System-Level Integration of Ventilation-Perfusion Matching by Hypoxic Pulmonary Vasoconstriction

by

Andrew Marquis

A dissertation submitted in partial fulfillment
of the requirements for the degree of
Doctor of Philosophy
(Molecular and Integrative Physiology)
in the University of Michigan
2022

Doctoral Committee:

Professor Daniel A. Beard, Co-Chair
Professor David J. Pinsky, Co-Chair
Professor Alberto Figueroa
Professor Vibha Lama
Professor Daniel Michele

Andrew Marquis

admarqui@umich.edu

ORCID iD: 0000-0001-7095-3569

© Andrew Marquis 2022

Dedication

This dissertation is dedicated to the more than 1 million Americans and 6.25 million people worldwide who have died from the COVID-19 Pandemic (statistics current as of May 2022).

"Life has to end. Love doesn't"

– Mitch Albom

Acknowledgements

There are countless people who have helped me to make this dissertation research at the University of Michigan possible - each to whom I owe my deepest gratitude. I begin by thanking my mentors David Pinsky, and Daniel Beard. I thank them for their unwavering belief in my capabilities, and in some of my darkest moments their prudent council that I am so much more than my putative PhD. As I embark on the next chapter of my life, I can only hope to emulate the leadership and compassion they possess. Many thanks are due to the members of the Pinsky and Beard labs for their encouragement, friendship, and support. I must specifically thank Patrick Robichaud, and Danica Petrovic-Djergovic whose instruction, guidance, and patience were instrumental in designing and performing experiments that made these research projects possible.

I thank my therapist, Stephanie Lin. Graduate school has strained, stretched, and broken my sense of self in ways I could not have prepared for. Despite my cynical disposition and tendency to seek nihilistic solutions, she helped me realize that I want to care, I do care, and above all it is important to care.

Finally, I would like to thank my wife and partner, Liz. They have been a fundamental pillar of support and continue to challenge me to become the truest version of myself. We came to University of Michigan as a bright-eyed newly engaged couple, and we will leave as a family. I could ask for no greater gift than this.

Table of Contents

Dedication ii

Acknowledgements iii

List of Tables ix

List of Figures x

List of Appendices xii

Abstract xiii

Chapter 1 Hypoxic Pulmonary Vasoconstriction and Ventilation-Perfusion Matching 1

1.1 Introduction 1

1.2 Scoping the Impact of Flow Distribution on Oxygen Uptake 3

1.2.1 Flow Distribution Between Two Pulmonary Gas Exchange Units 3

1.2.2 Flow Distribution Between Seven Pulmonary Gas Exchange Units 4

1.2.3 Flow Distribution Between Thousands of Pulmonary Gas Exchange Units 5

1.3 Phenotypes of HPV 7

1.3.1 Fetal Transition 7

1.3.2 Bi-phasic response 7

1.3.3 Clinical Considerations 8

1.4 Cellular and Molecular Mechanisms 14

1.4.1 Vasoconstrictive Effectors 14

1.4.2 Oxygen Sensors 17

1.4.3 Information Transducers 20

1.4.4 Endothelial Modulation 23

1.5 Major Themes 28

1.6 Aims of this Thesis 30

1.6.1 Specific Aim 1: Determine how V/Q ratios affects oxygen transport 30

1.6.2 Specific Aim 2: Determine how HPV regulates V/Q matching and oxygen transport 30

1.6.3 Specific Aim 3: Determine how proposed mechanisms of HPV could redistribute blood flow in response to airway occlusions 30

Chapter 2 On the Physiological Relationship Between Ventilation, Perfusion, and Oxygen Transport 35

2.1 Acknowledgements 35

2.2 Abstract 35

2.3 Introduction 36

2.4 Methods 39

2.4.1 Cardiac output, ventilation, and whole-body oxygen transport in exercise 39

2.4.2 Oxygen transport models 41

2.4.3 Steady state alveolar and vascular oxygen tension 45

2.4.4 Model parameterization 45

2.5 Results 46

2.5.1 Sensitivity of model behavior to apparent diffusion parameter 46

2.5.2 Vascular oxygen tension 47

2.5.3 Alveolar oxygen tension 48

2.5.4 Alveolar-vascular oxygen tension difference 48

2.6 Discussion 49

2.6.1 The optimal V/Q ratio for a single pulmonary gas exchange unit 49

2.6.2 Open v/s closed loop system 51

2.6.3 Potentially limiting model assumptions 52

2.6.4 Regional regulation of pulmonary perfusion and V/Q matching 54

2.6.5 Clinical considerations 55

2.6.6 Summary 56

Chapter 3 Hypoxic Pulmonary Vasoconstriction as a Regulator of Alveolar-Capillary Oxygen Flux: A Computational Model of Ventilation-Perfusion Matching 66

3.1 Acknowledgements 66

3.2 Abstract 66

3.3 Introduction 67

3.4 Methods 72

3.4.1 Model 72

3.4.2 Model parameterization 81

3.5 Results 88

3.5.1 Effect of HPV on regional hemodynamics 88

3.5.2 Effect of HPV on V/Q matching and regional alveolar-capillary oxygen flux 89

3.5.3 Effect of the fraction of inspired oxygen on HPV-mediated redistributions in hemodynamics, V/Q matching, and alveolar-capillary oxygen flux 90

3.5.4 Effect of airway occlusions on HPV-mediated redistributions in hemodynamics, V/Q matching, and regional alveolar-capillary oxygen flux 91

3.6 Discussion 92

3.6.1 Vascular network generation 92

3.6.2 Modeling of vascular mechanics 93

3.6.3 Modeling of oxygen transport 95

3.6.4 Empirical modeling of hypoxic pulmonary vasoconstriction 96

3.6.5 Model parameterization 100

3.6.6 Vascular recruitment 101

3.6.7 Summary of main findings 102

Chapter 4 How Different Oxygen Sensor Locations for Hypoxic Pulmonary Vasoconstriction affect Blood Flow, V/Q ratio, and Oxygen Flux Distribution 118

4.1 Acknowledgements 118

4.2 Abstract 118

4.3 Introduction 119

4.4 Methods 121

4.4.1 Model of V/Q matching 121

4.4.2 Models of HPV 121

4.4.3 Model parameterization 124

4.5 Results 125

4.5.1 Effect of HPV mechanisms on regional hemodynamics 125

4.5.2 Effect of HPV mechanisms on V/Q matching and regional alveolar-capillary oxygen flux 127

4.5.3 Effect of airway occlusions on HPV-mediated redistributions in hemodynamics, V/Q matching, and regional alveolar-capillary oxygen flux 128

4.6 Discussion 129

4.6.1 Conducted vascular response versus regional oxygen sensing as putative mechanisms underlying HPV 129

4.6.2 Modeling limitations 130

4.6.3 Summary 131

Chapter 5 Conclusions and Roadmap for the Future 146

5.1 Summary 146

5.2 Proposed Experimental Standard for Measuring HPV's Function 148

5.2.1 Defining HPV's function in terms of blood flow distribution 148

5.2.2 Measuring the Distribution of Alveolar Oxygen Tension 152

5.3 Future Experiments to Corroborate/Refute Model Simulations 153

5.3.1 V/Q Ratios Using Flow Rates v/s Tracer Signal Intensities 153

5.3.2 Validating Multi-scale Multi-Physics Model of V/Q Matching and HPV 154

5.3.3 Methods to Measure Molecular Signaling Events Distributed Throughout the Lungs 156
5.4 Future Model Refinements 157
5.5 Clinical Considerations for Interpreting V/Q Ratios 159
Appendix A 164
A.1 Steady state alveolar and vascular oxygen tension 164
A.1.1 Model A 164
A.1.2 Model B 164
A.1.3 Model C 165
A.1.4 Model D 166
A.1.5 Model E 166
A.1.6 Model F 166
A.2 Numerical stability for relaxing Model D and F to steady state 167
A.3 Sensitivity of model behavior to apparent diffusivity parameter 168
Appendix B 170
B.1 Network morphometry 170
B.2 Airway model 170
B.3 Effect of tidal volume on oxygenation 170
B.4 Effect of HPV and uniform vasoconstriction on regional oxygen tension distribution 170
B.5 Effect of airway occlusions on vascular tone from HPV 171
Bibliography 177

List of Tables

Table 2.1 **Model variables and parameters** 58

Table 2.2 **Model optimization and optimal diffusivity parameter** 59

Table 3.1 **Model variables, fixed parameters, and adjustable parameters** 103

Table 3.2 **Results from BELUGA Genetic Algorithm** 104

Table 3.3 **Standard Deviation (SD) and Correlations between parameters estimated by BELUGA Genetic Algorithm**. 105

Table 3.4 **Sensitivity Analysis** 106

Table 3.5 **Effect of HPV on regional flow, V/Q matching, and oxygenation** 107

Table 4.1 **Effect of HPV on regional flow, V/Q matching, and oxygenation** 132

Table 4.2 **Comparing the effects of two putative HPV mechanisms on regional flow, V/Q matching, and oxygenation in response to airway occlusions** 133

Table B.1 **Pulmonary vascular network and perfusion zone morphometry** 172

List of Figures

Figure 1.1 **Considering the scope of how blood flow distribution (V/Q matching) affects oxygen uptake in the pulmonary circulation.**..... 32

Figure 1.2 **Oxygen content of pulmonary venous outflow.** 33

Figure 1.3 **Summary of major signaling pathways proposed to mediate hypoxic pulmonary vasoconstriction**..... 34

Figure 2.1 **Empirical conversion of work rate to the cardiac output**..... 60

Figure 2.2 **Schematics of four open-loop pulmonary oxygen transport models** 61

Figure 2.3 **Schematics of two pulmonary closed-loop oxygen transport model**..... 62

Figure 2.4 **Contour plots for steady state oxygen tension in the alveolar space, vascular space, and the difference between them as a function of airflow and blood flow for Models A-D** 63

Figure 2.5: **Contour plots for steady state oxygen tension in the alveolar space, vascular space, and the difference between them as a function of airflow and blood flow for Models E and F** 64

Figure 2.6 **Least squares cost as a function diffusivity parameter, *D*** 65

Figure 3.1 **Schematic of multiscale multi-physics model of V/Q matching** 108

Figure 3.2 **Example of angiogenesis-inspired network generation algorithm**..... 109

Figure 3.3 **Morphometrically realistic pulmonary vascular networks** 110

Figure 3.4 **Whole-organ pressure-flow relationships** 111

Figure 3.5 **Fits from BELUGA Genetic Algorithm** 112

Figure 3.6 **Effect of HPV and uniform vasoconstriction on Network A regional perfusion, V/Q matching, and oxygen flux** 113

Figure 3.7 **Effect of HPV and uniform vasoconstriction on Network B regional perfusion, V/Q matching, and oxygen flux** 114

Figure 3.8 **Effect of HPV and uniform vasoconstriction on Network C regional perfusion, V/Q matching, and oxygen flux** 115

Figure 3.9 **Effect of the fraction of inspired oxygen on HPV-mediated redistributions in hemodynamics, V/Q matching, and oxygen flux** 116

Figure 3.10 **Effect of airway occlusions on HPV-mediated redistributions in hemodynamics, V/Q matching, and oxygen flux** 117

Figure 4.1 **Putative oxygen sensing mechanisms of hypoxic pulmonary vasoconstriction (HPV)** 134

Figure 4.2 **Distribution of vasomotor tone from HPV** 135

Figure 4.3 **Effect of HPV and uniform vasoconstriction on regional perfusion** 136

Figure 4.4 **Effect of HPV and uniform vasoconstriction on V/Q matching** 137

Figure 4.5 **Effect of HPV and uniform vasoconstriction on oxygen flux** 138

Figure 4.6 **Strategy to progressively occlude the airway** 139

Figure 4.7 **Effect of airway occlusions on tone from HPV** 140

Figure 4.8 **Effect of airway occlusions on HPV-mediated redistribution in hemodynamics** 141

Figure 4.9 **Effect of airway occlusions on HPV-mediated redistribution in V/Q matching** 142

Figure 4.10 **Effect of airway occlusions on HPV-mediated redistributions in oxygen flux** 143

Figure 4.11 **End-venous oxygen content as a function of the fraction of occluded alveoli**.. 144

Figure 4.12 **Proposed mechanism for HPV – multi-checkpoint system distributed throughout the tissue** 145

Figure 5.1 **Fluorescent Microspheres to Measure Rat Lung Blood Flow Distribution** 162

Figure 5.2 **Whole Body Oxygen Transport** 163

Figure A.1 **Numerical stability for approximating the fixed points of Model D** 169

Figure B.1 **Schematic of our airway model** 173

Figure B.2 **Effect of tidal volume on oxygenation** 174

Figure B.3 **Effect of HPV and uniform vasoconstriction on Network A regional oxygen tension distribution** 175

Figure B.4 **Effect of airway occlusions on the distribution of vascular tone from HPV This figure corresponds to simulations shown in Fig 3.10** 176

List of Appendices

Appendix A 164

Appendix B 170

Abstract

The lungs are a vital organ that facilitate several physiological processes, with gas exchange arguably being the most important, as the lungs are the only organ that directly interfaces with the atmosphere to deliver oxygen into the bloodstream. It is well appreciated that the regional overlap of airflow and blood flow, termed ventilation-perfusion (V/Q) matching, is a critical determinant of gas exchange efficiency and oxygen uptake. Decades of research efforts have revealed that pulmonary anatomy and gravity are major determinants of V/Q matching. It is also appreciated that the regulatory mechanism hypoxic pulmonary vasoconstriction (HPV) can also affect significantly affect and alter V/Q matching. In response to local hypoxia in the alveolar space, corresponding upstream pulmonary arteries vasoconstrict. This action of HPV is understood to redistribute pulmonary blood flow to regions of the organ that have adequate oxygen supply. However, there are gaps in our understanding of HPV's cellular/molecular basis and how HPV's function is integrated into the organ to affect V/Q matching at the system-level. This thesis leverages a systems-engineering perspective and computational modeling to reveal the mechanistic basis by which (Chapter 2) V/Q matching affects oxygenation, and (Chapter 3) how HPV affects V/Q matching and oxygenation. In Chapter 4 the model is used to test how putative locations of the HPV's oxygen sensors could redistribute blood flow and maintain oxygenation in response to a collapsed/occluded airway. These research efforts yield a new integrated understanding of how HPV is integrated within pulmonary vascular tissue and how it affects the distribution of blood flow, V/Q ratios, and oxygen uptake.

Chapter 1 Hypoxic Pulmonary Vasoconstriction and Ventilation-Perfusion Matching

1.1 Introduction

Gas exchange is perhaps the single most important process the lungs facilitate. In humans, the lungs are the only organ which directly interact with the atmosphere to deliver oxygen into the blood stream and play a major role in regulating plasma acid-base balance via the elimination of the metabolic waste product carbon dioxide. A major determinant of pulmonary gas exchange efficiency is the regional relationship between airflow and blood flow – a concept termed ventilation-perfusion (V/Q) matching. It is well appreciated that V/Q mismatching from a diversity of perturbations (ex: atelectasis, acute pulmonary embolism, pneumonia, etc.) can lead to inadequate gas exchange and subsequent blood gas derangements (1,2). Lungs are characterized by a fractal-like anatomy where hundreds of thousands parallel gas exchange units can compensate for small to moderate amounts of V/Q mismatching. In addition to the redundant anatomical structure of the lungs, it is well known that the force of gravity plays a significant role in V/Q matching (3,4). Consider a human standing upright – in this setting gravity leads to larger amount of blood flow the lowest part of the organ compared to the highest part. Additionally, the weight of the organ and extravascular tissue compresses the parenchyma (5). By extension, a subject's posture (ex: supine, prone, upright) has appreciable consequences on regional perfusion and V/Q ratios (1,2). For example: moving a patient into a prone position has been shown to improve V/Q matching and oxygenation (6). The relative contributions of anatomical structure and gravity to the distribution of air flow, blood flow, and V/Q ratios have been well studied and the literature review by Glenny et al. provides a thorough

review of these topics (7). Beyond anatomy and gravity, there is one more major factor that affects the distribution of perfusion within the lungs. This is the physiological mechanism of hypoxic pulmonary vasoconstriction (HPV). HPV is believed to operate by regionally sensing oxygen within the airway and then signaling the corresponding upstream arterioles to vasoconstrict. HPV functions to divert blood flow away from regions of the lungs with low oxygen supply (8). Put another way, HPV is a physiological feedback mechanism that helps to maintain oxygen uptake within a homeostatic range by altering the regional distribution of blood flow to match the regional distribution of airflow. The overall goal of the research presented in this thesis is to use a systems-engineering perspective illuminate how HPV affects V/Q matching to achieve adequate oxygen uptake.

The first observation of the HPV mechanism was by Euler et al. (in 1946) who demonstrated that ventilating a cat with pure oxygen lowered its pulmonary arterial pressure, whereas hypoxia raised it (9). They also observed that hypoxia-dependent vasoconstriction is modulated by carbon dioxide and the plasma acid-base balance, where alkalosis inhibits HPV while acidosis amplifies it. Some of the most impressive demonstrations of HPV include the use of double-lumen endotracheal tubes to differentially ventilate the left and right lungs. If one lung is ventilated with 100% oxygen and the other is ventilated with 4%, then a 95% diversion of pulmonary flow from the hypoxic to the hyperoxic lung is observed in miniature swine (10). Despite the reproducibility of the HPV phenotype across many mammalian species and countless studies over the past 75 years of investigation, the governing molecular pathways underlying this mechanism remain elusive and controversial. A review of the literature on the subject reveals a major gap: most studies investigating the molecular basis of HPV do ***NOT*** include measurements of V/Q ratios or use an experimental perturbation of air and/or blood flow distribution. This gap

is important considering the hypothesized physiological function of HPV to keep V/Q matching and oxygen uptake within homeostatic ranges. This chapter (a) reviews how ventilation and perfusion govern oxygen transport in the lungs; (b) outlines major phenotypes of HPV's function; (c) outlines critical cellular, molecular, and functional observations that have advanced the field's understanding of HPV; and (d) and delineates the research aims of the following chapters.

1.2 Scoping the Impact of Flow Distribution on Oxygen Uptake

1.2.1 Flow Distribution Between Two Pulmonary Gas Exchange Units

While V/Q matching is well appreciated as a major determinant of oxygen uptake, it is prudent to start with fundamental principles of biophysics to build a mechanistic understanding of how complex this phenomenon is. Let's begin by considering the simplest possible distributed network of pulmonary gas exchange depicted in Figure 1.1A. This diagram shows two pulmonary gas exchange units connected in parallel with blood flows q_1 and q_2 respectively, and a total blood flow through the network where $q_T = q_1 + q_2$. Assuming q_T is held constant, what values of q_1 and q_2 maximize oxygen uptake? If the two gas exchange units are identical (same volumes, air flows, and diffusion capacities), one might intuitively suggest $q_1 = q_2$ to be a satisfying and correct answer to this question. But what if there is reduced airflow to the top gas exchange unit? Given that regulatory mechanisms (such as HPV) plausibly operate in this scenario to divert blood flow away from under-ventilated regions, perhaps q_1 would be reduced? However, if q_1 is reduced then q_2 will proportionately increase due to our constraint of q_T being held constant. Reducing q_1 to improve V/Q matching of the top gas exchange unit would likely increase the oxygen concentration of the outflowing blood but increasing q_2 could plausibly

worsen V/Q matching and reduce the oxygen concentration of the outflow from bottom gas exchange unit. What should be appreciated here is that the oxygen concentration of the total outflow of this network is a function of how q_1 and q_2 (and corresponding airflows) are *distributed*.

1.2.2 Flow Distribution Between Seven Pulmonary Gas Exchange Units

Let's take this thought-experiment a step further and consider a more complex network depicted in Figure 1.1B. Here we have seven gas exchange units in parallel with an asymmetrically branching vascular network. Like the network in Figure 1.1A, we can ask a similar question of what distribution of these seven blood flows maximize oxygen uptake? This is substantially more complicated with additional gas exchange units, as to answer this question we need to know the corresponding seven air flows to each gas exchange unit AND how blood flow is apportioned through the intermediate vessel branches upstream of a gas exchange unit. For example, how does vasoconstriction of the blood vessel (reducing local blood flow) circled by the red oval affect oxygenation of the total pulmonary venous outflow? Upstream vasoconstriction will tend to reduce flow to the two downstream vessels and gas exchange units. Enforcing the constraint of constant total flow through the network, the other five will gas exchange units will necessarily have some level of increased blood flow. However due the structure of the vascular network, it is unlikely that these remaining five gas exchange units will have a uniform increase in blood flow. One plausible (albeit extreme) scenario is that that this excess flow will only be diverted to the top two gas exchange units while the bottom three maintain their original flow. The begs yet another question of what *redistribution* of flow through the network would best maintain oxygenation of the total venous outflow? But why stop here - what if we relax our assumption of the total flow through the network being constant and

allow it to increase, as there is a requisite increase in cardiac output during cardiovascular exercise? Does the increased total flow through the network change the optimal distribution of blood flow to oxygenate the blood stream? What about if the blood vessel circled by a red oval vasoconstricted during exercise?

1.2.3 Flow Distribution Between Thousands of Pulmonary Gas Exchange Units

I've taken these few preceding paragraphs to pose a series of questions regarding how the distribution of blood flow in these simple networks affects oxygen uptake but have purposefully not provided a complete answer these questions. This is because there are a potentially infinite number of ways blood flow (and corresponding V/Q ratios) can be distributed throughout a network, and the combinations of potential flow distributions only increases with more complex networks. Importantly, the complexity of the two simple networks shown in Figure 1.1 pales in comparison to that of true lungs – which are characterized by hundreds of thousands parallel gas exchange units. Basic science studies and clinical literature reports a that a V/Q ratios distribution for a healthy individual is log-normally distributed, centered around 1, and that the widening of this distribution (measured by log-scaled standard deviation) can be a symptom of pathological V/Q mismatching (2). It's quite remarkable to consider that only a narrow subset of all conceivably possible V/Q ratio distributions ensures adequate oxygenation of the bloodstream, as V/Q ratio distributions that do not conform to the log-normal pattern are considered pathological (11) – airway and vascular occlusions typically produce bimodal V/Q ratio distributions. While it is known that the anatomical similarity between the airway and vascular networks and regulation from mechanism like HPV enables V/Q matching and oxygenation to be maintained, we do not have a mechanistic understanding of how a given *distribution* of V/Q ratios produces a given oxygen concentration in the pulmonary venous

outflow; let alone how that distribution is regulated and/or redistributed in response to perturbations (ex: collapsed airway, pulmonary embolism).

In Figure 1.2 I present a conceptual way to organize how oxygenation of the pulmonary venous outflow is achieved using mathematical function notation. The use of this notation is not meant to be quantitatively or biophysically rigorous, but rather to clearly delineate in a stepwise manner how oxygenation of the bloodstream is achieved. First, is that pulmonary venous oxygen outflow is a function of V/Q matching ($P_{ven,O2}(VQ)$). Next is that V/Q matching is a function of anatomical structure, external forces such as gravity, and regulation from mechanisms like HPV ($VQ(x; \text{anatomy}, \text{gravity}, HPV)$). The quantity x is used here to indicate that VQ is a spatial probability distribution. Finally, physiological tone from HPV is a function of how oxygen within the alveolar space is regionally distributed ($HPV(x; P_{alv,O2}(x))$). I can nest these functions together to show that pulmonary venous oxygen is a non-trivial function of regional alveolar oxygen distribution ($P_{ven,O2}(VQ[x; HPV(x; P_{alv,O2}(x))])$). In many ways it is obvious, if not trivial, that oxygen content flowing out the lungs is dependent upon the oxygen available in the alveolar space. But this obvious point obscures the critical principle that is the *distribution* of these quantities and processes is what is most important. My emphasis on the importance of flow distribution is to highlight a major gap in the literature reviewed in the following sections. Within the field investigating the cellular and molecular basis of HPV, it is not standard to use measurements of V/Q ratios or flow distributions as a functional assessment. Rather, it is commonplace to measure HPV at the single cell level (patch-clamp electrophysiology of pulmonary arterial smooth muscle cells), single vessel level (isolated vessel myography), or whole-organ level (pressure-flow relationships in isolated-ventilated-perfused lungs). These

assays are certainly appropriate and useful, but they do not adequately capture the *distributed nature* of this physiological process.

1.3 Phenotypes of HPV

1.3.1 Fetal Transition

In the chronology of an organism's life, HPV makes its first appearance *in utero*. The fetus receives oxygenated blood via the placenta as the fetal airways are filled with amniotic fluid and do not have direct access to the atmosphere (12). While there are anatomical structures unique to the fetus that enable blood flow to effectively by-pass the fetal pulmonary circulation all together, such as the fetal ductus arteriosus which is a blood vessel that connects the aorta and main pulmonary artery (13), the pulmonary vascular resistance of fetal lungs is remarkably higher than those of newborn or adult (14,15). This can be explained by the function of HPV. *In utero,* HPV is active – the relatively low oxygen in the amniotic fluid-filled airway causes the pulmonary circulation to vasoconstrict and limit the blood flow through the developing lungs. At the moment of birth when the newborn takes its first breath of air there is now a supply of oxygen within the airways. HPV thus relaxes and the pulmonary circulation vasodilates to accommodate the necessary blood flow through the lungs so that the newborn can oxygenate their own blood. This profound physiological transition has led some to hypothesize that HPV in fully grown adults is an incidental remnant of a broader suite of mechanisms that have evolved to support fetal development (16). Some studies investigating HPV leverage the mechanism's fetal origins by using neonates or fetuses as research subjects, as they tend to have a stronger hypoxia-induced vasoconstrictive response compared to adults.

1.3.2 Bi-phasic response

The timescale of how HPV operates complicates our understanding of the mechanism. HPV is biphasic – meaning over the course of chronic hypoxia exposure there are two distinct phases of vasoconstriction (17). The first phase of vasoconstriction occurs within 10-20 minutes of hypoxia exposure. However, over the course of 2 or more hours, vasoconstriction continues to increase (18). The biphasic nature of HPV has been observed at multiple levels that include pulmonary arterial pressure (18), pulmonary artery diameter (19), and calcium influx within pulmonary arterial smooth muscle cells (PASMCs) (20). There has been a tremendous amount of effort from the field to differentiate between the governing molecular pathways that mediate phase 1 (acute) and phase 2 (chronic). The earliest study to observe the biphasic nature of HPV revealed that phase 2 contraction is endothelium-independent and the phase 1 is endothelium-dependent (17). More recent studies have implicated sensitization of Rho kinase activity in PASMCs as a major component of phase 2 constriction (20), and electrophysiological coupling of PASMCs to endothelial cells via gap junctions to be critical in phase 1 constriction (21). It also been observed that in addition to arterial vasoconstriction, pulmonary veins also constrict in response to hypoxia (22), and that pulmonary venous HPV is endothelium independent and is in magnitude greater than phase 2 arterial HPV. Despite this observation, there is a paucity of evidence implicating hypoxic pulmonary venous constriction in HPV's function to redistribute blood flow.

1.3.3 Clinical Considerations

High Altitude Pulmonary Edema

I conceptualize HPV as a negative feedback loop: with an adequate supply of oxygen, pulmonary arteries remain dilated; when there is a region with an inadequate supply of oxygen, HPV operates so that pulmonary arteries constrict to improve V/Q matching and ensure oxygen

uptake is within a homeostatic range. Despite this understanding of HPV, there are a number of situations where HPV's function can lead to pathology. One of the first observed disease states related to HPV is high-altitude pulmonary edema (HAPE) (23). At high altitudes the ambient air pressure is lower compared to sea level and thus there is a corresponding decrease in density of all gases – including oxygen. The net effect is that traveling to a high altitude can emulate sustained exposure to hypoxia and thus engage HPV. At the most extreme, prolonged pulmonary vasoconstriction can lead to elevated pressures in the pulmonary circulation and cause a mechanical stress-failure at the alveolar-capillary level and lead to edema (24). HAPE can be directly treated by supplemental oxygen and/or descending to a lower altitude (25), but can also be prophylactically prevented and managed by carbonic anhydrase inhibitors, such as acetazolamide, by augmenting the plasma acid-base balance and potentially augmenting the hypoxic ventilatory response (26).

Interestingly, people indigenous to high-altitude regions, like Tibet, have a blunted HPV response, which may be an evolutionary advantage to living in such a location (27). In a 2017 study, Peng et al. showed heterozygous hypoxia inducible factor 2α (HIF-2α) knockout mice have blunted physiological responses to chronic hypoxia – a phenotype consistent with Tibetans (28). Importantly, they also found that the Tibetan version of HIF-2α is associated with a low pulmonary vasoconstriction response; they proposed that the down regulation of HIF-2α contributes to the Tibetan adaptation and tolerance of hypoxia and high altitudes. At the molecular level, Yoo et al. has demonstrated that ambient hypoxia exposure can make HPV disappear by reducing a nonselective cationic current in rat pulmonary arterial smooth muscle cells (PASMCs) (29). However, to my knowledge it has not been tested if the Tibetan version of

HIF-2α is mechanistically related to Yoo et al.'s observation of a reduced nonselective cationic current in PASMCs.

Pulmonary Hypertension and Sex Differences

There is a significant overlap between literature on HPV and literature on hypoxia-induced pulmonary hypertension (PH). The World Health Organization recognizes five distinct classes of PH, and one of these is hypoxia-induced (30). While the etiology of PH is a complex topic (I recommend Burger et al.'s review (31)), it's interesting to note that some of the most reliable pre-clinical animal models of PH require chronic exposure to hypoxia. Even pre-clinical models that are focused on the idiopathic form of PH, like the Sugen-Hypoxia rat model, require chronic hypoxia exposure in addition to an infused vascular endothelial growth factor (VEGF) receptor antagonist (32). This reflects that hypoxia-induced PH is arguably the class of PH we understand best. When chronically exposed to hypoxia, HPV induces pulmonary arterial vasoconstriction. To maintain or generate more constriction, the pulmonary vasculature undergoes profound vascular remodeling, such as hypertrophy of pulmonary artery tunica media, and increased tortuosity of vascular pathways (33). To this end, there has been a tremendous number of studies investigating the mechanisms of hypoxia-induced pulmonary vascular remodeling in the context of PH (34). The mechanism(s) underlying phase 2 constriction of HPV could plausibly be upstream drivers of the genetic programs that mediate vascular remodeling. It is also more than likely that biological sex modulates HPV, as it has been observed that estradiol induces the release of prostaglandins, and this can inhibit the apparent vasoconstriction mediated by HPV by activating the endothelial nitric oxide synthase (eNOS) pathway (35–37). We can potentially gleam further insights into sex differences based on those observed in PH. Women are twice as likely to have PH compared to men, but men are more likely to have more severe

cases of PH compared to women (38). Thus estrogen/estradiol can be a negative modulator of pulmonary vasomotor tone and can be protective against severe cases of hypoxia-induced PH.

Lung Infections

There are many pathogens capable of infecting the lungs and compromising the organ's function – the most clinically extreme state being pneumonia (39). In addition to molecular assays to identify the specific species underlying an infection or pneumonia, clinical procedures such as a computed tomography (CT) scans can be used to determine the spatial region where infections could be localized based on characteristic patterns of focal edema and/or disrupted air and blood flow pattern on these radiological scans (40). While better stratification and differential diagnoses for pathogens underlying pneumonias are active areas of research (41,42), it has been broadly observed that lung infections tend to disrupt the function of HPV. The earliest clinical evidence of this was in 1991 and demonstrated that pneumonia can disrupt normal V/Q matching, and the degree of V/Q mismatching correlated with disrupted gas exchange (43). In 1997 it was observed that HPV is blunted during sepsis without adaptation over time (44). These clinical observations have also been corroborated by basic science studies of endotoxemia. Frank et al. demonstrated that acute endotoxemia with lipopolysaccharide (LPS) increases the peak HPV response, but that the effect is not sustained (45,46). The authors speculated that this phenomenon could be due to disrupted function of eNOS and NO generation, which was later confirmed in 2005 by Spohr et al. (47). Relatively recently in 2015, Jahn et al. showed that low-dose carbon monoxide prevented LPS-mediated impairment of HPV, which coincided with a decreased expression of inducible nitric oxide synthase (iNOS) (48). Most recently in 2020, Cui et al. demonstrated that bacillus anthracis edema toxin inhibits HPV through cAMP-mediated mechanisms in isolated ventilated perfused rat lungs (49). However,

without knowing the governing molecular pathways of HPV it is challenging to determine if there is a common mechanism by which infections disrupt HPV, or if there are a diversity of ways different infections which either directly inhibit or phenotypically mask HPV by altering pulmonary vascular tone.

Mechanical Loading and Exercise

A broad challenge the field faces is consistency in reproducing observations of HPV. This is not because HPV is difficult to stimulate, but rather because its function operates on the background of many other physiological processes and mechanical influences. In 1995 Morrell et al. used a balloon-tipped catheter to occlude the bronchus to the left lower lobe in supine human subjects and demonstrated that hypoxemia during lobar bronchial occlusion is caused by shunting of mixed venous blood (50). They also observed that in regions of the lung immediately adjacent to the obstructed region had reduced airway compliance, which could impair ventilation. It's plausible that this regionally reduced compliance could be a greater contributor to hypoxemia than a diversion of regional blood flow from regulatory mechanisms like HPV. McCann et al. lavaged pigs with a mild detergent (Tween) to disrupt alveolar mechanics, after which they observed that unstable alveoli stents open pulmonary vessels (51). This stenting may explain why HPV is impaired in disease states characterized by alveolar surfactant loss, such as acute respiratory distress syndrome (ARDS). In a 2011, Taylor et al. studied pulmonary capillary recruitment by measuring cardiac output and pulmonary capillary blood volume changed in response to saline infusion and exposure to hypoxia. Changes in blood flow, systolic pulmonary arterial pressure, and left ventricular diastolic function were not able to explain changed recruited pulmonary capillaries (52) – the authors speculate that HPV may play a role in mediating pulmonary capillary recruitment.

A common practice for laparoscopic surgical procedures is to inflate the abdominal cavity. This is called pneumoperitoneum, which provides more space to navigate and operate fiber optic cameras and surgical tools (53). A non-obvious advantage of a pneumoperitoneum is that it can improve V/Q matching and oxygen uptake, and it has been speculated that this is due to the compression of the lungs in the thoracic cavity and corresponding change in the distribution of airflow (54). In a 2013 study, Strang et al. compared pneumoperitoneum using CO_2 or air, and found that only CO_2 pneumoperitoneum improves V/Q matching and oxygenation, while air does not (55). A possible explanation for this difference is that CO_2 peritoneum makes blood pH more acidic, and this could potentiate HPV-mediated redistribution of pulmonary blood flow and corresponding improvement in V/Q matching.

Healthy lungs have reserve oxygen uptake capacity compared to the oxygen demand of systemic tissues during normoxia. However, exercise increases oxygen demand and drives a physiological response to recruit this reserve oxygen uptake capacity to meet the metabolic demands of systemic tissues (56). Roy et al. developed and validated a mathematical model of pulmonary blood flow heterogeneity, defined by the coefficient of variation (CV = standard deviation/mean), to investigate the effects of flow heterogeneity on oxygen update during exercise (57). Their model simulations predict that at baseline the lungs are capable of adequately oxygenating the blood stream over a range of heterogenous flow distributions (up to a CV of 3), but that highly heterogenous flow distributions are unable to adequately oxygenate the blood stream during exercise. Adequate oxygenation during exercise is only achieved with a relatively low blood flow CV (0.48), which suggests that local flow regulation, such as HPV, may play a role in maintaining V/Q matching and oxygen uptake during exercise.

1.4 Cellular and Molecular Mechanisms

As HPV is a homeostatic regulatory mechanism, my review of the molecular literature organized by (a) the vasoconstrictive effector; (b) the oxygen sensor; and (c) the information transducer that connects the sensor to the effector. Despite the large volume of research in this area over the past 75 years the molecular identify of the governing vasoconstrictive effectors, oxygen sensors, and information transducers all remain unclear. These research efforts have suggested numerous biomolecular complexes and entities as molecular integrators that range from ion channels that affect pulmonary arterial smooth muscle cell (PASMC) electrophysiology, redox signaling within and outside the mitochondria, signal transduction from prostanoids, and endothelial modulation. Many of these studies do not use measurements of V/Q ratios or blood flow distribution, even though it understood that HPV functions to regulate V/Q matching and the distribution of blood flow. Despite this gap in the literature, the studies reviewed here have enabled tremendous insight into the function of HPV. In Figure 1.3 I depict many (but not all) of the signaling pathways and mechanisms reviewed that could plausibly intersect to produce the function of HPV.

1.4.1 Vasoconstrictive Effectors

Smooth Muscle Cell Contraction: Extracellular v/s Intracellular Calcium

It is well known that vasoconstriction of pulmonary arteries (and blood vessels in general) is due to the contractile function of smooth muscle cells (SMCs) (58). Part of the contemporary understanding of SMC physiology is that their contraction is a calcium-dependent process – raising intracellular Ca^{2+} concentration is the rate-limiting stimulus to activate actin-myosin cross-bridge cycling. Additionally, long term maintenance of constriction is

accomplished through sensitization mechanisms that canonically involve the activity of Rho kinase. For a detailed and thorough treatment of vascular smooth muscle contraction, I recommend the 2018 literature review by Touyz et al. (58). In the context of HPV's molecular mechanism, we can reasonably expect that PASMC intracellular Ca^{2+} concentration and Rho kinase activity are necessary downstream factors to drive the vasoconstrictive effector function.

There is compelling and conflicting evidence for extracellular and intracellular sources of Ca^{2+} being necessary to drive HPV. The earliest studies of Ca^{2+} signaling in HPV showed that pharmacologically inhibiting L-type Ca^{2+} channels inhibit hypoxia-dependent constriction of pulmonary arteries (59–63) . More recent investigations have reached some consensus that L-type Ca^{2+} channels are unlikely to be a direct or solitary mediator but can certainly potentiate and/or modulate the mechanism (64,65). Yet there is also evidence that Ca^{2+} from the sarcoplasmic reticulum (including store operated Ca^{2+} entry) (66,67), and endoplasmic reticulum via canonical G-protein-IP3 signaling pathways (68) can affect the HPV response. A broad interpretation of these contrasting conclusions is that perhaps both extracellular and intracellular sources of Ca^{2+} contribute to the effector function of HPV. Connolly et al. posit an interesting hypothesis, where L-type Ca^{2+} channels primarily contribute to phase 1 of HPV, and Ca^{2+} from the sarcoplasmic reticulum and SOCE contributes to both phase 1 and 2 (64).

Unlike many other Ca^{2+} channels that have proposed, there is consistent evidence for transient receptor potential cation channel 6 (TRPC6) being a critical part of HPV across investigation from different research groups. Fuchs et al.'s landmark literature review on the role of TRP (transient receptor potential) channels in HPV presented for the first-time data showing that TRPC knock-out mice had effectively no acute (phase 1) HPV response, however phase 2 constriction was left entirely intact (69). Tang et al. provided greater clarity into this mechanism,

where they showed that TRPC6 is likely the critical isoform, as knock down of TRPC6 by siRNA reduced the acute HPV response by approximately 80% (70). Another study from Fuchs et al. demonstrated that diacylglycerol is sufficient to activate TRPC6 in the acute phase of HPV (71). It has also been shown that the activity of RhoA/Rho associated protein kinase (ROCK) signaling affects the expression of HIF-1α, and HIF-1α expression affects the expression and function of TRPC1 and TRPC6 channels in PASMCs (72).

Hypoxia-Mediated Inhibition of Kv Channels

There is profoundly compelling evidence that inhibition of Kv currents and subsequent depolarization of PASMC membrane potential is a key factor of HPV's molecular mechanism. The earliest study by Post et al demonstrated that inhibiting K^+ channels increased pulmonary arterial pressure in isolated lungs and inhibited whole cell K^+ currents in isolated PASMCs (73). Since this landmark observation, K-ATP, K-Ca, and "big" BK-Ca channels have been ruled out as the operative channels (74,75). In 2000, Osipenko et al advanced the field by expressing the O2-sensitive Kv channels Kv1.1, Kv1.2, and Kv1.5, and Kv3.1b in L929 (mouse fibroblast) cells and observed that hypoxia exposure only inhibited currents from Kv3.1b, and then confirmed the expression of Kv3.1b in PASMCs with RT-PCR and immunocytochemistry (76). Coppock et al. extended this observation the following year where they stained for the same O2-sensitive Kv channels as Osipenko and observed that Kv3.1b α-subunit and Kvβ.1, Kvβ1.2, and Kvβ1.3 accessory subunits expression dramatically increased along the distal branches of the pulmonary arterial tree (77). I emphasize that this observation is consistent with functional observations of HPV being most prominent at the intrapulmonary resistance arteries of the pulmonary vasculature (78).

Platoshyn et al. observed in 2001 that chronic hypoxia decreases mRNA expression of Kv channel α-subunits (Kv1.1, Kv1.5, Kv2.1, Kv4.3, and Kv9.3) and protein expression (Kv1.1, Kv1.5, and Kv2.1) in PASMCs but not in mesenteric artery SMCs (79). Functionally, this loss of Kv channels depolarized PASMCs and increased intracellular Ca^{2+} concentrations**.** This same group transfected Hek-293, COS-7, mesenteric artery SMCs with KCNA5 (which encodes the Kv1.5 channel) and overexpressed it in PASMCs in 2006 (80). They showed that Kv1.5 creates hyperpolarizing currents in all cell types tested, however only in PASMCs did hypoxia inhibit the current from Kv1.5 – suggesting that PASMCs have a unique hypoxia-sensing mechanism that operates to inhibit KCNA5 channel activity. It's important to emphasize that this hypoxia-mediated inhibition of Kv channels is unique to pulmonary arterioles and not observed in systemic arterioles – systemic blood vessels tend to vasodilate in response to hypoxia through a myriad a metabolism-mediated mechanisms (81,82). Platoshyn et al. again further complicated the understanding of Kv currents in HPV in 2007 when they investigated the heterogeneity of Ca^{2+} signal in HPVs (83). Using single cell patch-clamp and RT-PCR, they observed that "hypoxia-sensitive" cells expressed high amounts of Kv1.5 compared to "non-responder" cells. Perhaps most importantly, Kv1.5 channel knockout mice have impaired HPV (84). Despite the body of evidence for Kv channel inhibition being important for HPV, it remains unclear how the subsequent membrane depolarization leads to increased concentration of intracellular Ca^{2+} – particularly when one considers the current understanding that while voltage-gated L-type Ca^{2+} channels contribute to HPV, they are not essential for the mechanism.

1.4.2 Oxygen Sensors

Hypoxia Sensing by Pulmonary Arterial Smooth Muscle Cell Mitochondria

Plausible oxygen sensors for HPV include mitochondrial and non-mitochondrial redox enzymes. A major physiological role of molecular oxygen is to act as an electron sink which mitochondria respiratory complexes leverage to catalyze a sequence of biochemical reactions (tricarboxylic acid cycle) on various carbon substrates (ex: glucose and fatty acids) and ultimately produce ATP via oxidative phosphorylation (85). Thus, it is quite intuitive to hypothesize that the oxygen sensor for HPV lies within the mitochondria. Mitochondrial electron transport chain (ETC) complexes I, II, III, and IV have all been proposed as the putative oxygen sensor for HPV, however there is conflicting evidence amongst different investigations (86–92). Interestingly, hypoxia differentially affects reactive oxygen species (ROS) generation in PASMCs compared to coronary SMCs (CASMCs). Acute hypoxia exposure decreases ROS production in both cell types, however chronic hypoxia increases ROS production in PASMCs, unlike CASMCs which maintain decreased ROS levels (93).

Part of the historical challenge in determining which (if any) of the mitochondrial ETC complexes acts as HPVs oxygen sensor is identifying the specific ROS changed by hypoxia exposure that then connecting this to a downstream rise in intracellular Ca^{2+}. There is some consensus that generation of superoxide and dismutation into hydrogen peroxide are critical redox metabolites for HPV (94–97). The field has some mechanistic insight into how changes in PASMC redox status lead to HPV, as certain K+ channels (such Kv1.5) are intrinsically redox sensitive due to sulfhydryl groups (98). Of the studies testing the contribution ETC complexes to HPV, a recent one published by Dunham-Snary et al. in 2019 is particularly compelling (92). Their study showed that knockdown of NADH dehydrogenase iron-sulfur protein 2 (Ndufs2), a subunit of complex I, via siRNA in cultured PASMCs decreased normoxic production of

hydrogen peroxide, prevented the hypoxia-induced increase in intracellular Ca^{2+}, increased the NADH/NAD+ ratio, and decreased expression of Kv1.5 protein. This study also knocked down Ndufs1, another Fe-S ceneter within complex I, and other subunits proposed as putative oxygen sensors in complex III (Riske iron-sulfur protein), and complex IV (cytochrome c oxidase subunit 4 isoform 2). These knockdowns had no effects on hypoxia-mediated increase in intracellular Ca^{2+}. As exciting as these data are, I assert that further studies are needed to test if knocking down Nduf2 affects how changes in alveolar oxygen *distribution* alter the *distribution* of pulmonary blood flow to confidently claim complex I is the operative oxygen sensor for HPV. Additionally, this study only assessed phase 1 of HPV and not the longer time scale for phase 2. An earlier study by Paddenburg et al. in 2003 provides evidence that complex II (succinate dehydrogenase) is important for phase 2 of HPV (88). It is certainly plausible that different ETC complexes contribute to different times scales of the HPV response, which further complicates how the field needs to disentangle the factors mediating HPV.

Non-Mitochondrial Redox Signaling in Hypoxic Pulmonary Vasoconstriction

In addition to mitochondrial ETC complexes, non-mitochondrial ROS have been shown to contribute to HPV. Inhibiting NADPH oxidase has been shown to inhibit phase 1 of HPV (99), and inhibiting the pentose phosphate pathway (PPP) has been shown to reduce NADPH levels and the NADPH/NADP+ ratio (100). This study observed that inhibition of the PPP also increases soluble guanylate cyclase activity and inhibiting soluble guanylate cyclase potentiated the HPV response (100), so it's possible that PPP-derived NADPH modulates HPV by activating the canonical vascular nitric oxide (NO)-cyclic guanosine monophosphate (cGMP) vasodilation pathway (101). Beyond hydrogen peroxide-mediated inhibition of Kv currents, ROS signaling has been showed to activate RhoA during prolonged hypoxia exposure (102); however, it is

unclear if hydrogen peroxide or other redox metabolites are responsible for this increased Ca^{2+} sensitivity. ROS signaling has also been shown increase intracellular Ca^{2+} and PASMC contraction by ROS-dependent activation of PLCγ1, IP3 production, PKCε activation, and IP3R1 opening (103).

Multiple mitochondrial complexes, redox enzymes, and corresponding redox products have been shown to affect PASMC intracellular Ca^{2+} concentration which has provided a great deal of insight into HPV's molecular basis, but this has also seeded much controversy regarding the oxygen sensor underlying the mechanism. One such controversy is the operative mitochondrial ETC complex or complexes – as it seems very plausible that multiple mitochondrial ETC complexes act as oxygen sensors for HPV's mechanism. A parallel controversy is the relative contribution of Ca^{2+} sources to mediate or moderate HPV – perhaps the redox products of various mitochondrial complexes affect distinct Ca^{2+} channels? Given that there is no clear consensus on the critical source of Ca^{2+} (extracellular v/s intracellular – ryanodine v/s IP3, etc.) necessary to drive HPV, evidence showing that redox signaling can affect Ca^{2+} influx from any of these sources does not immediately or easily help the field resolve the mechanism. I reassert what I have identified as a major gap in the field here: most studies investigating HPV's cellular and molecular basis do not measure HPV's phenotype in terms of blood flow *distribution*. While the constellation of redox processes, signaling, and intersection with other canonical signal transduction pathways is certainly an area needing more investigation, the field could potentially rule out putative red herrings by using measurements of blood flow distribution as the standard to assess HPV's phenotype.

1.4.3 Information Transducers

Prostanoids

Many prostanoids have been proposed as signaling transducers within HPV's mechanism. These are a subclass of eicosanoids, consisting of prostaglandins, thromboxanes, and prostacyclins, and it well appreciated that the creation of these compounds by cyclooxygenases and lipoxygenases play roles in fatty acid and lipid signaling in a diversity of tissues (104). Some of the earliest evidence for prostanoids having a role in HPV was the observation that volatile halogens like isoflurane inhibit HPV (105), and that this inhibition can be abolished by cyclooxygenase inhibition (106). Additionally, the lungs are also known to produce both thromboxane (pulmonary vasoconstrictor) and prostacyclin (potent vasodilator) (107). The earliest investigations of prostanoid signaling in HPV primarily consisted of negative data, and definitively ruled out immune response-modulating leukotrienes as a vasoactive mediator for HPV (108–112). Yet there is a body of evidence suggesting that the activity of 15-lipoxygenase (15-LO) and corresponding product 15-hydroxyeicosatetranenoic acid (15-HETE) play a role in HPV's mechanism. Exogenous 15-HETE induces pulmonary vasoconstriction in a dose-dependent manner (113), and 15-HETE-induced constriction can be blocked by inhibiting Kv channels (114). Parsimoniously but in the oppositive signaling direction, it's also been shown that blocking 15-LO activity (synthesis of 15-HETE) prevents the hypoxia-mediated down regulation of Kv1.5 expression in PASMCs (115), and that hypoxia-mediated activation of 15-LO regulates the expression of Rho-associated kinase via G-protein and tyrosine kinase pathways (116).

In addition to 15-LO activity and 15-HETE, there is evidence that CYP450 epoxygenase-derived epoxyeicosatrienoic acids (EETs) and ceramide from neutral sphingomyelinase (nSMase) have roles in HPV's mechanism. It has been shown that 11,12-EET can induce

pulmonary vasoconstriction in a dose-dependent manner, and that both hypoxia and 11,12-EET can induce the translocation of a TRPC6-V5 fusion membrane to the PASMC membrane (117). Perhaps most importantly, this study also showed that full TRPC6 knockout mice did not have HPV response to hypoxia or 11,12-EET. It has been demonstrated that the hypoxia increases nSMase activity and corresponding levels of ceramide in cultured PASMCs, and that inhibition of nSMase prevents the hypoxia-induced inhibition of Kv currents and increase in pulmonary arterial pressure (118). Along these lines, it also been shown that inhibition of nSMase prevents the hypoxia-induced production of ROS in PASMCs, and in the opposite direction rotenone (inhibitor of mitochondrial ETC complex I) prevents the hypoxia-induced increase in ceramide (119).

Conducted Vascular Responses

Many studies investigating the cellular and molecular basis of HPV make an implicit assumption that the oxygen sensor is located within PASMCs. However, Wang et al. proposed and tested a novel hypothesis in 2012 where they speculated that the ideal location for an oxygen-sensor for HPV would be located at the alveolocapillary level, and then subsequent retrograde conducted vascular response through the endothelial gap junctions would induce PASMC contraction (120). In their study they demonstrated that HPV was largely attenuated by Connexin-40 (Cx40) specific and nonspecific gap junction uncouplers in the lungs of wildtype mice, and lungs from Cx40 knockout mice. Perhaps most importantly, they used intravital microcopy and real-time fluorescence imaging to reveal that hypoxia caused endothelial membrane depolarization in alveolar capillaries that propagated to upstream arterioles in wild type, but not Cx40 knockout, mice. From this same group in 2015, Goldenberg et al investigated the role of TRPV4 channels in HPV and showed that hypoxia-induced increase in pulmonary

artery pressure in wildtype mice was attenuated by both pharmacological inhibition of TRPV4 and in a TRPV4 knockout mice (121). This study also demonstrated that in cultured human PASMCS, inhibition of TRPV4 blocked hypoxia induced Ca^{2+} influx and myosin light chain phosphorylation. The authors speculate that TRPV4 may form a heteromeric channel with TRPC6 as the two channels coimmunoprecipitate from PASMCs, and there is no additive effect of TRPC and TRPV4 inhibition on Ca^{2+} influx. Also in 2015 from this same group, Tabeling et al showed that the translocation of TRPC6 to the PASMC membrane is downstream of nSMase activity and requires the cystic fibrosis transmembrane regulator (CFTR) to interact with TRPC6 as a chaperone (122). These studies outline a new frontier of research the field needs to contend with, as it forces investigators to consider and test the broad hypothesis that HPV is a mechanism distributed throughout the pulmonary vascular tissue, rather than being solely intrinsic to PASMCs.

1.4.4 Endothelial Modulation

There are countless substances that influence vasomotor tone and affect the distribution of blood flow. However, endothelial-derived nitric oxide (NO) and endothelins (ETs) are arguably the most ubiquitous endogenous substances that influence virtually every blood vessel's diameter. In the vasculature, the endothelial isoform of nitric oxide synthase (eNOS) is responsible for synthesizing NO. As a physiological gas, NO can easily diffuse across the vascular SMC membrane and activate guanylate cyclase. Guanylate cyclase then converts guanosine triphosphate (GTP) into cyclic guanosine monophosphate (cGMP). cGMP then activates protein kinase G (PKG), which has multiple cellular phosphorylation targets that operate to lower intracellular vascular SMC Ca^{2+} concentrations. NO is thus recognized as a potent vasodilator and much research has been performed to understand it's multifactorial roles

in protecting against various cardiovascular diseases - I recommend Farah et al.'s literature review for a thorough treatment of NO's influence on cardiovascular function (101). ETs can be considered to have the parallel opposite function of NO as one of the most potent endogenous vasoconstrictors. ETs are peptides primarily synthesized by the endothelium which bind to endothelin receptors expressed by neighboring SMCs in a paracrine manner. There are 3 ET isoforms (ET-1, -2, and -3), which have different binding affinities for two of GPCR receptors, ETA and ETB. The ETA receptors are selective for ET-1 and is primarily expressed on vascular SMCs, whereas the ETB receptor has similar binding affinity for all ET isoforms and is primarily expressed by endothelial cells. ETB receptor activation on endothelial cells has also been shown to activate eNOS and NO synthesis (123). I recommend Davenport et al.'s literature review for a deeper treatment of ET pharmacology (124).

Nitric Oxide

Some early investigations hypothesized that the mechanism of HPV operates by reducing NO activity during hypoxia. In other words, rather than hypoxia leading to a direct vasoconstrictive effector, hypoxia would remove a tonic vasodilating signal which produces an apparent vasoconstriction. The origin of this hypothesis is a 1980 study, where Weygandt et al sought to determine the mechanism of nitroglycerin-induced hypoxemia in patients with coronary artery disease and/or obstructive ventilatory disease (125) and observed that the reduction of blood oxygenation from nitroglycerin is explained by pulmonary vasodilation and corresponding disruption of V/Q matching (increased perfusion of poorly ventilation lung units). This hypothesis was directly scrutinized by Ogata et al. in 1992, where they used isolated porcine pulmonary artery rings suspended in an organ chamber and measured changes in isometric force. They observed that hypoxia significantly reduced endothelium-dependent

relaxation from acetylcholine and augmented the contractile response to phenylephrine. Perhaps most importantly, the augmentation of phenylephrine-mediated contraction by hypoxia was not seen in rings without endothelium, and removal of the endothelium enhanced hypoxic contraction (126). These data suggest that the suppression of NO synthesis is not the mechanism underlying HPV. Despite these negative data for NO signaling being the direct mediator of HPV, it's influence on HPV and basal vascular tone is non-trivial and has continued to be investigated in the context of HPV.

In 1993, Roberts et al. demonstrated that inhaled NO can reverse HPV potentiated by acidosis in a newborn lamb by increasing cGMP (127). Using an isolated-perfused lung preparation in 1996, Dumas et al measured how a variety of vasodilators affect HPV and HPV augmented by hypercapnic acidosis (74). In contrast to Robert et al, they conclude that NO can limit HPV, but not HPV potentiated by hypercapnic acidosis. The differences in these conclusions can potentially be explained by their differing model systems – it's plausible that the pulmonary vasculature of newborn lambs have a stronger HPV response than adult rabbits. In 2000, Weissman et al used an isolated-perfused rabbit lung preparation to demonstrate that NO can only oppose HPV as a vasodilator by stimulating cGMP synthesis, and that there was no evidence for a role of NO outside the canonical cGMP pathway (128). A major landmark in understanding NO signaling in general was the development of the first eNOS gene knockout (-/-) mice by Fagan et al in 1999 (129). They observed that eNOS (-/-) mice developed pulmonary hypertension when raised in mild hypoxia compared to wild type controls and eNOS (-/-) mice raised in normoxia. Importantly, this phenotype was rescued by acute inhalation of NO. The operative conclusion here is that eNOS derived NO is an important modulator of pulmonary

vascular responses to chronic hypoxia – despite the reality that NO signaling is unlikely to be the primary effector of HPV.

In 1998, Deem et al investigated the mechanism in which red blood cells (RBCs) augment HPV (130). Using isolated-ventilated-perfused lungs from rabbits, they demonstrated that HPV was greater when the lungs were perfused with larger hematocrits, and that expired NO varies inversely with hematocrit and decreased with hypoxia. Notably, eNOS inhibition eliminated RBC-dependence on HPV, which led the authors to speculate that this phenomenon is related to the scavenging of NO by RBCs. This same group furthered this line of investigation in 2000, where they performed similar experiments but used free hemoglobin and RBC ghosts (131). They observed free hemoglobin alters HPV in a similar manner to RBCs, whereas RBC Ghosts only mildly inhibited HPV and caused a small reduction in expired NO. This same year, Loer et al. explored in the same phenomenon with more granularity of hematocrits tested in a similar isolated-ventilated-perfused rabbit lung preparation (132). They showed that the magnitude of acute HPV is not altered by increased hematocrit but is reduced with reduced hematocrit. Additionally, they observed that hematocrit does not affect hypoxia-mediated changes in passive vascular elasticity. This enabled the authors to speculate that the RBC influence on HPV is perhaps due to flow-related mechanisms – this is perhaps some of the earliest evidence of flow-mediated vasodilation via the activation of eNOS (133). In 2003, Han et al. demonstrated that under hypoxia, RBCs consume NO faster compared to normoxia (134). We recommend Deem et al.'s 2004 review on how hemoglobin inactivates NO (135). To further complicate the modulatory role of NO signaling in HPV, Takemoto et al. in 2002 showed that hypoxia reduces the expression of eNOS in cultured endothelial cells by increasing Rho-kinase activity (136). The critical observation from this study was that blocking Rho-kinase with

hydroxyfasudil prevented the hypoxia-mediated decrease in eNOS expression in a dose dependent manner. Additionally, Nozik-Grayck et al. demonstrated in 2003 that eNOS activity is also able to generate superoxide, and inhibition of the bicarbonate-chloride anion exchange protein (AE2) reduced the extrusion of superoxide from the endothelium (137). These results represent an integrative observation where the canonical eNOS pathway and ROS signaling overlap to regulate pulmonary vascular tone and potentially modulate HPV.

Endothelin

The first studies to investigate the role of ET in HPV were in 1995, where Helset et al. observed increased ET-1 concentration in the perfusate that washed out of an isolated-perfused rat lung preparation when exposed to hypoxia compared to normoxia (138). Wang et al. also demonstrated that application of ETA receptor antagonist BQ123 can inhibit hypoxia-induced increase pulmonary vascular resistance. Like Wang et al., Jones et al. in 1999 showed that ETA receptor antagonist CI-1020 reduces hypoxia-induced contraction in small pulmonary arteries but not large arteries (139). However, the likelihood for ET being a primary effector of HPV significantly decreased in 1997, where Takeda et al. used double lung ventilation on humans to show that while circulating ET-1 increases with hypoxia exposure, the time scale is not consistent with the timescale of HPV - 20 minutes for peak increase in resistance v/s 40 minutes to peak ET-1 plasma concentration (140). In 2000, Sato et al. showed that the ETA antagonist BQ123 and nonselective ETA and ETB antagonist PD-145065 can inhibit HPV both *in vivo* in rats and in an isolated perfused rat lung preparation, unlike the ETB antagonist BQ788 (141). Sato et al. also observed that BQ123-mediated inhibition of HPV can be rescued by the application of glibenclamide – suggesting that ET-1 contributes to HPV via ETA-mediated suppression of KATP activity (141). In 2001, Liu et al. used isolated porcine pulmonary arteries

to show that endothelial denudation abolished HPV, but that it could be rescued when pretreated with ET-1 (142). In 2003, Goirand et al. and Zhang et al. independently connected ETA receptor activity to PASMC electrophysiology. Goirand et al. showed that glibenclamide (KATP channel inhibitor), charybdotoxin (BKCa channel inhibitor), and 4-aminopoyradine (Kv channel inhibitor) were able to partially rescue the inhibition of HPV by BQ123 (143). Zhang et al. showed that ETA activation operates through Gq-coupled GPCR (phospholipase C and inositol triphosphate) and ryanodine receptor pathways that raise intracellular Ca^{2+} concentration (144). We emphasize here that under hypoxic conditions, ETA activation can increase PASMC intracellular Ca^{2+} concentration via both external and internal stores of Ca^{2+}, in addition to modulating membrane potential via KATP channels. Taken together, these studies suggest that ET signaling potentiates the function HPV by priming the availability of Ca^{2+} ions. Additionally, it is plausible that ET signaling contributes to the generation and maintenance of phase 2 of HPV.

1.5 Major Themes

In this chapter, I have motivated the complexity of pulmonary air and blood flow distributions (V/Q matching) on the biophysics of oxygen uptake, outlined the major phenotypes of HPV, and reviewed the landmark observations that have advanced our understanding of HPV and current controversies regarding the cellular and molecular basis of this physiological mechanism. The defining challenge of cellular and molecular investigations has been to determine if a given protein and/or biomolecular complex is indeed a key mediator of the mechanism, or does it only modulate pulmonary vasomotor tone. Much of the contention within the field can be ascribed to one investigator producing evidence that a pathway could be a mediator, only for another to show contrasting evidence where the pathway can only modulate

HPV's response. There is a litany of factors on may consider when trying to resolve these disparate findings: the organism/species studied; the experimental preparation and variable(s) measured; pros and cons of genetic v/s pharmacological perturbations; and potentially many more. I call attention to the experimental preparation and variable(s) that are measured in studies of HPV's molecular mechanism. Remarkably, only a few studies investigating the molecular basis of HPV measure the distribution of blood flow within the lung. While the hypoxia-induced rise in PASMC Ca^{2+} concentration, constriction of pulmonary artery diameter, and increase in pulmonary arterial pressure are of indeed aspects of HPV, none of these measurements capture the essential physiology of HPV – to change the regional distribution of blood flow to match the distribution of airflow (oxygen in the airway). *The opportunity I take in this thesis is to advance the field by filling a fundamental gap in knowledge of how V/Q matching can optimize oxygenation due to HPV, and physiological or pathological disruptions of air or blood flow distribution.* I assert that the highest level of evidence to evaluate the contribution of a molecular entity to HPV is an experiment that measures pulmonary blood flow distribution. In such an experiment one can reasonably expect a pharmacological inhibitor or genetic knockout of the key effector mechanism of HPV to worsen V/Q matching. Similarly, we could also expect that inhibiting a modulating pathway that is NOT essential for HPV might alter the hypoxia-induced increase in pulmonary arterial pressure but leave the distribution of blood flow and V/Q ratios unaffected (reduce overall vasomotor tone, but HPV and V/Q matching would still be intact).

To circumvent the experimental challenges with measuring flow distribution and begin addressing this gap in the field, I use an integrative computational modeling approach to understand how HPV operates at the system level to maintain adequate oxygen uptake. My central hypotheses are: ***(1) regional regulation of blood flow distribution by HPV homogenizes***

regional alveolar-capillary oxygen flux; and (2) homogenization of regional alveolar-capillary oxygen flux maximizes the total delivery of oxygen into the bloodstream.

1.6 Aims of this Thesis

1.6.1 Specific Aim 1: Determine how V/Q ratios affects oxygen transport

In Chapter 2, I analyze a series of progressively more complicated models of pulmonary oxygen transport. The central question addressed by this study is "What V/Q ratio optimizes pulmonary oxygen uptake?" The results of our analysis conflict with the intuition that a V/Q ratio (of flow rates) equal to 1 maximizes oxygen uptake. We find that for all models, optimal oxygen uptake is typically associated with a V/Q ratio greater than 1. Moreover, we observe that oxygen uptake is not only dependent upon the V/Q ratio, but the absolute magnitude of air and blood flow.

1.6.2 Specific Aim 2: Determine how HPV regulates V/Q matching and oxygen transport

In Chapter 3, I develop a multi-scale multi-physics model of V/Q matching that consists of pulmonary vascular networks, airway mechanics and hemodynamics, oxygen transport, and an empirical model of HPV. This model is used to make functional predictions on how the mechanism of HPV alters the distribution of blood flow and oxygenation and test our central hypotheses.

1.6.3 Specific Aim 3: Determine how proposed mechanisms of HPV could redistribute blood flow in response to airway occlusions

In Chapter 4, I use the model developed in Chapter 3 as a platform to test how proposed mechanisms of HPV could affect the distribution of blood flow, V/Q ratios, and oxygen uptake

during the pathological case of an occluded or collapsed airway. Mechanisms tested include conducted vascular response originating at the alveolar-capillary boundary and transduced to the upstream arteries, and direct regional sensing by pulmonary resistance arteries. Simulations in this chapter further scrutinize our central hypotheses. Based on our results, we posit a hypothesis that HPV is mediated by a multi-checkpoint mechanism with multiple oxygen sensors distributed throughout the pulmonary vascular tissue.

Chapter 5 provides a summary of how HPV affects V/Q matching and oxygenation from a systems-engineering perspective. The implications for the findings presented in this thesis for understanding HPV and V/Q matching at the system-level are discussed, and recommendations for experiments to corroborate or disprove the results of the model simulations are proposed. Finally, an analysis of the additional unanswered questions related to how HPV affects V/Q matching and oxygenation, and areas of future research are considered.

Figure 1.1 ***Considering the scope of how blood flow distribution (V/Q matching) affects oxygen uptake in the pulmonary circulation.***

(A) Schematic of the simplest pulmonary vascular network - two pulmonary gas exchange units connected in parallel. q_T it the total blood flow through the network, q_1 and q_2 are the blood flows through the top and bottom gas exchange units, respectively. Motivating questions: What values for q_1 and q_2 maximize oxygen uptake? If q_1 is reduced by vasoconstriction and q_T is held constant so that q_2 increases, how does this affect the oxygen content of the pulmonary venous outflow? (B) Schematic of a pulmonary vascular network with 7 gas exchange units. Motivating question: How does vasoconstriction of the blood vessel (reduction in blood flow) marked by a red oval affect oxygenation of the pulmonary venous outflow?

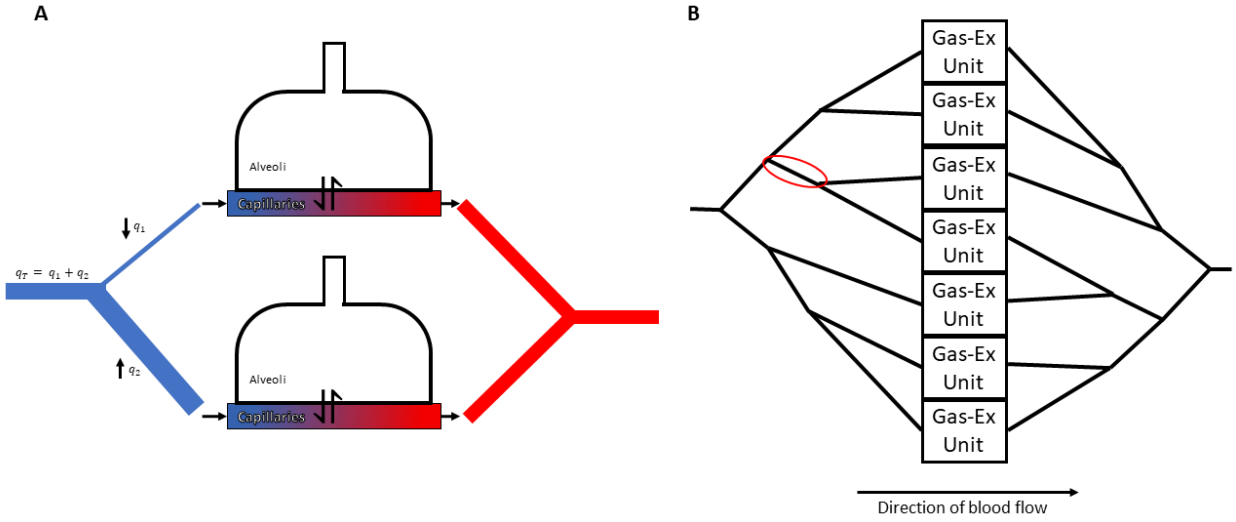
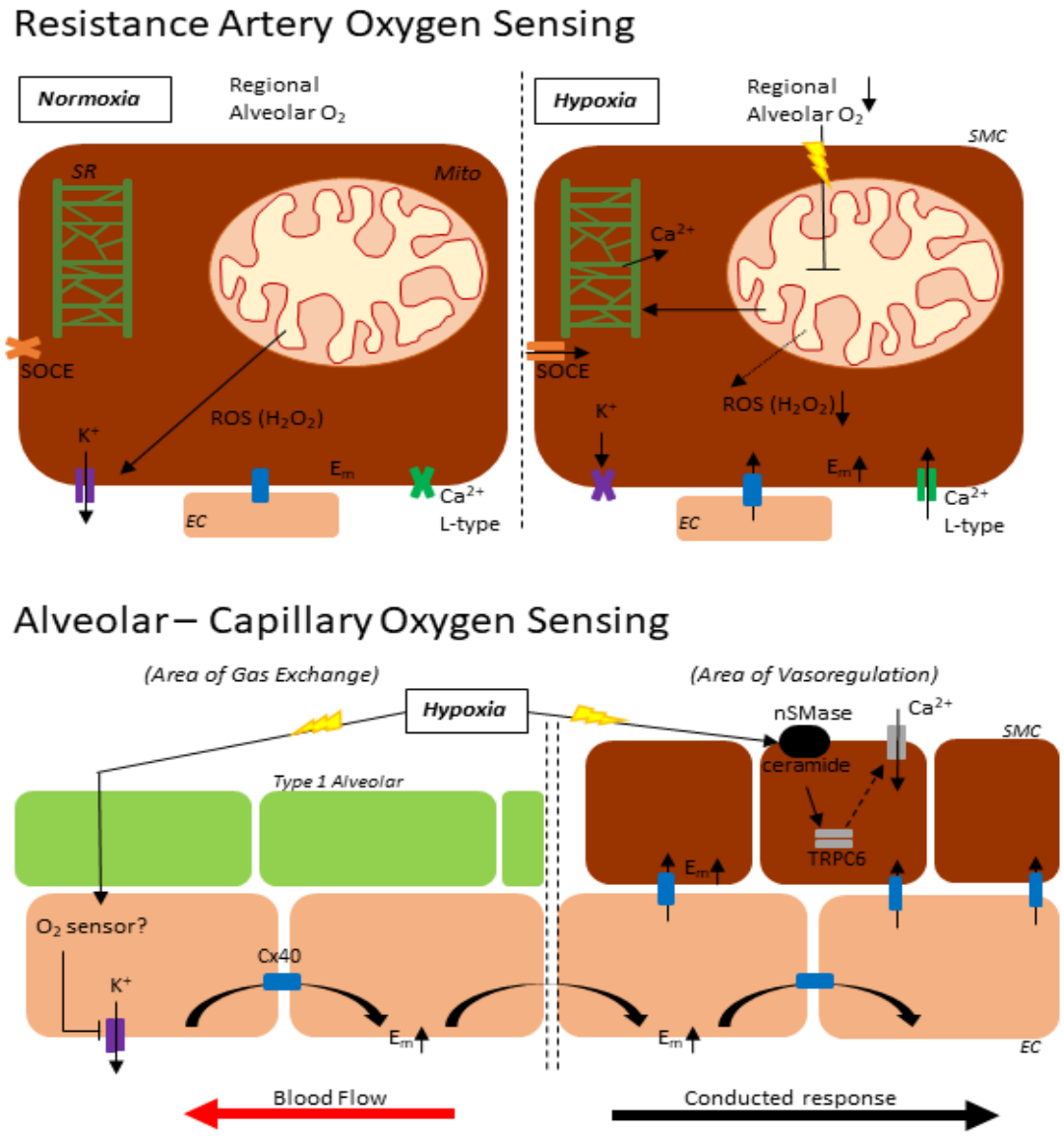


Figure 1.2 ***Oxygen content of pulmonary venous outflow.***

This is a conceptual way to delineate how oxygenation of the blood stream is achieved ventilation-perfusion matching. On the right is mathematical functions, and on the left is the equivalent in English sentences. $P_{ven,O2}$ *denotes the oxygen content of the pulmonary venous outflow.* VQ *denotes ventilation-perfusion matching -* x *is used indicate that* VQ *is a spatial probability distribution.* HPV *is the distribution of vascular tone from hypoxic pulmonary vasoconstriction.* $P_{alv,O2}$ *is the distribution of oxygen in the alveolar space.*

$P_{ven,O2}(VQ)$	Pulmonary venous oxygen content is a function of V/Q Matching
$VQ(x; \text{anatomy}, \text{gravity}, HPV)$	V/Q Matching (blood flow distribution) is a function of anatomy, gravity, and regulation from HPV
$HPV(x; P_{alv,O2}(x))$	HPV is a function of regional alveolar oxygen distribution
$P_{ven,O2}\left(VQ\left[x; HPV\left(x; P_{alv,O2}(x)\right)\right]\right)$	Pulmonary venous oxygen is a non-trivial function of regional alveolar oxygen distribution

Figure 1.3 ***Summary of major signaling pathways proposed to mediate hypoxic pulmonary vasoconstriction****. The signaling processes depicted here are not exhaustive, and there could be overlap of molecular events at distinct spatial locations. Ex: TRPC6 translocation could occur in PASMCs within a resistance artery. (Top) Resistance artery oxygen sensing. The mitochondrial ETC(s) are inhibited by hypoxia. Decreased production of ROS, such as H_2O_2, inhibits Kv currents and depolarizes the PASMC and activates L-type Ca^{2+} channels. A diversity of other mitochondrial process are augmented which activate the release of Ca2+ from the sarcoplasmic reticulum (SR) via IP3, ryanodine receptor, and/or store operated calcium entry (SOCE). (Bottom) Alveolar-capillary oxygen sensing. Hypoxia in the alveolar space stimulates a conducted vascular response that travels upstream in the oppositive direction of blood flow to depolarize PASMCs. Inhibition of Kv currents and activation of neutral sphingomyelinase (nSMase) and translocation of TRPC6 channels to PASMC membrane are potential mechanisms that operate at this spatial locus.*



Chapter 2 On the Physiological Relationship Between Ventilation, Perfusion, and Oxygen Transport

2.1 Acknowledgements

This chapter is undergoing peer-review to be published as an academic journal article. Special thank you to my co-authors David J. Pinsky and Daniel A. Beard.

2.2 Abstract

A major determinant of how the lungs deliver oxygen to the circulating blood is the regional matching of airflow and blood flow ¬- referred to as ventilation-perfusion (V/Q) matching. V/Q matching has great pathophysiological importance in the sequalae of conditions such as acute pulmonary embolism and atelectasis, yet how physiological V/Q matching is achieved remains poorly understood. This study aims to investigate how V and Q together govern oxygen transport, and theoretically determine the optimal ratio of air and blood flow to maximize oxygen uptake. To better understand how the ratio of flow rates affect oxygen uptake, we analyze a series of progressively more sophisticated models of V/Q matching in a single pulmonary gas exchange unit. Each model is analyzed using steady state analysis. Model predicted oxygen tensions are consistent with cardiac output and ventilation data measured in humans over a range of cardiovascular exercise intensities. The results of our analyses conflict with the intuition that a V/Q ratio equal to 1 maximizes oxygen uptake. We find that for all models, optimal oxygen uptake is typically associated with a V/Q ratio greater than 1. Moreover, we observe that oxygen uptake is not only dependent upon the V/Q ratio, but also on the absolute

magnitude of air and blood flow. When oxygen demand increases in exercise, air flow must increase more than cardiac output to maintain a given level of oxygenation in the systemic arterial blood. Thus, this analysis predicts the observed non-linear relationship between optimal air and blood flow rates that is observed experimentally.

2.3 Introduction

Efficient pulmonary gas exchange requires effective matching of airflow and blood flow—referred to as ventilation-perfusion (V/Q) matching. Conditions characterized by V/Q mismatching such as atelectasis or acute pulmonary embolism can inhibit gas exchange and lead to blood gas derangements (145). In clinical settings, V/Q matching can be measured either through the multiple inert gas elimination technique (MIGET) (146), or single photon emission computed tomography (SPECT) (147). The SPECT approach involves a patient inhaling and being infused with two distinct radiolabeled tracers. This enables a gamma camera to detect distinct ventilation and perfusion signals. V/Q scans obtained through SPECT allow physicians to identify regions where a patient's airway or vasculature have a disturbed pattern of flow or volume. A V/Q ratio equal to 1 is generally considered optimal (148). If we consider a single gas exchange unit, a larger V/Q ratio generally leads to greater uptake of oxygen but at the expense of potentially exhaling too much carbon dioxide. Similarly, a small V/Q ratio leads to decreased oxygen uptake at the expense of limiting the elimination of carbon dioxide (149). In the whole organ, V/Q ratios are distributed following a gravitational gradient, where larger V/Q ratios tend to be observed toward the top the organ and smaller V/Q ratios toward the bottom (3).

While both air and blood flow are volumetric flow rates (ex: L/min), clinical V/Q measurements do not reflect a direct ratio of flow values. For example, in the case of SPECT, a V/Q ratio image can be constructed based on the ratio of signal intensities associated with the

vascular and airway tracers (5). The assumption is that the relative amount of tracer delivered to a given region is proportional to the total flow to that region. However, application of this assumption invokes normalization and other post-processing steps (5). The result is a functional image that reflects regions of relatively high and relatively low V/Q ratios but is not a quantitative ratio of volumetric flows. Due to this implicit normalization step the "true" V/Q ratios could be obscured. Moreover, not only does the V/Q ratio potentially vary regionally, but the global (whole lung) V/Q ratio varies temporally during physiological challenges such as exercise. In exercise, cardiac output (CO) may increase by 4-fold compared to baseline conditions, while ventilation may increase by as much as 10-fold fold in healthy untrained subjects (151). The increase in CO in exercise is elicited in part by metabolism-mediated mechanisms to meet the increased oxygen consumption demands of systemic tissues (81,82,152). The increase in ventilation is elicited primarily by the respiratory chemoreflex, functioning to keep blood carbon dioxide and pH within a homeostatic range in response to increased rates of carbon dioxide generation (153). Regarding oxygen transport, as total CO increases during exercise, not only must the overall oxygen flux from air to blood increase, but also red cell transit times decrease with increasing blood flow. In other words, with increasing CO, commensurate increases in oxygen delivery from air to blood must be accomplished in less time. A situation in which a 1:1 ratio of blood to air flow were maintained in response to increases in oxygen demand during exercise would be expected to result in decreasing oxygenation of the systemic arterial blood. To maintain relatively constant oxygenation of the systemic arterial blood requires that air flow increases substantially more than blood flow does during exercise.

The goal of this study is to theoretically investigate the optimal ratio of air and blood flow in a single pulmonary gas exchange unit that maintains stable oxygenation of pulmonary

venous blood under different demand conditions. To this end, we analyze a sequence of progressively more sophisticated models of pulmonary oxygen transport: Model A is a simple linear compartmental formulation; Model B accounts for the nonlinear effect of hemoglobin on oxygen content; Model C accounts for the spatial profile of a pulmonary capillary; Model D accounts for both hemoglobin and spatial transport; and Model E and F both expand upon Model B and D respectively by accounting for the complete circulatory path and consumption of oxygen by systemic tissues. Each model is analyzed by determining the steady state oxygen tension of the alveolar space and pulmonary venous outflow. Our analysis reveals that oxygenation of the bloodstream is a non-linear function of air and blood flow, and our model-predicted relationships are consistent with published human cardiac output and ventilation data measured over a range of cardiovascular exercise intensities. Each of these models predict that oxygen uptake is not only dependent upon the ratio or air and blood flow, but the magnitude of air and blood flow. As observed experimentally, when oxygen demand increases in exercise, air flow must increase more than cardiac output to maintain a given level of oxygenation in the systemic arterial blood.

The major finding of this study is that the observed nonlinear relationship between whole-body ventilation and cardiac output emerges to maintain adequate arterial blood oxygenation during changes in whole-body oxygen demand. While it is well understood that ventilation at the whole-organ level increases during exercise to maintain blood carbon dioxide and pH levels, this ventilatory increase is also necessary to adequately oxygenate the bloodstream. Visualizations of steady state vascular and alveolar oxygen tension as functions of airflow and blood flow provide quantitative illustrations of how air flow and blood flow affect the transport of oxygen into the blood stream and how V and Q vary under physiological

conditions. Moreover, by simulating the behavior of a series of models of increasing complexity, the dependencies of pulmonary oxygen transport dynamics on nonlinear and spatially distributed flows are illustrated.

2.4 Methods

Our computational work has been implemented in MATLAB and the corresponding codes have been made available in the GitHub repository [https://github.com/beards-lab/simple-VQ-matching-O2-transport]. The following subsections explain how we:

- Process cardiopulmonary exercise testing (CPET) data from the literature
- Apply six increasingly complex models of pulmonary oxygen transport
- Use steady state analysis to find the steady state levels of oxygen tension in the alveolar and vascular space
- Identify the model based on fitting data from CPET data from the literature

2.4.1 Cardiac output, ventilation, and whole-body oxygen transport in exercise

To parameterize relationships between whole-body oxygen consumption, cardiac output, and ventilation during voluntary exercise, data were obtained from the prior literature. O'Donnell et al (151) report measurements on ventilation and oxyhemoglobin saturation as a function of work rate during voluntary upright bicycle exercise in human subjects (Figure 8BE of (151)). Data were reported for patients with pulmonary arterial hypertension and healthy controls. For the healthy controls, oxyhemoglobin saturation remained effectively unchanged (approximately 98% oxyhemoglobin saturation, corresponding to 125 mmHg oxygen tension by inverting the Hill function) over the observed range of exercise levels while ventilation increased as work rate increased. Figure 2.1D plots average data on whole-body ventilation (V) versus cardiac output

(Q). The figure also plots the line V = Q (dashed line) for comparison, illustrating how the difference between V and Q increases with increasing exercise level and oxygen demand. In the analysis that follows model predictions are compared to these data.

A relationship between whole-body oxygen demand (V_{O2}) and the rate of work performed is constructed from the data of Riley et al. (154), where they measured V_{O2} as a function work rate in human subjects performing cycle ergometry exercise. Data from this study is plotted in Figure 1B, illustrating a linear relationship between V_{O2} and work (W) in these subjects. The fit to this relationship illustrated by the solid line in the figure,

$$V_{O2} = aW + b, \qquad \text{Eqn. (1)}$$

is associated with regression coefficients $a = 7.5 \times 10^{-3}$ L/(min·watt) and $b = 0.65$ L/min.

The physiological relationship between cardiac output and oxygen demand is obtained based on the observation of Stringer et al. that that the arteriovenous oxygen difference ($C_A - C_V$) increases linearly with the fraction of maximum oxygen consumption rate ($\%V_{O2,Max}$) (155) and from Fick's law,

$$Q(C_A - C_V) = V_{O2}, \qquad \text{Eqn. (2)}$$

where Q is cardiac output (L/min), C_A is the arterial oxygen content (ml/100 ml), C_V is the venous oxygen content (ml/100 ml), and V_{O2} is the oxygen consumption rate (L/min). Substituting the liner relationship between ($C_A - C_V$) and V_{O2} we obtain

$$Q\left(c\frac{100 \times V_{O2}}{V_{O2,Max}} + d\right) = V_{O2}, \qquad \text{Eqn. (3)}$$

where $c = 0.10$ and $d = 5.72$ are the regression coefficients reported by Stringer et al. This relationship is illustrated in Figure 2.1A. Substituting Equation (1) into Equation (3), we obtain the following relationship between cardiac output and work:

$$Q = \frac{V_{O2,Max}(aW + b)}{100 \times (acW + cbad + V_{O2,Max}d)} \quad \text{Eqn. (4)}$$

The predicted relationships between cardiac output and V_{O2} (from Equation. (3)) and between cardiac output and work (Equation (4)) are plotted in panels A and C of Figure 2.1. Panel C shows that for an individual with a $V_{O2,Max}$ of 4.5 L/min, cardiac output varies from 5 L/min at baseline to 20 L/min at a maximal exercise state.

2.4.2 Oxygen transport models

Model A– Compartmental mass transport

The simplest manner to represent oxygen transport in the pulmonary circulation is a linear two-compartmental formulation in which a single alveolar compartment interacts with a single vascular compartment. The governing equations for this formulation are

$$\frac{dP_{alv}}{dt} = \frac{V(P_{air} - P_{alv}) - D(P_{alv} - P_{vasc})}{V_{alv}}, \text{and}$$

$$\frac{dP_{vasc}}{dt} = \frac{Q(P_{in} - P_{vasc}) + D(P_{alv} - P_{vasc})}{V_{vasc}}, \quad \text{Eqn. (5)}$$

where P_{alv} is the alveolar oxygen tension, P_{vasc} is the vascular oxygen tension, P_{air} is the oxygen tension in the ambient air, P_{in} is the oxygen tension of the deoxygenated blood entering the pulmonary circulation, V is the air flow, Q is the blood flow, D is the apparent diffusivity parameter, V_{alv} is the volume of the alveolar compartment, and V_{vasc} is the vascular compartment.

Model B – Oxygen-hemoglobin binding

Model A is extended to account for nonlinear oxygen-hemoglobin binding using a representation of the relationship between oxygen concentration and partial pressure in the blood:

$$C_{vasc} = \alpha P_{vasc} + C_{Hb} \frac{P_{vasc}^n}{P_{vasc}^n + P_{50}^n}, \quad \text{Eqn. (6)}$$

where C_{vasc} is the vascular oxygen concentration (mM), α is the solubility of oxygen in plasma/water, C_{Hb} is the concentration of hemoglobin binding sites, P_{50} is the oxygen tension where half of the oxyhemoglobin binding sites are occupied, and n is the Hill coefficient. The αP_{vasc} term represents freely dissolved oxygen, and the second term represents the oxygen bound to hemoglobin. The relationship between alveolar oxygen concentration and tension is given by

$$P_{alv} = \beta C_{alv}, \quad \text{Eqn. (7)}$$

where C_{alv} is the concentration of oxygen in the alveolar compartment, and β is the solubility of oxygen in the air. The governing differential equations for this model are thus given by:

$$\frac{dP_{alv}}{dt} = \frac{V(P_{air} - P_{alv}) - \alpha\beta D(P_{alv} - P_{vasc})}{V_{alv}}$$

$$\frac{dC_{vasc}}{dt} = \frac{Q(C_{in} - C_{vasc}) + \alpha D(P_{alv} - P_{vasc})}{V_{vasc}}. \quad \text{Eqn. (8)}$$

Model C – Spatially distributed vascular transport

A spatially distributed model is formulated by representing transport along a pulmonary capillary. Here, a one-dimensional formulation is employed where $P_{vasc}(t, x)$ is a function of time and *x*, the position along a capillary:

$$\frac{dP_{alv}}{dt} = \frac{V(P_{air} - P_{alv}) - D(P_{alv} - \langle P_{vasc} \rangle)}{V_{alv}}$$

$$\frac{\partial P_{vasc}}{\partial t} + \frac{Ql}{V_{vasc}} \frac{\partial P_{vasc}}{\partial x} = \frac{D}{V_{vasc}} (P_{alv} - P_{vasc}), \qquad \text{Eqn. (9)}$$

where l is the length of the capillary, and $\langle P_{vasc} \rangle(t) = \frac{1}{l} \int P_{vasc}(t, x) dx$ is the average oxygen tension across the capillary tube. The boundary condition $P_{vasc}(t, 0) = P_{in}$ is set as the pulmonary arterial oxygen tension.

Model D – Oxygen-hemoglobin binding and spatially distributed transport

This model integrates nonlinear oxygen-hemoglobin banding with spatially distributed transport. The governing differential equations are given by

$$\frac{dP_{alv}}{dt} = \frac{V(P_{air} - P_{alv}) - \alpha\beta D(P_{alv} - \langle P_{vasc} \rangle)}{V_{alv}}$$

$$\frac{\partial C_{vasc}}{\partial t} + \frac{Ql}{V_{vasc}} \frac{\partial C_{vasc}}{\partial x} = \frac{\alpha D}{V_{vasc}} (P_{alv} - P_{vasc}). \qquad \text{Eqn. (10)}$$

Like Model B, oxygen content is represented by constitutive relationships of Equation (6) and (7). The boundary condition $C_{vasc}(t, 0) = C_{in}$ represents oxygen content in the pulmonary arterial blood, where C_{in} is related to P_{in} by equation (6).

Model E – Oxygen-hemoglobin binding and oxygen consumption

In Models A-D it assumed that the oxygenation of blood entering the lung from the pulmonary artery is constant. Models E and F relax this assumption by assuming a relationship between total flow (Q) and whole-body oxygen consumption (V_{O2}), as illustrated in Figure 1, and captured by Equation (3). Invoking mass-balance via Fick's law, $Q(C_{vasc} - C_{in}) = V_{O2}$, and

substituting Equation (3), we obtain the following expression for C_{in}, the pulmonary arterial oxygen content, as a function of Q:

$$C_{in} = C_{vasc} - V_{O2}/Q. \quad \text{Eqn. (11)}$$

Substituting this expression into Equations (8) yields the governing differential equations for Model E:

$$\frac{dP_{alv}}{dt} = \frac{V(P_{air} - P_{alv}) - \alpha\beta D(P_{alv} - P_{vasc})}{V_{alv}}$$

$$\frac{dC_{vasc}}{dt} = \frac{-V_{O2} + \alpha D(P_{alv} - P_{vasc})}{V_{vasc}}. \quad \text{Eqn. (12)}$$

Like Models B and D, oxygen content is represented by constitutive relationships defined by equations (6) and (7). Equation (3) is used to determine V_{O2} from Q, and a conversion factor is used to recast units from L/min to mmol/min

Model F – Oxygen-hemoglobin binding, spatially distributed transport, and oxygen consumption

The governing differential equations for Model F are the same as Model D (given by equation (10)) with the only difference is the boundary condition for the oxygen concentration flowing into the lungs is

$$C_{vasc}(t, 0) = C_{vasc}(t, l) - \frac{V_{O2}}{Q}. \quad \text{Eqn. (13)}$$

Again, oxygen content is represented by constitutive relationships defined by equations (6) and (7), and equation (3) is used to determine V_{O2} from Q, and a conversion factor is used to recast units from L/min to mmol/min

2.4.3 Steady state alveolar and vascular oxygen tension

The steady-state behavior of each model is simulated by setting time derivatives to zero and determining the steady-state values of oxygen in the alveolar and vascular compartments. Details of these derivations are reported in Appendix A.

2.4.4 Model parameterization

Table 2.1 contains a list of all model variables, fixed parameters, and adjustable parameters. The only adjustable parameter in each model is the apparent diffusivity parameter, D. We fit each model to the data from O'Donnell et al by estimating D with the Nelder-Mead algorithm implemented via MATLAB's *fminsearch* function. At given cardiac output measurement from O'Donnell et al denoted as Q_i, we use our models to calculate the corresponding ventilation ($V_{i,pred}$) needed to ensure the vascular oxygen tension is at the physiological target of $P_T = 125$ mmHg. Similarly for ventilation measurements denoted as V_i, we calculate the corresponding blood flow ($Q_{i,pred}$) needed to ensure $P_T = 125$ mmHg. This optimization scheme seeks to minimize the objective function

$$J_V = \sum_i^N \left[V_i - V_{i,pred}\right]^2 \qquad \text{Eqn. (14)}$$

$$J_Q = \sum_i^N \left[Q_i - Q_{i,pred}\right]^2$$

$$J = J_V + J_Q.$$

The overall cost, J, is the sum of error in model predicted $Q_{i,pred}$ and $V_{i,pred}$ – where J_v and J_Q are summed with equal weights, assuming that uncertainties in the measures of V and Q are

roughly similar. Table 2.2 reports the minimum value of J for each model and the corresponding value of D.

2.5 Results

We calculate and plot the steady state oxygen tension in alveolar, vascular, and alveolar-vascular difference in oxygen tensions over a wide range of blood and air flows. These relationships are visualized in Figures 2.4 (open-loop models) and 2.5 (closed-loop models) as contour plots. Each line on alveolar and vascular panels is an isocline (level curve) that represents ventilation (V) as a function perfusion (Q) to maintain a fixed amount of oxygen in that compartment. For the alveolar-vascular difference in oxygen tension panels, these isoclines represent a fixed driving force underlying oxygen transport into the bloodstream. Each subpanel of these Figures has a dashed-black line representing the identity line, which can also be interpreted as where air flow is equal to blood flow, or a V/Q ratio of 1.

2.5.1 Sensitivity of model behavior to apparent diffusion parameter

To determine how the adjustable apparent diffusivity parameter affects model behavior we compute the contour plots in Figures 2.4 and 2.5 using a range of values for D. The results are visualized as animated .gif images to show how increasing D affects the oxygen tension isoclines (can be found in the github repository). For each model we observe that increasing D has a similar effect of linearizing the alveolar and oxygen tension isoclines. Moreover, the alveolar-vascular oxygen tension difference starts to vanish toward zero as D approaches larger and larger values. For model E, increasing D has zero effect on the alveolar oxygen tension isoclines – this is perhaps obvious as Equation (A10) does not depend on D. However, for the vascular and alveolar-vascular oxygen difference isoclines, increasing D produces a rightward

shift of every isocline. In other words, increasing the diffusivity decreases oxygenation's dependence on blood flow. Animated. gif's for model F have been excluded, as they are extremely computationally intensive to generate and model F has a similar dependence on the parameter D as model E.

The value of D used in generating the plots in Figures 4 and 5 is reported in Table 2. In Figure 6, we plot the cost function of Equation (14) as a function of the optimized diffusivity parameter, D. Three of the six models (A, C, E) we fit to the data do not have a well-defined minimum and monotonically decrease as the value of D is increased. For these models, increasing D toward infinity has diminishing returns on aligning with the data. In other words, the models best match the data in the flow-limited regime. Since at extremely large values of D the isoclines are linearized, we choose values of D at the "corner" of diminishing returns on model cost, which are also plotted on Figure 2.6.

2.5.2 Vascular oxygen tension

For a given vascular oxygen tension isocline in Figure 2.4 or 2.5, a given increase in blood flow requires a greater increase in ventilation to maintain constant oxygenation of the pulmonary venous blood. In other words, for all six of the models analyzed every vascular oxygen tension isocline is concave-up. This behavior is consistent across the four open-loop (A-D) and two closed-loop (E-F) models. For Models A and C, these isoclines appear nearly linear due to the relatively large value of the apparent diffusivity parameter (D) used. We use the 125-mm Hg isocline as a theoretical physiological value that the system aims to maintains, which should ideally cross through the data points from O'Donnell et al. depicted on these panels. Due to oxygen-hemoglobin binding the increase in oxygen content in the blood above 100 mmHg is minimal.

For models A and E, we can derive closed form expressions of these isolines. Using the analytic expression of steady state alveolar and vascular oxygen tension for model A in equations (A2) we find

$$V = \frac{P_{in}(P^*_{alv} - P^*_{vasc})Q}{P_{air}P^*_{vasc}D - (P^*_{alv}P_{in} + P_{air}P^*_{alv} - P_{air}P^*_{vasc})Q}, \quad \text{Eqn. (15)}$$

where P^*_{alv} and P^*_{vasc} are the steady state alveolar and vascular oxygen tensions respectively. We can perform a similar derivation for model E using equations (A10) to derive

$$V = \frac{\alpha\beta D V_{O2}}{\alpha P_{air}D - \alpha P^*_{vasc}D - V_{O2}}. \quad \text{Eqn. (16)}$$

Note that data from exercise studies show that V_{O2} is proportional to Q. Both equations (15) and (16) represent ventilation (V) as a function of perfusion (Q) and can be interpreted as curves that define optimal V/Q matching to ensure a specified oxygen tension in the pulmonary venous outflow.

2.5.3 Alveolar oxygen tension

One difference between the closed-loop models and the open-loop models is illustrated in the alveolar oxygen tension contour plots. Isoclines for alveolar oxygen tension in open-loop models (Figure 2.4) tend to have a saturating behavior as a blood flow increases (concave-down and bounded by $P_{air} = 150$ mmHg), whereas for closed-loop models (Figure 2.5) these isoclines are more like the contours seen in the vascular panels. For Model F, these isoclines are somewhat of a hybrid of Model E and the open-loop models as at a certain threshold the concave-up behavior ends the isoclines plateaus to no longer to depend on air flow.

2.5.4 Alveolar-vascular oxygen tension difference

Another important difference between the closed- (A-D) and open-loop (E-F) models is the alveolar-vascular oxygen tension difference. For Model A, this plot is symmetric across the identity line. For Models B and C, relative to Model A this relationship is subtly shifted down and to the right. For Model D, an interesting non-linearity emerges at V/Q ratios less than 1 and at small magnitudes. This non-linearity can be understood by observing the corresponding vascular and alveolar oxygen tension plots for Model D. For large V/Q ratios (due to large V rather than small Q), there is a region where the vascular and alveolar oxygen tensions are equal – in other words the oxygen difference is 0. This implies that at these V/Q ratios the oxygen in the bloodstream perfectly equilibrates with the oxygen in the alveolar space. The bulge seen at low V/Q ratios on the alveolar-vascular oxygen tension difference plot reflects the complexity of both air and blood flow limitation on the transport of oxygen into the bloodstream.

For Model E, one can appreciate that there is no dependence on air flow and oxygen uptake is entirely defined by blood flow. This can be explained by our assumption of oxygen consumption being dependent upon blood flow via Fick's law. For a fixed air flow, increasing blood flow increases the alveolar-vascular oxygen difference in a manner proportional to the reciprocal of blood flow. In other words, this panel is a demonstration of the assumed proportionality between blood flow and oxygen consumption. For Model F, we can see that there is a similar non-linearity of Model D at V/Q ratios less than 1 and at low magnitudes, however the bulge is sharper compared to Model D.

2.6 Discussion

2.6.1 The optimal V/Q ratio for a single pulmonary gas exchange unit

A major conclusion from this study is that there is a spectrum of air flows and bloods flows that lead to the same level of oxygenation of the blood stream. At the whole organ level,

data from a cardiopulmonary exercise test (CPET) study illustrates how ventilation increases from 10 L/min to 68 L/min from rest to the maximum measured workload, while cardiac output increases from 7 L/min to 17 L/s. These data indicate that whole-lung ventilation and cardiac output and are not matched one to one. The model-predicted vascular oxygen tension as functions of air and blood flow (Figures 4 and 5) further illustrates this concept as each isocline has a concave-up behavior, rather than aligning with the identity line. Each of the models considered in this study predict that a V/Q ratio greater than one is generally requires to maintain physiological oxygenation of the blood exiting the lung. There is no single optimal V/Q ratio. Rather the optimal ratio increases with increasing V and Q.

Simple closed-form expression for the vascular oxygen tension isoclines for Models A and E are obtained in Equations (15) and (16). These expressions suggest that optimal oxygenation of the bloodstream follows the relationship

$$V = \frac{AQ}{B - CQ}, \qquad \text{Eqn. (17)}$$

where $A, B,$ and C are arbitrary positive real-valued constants. Equation (17) has a vertical asymptote at $Q = B/C$, however this asymptote occurs at blood flows that are profoundly large and would be impossible to achieve under realistic conditions. While the whole-body ventilatory increase during exercise is regulated through plasma pCO2 and pH (153), equation (17) demonstrates that the resulting observed relationship between V and Q is also necessary to maintain stable oxygenation.

While there is some limited evidence that airflow can be redistributed via hypocapnic bronchoconstriction (156,157), it is broadly accepted that the regional distribution of airflow is not physiologically regulated (158,159). It follows that regulation of regional V/Q matching must

be accomplished by redistributing blood flow. Physiological regulatory mechanisms, such as hypoxic pulmonary vasoconstriction, may operate to keep the system within a local neighborhood of the curve defined by equation (17). Deviations from this curve (V/Q mismatching) could lead to blood gas derangements and thus be considered pathological. The vascular panel of Figures 4 for Model D shows that the 125-mmHg isocline locally appears to be linear near the identity line at values of air and blood flow that reflect a person at rest; these values only diverge from the identity at air and blood flows that reflect some level of cardiovascular exercise. We discuss below how the scale of a gas exchange unit (the whole organ v/s a lobe v/s as single acini) affect the interpretation of the theory derived in this study.

2.6.2 Open v/s closed loop system

Across both open-loop and closed-loop models analyzed in this study there is a consistent pattern of behavior in how V/Q matching affects oxygenation of the vascular compartment. All models predict a concave-up relationship, where to maintain a given amount of oxygen in the pulmonary venous outflow, airflow needs to be increased more than blood flow. However, accounting for oxygen consumption in the closed-loop models does alter the alveolar and alveolar-vascular oxygen difference contour plots. The alveolar-vascular oxygen difference represents the driving force underlying transport oxygen into the blood stream. Physiologically, this implies that oxygen consumption by systemic tissues influences the alveolar-(systemic) arterial oxygen difference – a variable commonly measured and used in clinical settings to diagnoses the cause of hypoxemia (160). Large alveolar-arterial (A-a) oxygen gradients tend to correlate with gas exchange problems such as decreased carbon monoxide diffusion capacity (DLCO) or right to left shunting of blood flow. However, these models complicate our understanding of this relationship in that the measuring the magnitude of air and blood flow to

the entire lung or a region (such as an anatomical lobe) could provide a more nuanced understanding of how a large A-a oxygen gradient is due to pathology within the lung, or within systemic tissues. Additionally, many models of pulmonary gas exchange assume that gas tensions in the alveolar and vascular spaces are perfectly equilibrated which justifies the use of a single compartment in these models [REF]. However, by using two-compartments our analysis shows that equilibration of the oxygen in alveolar and vascular spaces only occurs at extremely large V/Q ratios, as shown in the alveolar-vascular oxygen difference only being near zero toward the west and northwest portion of the contour plots. Thus, the conditions necessary for the gas tensions in the alveolar and vascular spaces to be perfectly equilibrated are potentially an area of further research.

The differences between the open- and closed-loop models analyzed in this study might also help interpret results from different experimental systems to study V/Q matching and may help reconcile conflicting perspectives in the literature. For example, models A-D would be most appropriate to compare to open-loop isolated-ventilated-perfusion lung preparations, and models E and F would be most appropriate to compare to *in vivo* physiology studies.

2.6.3 Potentially limiting model assumptions

Models D and F best fit the observed data likely because the transport process synergistically depends on the spatial distribution of oxygenation and oxygen-hemoglobin binding along the pulmonary capillary. Based on Figure 2.6 and Table 2.2's demonstration that Model D has the smallest least squares cost of all six models, one could broadly conclude that Model D is the best representative of the physiological system. However, since Model F more realistically represents the dependence of pulmonary arterial oxygen content on oxygen demand in exercise, Model F should be interpreted as better capturing gas exchange in exercise.

Regardless, neither model perfectly captures the observed data, and both invoke a set of simplifying assumptions.

One common assumption across all the models analyzed in this study is that a single pulmonary gas exchange unit represents the entire lung. True lungs operate as a distributed network of numerous gas exchange units operating in parallel. Considering a pulmonary acinus as the functional pulmonary gas exchange unit, the ratio of air and blood flow through this unit is what ultimately affects the transport of oxygen into the bloodstream. The models presented here can be thought of as just as well representing a sub-section of the lung as representing the whole organ. Thus, we expect that the predicted trends are valid not just at the whole-organ level, but also regionally. However, it is possible that the optimal V/Q ratio at the regional scale may differ than the comparison of whole lung ventilation and cardiac output. If we extrapolate the predictions of model D and F to this regional scale, then the emergent non-linear behavior of the alveolar-vascular oxygen difference might be of major physiological significance (ex: nonperfused pulmonary capillaries become perfused when the distribution of blood flow is altered). However, without direct measurements of air and blood at this scale this remains a model prediction in need of experimental corroboration/refutation. By the nature of our steady state analysis, the actual length (l) of the vessels used in the spatially distributed models is arbitrary and can be lumped into the apparent diffusivity parameter, D. Yet true lungs are never actually at steady state, and thus the length of a capillary or capillary bed (and by extension the scale/size of the gas exchange unit) is likely an important factor when considering settings where kinetics and dynamics dominate the system. Non-perfused capillaries becoming perfused is a salient example, as in humans at rest only a fraction of pulmonary capillaries are actively perfused; during exercise more capillaries are recruited via increased perfusion pressure and/or

cardiac output (161–163). Recruitment could potentially lead to more nuances in the optimal V/Q ratio at regional scale to ensure adequate oxygenation.

The major limitation for open-loop models A-D is the assumption of a fixed oxygen tension entering the pulmonary circulation (P_{in}), as this assumption implies that oxygen consumption (V_{O2}) and cardiac output (Q) vary in a simple proportion to maintain a constant oxygen tension flowing into the pulmonary circulation, a simplification that is not accurate (164). Metabolism-perfusion matching in the periphery is the parallel physiological function that ventilation-perfusion matching in the lungs supports. Models E and F account for the observed whole-body relationship between peripheral oxygen consumption and cardiac output. At the whole-body level the relationship between cardiac output and peripheral demand is mediated through autonomic mechanisms including the central and peripheral chemo- and baroreflexes. At the local level, metabolism-mediated vasodilating factors are released in response to increasing oxygen demand (165,166). The largest limitation to our representation of the relationship between Q and VO2 is that it does not account for any decoupling of oxygen consumption and perfusion that could plausibly occur in a disease state. Moreover, our formulation does not account for transient dynamic changes that occur in response to a change in demand. Thus, Models E and F are only appropriate for analyzing the steady state.

2.6.4 Regional regulation of pulmonary perfusion and V/Q matching

The concept of V/Q matching broadly refers to the distribution of air flow, blood flow, and V/Q ratios throughout the organ. It follows that the distribution of V/Q ratios are a critical determinant of the lung's abilities to oxygenate the blood stream. The fractal-like nature of the airway and pulmonary vascular tree produce heterogenous distributions of air flow and blood flow respectively (167). Despite these sources of heterogeneity, air flow and blood flow are

generally well matched (7), and V/Q mismatching is recognized as a pathological state (168). Numerous studies investigating the factors that influence and regulate the distribution of V/Q ratios have revealed that the interwoven anatomy of the airways and vascular tree, gravity and posture, and physiological regulatory mechanisms, such as hypoxic pulmonary vasoconstriction, all contribute to the distribution of V/Q ratios. For example, Glenny et al measured the distribution of regional perfusion in swine subjects in response to perturbations in gravity in parabolic flight (169). They showed that while gravity and anatomical structure contribute to the distribution of pulmonary blood flow, the anatomical structure is a primary determinant of regional perfusion.

The simple models analyzed in the present study do not represent mechanisms that may be responsible for achieving the predicted physiological oxygenation of pulmonary venous blood. However, previous work from our group has modeled pulmonary oxygen transport through a distributed vascular network and included an empirical mechanism for hypoxic pulmonary vasoconstriction (170). In contrast to the more standard interpretation that hypoxic pulmonary vasoconstriction does not play a physiological role (171), simulations with our model predict that hypoxic pulmonary vasoconstriction could significantly contribute to the resting distribution of V/Q ratios and oxygen uptake. Hypothetical regulatory mechanisms such as hypoxic pulmonary vasoconstriction potentially could function to govern regional pulmonary perfusion (and thus V/Q ratios) to be within a local neighborhood of the optimal curve predicted by the gas exchange models analyzed here.

2.6.5 Clinical considerations

Our model analysis predicts that the nonlinear concave-up relationship between V and Q that is observed at the whole-body level in exercise is operative at the regional level in the

heterogeneously ventilated and perfused lung. This prediction may potentially impact the interpretation of clinical regional V/Q imaging. Under physiological conditions we do not expect a simple linear proportional relationship between regional V and Q levels. However, the nonlinearity of this relationship may be clearly apparent only at extreme regional values of V and Q under basal conditions.

The models presented in this study could also be a biophysical basis for pharmacokinetic modeling to predict how the matching of air and blood flow affect an inhaled compound entering the blood stream, or how a substance is eliminated from the body by exhalation. The most immediate application could be for the administration of physiological gases such as supplemental oxygen, nitric oxide (NO), carbon monoxide (CO), or hydrogen sulfide (HS), however the mechanistic framework can also be expanded to model other inhaled drugs such as insulin, prostacyclin, β-agonists, etc.

2.6.6 Summary

In this study we sought to determine the optimal relationship between ventilation and perfusion to maintain physiological oxygen uptake. We analyzed a suite of progressively more complicated models of pulmonary oxygen transport. Our study reveals that when V/Q ratios are computed using true flow rates, a V/Q ratio equal to one does not necessarily maximize oxygen uptake. Model simulations suggest that there is a wide range of plausible values ventilation, perfusion, and corresponding V/Q ratios could take on to adequately oxygenate the bloodstream. The observed whole-body nonlinear relationship between V and Q (Figure 1) is required to maintain constant oxygenation of the blood (Figures 4 and 5). Moreover, the ventilatory increase observed during exercise to breathe off excess carbon dioxide serves a dual purpose of also maintaining oxygenation of the systemic arterial blood. This relationship is expected to reflect

the relationship between V and Q on a regional level in the heterogeneously perfused and ventilated lung in vivo.

Table 2.1 ***Model variables and parameters***

Variables				
Name	**Units**	**Interpretation**	**Reference**	**Value**
P_{alv}	mmHg	Alveolar oxygen tension	-	-
P_{vasc}	mmHg	Vascular oxygen tension	-	-
C_{vasc}	mM	Vascular oxygen concentration	-	-
V	L/min	Air flow	-	-
Q	L/min	Blood flow	-	-
Parameters				
Name	**Units**	**Interpretation**	**Reference**	**Value**
P_{air}	mmHg	Atmospheric oxygen tension	-	150
P_{in}	mmHg	Pulmonary arterial oxygen tension	-	45
α	mM/mmHg	Oxygen solubility in water	(172)	$1.3x10^{-3}$
β	mmHg/mM	Oxygen solubility in air	(172)	16.8
P_{50}	mmHg	Half-max hemoglobin saturation	(173)	30
n	Unitless	Hill exponent	(173)	2.7
C_{Hb}	mM	Concentration of oxy-hemoglobin binding sites	(174)	8.4
l	Cm	Length of capillary tube	-	1
$V_{O2,Max}$	L/min	Maximum oxygen consumption rate	(154)	4.5
D	ml/s	Apparent diffusivity	-	See Table 2.2

Table 2.2 ***Model optimization and optimal diffusivity parameter.*** *J denotes the final least squares cost (equation (14)), and D is the value of the apparent diffusivity parameter used to generate the plots in Figure 2.4 and 2.5.*

Model	***J***	***D***
A	5.03×10^3	500
B	989.47	2200
C	$4.15\text{x}10^3$	80
D	86.83	380
E	$1.19\text{x}10^3$	3400
F	663.41	536.36

Figure 2.1 ***Empirical conversion of work rate to the cardiac output.***

(A-C) The square points denote reference values for resting and exercising cardiac output for an average fit individual with $V_{O2,Max} = 4.5$ L/min. (A) Cardiac output as a function of percent of $V_{O2,Max}$ – corresponds to Equation (3) and the curve is derived from Stringer et al's observation of the arteriovenous oxygen difference having a linear relationship with $V_{O2,Max}$ (6). (B) Oxygen consumption rate (V_{O2}) as a function of work rate – corresponds to Equation (1). Discrete data points are from Riley et al (7). (C) Cardiac output as a function of work rate. Each curve uses a different value for $V_{O2,Max}$ to demonstrate how the choice of this free parameter affects the empirical relationship. (D) Ventilation versus cardiac output. Data points were originally reported in O'Donnell et al (5) as ventilation versus work rate. The values for measured work rate were converted to cardiac output using the relationship shown in panel C. The dashed line is the identity (x=y).

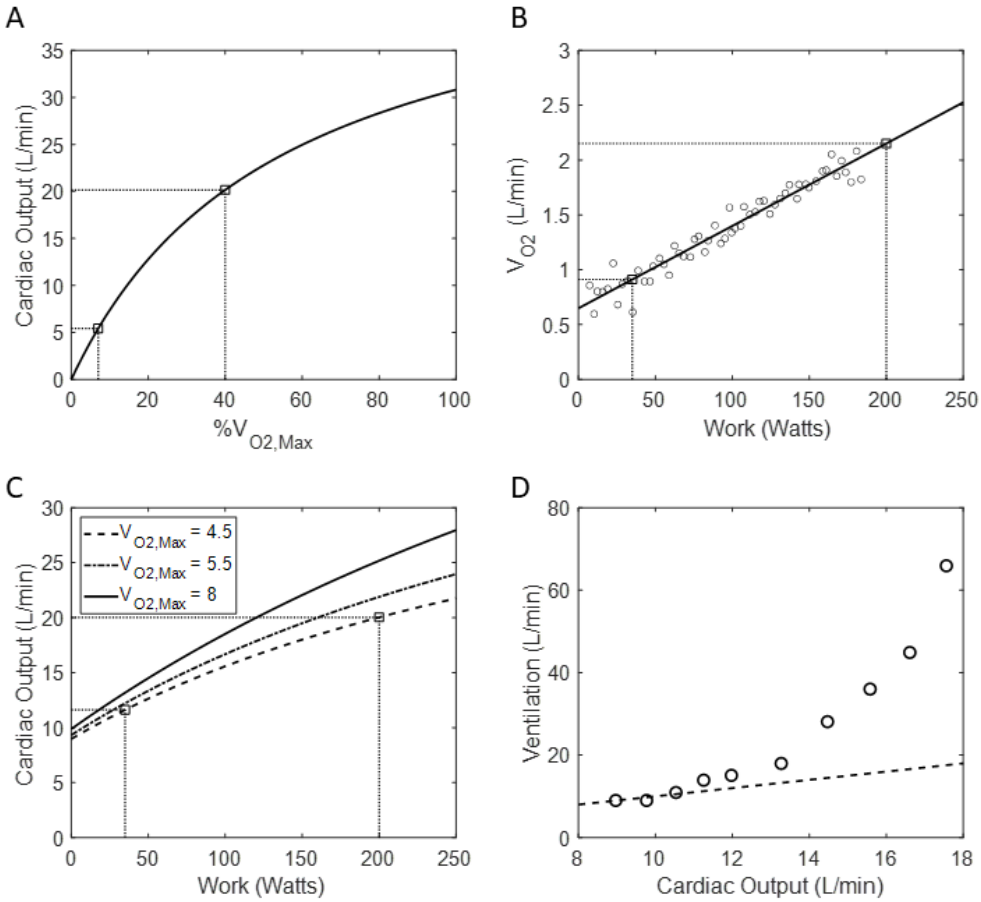


Figure 2.2 ***Schematics of four open-loop pulmonary oxygen transport models****. (A) Liner compartmental formulation where the vascular and alveolar vascular space are compartments. (B) Expands upon Model A by incorporating a solubility rule that accounts for the nonlinear effects of hemoglobin on oxygen solubility. (C) Expands upon Model A by accounting for the spatial profile of a pulmonary capillary. (D) Combines the complexities (hemoglobin and spatial transport) of Models B and C.*

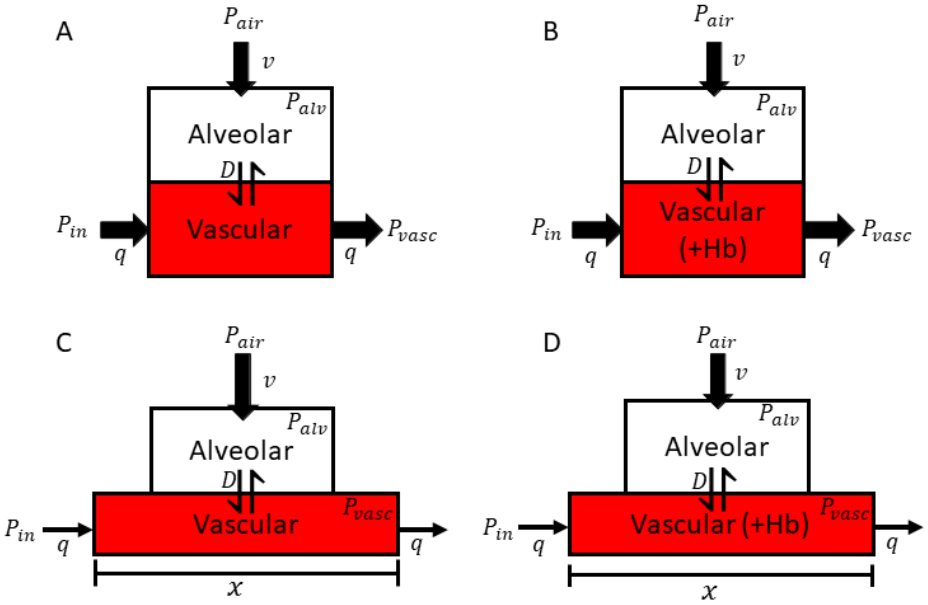


Figure 2.3 ***Schematics of two pulmonary closed-loop oxygen transport model.*** *(E) Compartmental formulation where oxygen enters the vascular space from the alveolar space and is consumed by the systemic tissues. Like Model B, this one also accounts for hemoglobin's effect on oxygen solubility (F). Expands upon Model E by accounting for the spatial profile of a pulmonary capillary. This model is closed-loop version of Model D.*

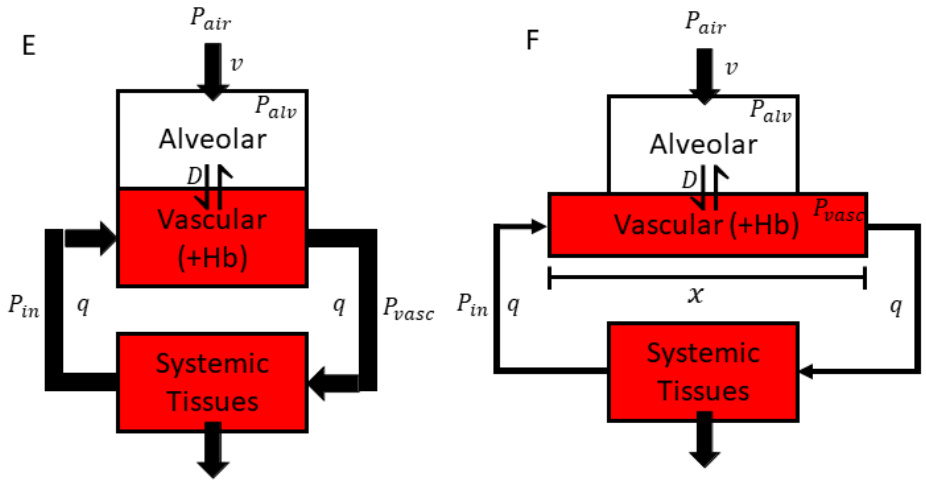


Figure 2.4 ***Contour plots for steady state oxygen tension in the alveolar space, vascular space, and the difference between them as a function of airflow and blood flow for Models A-D.*** *From left to right, the column corresponds to Model A-D. From top to bottom, the rows represent the oxygen tension of the alveolar space, vascular space, and alveolar-vascular difference. Each line is an isocline for a fixed amount of oxygen. The black circles on the vascular panels are the same data points shown in Figure 2.1D from O'Donnell et al. The solid black line on the vascular panels is the is 125 mmHg isocline – a physiological target value the body aims to maintain, and corresponds to the average value of the data from O'Donnell et al. The dashed black line is the identity line (y=x).*

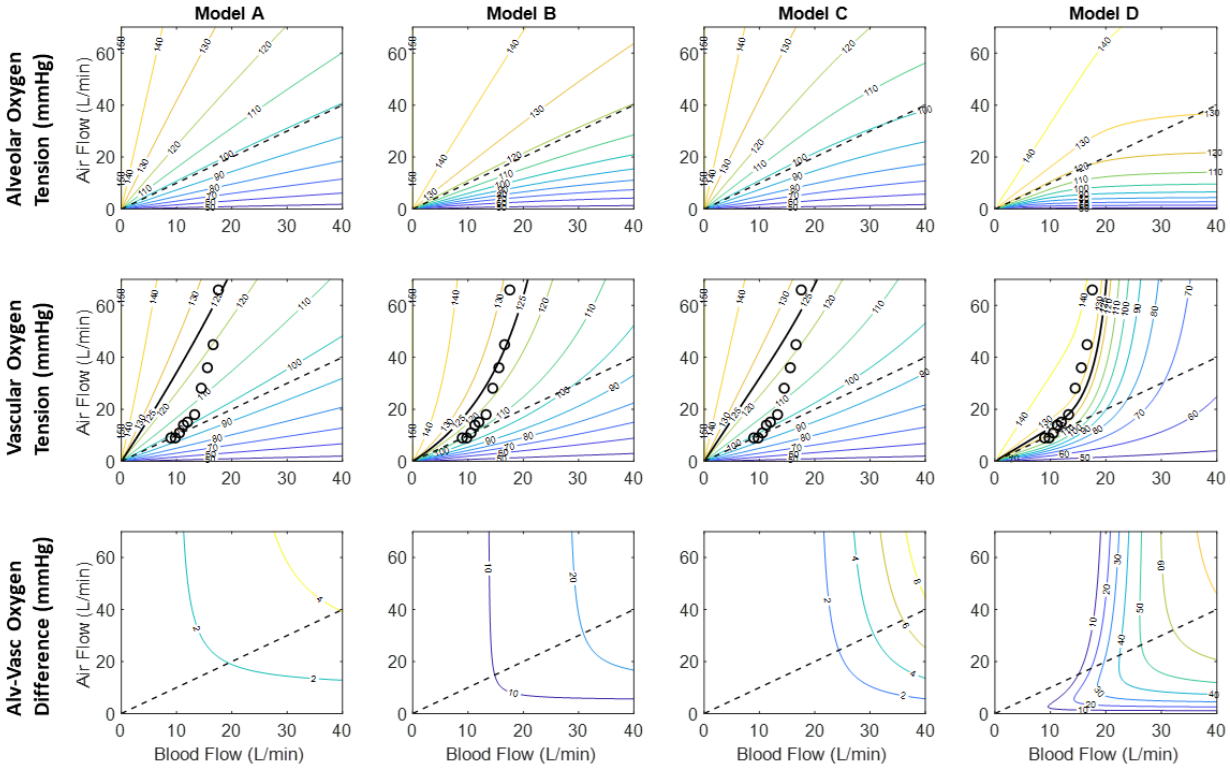


Figure 2.5: ***Contour plots for steady state oxygen tension in the alveolar space, vascular space, and the difference between them as a function of airflow and blood flow for Models E and F.*** *From left to right, the column corresponds to Models E and F. From top to bottom, the rows represent the oxygen tension of the alveolar space, vascular space, and alveolar-vascular difference. Each line is an isocline for a fixed amount of oxygen. The black circles on the vascular panels are the same data points shown in Figure 2.1D from O'Donnell et al. The solid black line on the vascular panels is the is 125 mmHg isocline – a physiological target value the body aims to maintain, and corresponds to the average value of the data from O'Donnell et al. The dashed black line is the identity line (y=x).*

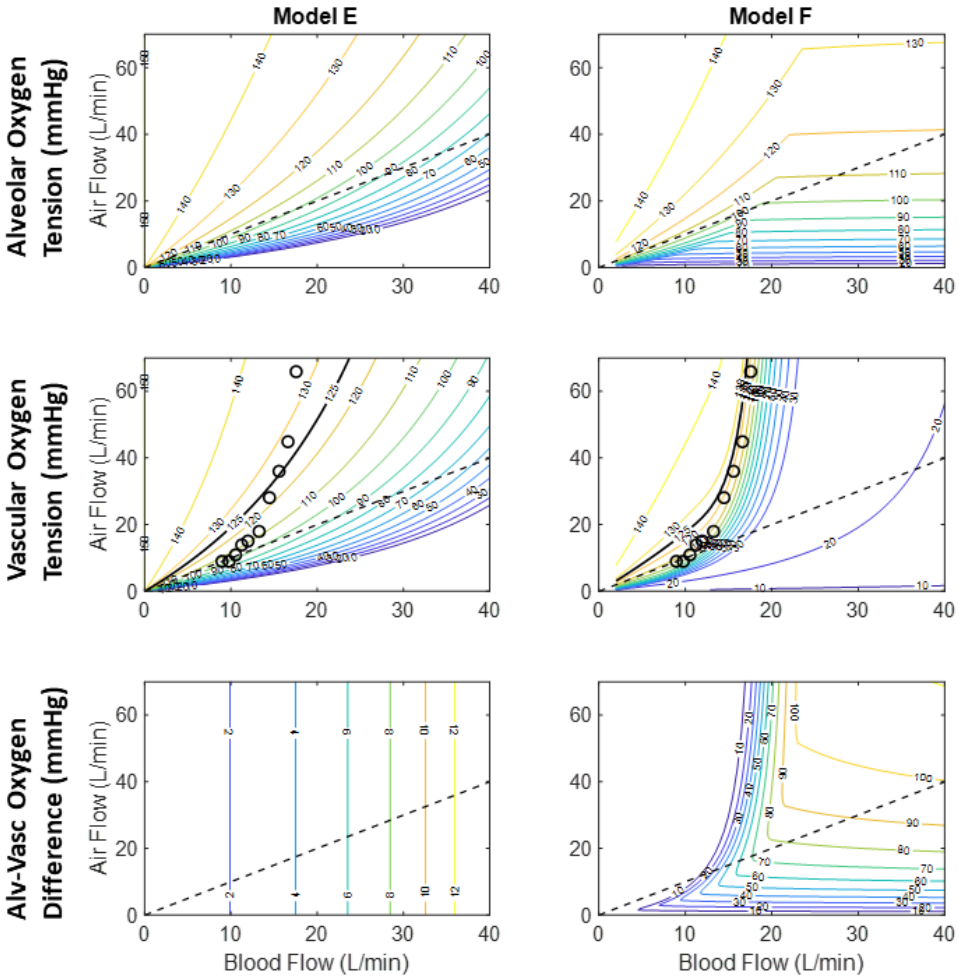
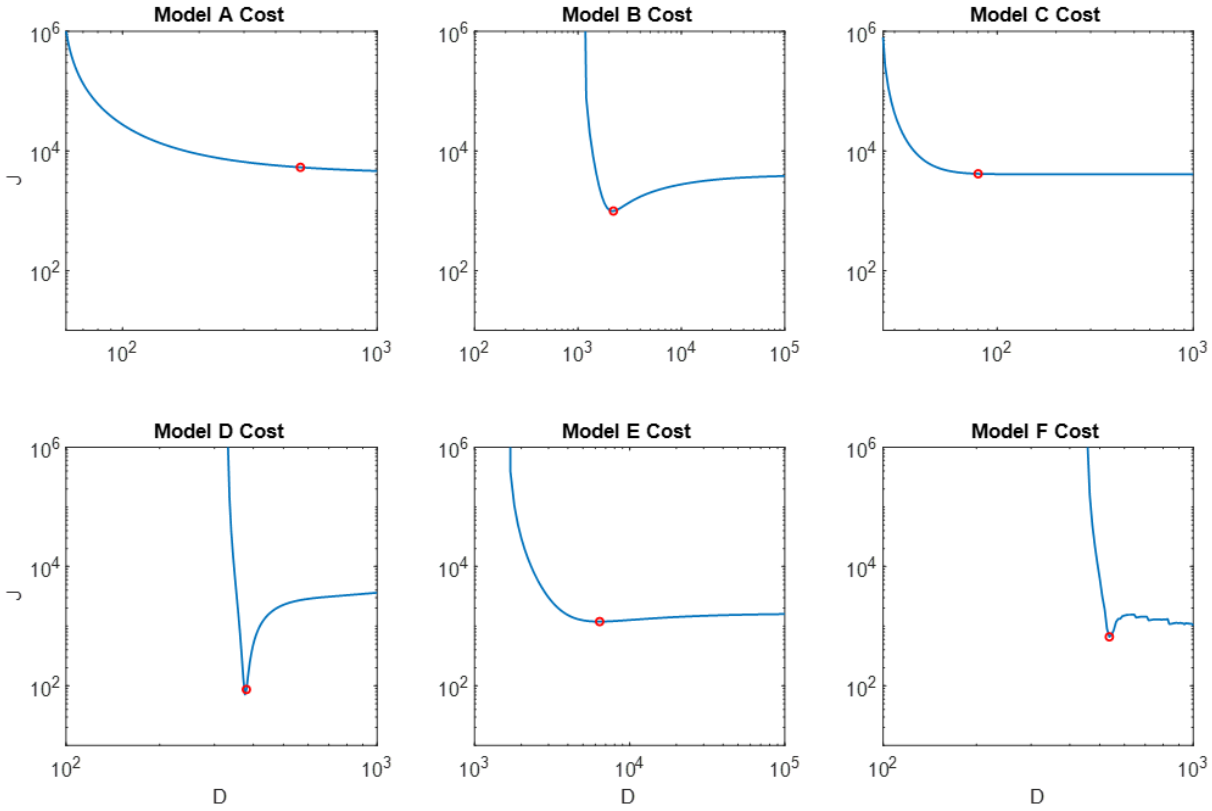


Figure 2.6 ***Least squares cost as a function diffusivity parameter, D****. Each panel corresponds to one of the six models analyzed. On the x-axis the value of the parameter, D, and on the y-axis is the value of the cost function in equation 14. Red circles indicate the values of D used to generate the contour plots in Figures 2.4 and 2.5 and are also reported in Table 2.2*



Chapter 3 Hypoxic Pulmonary Vasoconstriction as a Regulator of Alveolar-Capillary Oxygen Flux: A Computational Model of Ventilation-Perfusion Matching

3.1 Acknowledgements

This chapter has been previously published under open license of the Public Library of Science Computational Biology (170) and is reproduced here. This work was supported by National Institutes of Health grants T32-HL12542, 1F31HL149277-01A1, R01HL15092, and R01-HL139813. Special thank you to my co-authors Filip Jezek, David J. Pinsky, and Daniel A. Beard.

3.2 Abstract

The relationship between regional variabilities in airflow (ventilation) and blood flow (perfusion) is a critical determinant of gas exchange efficiency in the lungs. Hypoxic pulmonary vasoconstriction is understood to be the primary active regulator of ventilation-perfusion matching, where upstream arterioles constrict to direct blood flow away from areas that have low oxygen supply. However, it is not understood how the integrated action of hypoxic pulmonary vasoconstriction affects oxygen transport at the system level. In this study we develop and make functional predictions with a multi-scale multi-physics model of ventilation-perfusion matching governed by the mechanism of hypoxic pulmonary vasoconstriction. Our model consists of (a) morphometrically realistic 2D pulmonary vascular networks to the level of large arterioles and venules; (b) a tileable lumped-parameter model of vascular fluid and wall mechanics that accounts for the influence of alveolar pressure; (c)

oxygen transport accounting for oxygen bound to hemoglobin and dissolved in plasma; and (d) a novel empirical model of hypoxic pulmonary vasoconstriction. Our model simulations predict that under the artificial test condition of a uniform ventilation distribution (1) hypoxic pulmonary vasoconstriction matches perfusion to ventilation; (2) hypoxic pulmonary vasoconstriction homogenizes regional alveolar-capillary oxygen flux; and (3) hypoxic pulmonary vasoconstriction increases whole-lobe oxygen uptake by improving ventilation-perfusion matching.

3.3 Introduction

The pulmonary circulation exhibits several unique features when compared to systemic circulation. In a healthy individual, mean systemic arterial blood pressure tends to be between 90-110 mmHg, whereas mean pulmonary arterial pressure tends to be between 15-20 mmHg. Since the lungs are perfused with the entire cardiac output, they are perfused with the largest flow at the lowest perfusion pressure of any organ. At the regional level, flow in the pulmonary circulation is regulated via unique mechanisms. In response to hypoxia, systemic arteries tend to dilate. At the whole-body level this response is mediated by neural mechanisms such as the central and peripheral chemoreflex (152). At the local level, metabolism-mediated vasodilating factors are released in response to increasing oxygen demand. One potential metabolic factor is extracellular ATP, which can act as a vasodilator through the activation of P2Y2 receptors (81,82). Pulmonary arteries however, constrict in response to low oxygen in the alveolar space (175,176). This phenomenon is referred to as hypoxic pulmonary vasoconstriction (HPV) and is believed to operate on a regional level by directing blood flow away from airway regions that have low oxygen supply (176).

Efficient pulmonary gas exchange requires effective matching of airflow and blood flow – referred to as ventilation-perfusion (V/Q) matching. In large mammals, such as humans, V/Q ratios are significantly influenced by gravity, resulting in increased blood flow through the lowest part of the organ (177). The weight of the organ and extravascular tissue compresses the parenchyma (178). By extension, a subject's posture (ex: supine, prone, upright) has appreciable consequences on regional perfusion and V/Q ratios (4). Moving a patient into a prone position has been shown to improve V/Q matching and oxygenation (6). However, very little is known about how V/Q matching is actively regulated through physiological regulatory mechanisms. While the ability of central and peripheral chemoreflexes to alter the rate and depth of the ventilation for the whole organ is well appreciated, regulation at the regional level is not understood (152). Similarly, bronchoconstriction and bronchodilation of the airway have been well studied and discussed in the context of asthma (156,157). There are a few experimental studies which suggest that hypocapnic bronchoconstriction could be an important regulatory mechanism for V/Q matching, but the evidence has not definitely proven the role of this mechanism (179,180). To our knowledge there is no evidence to suggest that the small airways sense airway oxygen and physiologically regulate the distribution of air flow (159,181). HPV is understood to be the major homeostatic feedback mechanism which physiologically maintains adequate V/Q matching. Chronic exposure to high altitude and inappropriate activation of HPV have also been implicated in the development of pulmonary arterial hypertension (168,182–184).

The molecular basis of HPV remains elusive. A common perspective is that the oxygen sensor, transducer, and vasoconstrictive effector must all be contained within pulmonary arterial smooth muscle cells (168). From this perspective, several pathways including modulation of endothelin signaling, and regulation of prostacyclin synthesis have been proposed as the

molecular integrators of HPV. However, functional studies investigating these specific pathways have been unable to demonstrate their role in mediating the phenomenon (185). Kuebler and coworkers have proposed a signal transduction pathway for HPV wherein an oxygen-sensitive sphingomyelinase and the cystic fibrosis transmembrane regulator (CFTR) induce the translocation of TRPC6 calcium channels to the membrane of vascular smooth muscle cells in the smallest arterioles that perfuse the alveoli (122). In this mechanism, membrane depolarization initiates at the alveolocapillary level, and a conducted wave of depolarization then propagates along the endothelium in the opposite direction of blood flow through connexin-40 gap junctions (120). Dunham et al. have also recently proposed a pathway for HPV in which hydrogen peroxide generated by nicotinamide adenine dinucleotide dehydrogenase iron-sulfur protein 2 (Ndufs2—a core subunit of mitochondrial complex 1) regulates the activity of Kv1.5 ion channels on pulmonary arterial smooth muscle cells (92).

A popular perspective in the V/Q matching literature is that HPV is not important under normoxic conditions as major changes in pulmonary arterial pressure or total pulmonary vascular resistance are generally only observed when alveolar oxygen falls below 80 mmHg. This view is supported by experiments in Arai et al (171). The authors hypothesized that some of the heterogeneity in pulmonary blood flow present in the normal human lung in normoxia is due to HPV. To test this, they exposed human subjects to mild hyperoxia and measured blood flow heterogeneity via arterial spin labeling. Their results show that under mild hyperoxia that there was little change in the distribution of blood flow compared to normoxic conditions and conclude that HPV does not affect pulmonary perfusion heterogeneity in normoxia. We are skeptical of hyperoxia exposure being an effective perturbation to uniformly inhibit HPV, and the conclusions of this study. Under normoxic conditions there is heterogeneity in the

distribution of airflow and oxygen in the airway. This means that there are likely some regions of lung where HPV could be activated. Under hyperoxic conditions the average oxygen content in the airway certainly increases, however the heterogeneity of the airway oxygen distribution is likely unchanged—as demonstrated by experiments where airflow distribution is measured when a pig is ventilated on different fractions of inspired oxygen (181). Given that HPV operates to alter the blood flow distribution to mirror the airflow distribution, and that hyperoxia exposure does not alter the distribution of airflow, we assert that the role of HPV in affecting blood flow distribution in normoxia remains an open question. Effective inhibition of HPV by transgenic or pharmacological manipulation could potentially decouple the oxygen sensor from the vasoconstrictive effector. Our skepticism of global hyperoxia not being an effective way to inhibit HPV could be reconciled by measuring the distribution of alveolar oxygen tension. However, routine clinical measurements of alveolar oxygen are an indirect extrapolation using an empirical formula based on blood gas measurements and only represent the average alveolar oxygen tension (186). It is likely that HPV function would be most apparent during hypoxia exposure, conditions where oxygen consumption is increased (cardiovascular exercise), or when there are significant structural occlusions of the vasculature (ex: pulmonary embolism) or airway (ex: inhaled foreign body).

Given the complexity of V/Q matching, there have been many efforts to computationally-model the physiology of pulmonary gas exchange. Compartmental formulations have been useful to scrutinize system-level regulation by neuro-humoral mechanisms, as well as effects of binding and buffering of oxygen and carbon dioxide (187,188). There are also structural models which have been constructed to investigate the impact of airway and vascular geometry on regional flow distribution (189–191). These types of models have been critical in informing our current

understanding of how gravity and posture impact that distribution of blood flow. These structural models offer a direct way to translate patient-specific geometries to functional predictions. Burrowes et al. model how pulmonary emboli will redistribute blood flow, and the impact of oxygenation of red blood cells (189). They predict that occluding 80% of the vascular network will increase the mean red blood cell transit time above the time needed to fully saturate the cell's hemoglobin. More recent work from Burrowes et al. use an empirical model HPV on top of their structural model to predict the role of this mechanism in acute pulmonary embolism (192).

While there are many factors that influence V/Q matching, the goal of this study is to understand how the integrated action of HPV affects V/Q matching and regional alveolar-capillary oxygen flux throughout a lobe of the lungs. We present a multi-scale multi-physics computational model of V/Q matching in rat lungs where the critical components are: (a) an algorithm to generate morphometrically realistic pulmonary vascular networks; (b) a tileable lumped-parameter model of vascular fluid and wall mechanics; (c) oxygen transport accounting for oxygen bound to hemoglobin and dissolved in plasma; and (d) a novel empirical model of HPV based on the conducted vascular response mechanism proposed by Wang et al. (87). A schematic of our model is shown in Figure 3.1. The model is calibrated to data available in published literature. Our model simulations predict that under the artificial test condition of a uniform ventilation distribution (1) HPV matches perfusion to ventilation; (2) HPV homogenizes regional alveolar-capillary oxygen flux; and (3) HPV increases whole-organ oxygen uptake by improving V/Q matching.

3.4 Methods

Our computational work has been implemented in MATLAB and the corresponding codes have been made available in the GitHub repository *https://github.com/drewzeewoozee/VQmodel*. Table 1 contains a list of all model variables, fixed parameters, and adjustable parameters. The following subsections explain how we:

- Generate morphometrically realistic vascular networks
- Derive equations that govern vascular fluid mechanics
- Derive equations that govern oxygen transport
- Derive equations of an empirical model of HPV

The major novel features are the empirical model of HPV, and the integration of these sub-models into a multi-scale multi-physics framework that enables us to understand how the regulation of blood flow distribution impacts oxygen transport.

3.4.1 Model

Distributive branching networks

To generate the topology of vascular networks we adapt the angiogenesis-inspired distributive branching algorithm of Wang et al. (195). Wang et al.'s original algorithm requires a domain of mesh points for the network to span and uses a purely dichotomous branching mechanism to "fill" the space bounded by the mesh points. Our algorithm similarly requires a user supplied domain of points. We generated various shaped 2-dimensional domains of mesh points by using a finite-element meshing algorithm (PolyMesher) (196). Each iteration of our algorithm adds a new node to the network. Network nodes can be one of four types: 0 — the network "root" — there is only one of these in a given network; 1 — "normal" nodes which have

a single parent and a single daughter; 2 — "bifurcation" nodes which have a single parent and two daughters; and 3 — "terminal" nodes which have a single parent and no daughters. Our algorithm in pseudo-code is illustrated in Figure 3.2. This algorithm requires user inputs of Δg — the grow size distance for each node, K — the number of nodes to generate, x and y — the x and y coordinates of the mesh points, and r — a 2×1 vector specifying the location of the root node.

The output of our algorithm is an undirected graph which describes the topological connectedness of a vascular network. To interpret each branch of the network as a vessel we assign them a length and radius. This allows us to validate the morphology of our networks by comparing them to experimental data. The data set we compare our networks to reports the length and radius of rat pulmonary arterial networks using the Diameter-defined Strahler ordering system (197). To make such comparisons, we first determine the vessel segments—network branches in between bifurcation nodes. We assign a radius to each vessel segment based on Poiseuille's law:

$$\Delta P = \frac{8\mu(Hct, r)lQ}{\pi r^4} \qquad \text{Eqn. (1)}$$

where ΔP is the pressure drop across the segment, μ is the viscosity of blood, l is the length of the segment, Q is the volumetric flow rate, and r is the radius of the segment. We use Pries et al.'s nonlinear viscosity law [36] for $\mu(Hct, r)$ to account for the rheological properties of blood flow in the microcirculation (Fahraeus and Fahraeus-Lindqvist effects). We set the flow rate in each segment by first determining the area of each perfusion zone. A perfusion zone is defined as the area spanned by mesh points closest to a terminal branch in the network — conceptually similar the Voronoi diagram (198). We assign a flow through a terminal segment proportional to the area it perfuses. Using the topology of the network, we back-calculate the flow in each

segment of the network. To estimate the pressure drop for each segment, we assume that $\Delta P = ql/k$, where q is the flow through the vessel segment, and k is a constant hydraulic conductivity per unit length (μm^2/mmHg/s). Equations (1) is numerically solved to determine r, the radius of each vessel segment.

Once we have assigned a radius to each vessel segment, we categorize their orders by the diameter-defined Strahler system as detailed in Jiang et al. (197). We then compare the length and radius of each Strahler order in our vascular networks to Jiang et. al.'s morphometric data. We manually calibrate our network anatomy to the morphometric data by adjusting the size and shape of the finite-element meshes generated by Polymesher, and adjusting the value of k to achieve reasonable fits to the morphometric data in Figure 3.3.

Vascular mechanics

We represent fluid mechanics through the vascular network using a tileable lumped-parameter model following the bond graph approach of Safaei et al. (199). Figure 1B shows how the mechanics of each vessel segment may be represented as an equivalent RC electric circuit. The wall of each vessel segment is equivalent to Voigt body model. For each segment, the change in vessel wall pressure is given by

$$C\frac{dP_v}{dt} = q_{in} - q_{out} \qquad \text{Eqn. (2)}$$

where Pv is the vessel wall pressure, C is the vessel compliance, and qin and qout are the flow in and out of the vessel respectively. The lumenal outlet pressure of each segment is determined by

$$P_{out} - P_{alv} = R_D(q_{in} - q_{out}) \qquad \text{Eqn. (3)}$$

where P_{alv} is the external alveolar pressure, P_{out} is the lumenal vessel outlet pressure, and R_D is the vessel-wall resistance. Inlet flow qin is governed by

$$L\frac{dq_{in}}{dt} + Rq_{in} = P_{in} - P_{out}, \quad \text{Eqn. (4)}$$

where L is the blood inertance, R is the hydraulic resistance, and P_{in} is the inlet pressure. Eqs (2-4) constitute a system of two ordinary differential equations where and qin are the state variables and P_{out} and q_{out} are the conditions at the boundary of a given vessel segment. We assume hydraulic resistance R is a non-linear quantity that depends on the volume of the vessel segment and is represented by

$$R = R_0\left(\frac{V_0}{V}\right)^2 \quad \text{Eqn. (5)}$$

where R_0 is the resistance, V_0 is the fluid volume at an idealized equilibrium, and V is the instantaneous volume of the vessel segment, given by

$$V = CP_v, \quad \text{Eqn. (6)}$$

which holds for all vessel segments.

For an arterial bifurcation, flow from a parent segment is partitioned into two daughter segments. Pin for the daughter segments is specified as the Pout of the parent segment. q_{out} of the parent segment is specified by conservation of flow with

$$q_{out,p} = q_{in,d1} + q_{in,d2}, \quad \text{Eqn. (7)}$$

where $p, d1$, and $d2$ denote parent and daughter segments respectively. Terminal arterioles connect to capillary segments whose mechanics are represented in the same manner. By conservation of flow and pressure balance we have $q_{out,cap} = q_{in,cap}$, and $P_{in,cap} = P_{out,art}$, where art and cap denote arterial and capillary segments. Capillary segments drain into a venous

network that is topologically equivalent to the arterial network. Similarly, we have $q_{out,cap} = q_{in,ven}$, and $P_{in,ven} = P_{out,cap}$, where ven denotes the venous segments. For a venous bifurcation, flow through two "partner" segments merges into a confluent segment. Conservation of flow and pressure balance requires

$$q_{in,c} = q_{out,a} + q_{out,b}, \text{ and} \quad \text{Eqn. (8)}$$

$$P_{v,a} + R_D\left(q_{in,a} - q_{out,a}\right) = P_{v,b} + R_D(q_{in,a} - q_{out,b}) \quad \text{Eqn. (9)}$$

where *a* and *b* denote the "partner" segments and *c* denotes the confluent segment. Since q_{out} is an initial condition, we need to solve for $q_{out,a}$ and $q_{out,b}$ equations (8) and (9) can be solved to yield

$$q_{out,a} = \frac{P_{v,a} - P_{v,b} + R_{D,b}q_{in,c} + R_{D,a}q_{in,a} - R_{D,b}q_{in,b}}{R_{D,a} + R_{D,b}}, \quad \text{Eqn. (10)}$$

$$q_{out,b} = \frac{P_{v,a} - P_{v,b} + R_{D,a}q_{in,c} + R_{D,b}q_{in,b} - R_{D,b}q_{in,a}}{R_{D,a} + R_{D,b}}. \quad \text{Eqn. (10)}$$

Airway and vascular oxygen transport

We treat a single capillary vessel segment interacting with an alveolar compartment as the gas exchange unit. Although pulmonary capillary blood flow resembles a sheet of fluid moving across the alveoli (200,201), our model does not explicitly represent this spatial feature of the gas exchange unit. Instead we use a lumped compartmental approach and represent the diffusion capacity as an apparent diffusion parameter (D_{O2}) that we estimate in the Model Parameterization section.

For the airway, we use a simplified compartmental model to represent oxygen transport which is shown in Fig A.1. We assume fixed volumes for the airways, and variable volumes for the alveolar compartments. Equations in this section are derived based on compartmental mass-balance. In the airway, oxygen content is represented by partial pressure (mmHg). For oxygen

dissolved in the blood there is a non-linear relationship between blood oxygen partial pressure and blood oxygen concentration due to oxygen being bound to hemoglobin.

Airway1 represents the proximal airway and interacts with atmospheric air, airway2 connects to airway1, and all the alveolar compartments. Airway2 functions as a mixing compartment and is representative of the anatomical dead-space. The model is driven by two empirical functions:

$$Q_{air}(t), Q_v^* \sin(2\pi R_R t), \text{ and,} \quad \text{Eqn. (12)}$$

$$P_{alv}(t) = P_{alv}^* \sin(2\pi R_R t) \quad \text{Eqn. (13)}$$

where Q_V^* is the magnitude of air flow (ml/s), P_{alv}^* is the amplitude of the alveolar pressure, and RR is the number of breaths per second. The oxygen mass balance in airway1 is governed by

$$\frac{dP_{airway1,O2}}{dt} = \begin{cases} \frac{Q_{air}}{V_{airway1}}[P_{air,O2} - P_{airway}] & Q_{air} \geq 0 \\ -\frac{Q_{air}}{V_{airway1}}[P_{airway2,O2} - P_{airway1,O2}] & Q_{air} < 0 \end{cases} \quad \text{Eqn. (14)}$$

where $P_{airway1,O2}$ is the partial pressure of oxygen in $airway1$, $V_{airway1}$ is the volume of air in $airway1$, and P_{air} is the partial pressure of oxygen in the atmosphere. Oxygen mass balance in $airway2$ is governed by

$$\frac{dP_{airway2,O2}}{dt} = \begin{cases} \frac{Q_{air}}{V_{airway2}}[P_{airway1,O2} - P_{airway2,O2}] & Q_{air} \geq 0 \\ -\frac{\sum_{i=1}^{M}[P_{alv,O2,i} - P_{airway1,O2,i}]}{V_{airway1}} & Q_{air} < 0 \end{cases} \quad \text{Eqn. (15)}$$

where $P_{airway2,O2}$ is the partial pressure of oxygen in $airway2$, M is the number of perfusion zones, q_i is the airflow to the i'th alveolar compartment (mL/s), $P_{alv,O2,i}$ and is the partial

pressure of oxygen in the i'th alveolar compartment such that $Q_{air}(t)$=$\sum_{i=1}^{M} q_i(t)$. For the i'th alveolar compartment, change in volume is given by

$$\frac{dV_{alv,i}}{dt} = q_i \quad \text{Eqn. (16)}$$

or,

$$V_{alv,i}(t) = V_{0,i} + \frac{q_i}{2\pi R_R}(1 - \cos(2\pi R_R t)) \quad \text{Eqn. (17)}$$

where $V_{0,i}$ is the initial volume of the i'th alveolar compartment. The mass (in moles) of oxygen in the i'th alveolar compartment is given by

$$\frac{dM_{alv,i}}{dt} = \begin{cases} \frac{q_i}{\beta} P_{airway2,O2} - \alpha D_{O2}[P_{alv,O2,i} - P_{O2,i}] & Q_{air} \geq 0 \\ \frac{q_i}{\beta} P_{alv,O2,i} - \alpha D_{O2}[P_{alv,O2,i} - P_{O2,i}] & Q_{air} < 0 \end{cases} \quad \text{Eqn. (18)}$$

where α is the Henry solubility coefficient for oxygen in a fluid (mol/L/mmHg), β is the solubility of oxygen in gas (mmHg L/mol), D_{O2} is the apparent diffusion capacity of oxygen across the alveolar-capillary boundary, $P_{alv,O2}$ is the partial pressure of oxygen in the i'th alveolar compartment, and $P_{O2,i}$ is the partial pressure of oxygen in the i'th capillary vessel segment. The oxygen partial pressure in the alveoli is computed by

$$P_{alv,O2,i}(t) = \beta \frac{M_{alv,i}(t)}{V_{alv,i}(t)}. \quad \text{Eqn. (19)}$$

Equation (18) is cast in units of total mass of oxygen per unit time. Equation (19) is used to calculate the corresponding oxygen partial pressure in the alveolar compartment.

To represent oxygen within the blood, we account for oxygen both freely dissolved in plasma and that bound to hemoglobin, so that

$$C_{O2} = \alpha P_{O2} + HctC_{Hb}\left(\frac{P_{O2}^n}{P_{O2}^n + P_{50}^n}\right) \quad \text{Eqn. (20)}$$

where C_{O2} is the concentration of oxygen (total moles per L), P_{O2} is the partial pressure of oxygen (mmHg), C_{Hb} is the average concentration of hemoglobin binding sites in a red blood cell (mol/L), P_{50} is the oxygen partial pressure in which half the hemoglobin binding sites are bound to oxygen, and n is the Hill-coefficient. For the i'th capillary compartment, change in oxygen concentration is given by

$$\frac{dC_{O2,i}}{dt} = \frac{q_{in,i}\left(C_{O2,input} - C_{O2,i}\right) + \alpha D_{O2}(P_{alv,i} - P_{O2,i})}{V_{cap,i}}, \quad \text{Eqn. (21)}$$

where $q_{in,i}$ is the inlet flow rate for the i'th capillary segment, and $V_{cap,i}$ is the volume of the i'th capillary segment. We assume that there is no partitioning of hematocrit or uptake of oxygen in the arterial network. For the j'th venous segment, change in oxygen concentration is given by

$$\frac{dC_{O2,j}}{dt} = \frac{q_{out,a}\left(C_{O2,a} - C_{O2,j}\right) + q_{out,b}(C_{O2,b} - C_{O2,j})}{V_{ven,j}}, \quad \text{Eqn. (22)}$$

where a and b represent the upstream venous segments that become confluent with the j'th venous segment, and $V_{ven,j}$ is the instantaneous volume of the j'th venous segment.

Empirical hypoxic pulmonary vasoconstriction

Our empirical representation of hypoxic pulmonary vasoconstriction (HPV) is inspired by Wang et al. (120) , in which they demonstrate that connexin-40 gap junctions facilitate the transduction of a wave of depolarization from the alveolar-capillary boundary upstream to the arterioles and arteries. For the i'th perfusion zone, the HPV signal generated by the oxygen content in the alveoli is represented by

$$S_i = \exp\left(\frac{-P_{alv,O2,i}}{P_{HPV}}\right) \quad \text{Eqn. (23)}$$

where S_i is a unitless signal, and P_{HPV} is a parameter representing the sensitivity of HPV to oxygen partial pressure in the alveolar space. An implicit assumption built into equation (23) is that HPV senses and generates a signal across all possible values of $P_{alv,O2,i}$. The exponential form of equation (23) was chosen so that S_i was strictly positive and decreasing as a function of alveolar oxygen. In other words, the less oxygen in the alveolar space, the greater the HPV signal, Si. The target tone of the j'th arterial segment is given by

$$T_{j,\infty} = \left(\sum_{k=1}^{N_k} S_k \exp\left[-\frac{l_k}{\lambda}\right]\right)(T_{Max} - T_{min}) + T_{min} \quad \text{Eqn. (24)}$$

where N_k is the number of perfusion zones that the j'th arterial segment feeds into, k is the index of those perfusion zones, l_k is the path length from the perfusion zone to the mid-line of the j'th segment, λ is a length constant governing the spatial decay of the transduced signal, and T_{Max} and T_{min} are unitless scaling parameters. The summation in equation (24) represents the cumulative HPV signal in the j-th vessel segment influenced by the k-many downstream perfusion zones. The strengths of the HPV signals, S_k, are weighted by an exponential spatial decay of signal strength along the length of the signal. This exponential functional form is justified by experimental studies on conducted vascular responses (201,202). The cumulative HPV signal is re-scaled by T_{Max} and T_{min} so that these parameters define the upper and lower bounds of the target vessel tone, $T_{j,\infty}$. The instantaneous tone of the j'th arterial segment is governed by first order

$$\tau \frac{dT_j}{dt} = T_{j,\infty} - T_j \quad \text{Eqn. (25)}$$

where τ is a time constant. Equation (25) operates as a linear filter to smoothly relax the instantaneous vessel tone, T_j, toward the target vessel tone, $T_{j,\infty}$. The vessel tone variable T_j is assumed to govern arterial vessel diameter (resistance) and stiffness. This is incorporated into our lumped-parameter vascular mechanics framework by adjusting the resistances and compliances of each arterial vessel segment by

$$R_j = R_{0,j} T_j, \text{ and} \quad \text{Eqn. (26)}$$

$$C_j = \frac{C_{0,j}}{T_j}, \quad \text{Eqn. (27)}$$

where R_j and C_j are the resistance and compliance of the j'th segment, and $R_{0,j}$ and $C_{0,j}$ are the corresponding fixed nominal estimates of those parameters. The motivation behind the functional forms of eqations (26) and (27) is that an increased vessel tone will increase vascular resistance and decrease the vessel compliance (increase stiffness) simultaneously. The vessel-wall resistance $R_{D,j}$ is computed by

$$R_{D,j} = \frac{v}{C_j} \quad \text{Eqn. (28)}$$

where v is the constant vessel relaxation speed and is recomputed whenever C_j is altered by the action of HPV.

3.4.2 Model parameterization

Vascular network morphometry

We use our distributive branching algorithm to generate a synthetic population of 3 rat lungs as shown in Fig 3.3 and Table B.1. Each vascular network is intended to represent a lobe of the rat lung. The shape of each mesh used to generate the vascular networks was chosen to emulate the shape of lungs lobes. We analyze the morphometry of these vascular networks with diameter-defined Strahler Ordering and compare our networks to the data from Jiang et al. (197), where they measured the length and radius of silicone-elastomer casts of rat pulmonary arterial vascular trees. Qualitatively, our networks capture the fractal-like branching pattern of true pulmonary arterial trees. To calibrate our model morphometry to the data in Jiang et al (197), we manually adjusted the hydraulic conductivity per unit length (k). Manual calibration required to find a satisfactory value for k was minimal, as we primarily varied it by orders of magnitude, and found k = 1012 μm2/mmHg/s to be in good agreement with the data from Jiang et al.

Vascular mechanics

To specify the vascular mechanics parameters (R_0, C_0, R_D, and L) for each arterial and venous vessel segment, we use the estimators defined in (199) (see Table 3.1). For R0 we use Poiseuille's law shown in equation (1) as the estimator. Treating vessels as composed of a homogenous linear elastic material,

$$C_0 = \frac{2\pi r^3 l}{hE} \qquad \text{Eqn. (29)}$$

where E is the Young's modulus and h is the vessel thickness. We use an estimated value for E from Blanco et al. [43]. Vessel wall thickness h is calculated using the following relation:

$$h = r(ae^{br} + ce^{dr}),$$ Eqn. (30)

where a, b, c, and d are the fitting parameters also taken from Blanco et al. (203). The vessel-wall resistance RD is estimated by

$$R_D = \frac{v}{C},$$ Eqn. (31)

where v is the time constant for stress relaxation (see Table 1). The hydraulic intertance L is estimated by

$$L = \frac{\rho}{\pi r^2},$$ Eqn. (32)

where ρ is the blood density.

For the capillary segments, we set R_0 and L to the same value as the upstream arterial segment, and use the estimator defined by equation (31) for R_D. We set capillary compliance (C) by

$$C = \frac{V_{cap,j,un}}{\Delta P},$$ Eqn. (33)

where $V_{cap,j,un}$ is the unstressed blood volume of the j-th capillary segment, and ΔP is the arteriolar-venular pressure drop. ΔP is set to 1 mmHg, $V_{cap,j,un}$ is defined by

$$V_{cap,j,un} = 0.7 a_j V_{cap,Total}$$ Eqn. (34)

where $V_{ca[.Total}$ is the total capillary blood volume, and a_j is the fraction of area the corresponding perfusion zone occupies in the total area of the network domain. The 0.7 factor reflects the assumption that when the vessels are unstressed they contain 70% of the potential

maximum total volume, as estimated by Gelman (204). We assume that one half of the total pulmonary blood volume is in the capillaries, one quarter of the total pulmonary blood volume is in the arteries, and the other quarter is in the veins. Thus, is $V_{cap,Total}$ defined by

$$V_{cap,Total} = 2\pi \sum_{i=1}^{N} r_i^2 l_i \quad \text{Eqn. (35)}$$

where N is number of arterial (or venular) segments in the network, and r_i and l_i are the radius and length of i-th segment. The summation in equation (35) is multiplied by π as we are computing the volume of blood in idealized cylindrical vessels, and is multiplied by 2 as we assume the venous network morphometry mirrors the arterial network.

To confirm that our model recapitulates realistic hemodynamics, we compare our simulations to data from isolated-ventilated-perfused rat lung experiments (185,205). In these experiments, the lungs and heart are excised en bloc from an animal. The left and right ventricle are punctured with cannulae so that the pulmonary circulation can be perfused, and the trachea is cannulated with a ventilator tube to control the airway pressure. The organ is kept in Zone 3 conditions (alveolar pressure is less than the venous pressure) and the whole organ flow rate is varied to measure the arterial-venous pressure-drop as an indicator of pulmonary vascular resistance. Molthen et al used papaverine during all of these experiments (205). Thus, data from this study are considered to represent a maximally dilated scenario. Chlopicki et al. investigated putative molecular mechanisms of HPV by applying a variety of pharmacological agents to an isolated-ventilated-perfused rat lungs while ventilated with normoxic (21% O2, 5% CO2, N2 balance) and hypoxic (5% CO2, 95% N2) gaseous mixtures (185). We have taken data points from this study where lungs were ventilated with normoxic and hypoxic gaseous mixtures without the presences of vasoactive pharmacological agents. The hypoxic condition is considered

to represent a maximally vasoconstricted scenario, and the normoxic condition is considered a physiological baseline. Simulations run under conditions that emulate these experiments are compared to the data to determine upper and lower bounds for our model's pressure-flow relationships. We introduce a global vascular tone parameter T^* (unitless) that is multiplied against the vascular resistance parameters (R_0) and divides the compliance parameters (C_0) — similar to equations (26) and (27). By manually adjusting the value of T^* we are able to shift the pressure-flow relationship to a more constricted or dilated scenario. Fig 3.4 shows how our model compares to the data. The model simulation curves that are near the 95% N2 (Chlopicki) data point were run with T∗ = 0.8, and the curves near the Paperavine (Molthen) data points were run with T∗ = 0.5.

Oxygen transport and regulation by HPV

To calibrate our oxygen transport and empirical model of HPV, we compare our simulations to human experiments done by Cheng et al, in which they measure pulmonary arterial pressure, ventilation, cardiac output, and systemic arterial oxygen partial pressure while inspiring normal (21% O2, 5% CO2) or hypoxic (10% O2, 5% CO2) air (206). We re-scale the human valued cardiac output and ventilation measurements to reflect that of an adult rat (350 g, 80 mL/min) so that

$$Q_P^* = Q_{P,Cheng}\frac{CO_{Rat,ref}}{CO_{Human,ref}} \text{ and,} \quad \text{Eqn. (36)}$$

$$Q_V^* = Q_{V,Cheng}\frac{CO_{Rat,ref}}{CO_{Human,ref}} \quad \text{Eqn. (37)}$$

Where Q_P^* and Q_V^* are the magnitude of total blood flow and ventilation through the model respectively, $Q_{P,Cheng}$ and $Q_{V,Cheng}$ are the cardiac output and ventilation data from Cheng et al

respectively, $CO_{Rat,ref}$ is a reference value for the basal cardiac output of an adult rat, and $CO_{Human,ref}$ is a reference value for the basal cardiac output of an adult human (5 L/min). We note that the hypoxia exposure activates the chemoreflex and local metabolism-mediated vasodilation to increase cardiac output. Thus there is a change in the total flow-rate through the pulmonary circulation independent of the action of HPV or other oxygen-sensitive pulmonary vasoregulation.

To specify the oxygen sensitivity parameter, P_{HPV}, we consider the observation that major changes in mean pulmonary arterial pressure or total pulmonary resistance from HPV are generally only observed when alveolar oxygen falls below 80 mmHg (207). With this in mind we want to ensure that the HPV signal (S) is equal to 1/2 when alveolar oxygen is 80 mmHg (S is bounded by the interval (0,1)). This is achieved by solving equation (23) for P_{HPV}. Substituting S = 1/2 and $P_{alv,O2}$ to 80 mmHg yields

$$P_{HPV} = -\frac{P_{alv,O2}}{\ln(S)} = \frac{80}{\ln(2)} = 115.42 \approx 115 \quad \text{Eqn. (38)}$$

We use the cardiac output, ventilation, and pulmonary arterial pressure measurements from Cheng et al. as boundary conditions (data inputs) for our model simulations and compare the oxygen partial pressure in the primary vein of our model to the systemic arterial oxygen blood gas measurements from Cheng et al. (206). The parameters representing apparent oxygen diffusivity (D_{O2}), maximum tone from HPV (T_{Max}), and minimum tone from HPV (T_{min}) are empirical quantities that are not able to be experimentally measured. We calibrate the model prediction of blood oxygenation by optimizing these parameters with the BELUGA Genetic Algorithm implemented in MATLAB (208). This optimization scheme seeks to minimize the objective function

$$J = \sum_{i=1}^{2} \left(P_{O2,D,i} - P_{O2,M,i}\right)^2, \quad \text{Eqn. (39)}$$

where $P_{O2,D}$ and $P_{O2,M}$ denote the data from Cheng et al. and model prediction of oxygen tension in the primary vein respectively. i = 1 is the normoxia condition, and i = 2 is the hypoxia condition. The model is solved over 120 respiratory cycles and the primary vein oxygen tension is averaged over the last 2 respiratory cycles. We run BELUGA for 30 generations with 100 individuals and allow for mutation. (During these BELUGA runs we set τ = 2 s so that the model reaches steady state in less simulation time. The operative condition is that $\tau > RR$, so that the HPV model is able to average over at least one respiratory cycle). Table 2 shows the values of our model predicted oxygen tension, final cost from equation (39), and values of the optimized parameters. Fig 3.5 graphically shows how the model predicted oxygen tension compares to the data. We also report the standard deviation of each parameter estimate and correlations between them in Table 3.3. One can observe that T_{Max} and T_{min} are highly correlated for all three networks. This is an expected result, and these two parameters are directly subtracted from each other in equation (24) of the empirical HPV model.

Sensitivity Analysis

To assess the sensitivity of model prediction on the variation in model parameters we perform a sensitivity analysis on the parameters listed in Table 3.4. We exclude parameters from this analysis that were involved in network generation or specific to each vessel segment to focus on parameters that influence system level function. Some parameters that have been directly measured have been excluded (α—solubility of oxygen in plasma, β—solubility of oxygen in air, ρ—density of blood, CHb—oxyhemoglobin binding site concentration). We vary the baseline of each parameter ±10%. Our sensitivity index is defined as

$$S = 100 \times \left(\frac{P_{O2,i} - P_{O2,ref}}{P_{O2,ref}} \right) \quad \text{Eqn. (40)}$$

where S_i is the sensitivity of the i-th parameter of interest (percent change in oxygen leaving the pulmonary circulation), and $P_{O2,ref}$ and $P_{O2,i}$ are the model simulated oxygen tensions in the primary vein run with all parameters fixed at their nominal values and the i-th parameter perturbed, respectively. The nominal parameter values are listed in Table 3.1, and we treat the BELUGA estimated values for D_{O2}, T_{Max}, and T_{min} as their nominal values.

Results of our sensitivity analysis are shown in Table 3.4. The most sensitive parameters are hematocrit (Hct), where a 10% perturbation results in a ~13% change in S, and the oxygen concentration entering the pulmonary circulation ($C_{O2,input}$), where a 10% perturbation results in a ~8% change in S. Of the BELUGA estimated parameters, T_{Max} is the most sensitive ($S \approx 5.5$), Tmin is mildly sensitive ($S \approx 1.5$), and DO2 is relatively insensitive ($S \approx 0.1$).

3.5 Results

3.5.1 Effect of HPV on regional hemodynamics

To determine the effect of HPV on flow distribution, we run simulations with and without our empirical HPV model. We also simulate the effect of uniform vasoconstriction (UVC) by setting T^* = 0.8 as a control. These simulations were run with an artificial condition of uniform airflow distribution (each alveolar compartment receives airflow that is proportional to its size). In the absence of regulation by HPV, our model predicts that shorter path lengths tend to have greater flow compared to longer path lengths as shown in Figs 3.6A, 3.7A and 3.8A. However, in the presence of regulation by HPV one can appreciate that there is a homogenization of blood flow. UVC reduces the total flow through the network similar to HPV,

however the distribution of flow is very similar to the simulation run without variation for capillary blood flow decreases for all three networks (Table 3.5).

Another way to interrogate the hemodynamic effects of HPV is to observe the red blood cell (RBC) transit time distribution. Experimentally, the RBC transit time distribution can be measured via an indicator-dilution experiment. In these experiments a vascular bed with a defined single inlet and outlet is identified. Then the inlet is then perfused with a bolus of tracer dye (ex: Evan's Blue, FITC conjugated dextran), and then the washout is measured at the outlet (209). The time series of tracer dye concentration at the inlet, $C_{in}(t)$ and concentration at the outlet, $C_{out}(t)$, are related by

$$C_{out}(t) = C_{in}(t) * h(t) = \int_0^\infty C_{in}(s)h(t-s)ds \quad \text{Eqn. (41)}$$

where $*$ is the convolution operator, and h(t) is a probability distribution of times it could take for a RBC to traverse the vascular bed. Figs 3.6E, 3.7E, and 3.8E show the RBC transit time distributions for each of our model networks. In the absence of regulation by HPV our model networks have some paths that are highly perfused and other paths that are barely perfused at all. In Figs 3.6E, 3.7E, and 3.8E we show how the action of HPV homogenizes $h(t)$ and increases the mean transit time for all three of our vascular networks. We emphasize that an increased transit time implies that a RBC will have more opportunity to acquire oxygen as it traverses the pulmonary circulation.

3.5.2 Effect of HPV on V/Q matching and regional alveolar-capillary oxygen flux

The consequence of homogenization of capillary blood flow and RBC transit times is that V/Q matching becomes more homogeneous as the whole organ coefficient of variation decreases for all three networks, as shown in Table 5 and illustrated in Figs 3.6BF, 3.7BF, and 3.8BF. UVC

shifts the V/Q ratio to the right, which reflects that there are more perfusion zones with large V/Q ratios (due to low blood flow) under this condition. Moreover, regional alveolar-capillary oxygen flux is also more evenly distributed throughout the organ with physiological control from HPV. This is graphically shown in Figure 3.6CG, 3.7CG, and 3.8CG and can also be understood by observing that the coefficient of variation for regional alveolar-capillary flux decreases for all three networks with the action of HPV (see Table 3.5). Perhaps more importantly, the presence of HPV increases the whole-organ oxygen transport into the bloodstream, and the end total amount of oxygen leaving the pulmonary circulation. UVC has variable effects on the distribution of alveolar-capillary oxygen flux, and does increase the amount of oxygen entering the bloodstream—although not as much as HPV. These results are summarized in Table 3.5.

3.5.3 Effect of the fraction of inspired oxygen on HPV-mediated redistributions in hemodynamics, V/Q matching, and alveolar-capillary oxygen flux

Simulations illustrated in Figs 3.6, 3.7, and 3.8 are run under normoxic conditions—the fraction of inspired oxygen ($F_{i,O2}$) is set to 21%, which corresponds to a partial pressure of 150 mmHg. To determine how the $F_{i,O2}$ influences HPV-mediated redistributions in blood flow, V/Q ratios, and oxygen flux, we performed a series of simulations where we set $F_{i,O2}$ to 10%, 15%, 21%, and 50%. The results of these simulations for Network A are shown in Fig 3.9 (results from the Networks B and C are similar and not shown). These simulations predict that the distribution of blood flow, V/Q ratios, and RBC transit time is homogenized with decreasing fractions of $F_{i,O2}$ (Figs 3.9ABDE). Larger $F_{i,O2}$ flattens the distribution of oxygen flux (Fig 3.9C). This is reflected by the decreased CV for $F_{i,O2}$below 21%—indicating that the distribution is being homogenized as $F_{i,O2}$ gets smaller (Fig 3.9E). Moreover, the mean oxygen flux decreases (leftward shift in the distribution) with a smaller $F_{i,O2}$.

3.5.4 Effect of airway occlusions on HPV-mediated redistributions in hemodynamics, V/Q matching, and regional alveolar-capillary oxygen flux

HPV is understood to direct blood flow away from regions of the lung that are under ventilated and have a poor oxygen supply. We simulate this behavior by setting alveolar airflows $q_i = 0$. For these simulations we hold the bulk airflow (Q_V^*) constant, so that occluding a single alveolus will result in an increased airflow to the unoccluded alveoli. We occlude the airway of the most southwestern perfusion zone, and progressively occlude more perfusion zones following the structure of the vascular network. The results of these simulations for Network A are shown in Fig 10 (results from Networks B and C are similar and not shown). These simulations predict that HPV directs blood flow away from the regions with occluded alveoli (Figs 10A-C). As the fraction of occluded alveoli increases there is a gradual decrease in the end-venous oxygen tension (Fig 10D); a gradual increase in the Pearson correlation between regional ventilation and regional blood flow (Fig 10E), and an increase the heterogeneity of V/Q ratios and regional oxygen flux (Fig 10F). Alveolar occlusions produce bimodal V/Q ratio and oxygen flux probability densities (Figs 10HI), however the changes to the blood flow distribution are mild in comparison. This is also reflected by the small gradual increase in the blood flow coefficient of variation shown in Fig 10F. When we run these simulations without HPV, there is no change in the blood flow distribution in response to the airway occlusions (simulations not shown). Moreover, there is decrease in the end-venous oxygenation compared to simulations with HPV — for Network A there is approximately 78 and 64 mmHg of oxygen with 28% of the alveoli occluded with and without HPV respectively.

3.6 Discussion

We constructed an integrated model of distributed gas exchange and regional blood flow control in lung tissue to investigate mechanisms regulating V/Q matching. In an isolated gas exchange unit, increasing the upstream vascular resistance would decrease blood flow, reduce RBC transit time, and thus improve oxygenation. Yet a change in flow to a single unit will impact other gas exchange units in the network. Regional flows and gas exchange throughout the lung are coupled in a complex nonlinear manner. The overarching goal of this study was to gain insight into how this distributed multi-scale system works.

Specifically, this study presents the derivation of, and predictions from a multi-scale multi-physics model of ventilation-perfusion matching. This model consists of morphometrically realistic vascular networks, vascular fluid mechanics, oxygen transport, and an empirical model of hypoxic pulmonary vasoconstriction. The HPV model integrates flow regulation with oxygen transport in a physiologically realistic manner, and facilitates simulations and functional predictions of how active regulation from HPV affects blood flow and oxygen transport at the local and system level.

3.6.1 Vascular network generation

Our novel distributive branching algorithm provides an efficient way to generate a vascular network over a 2D domain of any shape. While the present study is focused on lungs, this algorithm could be applied to generate vascular networks in any tissue of interest. Another potential use of this algorithm would be to impute missing data from vascular networks acquired from segmenting images from CT, MRI, or other radiological scans. One limitation of our generated networks is that they are two dimensional, whereas true vascular networks exist in 3-dimensional space. We chose to work with 2D domains to reduce the computational cost and

simplify the interpretation of spatial results. However, the operating principle of this algorithm can be easily extended to three dimensions. In future work we plan to generate 3D networks with this approach and compare/contrast them with true animal and human vascular geometries.

Another limitation of our network generation algorithm is our assumption of a constant hydraulic conductivity per unit length, in the form of the adjustable parameter k. This assumption was used to assign a radius to each vessel segment, where Poiseuille's law to was used impose conservation of flow as the operative constraint. The parameter k was treated as an adjustable parameter. While this approach results in morphometrically realistic networks, how we assign radii to vessel segments could potentially be improved by using a different constraint other than Poiseulle's law. Murray's law, and related derivatives, represent potential alternative choices (210,211). shown in Fig 4, and the regional distribution of flow as shown in Figs 3.6AD, 3.7AD, and 3.8AD. In Fig 3.4, one can observe that Network B does not fit the data as well as Network's A and C, as it appears to be mechanically stiffer. This is likely a result of how we assign radii to vessel segments in the network generation step, as discussed previously. There is a major bifurcation close to root of Network B, which results in there being effectively two parallel networks.

3.6.2 Modeling of vascular mechanics

We simulate hemodynamics using a lumped-parameter model inspired by the bond graph approach of Safaei et al (199). We have extended Safaei's vessel segment model by adding a variable pressure source (represents the mechanical pressure of the airway) and deriving and implementing the flow and pressure balance boundary conditions for a venous network (when flows from two segments become confluent in a larger segment). Our primary interest was in representing the spatial distribution of blood flow in a deterministic manner. The model

presented in this study is capable of capturing both the whole-organ mechanics as shown in Fig 3.4, and the regional distribution of flow as shown in Figs 3.6AD, 3.7AD, and 3.8AD. In Fig 3.4, one can observe that Network B does not fit the data as well as Network's A and C, as it appears to be mechanically stiffer. This is likely a result of how we assign radii to vessel segments in the network generation step, as discussed previously. There is a major bifurcation close to root of Network B, which results in there being effectively two parallel networks.

In real lungs, the CV of blood flow is dependent upon the size of the region observed. This is due to the fractal properties of blood vessel branching and blood flow in the pulmonary circulation. Glenny et al. (212) report a blood flow CV of 0.35 when sampling 0.53 mm3 volumes of rat lung and a fractal dimension of 1.12. The blood flow CV we report from simulations without regulation from HPV are approximately 2.2, and with regulation from HPV the CV becomes approximately 1.2. On average, our perfusion 750 μm^2 (0.75×10^{-14}). The linear dimension of an average perfusion from our model is$\sqrt{0.75 \times 10^{-4} = 0.027}$ mm, and we could extrapolate the volume to be $(0.27\ mm)^3 = 2.05 \times 10^{-5}$. Using the fractal relationship reported in Glenny et al., we can extrapolate that a sampling volume of 2.05×10−5 mm3 corresponds to a CV of 1.01. Our predicted blood flow distributions are thus in the realm of reality, but do appear to overestimate the heterogeneity. This is likely due to the relatively small number of simulated perfusion zones — there are approximately 100 perfusion zones in each network, whereas Glenny et al. used 1000's of sampling volumes when analyzing blood flow distribution in the entire rat lung.

It has been observed that there is an uneven partitioning of hematocrit that is discharged into daughter vessels at bifurcations (213). This phenomenon has implications for both oxygen transport, and rheology. We used to Preis et al.'s non-linear viscosity law as a compromise

between accounting rheological complexities and minimizing computational cost (214). This empirical viscosity law enables one to compute viscosity as a function of vessel segment radius and hematocrit. However, our implementation leverages the apparent viscosity's dependence on radius while assuming that hematocrit is constant in every vessel segment. To our knowledge, no study has measured the uneven partitioning of hematocrit in the pulmonary circulation, so we do not have adequate data so specify a model that captures this phenomenon. It is plausible to consider that the uneven distribution of red blood cells would lead to a heterogeneous distribution of apparent viscosities throughout the pulmonary vasculature and that could major consequences on the lungs regulate blood flow distribution.

3.6.3 Modeling of oxygen transport

Modeling of oxygen transportOur oxygen transport model was derived on the basis of compartmental mass-balance. A variety of models have been derived to capture the mechanics and transport properties in sheet flow (200,201). Given that smallest vessel segments in our model are not the size of pulmonary capillaries, we reasoned that using a sheet flow model would add unnecessary computational expense. Instead, we treat a single capillary vessel segment interacting with an alveolar compartment as the gas exchange unit. We justify this choice by representing the diffusion of oxygen across the alveolar-capillary boundary with an apparent oxygen diffusivity parameter, D_{O2}. The function of sheet flow is that it increases the surface area of the blood-air interface. We can interpret increasing D_{O2} as increasing the surface area of the blood-air interface.

In Fig 3.5 and Table 3.2, we can observe that the model struggles to capture the hypoxic condition. This is a result of two interacting phenomena. (1) We do not account for physiological changes in systemic oxygen consumption under hypoxic conditions. In other words, we assume

that the oxygen concentration entering the pulmonary circulation is the same under normoxic and hypoxic conditions, as the model does not have a closed-loop of circulation. (2) How we account for oxygen bound the hemoglobin and freely dissolved in plasma. Even under hypoxic conditions, the model is still operating on the relatively plateaued portion on the oxyhemoglobin dissociation curve above the half-max saturation. In this region of the curve, it takes a large change in oxygen concentration to see a change in oxygen tension. The model fits to the hypoxic conditions could potentially be improved by accounting for the closed-loop circulation and a physiological representation of oxygen consumption.

3.6.4 Empirical modeling of hypoxic pulmonary vasoconstriction

There is currently no consensus in the field regarding the governing molecular pathways which underlie hypoxic pulmonary vasoconstriction. Our model is inspired by the conducted response pathway proposed by Keubler and colleagues. Conducted vascular responses offer a mechanistic explanation of how information regarding oxygen content in the alveolar space is transduced to the pulmonary arteries which control the distribution of blood flow. Wang et al. (120) demonstrates that the connexin-40 hemmichannel gap junction is essential for HPV in mice. Genetic deletion of connexin-40 abrogated the depolarization of the endothelium in the pulmonary arterioles and vasoconstriction when the mice were exposed to hypoxia. Based on their experiments they conclude that conducted vascular responses from the alveolar-capillary boundary to the upstream pulmonary arteries mediate HPV. Follow up work from this group claims that the upstream oxygen sensor is an oxygen-sensitive sphingomyelinase which ultimately activates the CFTR to act as a chaperone to ferry TRPC6 calcium channels to the membrane of vascular smooth muscle cells near the alveolar-capillary boundary (215).

If we accept the assumption that conducted vascular responses do indeed mediate HPV, then it would follow that any oxygen-sensitive pathway that results in the depolarization of the endothelium at or near the alveolar-capillary boundary could contribute to activation of HPV. Coincidentally, recent work by Duham et al. has proposed a pathway for HPV in which hydrogen peroxide generated by nicotinamide adenine dinucleotide dehydrogenase iron-sulfur protein 2 (Ndufs2) regulates the activity of Kv1.5 ion channels on the pulmonary arterial smooth muscle cells (92). Given that Ndufs2 is a core subunit of mitochondrial complex 1, it is intuitive to expect the redox processes which mitochondria facilitate would be involved in oxygen-sensitive vasoregulation.

The empirical model of HPV derived in this study is a minimal representation of the conducted vascular response pathway. A more detailed model of conducted vascular responses would represent the electrophysiology of the blood vessel wall (membrane potential, intracellular calcium concentration of pulmonary arterial smooth muscle cells, etc). Simulations with our model predict that under an artificial test condition of having a uniform airflow distribution, the activation of HPV matches perfusion to ventilation. Under this test condition, the distribution of blood flow is homogenized. The critical prediction from our empirical HPV model is that homogenization of blood flow and V/Q ratio distributions improves oxygen transport into the bloodstream. We report this in terms of the homogenization of regional alveolar-capillary oxygen flux, increased whole-organ alveolar-capillary oxygen mass transport, and increased oxygen within the primary vein (Figs 6, 7, 8, and 9, and Table 5). A caveat on to these interpretations is our use of a fixed arterial-venous pressure drop of 25 mmHg. In reality vascular pressure, flow, and resistance are all dynamic quantities influenced by a number of pathophysiological systems. Using a fixed arterial-venous pressure drop allows us to assess how

physiological regulation of vascular resistance by HPV affects both total blood flow through the pulmonary circulation and the regional distribution of flow throughout the network. We emphasize that in Table 5 the total flow and vascular resistance are similar between the HPV and uniform vasoconstriction (UVC) simulations, while HPV does a much better job at improving oxygenation compared to UVC. The differences in the ability of HPV and UVC to affect oxygen uptake is explained by how they alter the distribution of blood flow and V/Q matching.

Measurements of pulmonary flow distribution in pigs have been performed by Hlasta et al. and Starr et al. using a microsphere infusion technique (159,181). They observe that the HPV response is spatially heterogeneous, and conclude that this heterogeneity may be related to baseline heterogeneity of the airflow distribution. We performed a series of simulations where we occluded alveolar compartments to explore the effects of a non-uniform airflow distribution (Fig 3.10). We observe that our model is indeed able to divert blood flow away from regions with occluded alveoli and limited oxygen supply. However, these simulations are still limited. One limitation is that we do not have an accurate representation of realistic and heterogeneous airflow distributions. The homogenization of blood flow by HPV that our model predicts is a consequence of the uniform air flow distribution we use. The heterogeneity of real pulmonary airflow distributions are almost certainly related to the anatomical structure of the airway. Interestingly, in a healthy individual airflow and blood flow are both heterogeneously distributed yet the V/Q ratios are still well matched. There is currently no uniformly accepted explanation of why V/Q ratios are well matched, but it is likely combination of the interwoven nature of airway and vascular anatomies, passive phenomena such as the influence of gravity, and the physiological regulatory mechanisms (such as HPV). Future model development will need to integrate our model of vascular flow regulation with a model of airflow through a realistic

network structure to systematically evaluate the contribution of regulation by HPV and anatomical geometry to basal V/Q matching. A second limitation is that the simulated diversion of blood flow away from regions with occluded alveoli is milder than we expect to observe in a real a true lung. This is most likely a limitation of our assumption that the vasoconstrictive ability of every vessel segment is bounded by the same maximum and minimum tone (T_{Max} and T_{min}). Fig B.4 shows how the tone from HPV in each vessel segment corresponding to the simulations in Fig 3.10. One can appreciate the largest tones tend to be in the distal segments and near regions with zero airflow, whereas the more proximal segments tend to have lower tone. This is explained by the mathematical form (exponential decay) of how we assume these signals are conducted upstream through vessel walls. An improved version of the model may require tone parameters that are unique to each size (ex: Strahler order) of vessel segment or represents the electrophysiology of pulmonary endothelium and vascular smooth muscle cells.

To our knowledge, this is the first study to explore how the integrated action of HPV regulates V/Q matching and oxygen transport throughout the lungs. A limitation of the predictions we have presented is that we have only accounted for regulation by HPV. We have not represented the central and peripheral chemoreflexes which alter the cardiac output and rate and depth of ventilation in response to changes in circulating and oxygen and carbon dioxide (plasma acid-base balance). Moreover, we have not accounted for the influence of gravity on the distribution of blood flow and V/Q ratios. The importance of posture on pulmonary blood flow distribution and V/Q matching is well appreciated. This knowledge has been leveraged in clinical settings to improve V/Q matching and oxygen uptake in patients by moving them into a prone position (216). Integrating these mechanisms into our model would provide a framework to understand the whole-body consequences of and influences on V/Q (mis)matching.

3.6.5 Model parameterization

The model presented in this study is fairly complex and is comprised of many parameters. When possible, we set parameters to values that have been measured and reported in the literature. Some parameters however, are empirical in nature and are not directly measurable. In particular, the maximum and minimum tone (T_{Max} and T_{min}) in our HPV model, and the apparent oxygen diffusivity (D_{O2}). Thus we set values for these parameters by estimating them. Algebraically, T_{Max} and T_{min} are subtracted from one another in the model. From the standpoint of structural identifiability, estimating both of these parameters bodes for an ill-conditioned optimization problem. Given that there are no data available to inform how we set these parameters a priori, this becomes a circular problem of not knowing what value to keep one parameter fixed at while we estimate the other. This issue is what ultimately led us to use BELUGA, a genetic algorithm. Using BELUGA enabled us to optimize both of these parameters. This in contrast to gradient-based methods (ex: Levenberg-Marquardt) which are much more susceptible to numerical instability and/or non-reproducible results from parameter unidentifiability [57]. After estimating T_{Max}, T_{min}, and D_{O2} we performed a retrospective sensitivity analysis to understand how these and the other model parameters influence the ability of our model to simulate oxygen uptake. We found that hematocrit (Hct) and the oxygen concentration entering the pulmonary circulation ($C_{O2,input}$) were the most sensitive model parameters. Interestingly, increasing Hct decreased the end-venous oxygen tension and decreasing Hct increased the end-venous oxygen tension. While this may appear paradoxical, perturbing Hct did not dramatically change the oxygen concentration in the blood, rather it shifted the blood oxygen concentration-partial pressure relationship. In other words, an increase in Hct will result in a specified blood oxygen concentration corresponding to a smaller partial

pressure. The other interesting result that emerged from our sensitivity analysis was that D_{O2} is a relatively insensitive parameter. We interpret this result to indicate that our model's ability to uptake oxygen is primarily flow-limited, rather than diffusion-limited. This reinforces the importance of how blood flow distribution is regulated, as altering flow in one segment of the vascular network affects the flow in all other segments of the network.

3.6.6 Vascular recruitment

Krogh first demonstrated the phenomenon of pulmonary capillary recruitment, whereas total blood flow to the lungs increases, previously unperfused capillaries open up and become perfused (161–163). The net effect is that the average RBC transit time tends to stay the same over a range of cardiac outputs. This enables the blood in the pulmonary circulation to be sufficiently oxygenated despite the increased cardiac output and oxygen demand from the systemic tissues. In our model, increases in perfusion pressure and flow lead to increases in microvascular volume via the lumped pressure-volume relationship (6). The limitation of this representation of vascular recruitment is that it does not directly represent vascular networks that are collapsed/non-perfused and then become recruited. In Fig 3.10D, we can see that the end-venous oxygenation decreases as the fraction of occluded alveoli is increased. While this result intuitively makes sense, it is reasonable to expect a true lung would be more resilient to this type of challenge due the mechanism of capillary recruitment. A downside to function enabled by capillary recruitment is that it could be a major contributor to challenges in diagnosing chronic pulmonary embolism (PE). Hypoxemia is uncommon in chronic PE and is often identified during a diagnostic work-up in patients with unexplained pulmonary arterial hypertension (217). A future version of the model presented in this study will require a biophysical representation of capillary recruitment to capture to nuances of these disease states.

3.6.7 Summary of main findings

In conclusion, we have developed an integrative computational model of V/Q matching mechanics, oxygen transport, and the physiological mechanism of HPV. Our model simulations predict that under the artificial test condition of a uniform ventilation distribution (1) HPV matches perfusion to ventilation; (2) HPV homogenizes regional alveolar-capillary oxygen flux; and (3) HPV increases whole-organ oxygen uptake by improving V/Q matching.

Table 3.1 ***Model variables, fixed parameters, and adjustable parameters.*** *Values are omitted if they are time varying or defined for each vessel segment. For the adjustable parameters estimated by the BELUGA Genetic Algorithm, values are reported for each network (A,B,C).*

Variables					
Name	Units	Interpretation	Estimator	Reference	Value
q_{in}	ml/s	flow rate into a vessel segment	-	-	-
q_{out}	ml/s	flow rate out of a vessel segment	-	-	
P_v	mmHg	wall pressure of a vessel segment	-	-	-
P_{in}	mmHg	inlet pressure of a vessel segment	-	-	-
P_{out}	mmHg	outlet pressure of a vessel segment	-	-	-
V	ml	volume of blood in a vessel segment	-	-	-
C_{O2}	mol/L	concentration of O_2 in a vessel segment	-	-	-
P_{O2}	mmHg	partial pressure of O_2 in a vessel segment	-	-	-
V_{alv}	ml	volume of air in an alveoli	-	-	-
M_{alv}	mol	mass of O_2 in an alveoli	-	-	-
$P_{alv,O2}$	mmHg	partial pressure of O_2 in an alveoli	-	-	-
$P_{airway,i}$	mmHg	partial pressure of O_2 in the i'th airway	-	-	-
T	unitless	vasoactive tone in a vessel segment	-	-	-
Fixed Parameters					
Name	Units	Interpretation	Estimator	Reference	Value
l	cm	vessel segment length	from network	[38]	-
r	cm	vessel segment radius	Eq (1)	[38]	-
R_0	mmHg s/ml	nominal vessel segment resistance	$R_0 = \frac{8\mu(r,\mathrm{Hct})l}{\pi r^4}$	[38]	-
E	mmHg	elastic modulus of a blood vessel	-	[43]	10,000
h	mm	vessel wall thickness	$h = r(ae^{br} + ce^{dr})$	[43]	-
a	mm	empirical constant for h estimator	-	[43]	0.2802
b	mm	empirical constant for h estimator	-	[43]	-0.5053
c	mm	empirical constant for h estimator	-	[43]	0.1324
d	mm	empirical constant for h estimator	-	[43]	-0.01114
C_0	ml/mmHg	Nominal vessel segment compliance	$C_0 = \frac{\pi r^3 l}{Eh}$	[38]	-
v	s	vessel relaxation speed	-	[38]	0.01
R_D	mmHg s/ml	vessel wall resistance	$R_D = \frac{v}{C}$	[38]	-
ρ	kg/m^3	density of blood	-	[38]	1060
L	mmHg s^2/ml	vessel segment intertance	$L = \frac{\rho l}{\pi r^2}$	[38]	-
α	mol/L/mmHg	O_2 solubility in plasma	-	[44]	1.3×10^{-6}
β	mmHg/L/mol	O_2 solubility in air	-	[44]	5.95×10^{-5}
C_{Hb}	mol/L	Oxyhemoglobin binding site concentration	-	[45]	0.0213
Hct	unitless	hematocrit—fraction of blood made out of RBCs	-	-	0.4
n	unitless	Hill exponent for Hb saturation	-	[46]	2.6
P_{50}	mmHg	partial pressure of O_2 where Hb is half saturated	-	[46]	36
$C_{O2,input}$	mol/L	O_2 entering pulmonary circulation	-	-	7.84×10^{-3}
R_R	1/s	respiratory frequency	-	-	1.17
Q_P^*	ml/s	perfusion magnitude	$Q_P^* = Q_{P,\mathrm{Cheng}} \frac{CO_{\mathrm{Rat,ref}}}{CO_{\mathrm{Human,ref}}}$	[47]	0.66
Q_V^*	ml/s	ventilation magnitude	$Q_V^* = Q_{V,\mathrm{Cheng}} \frac{CO_{\mathrm{Rat,ref}}}{CO_{\mathrm{Human,ref}}}$	[47]	2.97
P_{alv}^*	mmHg	alveolar pressure amplitude	-	-	0.75
P_{HPV}	mmHg	HPV O_2 sensitivity	$P_{HPV} = \frac{80 \text{ mmHg}}{\ln(2)}$	Eq (38)	115
λ	mm	HPV signal spatial decay constant	-	[42]	100
τ	s	HPV time constant	arbitrarily fixed	-	30
Adjustable Parameters					
Name	Units	Interpretation	Estimator	Reference	Value
D_{O2}	ml/s	apparent alveolar-capillary O_2 diffusivity	BELUGA GA	[48]	(3.36, 14.60, 0.95)
T_{Max}	mm	HPV maximum vessel tone	BELUGA GA	[48]	(1.49, 1.48, 1.49)
T_{min}	mm	HPV minimum vessel tone	BELUGA GA	[48]	(0.49, 0.48, 0.31)

Table 3.2 ***Results from BELUGA Genetic Algorithm****. The top block contains oxygen tensions from Cheng et al., and most fit individuals for each network from BELUGA optimization. The middle block contains the value of our objective function for each network from the most fit individuals. The bottom block contains the best fit parameter values for each network.*

	Network A	Network B	Network C	Cheng et al.
$P_{O2,M}$ (FiO2 = 0.21)	92.51	89.30	92.25	98.31
$P_{O2,M}$ (FiO2 = 0.10)	57.76	60.50	61.68	49.09
J	104.92	196.97	159.64	
D_{O2}	3.36	14.60	0.95	
T_{Max}	1.49	1.48	1.49	
T_{min}	0.49	0.48	0.31	

Table 3.3 ***Standard Deviation (SD) and Correlations between parameters estimated by BELUGA Genetic Algorithm***.

Network A				**Network B**				**Network C**			
	D_{O2}	T_{Max}	T_{min}		D_{O2}	T_{Max}	T_{min}		D_{O2}	T_{Max}	T_{min}
SD	1,025.9	13.52	4.22	SD	1,952.4	12.80	4.08	SD	1,213.1	13.66	3.04
D_{O2}	1	0.20	0.19	D_{O2}	1	0.41	0.45	D_{O2}	1	0.20	0.19
T_{Max}	-	1	0.96	T_{Max}	-	1	0.96	T_{Max}	-	1	0.97
T_{min}	-	-	1	T_{min}	-	-	1	T_{min}	-	-	1

Table 3.4 ***Sensitivity analysis****. Percent change in oxygen tension of the primary vein given a ±10% perturbation in nominal parameter value. *—The sensitivity index is less than 0.01.*

Parameter		Network A	Network B	Network C
E	+10%	5.79	5.06	4.12
	−10%	−6.40	−4.92	−4.06
v	+10%	−0.12	−0.02	0.11
	−10%	−0.28	0.00	−0.08
Hct	+10%	−11.40	−11.26	−10.55
	−10%	16.10	17.46	16.33
n	+10%	−3.39	−3.59	−3.43
	−10%	3.44	4.50	4.17
P_{50}	+10%	1.51	2.28	2.80
	−10%	−1.94	−2.54	−2.62
$C_{O2,input}$	+10%	8.70	9.31	9.55
	−10%	−7.57	−7.81	−7.71
R_R	+10%	−0.20	−0.30	−0.47
	−10%	0.87	0.53	0.84
Q_V^*	+10%	2.88	2.07	2.02
	−10%	−3.11	−2.09	−1.85
P_{alv}^*	+10%	−0.32	0.14	0.00*
	−10%	−0.21	0.26	0.42
P_{HPV}	+10%	1.97	1.83	1.54
	−10%	−2.66	−2.09	−1.60
λ	+10%	0.70	0.25	0.30
	−10%	−1.28	−0.29	−0.25
D_{O2}	+10%	−0.20	−0.01	0.03
	−10%	−0.28	−0.08	−0.04
T_{Max}	+10%	6.28	6.33	5.26
	−10%	−6.41	−5.60	−4.83
T_{min}	+10%	2.81	1.53	1.16
	−10%	−3.09	−1.52	−1.37

Table 3.5 ***Effect of HPV on regional flow, V/Q matching, and oxygenation.*** *Model simulations were performed with uniform vasoconstriction (UVC), and with and without regulation by HPV. All simulations used a fixed 25 mmHg arterial-venous pressure drop. The top block summarizes how HPV and uniform vasoconstriction (UVC) affects the total flow through the organ, and the variability of blood flow, V/Q ratio by the Coefficient of Variation (CV = μ/σ). The bottom block summarizes how HPV impacts the oxygenation in terms of the total alveolar-capillary oxygen mass flux, oxygen mass flux CV, oxygen mass flux normalized to total oxygen flux, venous oxygen tension, and venous oxyhemoglobin saturation.*

	Network A			Network B			Network C		
	w/o HPV	w/ HPV	UVC	w/o HPV	w/ HPV	UVC	w/o HPV	w/ HPV	UVC
Total Flow (ml/s)	1.10	0.38	0.26	2.32	0.62	0.60	1.77	1.07	0.46
Total Resistance (mmHg s/ml)	28.03	80.13	117.64	13.32	49.45	51.16	17.47	28.78	67.13
Flow CV	2.47	1.28	2.42	2.35	1.42	2.44	2.09	1.08	2.35
V/Q CV	3.42	1.24	2.45	1.78	1.65	2.75	3.39	1.36	1.65
Total Alv-cap O_2 flux (mmol/s)	4.6	11.6	5.0	29.7	70.1	28.8	3.8	5.6	2.3
Alv-cap O_2 flux CV	0.30	0.25	0.26	0.25	0.27	0.28	0.52	0.48	0.58
O_2 flux CV / Total O_2 flux (s/mol)	66.19	22.14	51.9	8.37	3.84	9.71	139.19	87.23	256.33
Venous O_2 (mmHg)	81.26	100.20	78.03	56.66	96.45	61.72	54.79	74.63	60.57
Venous O_2 (%)	0.94	0.97	0.93	0.85	0.96	0.87	0.84	0.92	0.87

Figure 3.1 ***Schematic of multiscale multi-physics model of V/Q matching****. Block (A) illustrates the whole-lobe vascular network model. Black lines represent blood vessels, and colored regions represent discrete zones of perfusion. The network geometry is agnostically generated by a space-filling algorithm inspired by Wang et a. Block (B) shows how the mechanics of each vessel segment is represented as an equivalent circuit. Intravascular pressure (P_V) and flow into the vessel (q_{in}) are the state variables; inlet pressure (P_{in}) and flow out of the vessel (q_{out}) are the initial conditions at boundaries for a given vessel segment; outlet pressure (P_{out}) is an algebraic constraint; time-varying alveolar pressure (P_{alv}) is a dynamic pressure source; and hydraulic resistance (R), inertance (L), compliance (C), and vessel wall resistance (R_D) are anatomical parameters calculated from the geometry of the vessel segment (length and radius) and can be modulated by vasoregulation (purple boxes). Block (C) depicts a representative gas exchange unit. Gases flowing through the capillary tube are exchanged with an alveolar compartment. Block (D) portrays the oxygen-sensitive vasoregulatory mechanism hypoxic pulmonary vasoconstriction (HPV). Hypoxia in the alveolar space induces conducted vasoconstriction. Conducted vascular responses are spatially propagated in a upstream through the endothelium – these responses modulate the values of the anatomical parameters (R, C, and R_D) in the arterial network.*

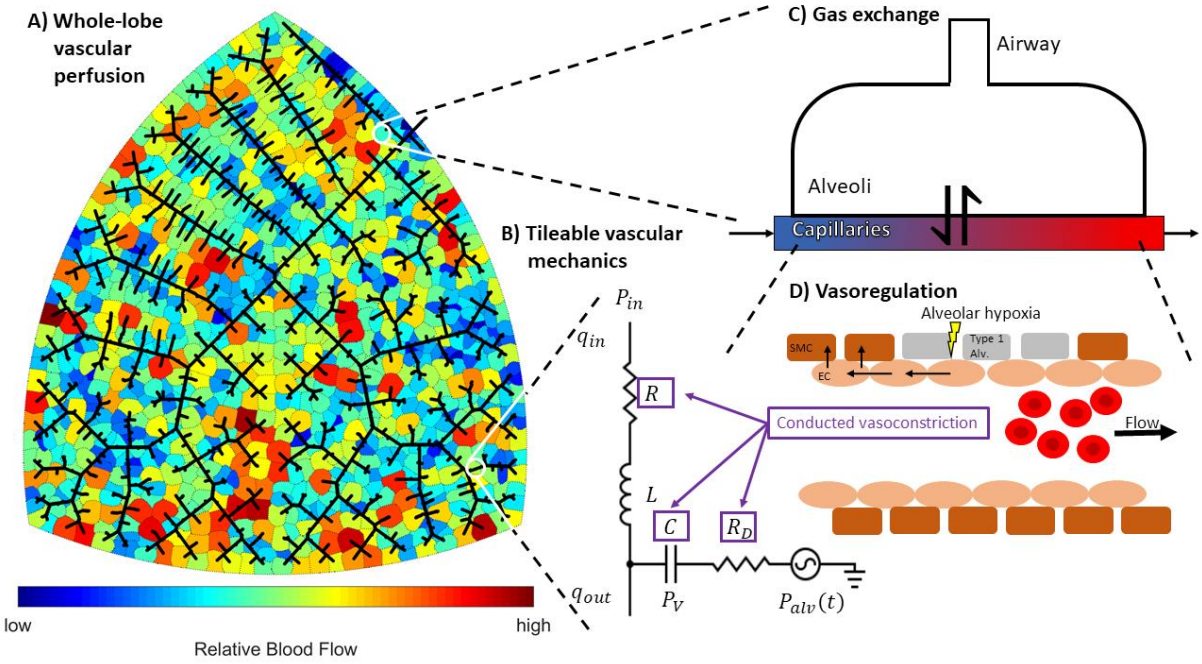


Figure 3.2 ***Example of angiogenesis-inspired network generation algorithm.*** *Blue points define a mesh that the algorithm seeks to cover with a network. The black and red dots are the nodes generated by each iteration of the algorithm; red nodes denote network terminals; black lines are connections between nodes. The black scale bar is 1000 μm. The first two nodes (1 and 2) are manually specified by the user. The algorithm determines the mesh points furthest from the network. For nodes 3-5, the southwest corner is the furthest mesh point. For node 6, the southeast corner is furthest and then for node 7 the southwest corner is furthest. For node 8, the southeast corner is the furthest point and is connected to closest node of the network—node 6. The northern most mesh point is furthest from both node 7 and 8. Node 9 is connected to node 2 since it is the closest node in the existing network. To implement the user needs to supply a domain of points to cover, the "grow distance" between nodes, and the number of nodes to generate.*

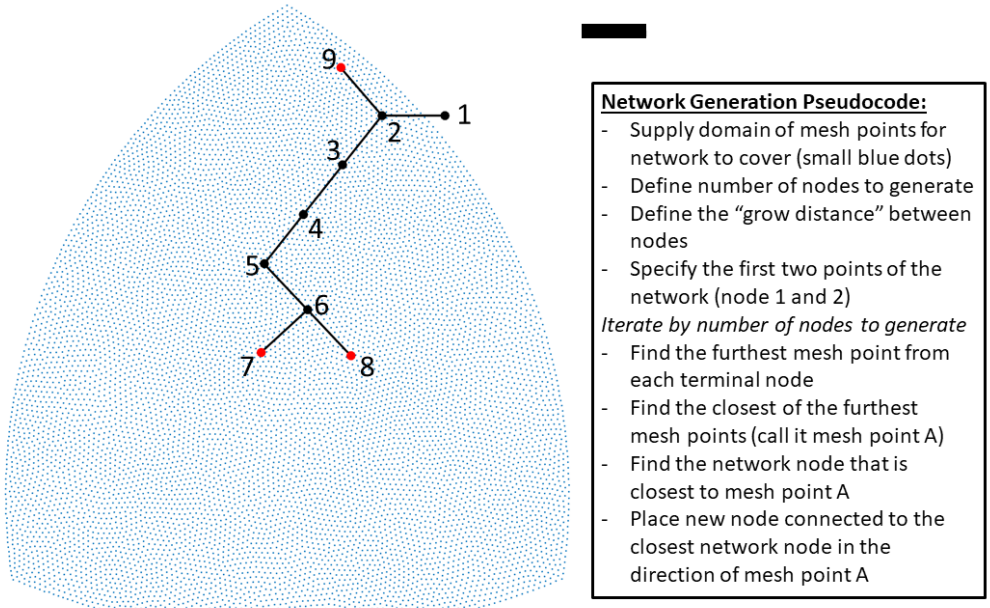


Figure 3.3 ***Morphometrically realistic pulmonary vascular networks****. (A,B,C) Synthetic population of rat lungs. Blue dots are the finite-element mesh points made by Polymesher, the cyan circles denote the root node for each network, the black lines represent the network topology, and the red squares denote the network terminals. The black scale bar is 3000 μm. All networks were made with 1,000 nodes and Δg set to 50 μm. Note that the radius of each vessel is not plotted to size. The total area spanned by each finite element mesh is the same. (D, E) Comparison of our network geometries to measured diameters and lengths as a function of diameter-defined Strahler orders from silicone elastometer casts of rat pulmonary arterial trees in Jiang et al.*

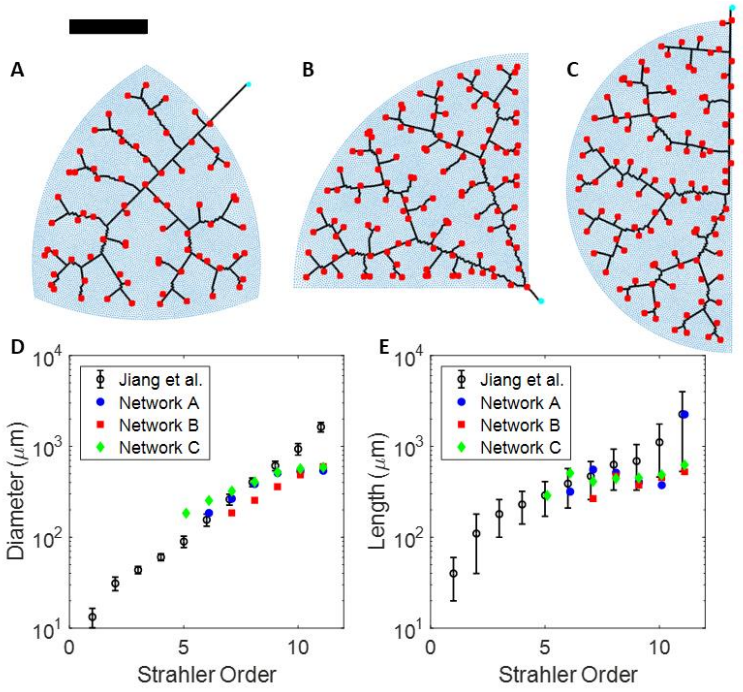


Figure 3.4 ***Whole-organ pressure-flow relationships.*** *Discrete data points are taken from isolated-perfused-ventilated lung experiments performed in Molthen et al. and Chlopicki et al. Simulations are run under Zone 3 conditions (venous outlet pressure (7 mmHg) > alveolar pressure (6 mmHg)). The model simulation curves that are near the 95% N2 (Chlopicki) data point were run with $T^* = 0.8$, and the curves near the Papaverine (Molthen) data points were run with $T^* = 0.5$.*

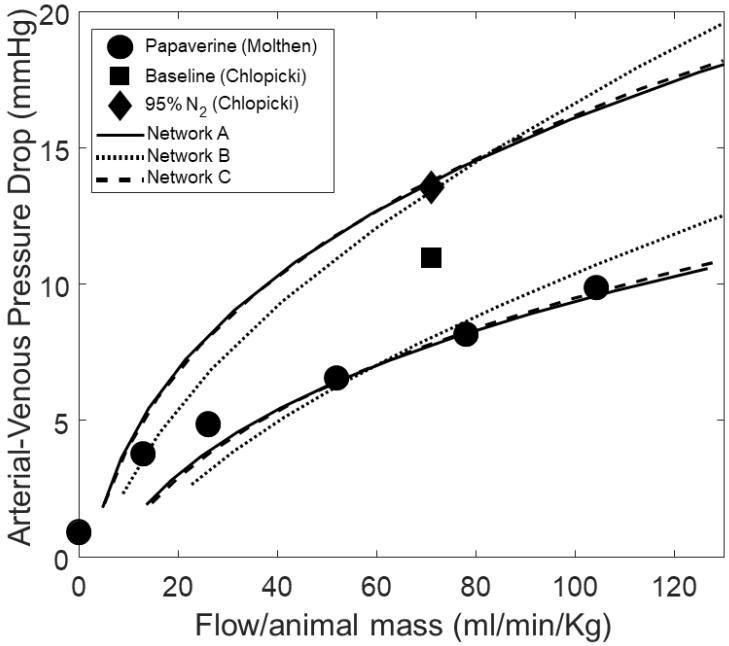


Figure 3.5 ***Fits from BELUGA Genetic Algorithm****. (A) Oxygen partial pressure in the pulmonary vein. The block circle and error bars denote data from Cheng et al., the blue circle denotes network A, the red square denotes network B, and the green diamond denotes network C. The plotted point is the best fit individual from BELUGA (parameters reported in Table 2). (B) The same data and results from (A) but expressed in terms of oxyhemoglobin saturation.*

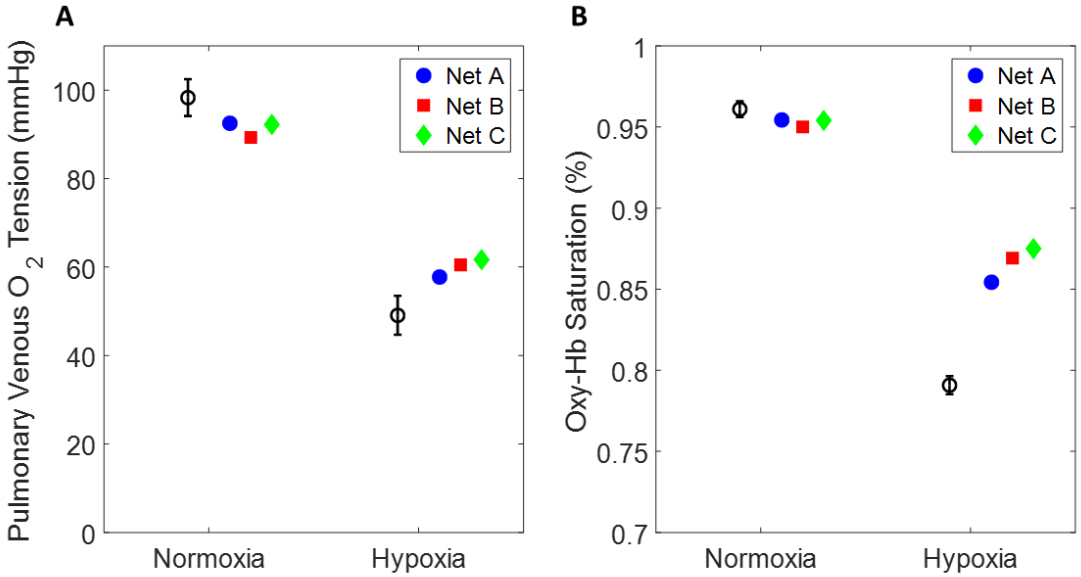


Figure 3.6 ***Effect of HPV and uniform vasoconstriction on Network A regional perfusion, V/Q matching, and oxygen flux****. (A-C) Leftmost column of networks are without regulation from HPV, middle column of networks are with regulation from HPV, and the rightmost column of networks are with uniform vasoconstriction, where $T^* = 0.8$ is used for the global vascular tone. The black scale bar is 1000 μm. (A) Perfusion in the capillary compartments; (B) Ventilation-perfusion (V/Q) ratios in the capillary compartments; (C) Oxygen flux in the capillary compartments. (D-G) Blood flow, RBC transit times, V/Q ratios, and oxygen flux expressed as probability densities—calculated with a kernel density estimator. (D) Distribution of flow; (E) RBC transit times normalized to mean transit time; (F) Distribution of V/Q ratios; (G) Distribution of oxygen flux.*

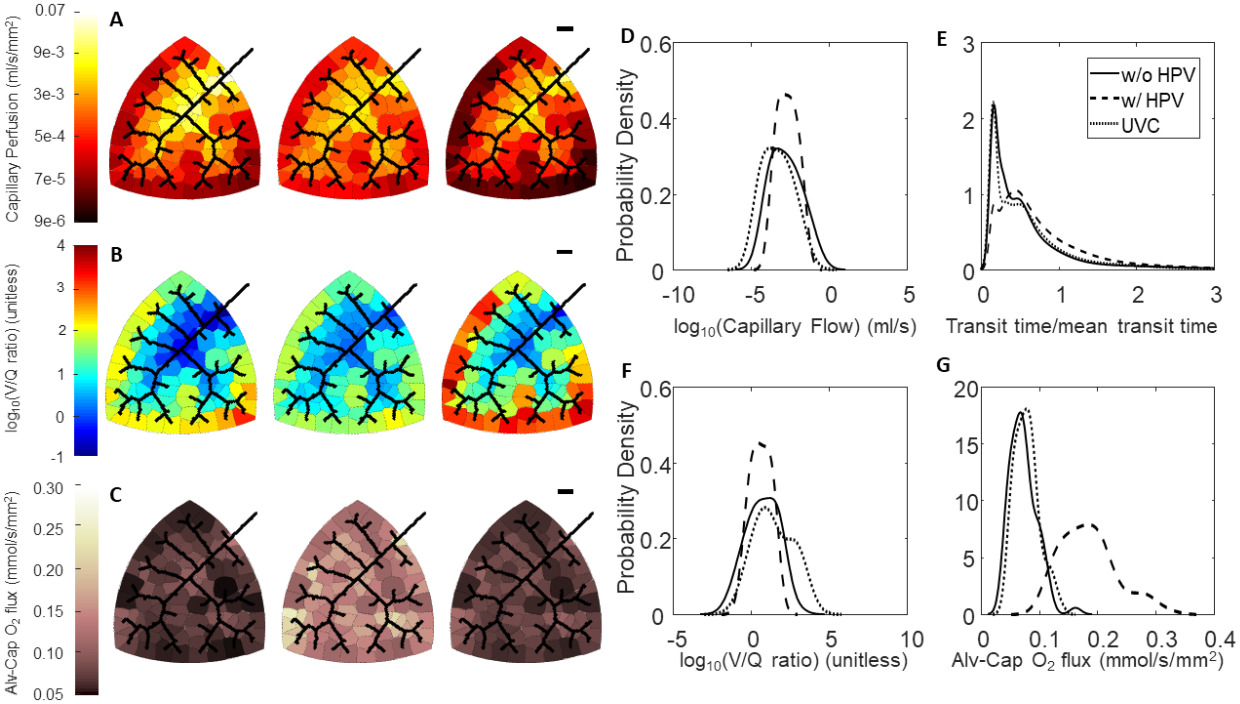


Figure 3.7 ***Effect of HPV and uniform vasoconstriction on Network B regional perfusion, V/Q matching, and oxygen flux****. (A-C) Leftmost column of networks are without regulation from HPV, middle column of networks are with regulation from HPV, and the rightmost column of networks are with uniform vasoconstriction, where $T^* = 0.8$ is used for the global vascular tone. The black scale bar is 1000 μm. (A) Perfusion in the capillary compartments; (B) Ventilation-perfusion (V/Q) ratios in the capillary compartments; (C) Oxygen flux in the capillary compartments. (D-G) Blood flow, RBC transit times, V/Q ratios, and oxygen flux expressed as probability densities—calculated with a kernel density estimator. (D) Distribution of flow; (E) RBC transit times normalized to mean transit time; (F) Distribution of V/Q ratios; (G) Distribution of oxygen flux.*

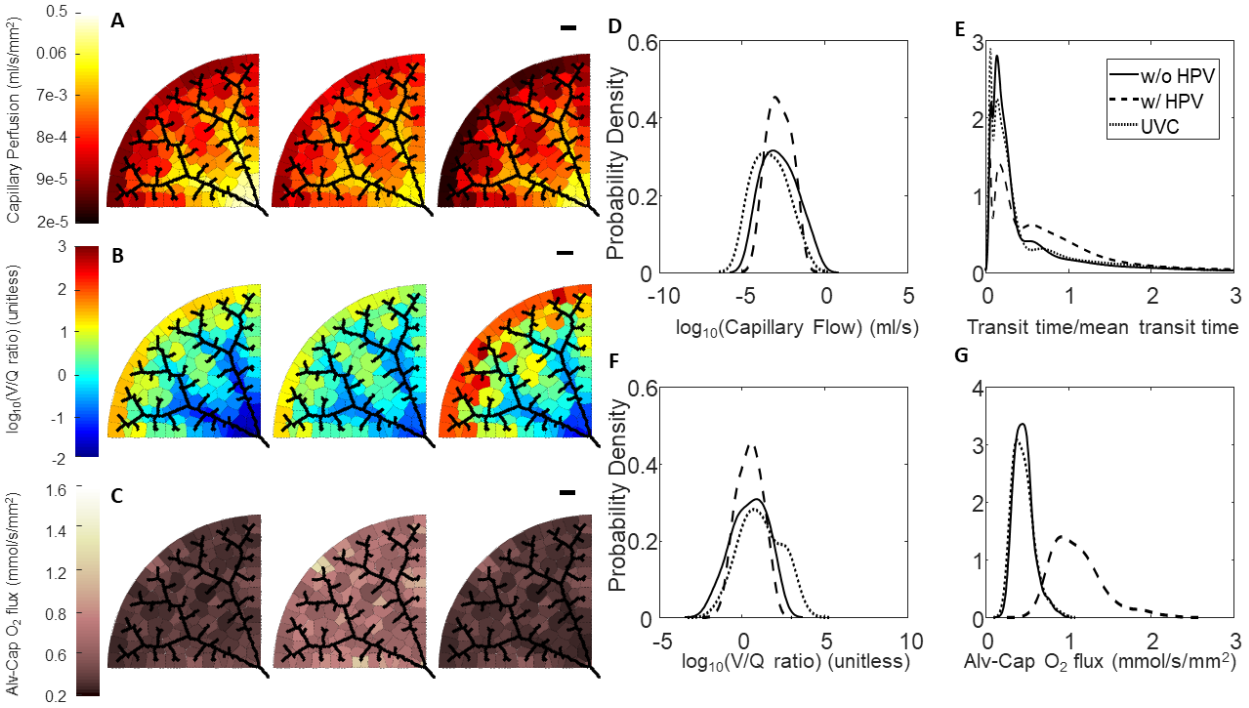


Figure 3.8 ***Effect of HPV and uniform vasoconstriction on Network C regional perfusion, V/Q matching, and oxygen flux****. (A-C) Leftmost column of networks are without regulation from HPV, middle column of networks are with regulation from HPV, and the rightmost column of networks are with uniform vasoconstriction, where $T^* = 0.8$ is used for the global vascular tone. The black scale bar is 1000 μm. (A) Perfusion in the capillary compartments; (B) Ventilation-perfusion (V/Q) ratios in the capillary compartments; (C) Oxygen flux in the capillary compartments. (D-G) Blood flow, RBC transit times, V/Q ratios, and oxygen flux expressed as probability densities—calculated with a kernel density estimator. (D) Distribution of flow; (E) RBC transit times normalized to mean transit time; (F) Distribution of V/Q ratios; (G) Distribution of oxygen flux.*

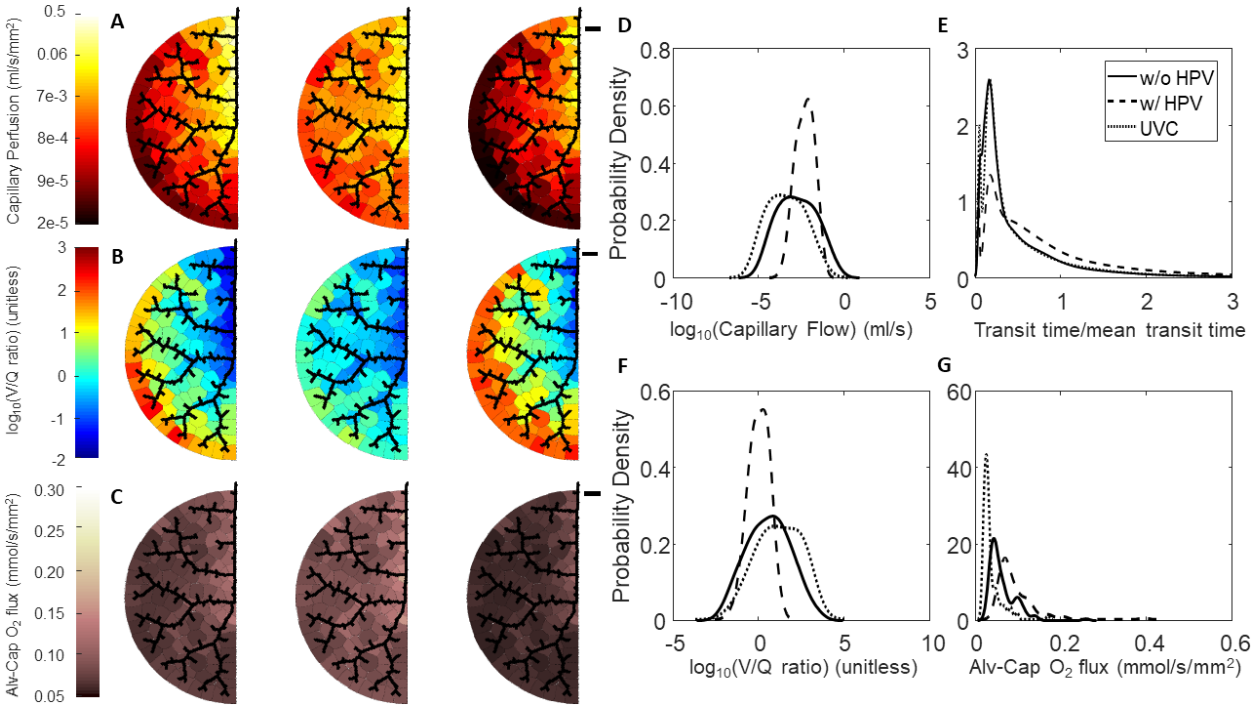


Figure 3.9 ***Effect of the fraction of inspired oxygen on HPV-mediated redistributions in hemodynamics, V/Q matching, and oxygen flux****. (A) Distributions of capillary blood flow; (B) Distributions of V/Q ratios; (C) Distributions of oxygen flux; (D) RBC transit time distributions; (E) Coefficient of variation of blood flow, V/Q ratio, and oxygen flux plotted as a function Fi,O2.*

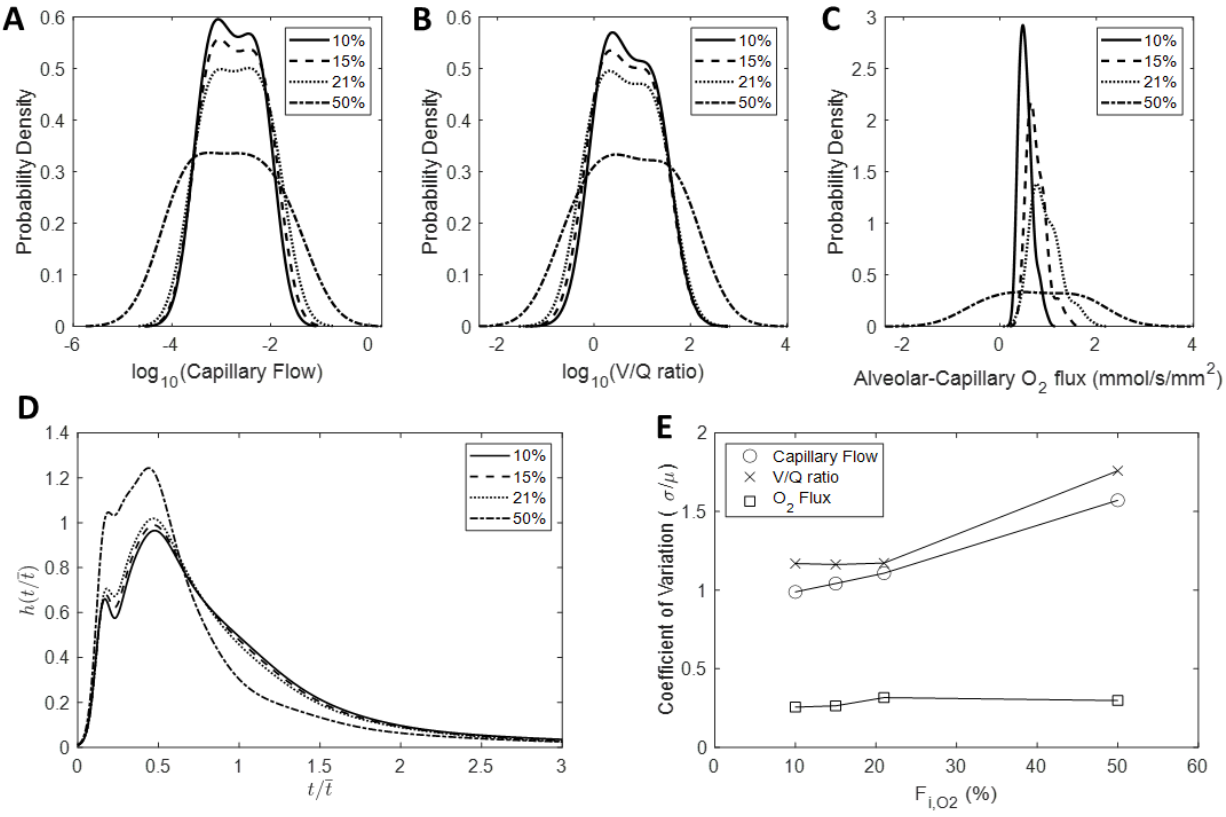
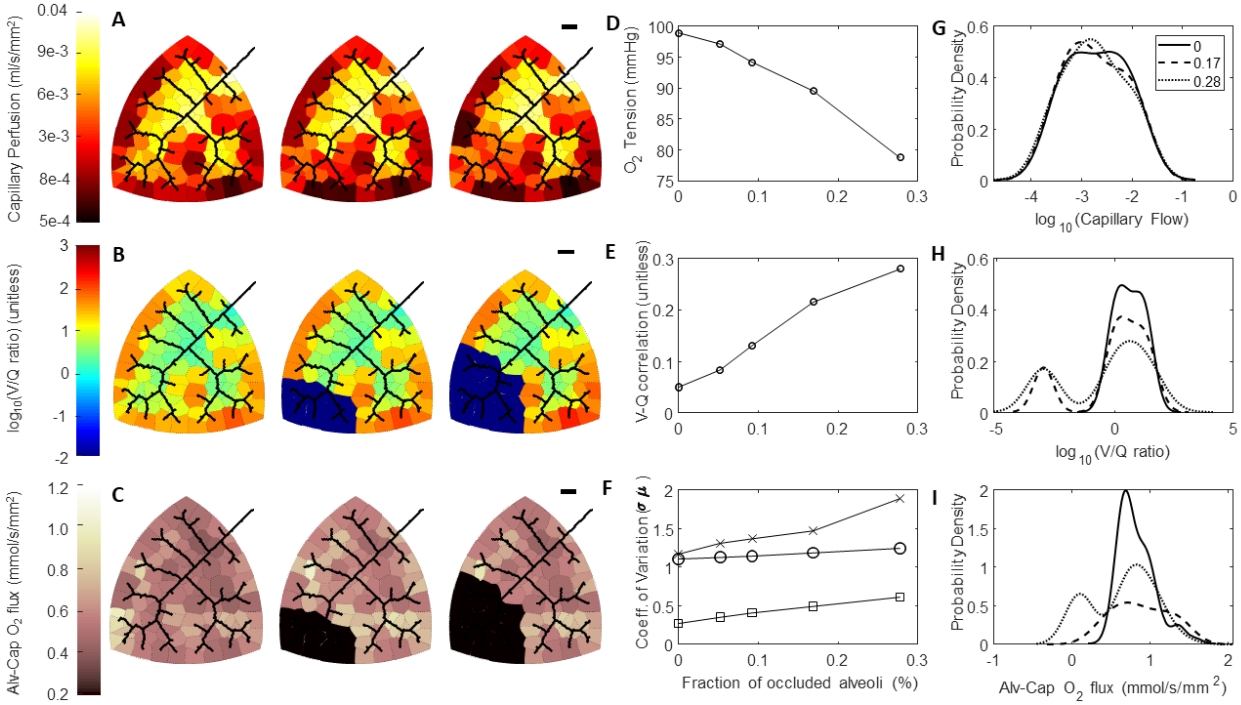


Figure 3.10 ***Effect of airway occlusions on HPV-mediated redistributions in hemodynamics, V/Q matching, and oxygen flux.*** *(A-C) Leftmost column of networks are with 0% of the alveoli occluded, middle column of networks are with 17% of the alveoli occluded, and the rightmost column of networks are with 28% of the alveoli occluded. The first airway occlusion is at the most southwestern perfusion zone, and progressive airway occlusions are made following the structure of the vascular network. The black scale bar is 1000 μm. (A) Perfusion in the capillary compartment; (B) Ventilation-Perfusion (V/Q) ratios in the capillary compartment; (C) Oxygen flux in the capillary compartments; (D) End-venous oxygen tension as a function of the fraction of occluded alveoli; (E); Pearson correlation between ventilation and perfusion as a function of the fraction of occluded alveoli; (F) Coefficient of Variation for blood flow (circles), V/Q ratios (x's), and oxygen flux (squares); (G) Distribution of blood flow; (H) Distribution of V/Q ratios; (G) Distribution of oxygen flux.*



Chapter 4 How Different Oxygen Sensor Locations for Hypoxic Pulmonary Vasoconstriction affect Blood Flow, V/Q ratio, and Oxygen Flux Distribution

4.1 Acknowledgements

This chapter is undergoing peer-review to be published as an academic journal article. Special thank you to my co-authors David J. Pinsky and Daniel A. Beard.

4.2 Abstract

Hypoxic pulmonary vasoconstriction (HPV) is a physiological regulatory mechanism where upstream pulmonary arteries vasoconstrict in response to alveolar hypoxia. Despite a tremendous amount of research to ascertain the cellular and molecular basis of this phenomenon, it remains elusive and controversial. In this study we use a previously published computational model of ventilation-perfusion (V/Q) matching to simulate how two proposed mechanisms of HPV can redistribute blood flow, V/Q ratios, and regional oxygen flux. One mechanism assumes that pulmonary arteries directly sense oxygen in adjacent alveoli (regional oxygen sensing), and the other assumes that the oxygen sensor lies at the alveolar-capillary oxygen which initiates a conducted wave of depolarization that travels through the endothelium to the upstream pulmonary arteries (conducted vascular responses). Our model simulations predict that (1) both conducted vascular responses and regional oxygen sensing can redistribute blood flow, improve V/Q matching, and oxygenation of bloodstream; (2) at baseline, the conducted vascular response mechanism does a better job at oxygenating the blood stream by altering the distribution of blood flow as the regional oxygen sensing mechanism behaves similarly to uniformly constricting

every artery; and (3) in response to occlusions of the airway, the regional oxygen sensing mechanism does a better job at diverting blood flow away from the under ventilated region of the lungs and maintain oxygenation of the bloodstream compared to the conducted vascular response mechanism. Based on these model simulations, we propose that it is possible both oxygen sensing mechanisms underly and potentially interact to produce the integrated function of hypoxic pulmonary vasoconstriction.

4.3 Introduction

Hypoxic pulmonary vasoconstriction (HPV) is a physiological mechanism wherein pulmonary arteries vasoconstrict in response to alveolar hypoxia (8). This mechanism is understood to redistribute pulmonary blood flow to areas of the lung that are adequately ventilated and operates to maintains adequate oxygenation of the bloodstream. In clinical settings HPV's function is known to affect ventilation-perfusion (V/Q) matching, which refers to the overlap of airflow and blood flow within the lungs and is known to be a critical determinant of gas exchange efficiency (1,2). Despite this mechanism being first observed in 1946 and more than 75 years of research the identity of the governing molecular pathways mediating this mechanism remain elusive and controversial (9). Many studies have identified pulmonary arterial smooth muscle cells (PASMC) as the functional mediator of vasoconstriction, and many unique oxygen-sensitive features of PASMC biology have been hypothesized to be important for HPV. Some hypotheses include mitochondrial redox products from electron transport chain (ETC) complexes inhibit the activity of Kv channel currents (92,218), others hypothesis include the activity of many types (L-type, store-operated calcium entry, TRPC6, etc.) of calcium channels (69,219), and more include various combinations and sequences of interactions between these biomolecular entities (65,89). A more recent study by Wang et al postulates a unique hypothesis

for HPV not originating within PASMCs (120). They propose that oxygen sensing originates at the level of the alveolar-capillary interface, wherein some oxygen sensor initiates a conducted wave of depolarization that travels through the endothelium to the upstream pulmonary arteries and then induces vasoconstriction. This study identifies connexin-40 hemichannels as the unique gap junction that could be responsible, and follow-up studies from this group implicate neutral sphingomyelinase as the upstream oxygen sensor (122).

The goal of this study is to test how an HPV mechanism based on (a) oxygen sensing at the PASMC level versus (b) oxygen sensing at the alveolar-capillary level can affect changes in pulmonary blood flow distribution, V/Q matching, and oxygenation of the blood stream. These two mechanisms are compared to each other using a previously published computational model of V/Q matching (170). The model used includes representations of spatially distributed vascular networks, vascular fluid and wall mechanics coupled to the airway, oxygen transport accounting for oxyhemoglobin binding, and empirical implementations of HPV. We test these two mechanisms by simulating regional decrease in ventilation as if an airway collapsed or became occluded (220) and determining how effective they are at maintaining oxygenation of pulmonary venous outflow. Our model simulations predict that both locations of oxygen-sensing can alter the distribution of blood flow, V/Q matching, and improve oxygenation. The redistributions from the model based on sensing oxygen at the level of PASMCs are similar to a control simulation where every vessel segment is maximally vasoconstricted; unlike the model based on conducted vascular responses which robustly homogenize the regional distribution of blood flow and V/Q ratios. However, when challenged with an airway occlusion perturbation, the model based on oxygen sensing at the level of the PASMC does a better job than the model based on oxygen

sensing at the level of the alveolar-capillary interface at maintaining oxygenation of the blood stream.

4.4 Methods

4.4.1 Model of V/Q matching

The details of our computational model of ventilation-perfusion matching can be found in our previously published study (170) (Chapter 3). This study includes the details of how the model is derived and verified. For the sake of brevity, details excluded from this present study include how spatially distributed vascular networks are generated and radius and length are assigned to each vessel; how compartmental vascular fluid and wall mechanics based on electrical circuits are implemented; and the mass balance underlying oxygen transport that accounts for oxyhemoglobin binding.

4.4.2 Models of HPV

Figure 4.1 illustrates the two putative HPV mechanisms we consider in this study.

Alveolar-capillary oxygen sensing

This representation of hypoxic pulmonary vasoconstriction (HPV) is inspired by Wang et al. (120), in which they demonstrate that connexin-40 gap junctions facilitate the transduction of a wave of depolarization from the alveolar-capillary boundary upstream to the arterioles and arteries. This model was originally derived in implemented in our previous study (170) and is included here for completeness.

For the i'th perfusion zone, the HPV signal generated by the oxygen content in the alveoli is represented by

$$S_i = \exp\left(\frac{-P_{alv,O2,i}}{P_{HPV}}\right), \quad \text{Eqn. (1)}$$

where S_i is a unitless signal, $P_{alv,O2,i}$ is the oxygen tension in the alveolar space of i'th perfusion zone, and P_{HPV} is a parameter representing the sensitivity of HPV to oxygen partial pressure in the alveolar space. An implicit assumption built into equation (1) is that HPV senses and generates a signal across all possible values of $P_{alv,O2,i}$. The exponential form of equation (1) was chosen so that S_i was strictly positive and decreasing as a function of alveolar oxygen. In other words, the less oxygen in the alveolar space, the greater the HPV signal, S_i. The target tone of the j'th arterial segment is given by

$$T_{j,\infty} = \left(\sum_{k=1}^{N_k} S_k \exp\left[-\frac{l_k}{\lambda}\right]\right)(T_{Max} - T_{min}) + T_{min} \quad \text{Eqn. (2)}$$

where N_k is the number of perfusion zones that the j'th arterial segment feeds into, k is the index of those perfusion zones, l_k is the path length from the perfusion zone to the mid-line of the j'th segment, λ is a length constant governing the spatial decay of the transduced signal, and T_{Max} and T_{min} are unitless scaling parameters. The summation in equation (2) represents the cumulative HPV signal in the j-th vessel segment influenced by the k-many downstream perfusion zones. The strengths of the HPV signals, S_k, are weighted by an exponential spatial decay of signal strength along the length of the signal. This exponential functional form is justified by experimental studies on conducted vascular responses (201,202). The cumulative HPV signal is re-scaled by T_{Max} and T_{min} so that these parameters define the upper and lower bounds of the target vessel tone, $T_{j,\infty}$. The instantaneous tone of the j'th arterial segment is governed by first order linear filter

$$\tau \frac{dT_j}{dt} = T_{j,\infty} - T_j \quad \text{Eqn. (3)}$$

where τ is a time constant. Equation (3) operates as a linear filter to smoothly relax the instantaneous vessel tone, T_j, toward the target vessel tone, $T_{j,\infty}$. The vessel tone variable T_j is assumed to govern arterial vessel diameter (resistance) and stiffness. This is incorporated into a lumped-parameter vascular mechanics framework by adjusting the resistances and compliances of each arterial vessel segment by

$$R_j = R_{0,j} T_j, \text{ and} \quad \text{Eqn. (4)}$$

$$C_j = \frac{C_{0,j}}{T_j}, \quad \text{Eqn. (5)}$$

where R_j and C_j are the resistance and compliance of the j'th segment, and $R_{0,j}$ and $C_{0,j}$ are the corresponding fixed nominal estimates of those parameters. The motivation behind the functional forms of equations (4) and (5) is that an increased vessel tone will increase vascular resistance and decrease the vessel compliance (increase stiffness) simultaneously. The vessel-wall resistance $R_{D,j}$ is computed by

$$R_{D,j} = \frac{v}{C_j} \quad \text{Eqn. (6)}$$

where v is the constant vessel relaxation speed and is recomputed whenever C_j is altered by the action of HPV.

Regional oxygen sensing

This representation of HPV is broadly inspired by the broad hypothesis that pulmonary arteries directly sense the oxygen in adjacent alveoli and is implemented in a manner similar to conducted vascular response model. For the j'th vessel segment, the HPV signal is represented by

$$S_j = \exp\left(\frac{-P_{alv,O2,near}}{P_{HPV}}\right), \quad \text{Eqn. (7)}$$

where $P_{alv,O2,near}$ is the oxygen tension of the nearest alveoli. We determine the nearest alveoli by each calculating the mid-point of each vessel segment and then identify the perfusion zone that mid-point is located in. The target tone of the j'th arterial segment is given by

$$T_{j,\infty} = S_j(T_{Max} - T_{min}) + T_{min}. \quad \text{Eqn. (8)}$$

This is incorporated into our lumped-parameter vascular mechanics framework by adjusting the resistances and compliances of each arterial vessel segment as shown in equations (4-6).

4.4.3 Model parameterization

To calibrate our models, we compare our simulations to human experiments done by Cheng et al, in which they measure pulmonary arterial pressure, ventilation, cardiac output, and systemic arterial oxygen partial pressure while inspiring normal (21% O2, 5% CO2) or hypoxic (10% O2, 5% CO2) air (206). We re-scale the human valued cardiac output and ventilation measurements to reflect that of an adult rat (350 g, 80 mL/min) so that

$$Q_P^* = Q_{P,Cheng}\frac{CO_{Rat,ref}}{CO_{Human,ref}} \text{ and,} \quad \text{Eqn. (9)}$$

$$Q_V^* = Q_{V,Cheng}\frac{CO_{Rat,ref}}{CO_{Human,ref}} \quad \text{Eqn. (10)}$$

Where Q_P^* and Q_V^* are the magnitude of total blood flow and ventilation through the model respectively, $Q_{P,Cheng}$ and $Q_{V,Cheng}$ are the cardiac output and ventilation data from Cheng et al respectively, $CO_{Rat,ref}$ is a reference value for the basal cardiac output of an adult rat, and $CO_{Human,ref}$ is a reference value for the basal cardiac output of an adult human (5 L/min). We note that the hypoxia exposure activates the chemoreflex and local metabolism-mediated

vasodilation to increase cardiac output. Thus, there is a change in the total flowrate through the pulmonary circulation independent of the action of HPV or other oxygen-sensitive pulmonary vasoregulation. We use the cardiac output, ventilation, and pulmonary arterial pressure measurements from Cheng et al. as boundary conditions (data inputs) for our model simulations and compare the oxygen partial pressure in the primary vein of our model to the systemic arterial oxygen blood gas measurements from Cheng et al. (206).

In our previous study we also estimated the parameter T_{min} and T_{Max}, however this parameter robustly converged to 0.5 and 1.5 respectively, so we fixed them at these values. The one parameter we estimate is the apparent oxygen diffusivity (D_{O2} - ml/s) as it is an empirical quantity.

We calibrate the model prediction of blood oxygenation by optimizing D_{O2} by hand. This is done so by minimizing the objective function

$$J = \sum_{i=1}^{2} \left(P_{O2,D,i} - P_{O2,M,i}\right)^2, \quad \text{Eqn. (11)}$$

where $P_{O2,D}$ and $P_{O2,M}$ denote the data from Cheng et al. and model prediction of oxygen tension in the primary vein respectively. i = 1 is the normoxia condition, and i = 2 is the hypoxia condition. The model is solved over 120 respiratory cycles and the primary vein oxygen tension is averaged over the last 2 respiratory cycles. For the conducted vascular response HPV model, we find $D_{O2} = 3.36$, and for the regional oxygen sensing HPV model we find $D_{O2} = 1.70$ to be the values that best fit the data from Cheng et al.

4.5 Results

4.5.1 Effect of HPV mechanisms on regional hemodynamics

We compare simulations of the two HPV models with the context of control model simulations – a negative without any form of regulation an HPV mechanism and a positive where uniform vasoconstriction (UVC) is applied by setting $T_{j,\infty}$ to T_{max} for every segment in the model. These simulations where run with a uniform airflow distribution (each alveolar compartment receives airflow that is proportional to its size). Figure 4.2 depicts the tone (T) from our HPV models in each vessel segment. One can appreciate that when looking from distal to proximal segments, the conducted vascular response mechanism tends to decrease, whereas the regional oxygen sensing mechanism increases. In the absence of regulation by HPV, our model predicts that shorter path lengths tend to have greater flow compared to longer path lengths as shown in Figure 4.3A. The UVC simulation reduces the total flow through the network, but the distribution of flow is similar to the simulation run without regulation from HPV but shifted to lower flows. Both HPV mechanism simulations alter the distribution of flow, which is summarized by the reduced coefficient of variation for capillary blood flow in Table 4.1. However, we can see in Figure 4.3E that the conducted vascular response mechanism robustly homogenizes the distribution of flow compared to regional oxygen sensing mechanism.

Another way to interrogate the hemodynamic effects of HPV is to observe the red blood cell (RBC) transit time distribution. Experimentally, the RBC transit time distribution can be measured via an indicator-dilution experiment. In these experiments a vascular bed with a defined single inlet and outlet is identified. Then the inlet is then perfused with a bolus of tracer dye (ex: Evan's Blue, FITC conjugated dextran), and then the washout is measured at the outlet (209). The time series of tracer dye concentration at the inlet, $C_{in}(t)$ and concentration at the outlet, $C_{out}(t)$, are related by

$$C_{out}(t) = C_{in}(t) * h(t) = \int_0^\infty C_{in}(s)h(t-s)ds \quad \text{Eqn. (12)}$$

where $*$ is the convolution operator, and $h(t)$ is a probability distribution of times it could take for an RBC to traverse the vascular bed. Figure 4.3F shows the RBC transit time distributions for each of our model simulations. This panel shows that in the absence of regulation by HPV our model networks have some paths that are highly perfused and other paths that are barely perfused at all, and how the action of HPV from both mechanisms homogenizes $h(t)$ and increases the mean transit time. We emphasize that an increased transit time implies that an RBC will have more opportunity to acquire oxygen as it traverses the pulmonary circulation. While both HPV mechanisms do increase the average RBC transit time, the effect from the conducted vascular response mechanism is slightly more compared to the regional oxygen sensing mechanism.

4.5.2 Effect of HPV mechanisms on V/Q matching and regional alveolar-capillary oxygen flux

The effect of more evenly distributing capillary blood flow and RBC transit times is that V/Q matching becomes more homogenous as the whole organ coefficient of variation decreases as shown in Table 4.1 and illustrated in Figure 4.4. Compared to the simulation run without regulation from HPV, UVC shifts the V/Q ratio to the right – reflecting that there are more perfusion zones with large V/Q ratios (due to low blood flow) under this condition. While the conducted vascular response mechanism robustly homogenizes the V/Q ratio distribution, the regional oxygen sensing mechanism does not and somewhat resemble the behavior of the UVC simulation – there is a shift toward large V/Q ratios, but not as many or as extreme as UVC. Moreover, the larger context of V/Q matching is how it affects regional alveolar-capillary

oxygen flux. In Figure 4.5 one can appreciate that both HPV mechanisms increase the whole-organ oxygen transport into the bloodstream, and the end total amount of oxygen in the pulmonary venous outflow. These results are summarized in Table 4.1.

4.5.3 Effect of airway occlusions on HPV-mediated redistributions in hemodynamics, V/Q matching, and regional alveolar-capillary oxygen flux

Since HPV is understood to direct blood flow away from regions of the lungs that are under ventilated and have poor oxygen supply, we benchmark the behavior of both HPV models by setting alveolar airflows to zero to emulate a collapsed or occluded airway. For these simulations we hold the bulk airflow constant so that occluding a single alveolus will result in an increased airflow to all unconcluded alveoli. Figure 4.6 illustrates how we occlude the airway of the most southwestern perfusion zone, and progressively occlude more perfusion zones following the structure of the vascular network. In Figure 4.7 we depict the tone from our HPV models (T) for each vessel segment in response to airway occlusions. One can appreciate that the regional oxygen sensing mechanism has maximal tone in vessel segments in regions of the lung where the airway is occluded, whereas the conducted vascular response mechanism has limited transduction of tone to upstream segments. In Figure 4.8 we can see how both HPV mechanisms direct blood flow away from the regions with occluded alveoli, however the regional oxygen sensing mechanism appears to do a better job of directing blood flow away from the occluded airways. Airway occlusions produce bimodal V/Q ratios and oxygen flux probability densities shown in Figures 4.9G and 4.10G respectively. Perhaps most importantly, as the fraction of occluded alveoli increases there is a gradual decrease in the end-venous oxygen tension (Figure 4.11). Interestingly, the regional oxygen-sensing mechanism is better able to maintain stable

oxygenation compared to the conducted vascular response as more and more of the airway is occluded. Table 4.2 summarizes the results of these airway occlusion simulations.

4.6 Discussion

4.6.1 Conducted vascular response versus regional oxygen sensing as putative mechanisms underlying HPV

Regarding the cellular and molecular basis of the HPV, arguably the dominant hypothesis the field broadly accepts is that PASMCs within pulmonary resistance arteries directly sense the oxygen of adjacent alveoli (92). A more recent hypothesis is that the oxygen sensor underlying HPV lies at or near the alveolar-capillary interface and a wave of depolarization is propagated upstream through the endothelium to corresponding upstream arteries (120). The computational analysis in this present study is not sufficient to make any claims about the validity of molecular limitations of these research efforts, however a broad criticism we can make of the field is most of these studies use patch-clamped PASMCs (114), isolated pulmonary arteries (221), or isolated-ventilated-perfused lungs (65) as their functional assessment of vasoconstriction in HPV. These assays and modes of measurement are certainly valuable, have provided critical insight, and will continue to provide insight, but they all fail to capture the system-level function of HPV – to affect the distribution of blood flow in order to optimize V/Q matching and oxygen uptake.

This present study leverages a previously published integrated model of distributed gas exchange and regional blood flow control to understand how different mechanisms that could underly HPV would affect system-level function of V/Q matching and oxygenation of the bloodstream. We have derived and implemented empirical versions of both regional oxygen sensing and conducted vascular response mechanisms within the framework of our multiscale

model of V/Q matching. The results of our model simulations with these two mechanisms complicates our understanding of HPV. Under baseline conditions, it appears that the conducted vascular response mechanism does a better job than regional oxygen sensing at redistributing blood flow and V/Q ratios in a manner that is distinct from uniform vasoconstriction. However, when these models are challenged with occlusions of the airway the regional oxygen sensing mechanism appears to do a better job as directing blood flow away from the under ventilated region of the lung and maintaining oxygenation of the bloodstream. Based on these conflicting results, we posit that it is possible that both mechanisms are valid and potentially intersect to produce the integrated function of HPV in real lungs. Bakhramov et al demonstrated that PASMCs only exhibit hypoxia-dependent vasoconstriction when they are depolarized (78). Perhaps conducted waves of depolarization acts a permissive signal for hypoxia-dependent molecular events in PASMCs to fully manifest as vasoconstriction? To put another way, the molecular basis of HPV could operate based on a multi-checkpoint system with oxygen sensing occurring at multiple locations and then converge on PASMCs as the effector of vasoconstriction. In Figure 4.12, we depict how a multi-checkpoint system could potentially operate. This Figure is certainly non-exhaustive, but we have attempted to depict many ion channels and other biomolecular complexes that have been implicated as potential integrators of HPV.

4.6.2 Modeling limitations

The empirical implementations of both HPV mechanisms in this study are simplifications of how HPV works in real lungs. The signal variable, S, we use could potentially be interpreted as membrane potential, but there are certainly more robust ways to represent this electrophysiology, such as the cable equation (222). Despite this limitation, these empirical

models serve as conceptual steppingstones and challenge the field of view V/Q matching the function of HPV from systems perspective. Along this line, to adequately assess our hypothesis that HPV operates as a multi-checkpoint system a biophysical rather than empirical model of pulmonary endothelial and SMC electrophysiology will likely be necessary. However, developing such a model is constrained by lack of spatial and temporal data of electrochemical and molecular events throughout the lungs – not to mentions measurements of blood flow distribution and V/Q ratios. This is perhaps the largest limitation of our empirical HPV models and our multiscale multi-physics model of V/Q matching – generating the necessary biological data that are spatially and temporally resolved to validate and/or scrutinize them.

4.6.3 Summary

In conclusion, we use an integrative computational model of V/Q matching to explore how different molecular mechanisms of HPV could affect the distribution of blood flow, V/Q ratios, and oxygenation. Our model simulations predict that (1) both conducted vascular responses and regional oxygen sensing can redistribute blood flow, improve V/Q matching, and oxygenation of bloodstream; (2) at baseline, the conducted vascular response mechanism does a better job at oxygenating the blood stream by altering the distribution of blood flow as the regional oxygen sensing mechanism behaves similarly to uniformly constricting every artery; and (3) in response to occlusions of the airway, the regional oxygen sensing mechanism does a better job at diverting blood flow away from the under ventilated region of the lungs and maintain oxygenation of the bloodstream compared to the conducted vascular response mechanism. Based on these model simulations, we propose that it is possible both oxygen sensing mechanisms underly and potentially interact to produce the integrated function of hypoxic pulmonary vasoconstriction.

Table 4.1 ***Effect of HPV on regional flow, V/Q matching, and oxygenation.*** *Model simulations were performed without regulation form HPV, with uniform vasoconstriction (UVC), and two implementations of HPV – one mediated by conducted vascular responses and the other by regional oxygen sensing. The top block summarizes how HPV and uniform vasoconstriction (UVC) affects the total flow through the organ, and the variability of blood flow, and V/Q ratios by the coefficient of variation (CV= μ/σ). The bottom block summarizes how HPV impacts the oxygenation in terms of the total alveolar alveolar-capillary oxygen flux, oxygen mass flux CV, oxygen mass flux normalized to total oxygen flux, venous oxygen tension, and venous oxyhemoglobin saturation.*

	w/o HPV	**UVC**	**Conducted**	**Regional**
Total Flow (ml/s)	1.09	0.26	0.33	0.24
Total Resistance (s × mmHg/ml)	28.39	118.79	93.70	128.71
Flow CV	2.48	2.42	1.16	1.69
V/Q CV	5.32	7.70	1.22	3.93
Total Alv-cap O_2 flux (mmol/s)	4.44	4.51	11.21	6.25
Alv-cap O_2 flux CV	0.25	0.26	0.25	0.21
O_2 flux CV/Total O_2 flux (s/mol)	57.41	58.02	22.67	49.54
Venous O_2 (mmHg)	55.50	75.90	100.86	93.00
Venous O_2 (%)	0.75	0.87	0.96	0.96

Table 4.2 ***Comparing the effects of two putative HPV mechanisms on regional flow, V/Q matching, and oxygenation in response to airway occlusions.*** *Model simulations were performed with two implementations of HPV – one mediated by conducted vascular responses and the other by regional oxygen sensing. The "Baseline" columns refer to simulations run without airway occlusions, and the "Occluded" columns refer to simulations run with the airway occluded (28%). The top block summarizes how HPV and uniform vasoconstriction (UVC) affects the total flow through the organ, and the variability of blood flow, and V/Q ratios by the coefficient of variation (CV= μ/σ). The bottom block summarizes how HPV impacts the oxygenation in terms of the total alveolar alveolar-capillary oxygen flux, oxygen mass flux CV, oxygen mass flux normalized to total oxygen flux, venous oxygen tension, and venous oxyhemoglobin saturation.*

	Conducted		**Regional**	
Airway Status	**Baseline**	**Occluded**	**Baseline**	**Occluded**
Total Flow (ml/s)	0.33	0.34	0.24	0.25
Total Resistance (mmHg/ml)	93.70	91.56	128.71	1.21×10^2
Flow CV	1.16	1.30	1.69	1.83
V/Q CV	1.22	2.01	3.93	3.11
Total Alv-cap O_2 flux (mmol/s)	11.21	6.45	6.25	3.66
Alv-cap O_2 flux CV	0.25	0.70	0.31	0.75
O_2 flux CV/Total O_2 flux (s/mol)	22.67	109.91	49.54	206.05
Venous O_2 (mmHg)	100.86	73.32	93.00	82.45
Venous O_2 (%)	0.96	0.92	0.96	0.94

Figure 4.1 ***Putative oxygen sensing mechanisms of hypoxic pulmonary vasoconstriction (HPV)****. The left panel depicts a mechanism where oxygen sensing is located at the alveolar-capillary interface, and a wave of depolarization is transduced through the endothelium to the upstream pulmonary arteries. The right panel depicts a mechanism where pulmonary arteries directly sense the oxygen from directly adjacent alveoli.*

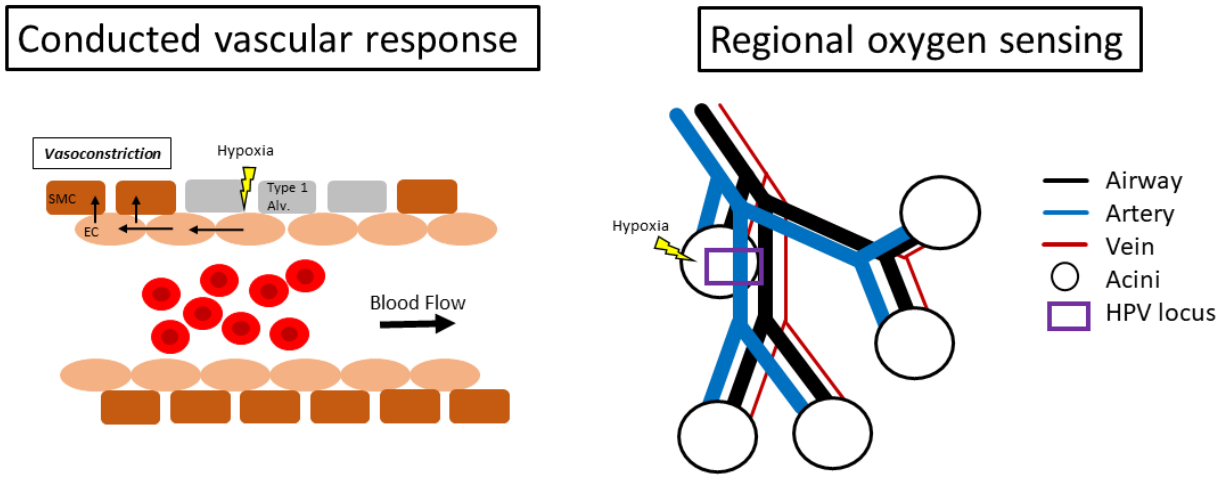


Figure 4.2 ***Distribution of vasomotor tone from HPV.*** *(A) Simulation run without regulation from HPV. (B) Simulation run with uniform vasoconstriction (UVC). (C) Simulation run with the conducted vascular response model of HPV. (D) Simulation run with the regional oxygen sensing model of HPV.*

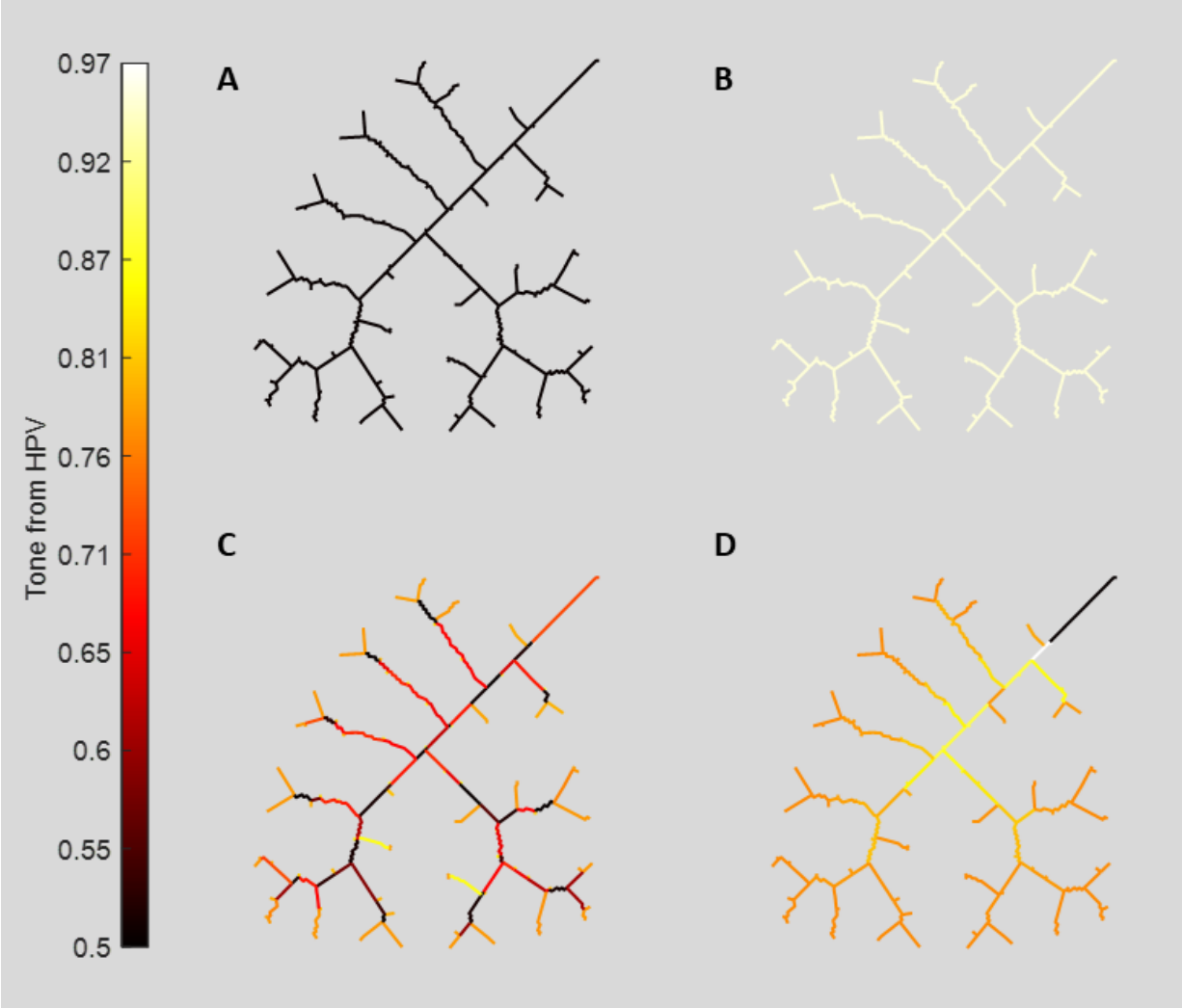


Figure 4.3 ***Effect of HPV and uniform vasoconstriction on regional perfusion.*** *(A) Simulation run without regulation from HPV. (B) Simulation run with uniform vasoconstriction (UVC). (C) Simulation run with the conducted vascular response model of HPV. (D) Simulation run with the regional oxygen sensing model of HPV. (E) Distribution of flow. (F) RBC transit times normalized to mean transit time.*

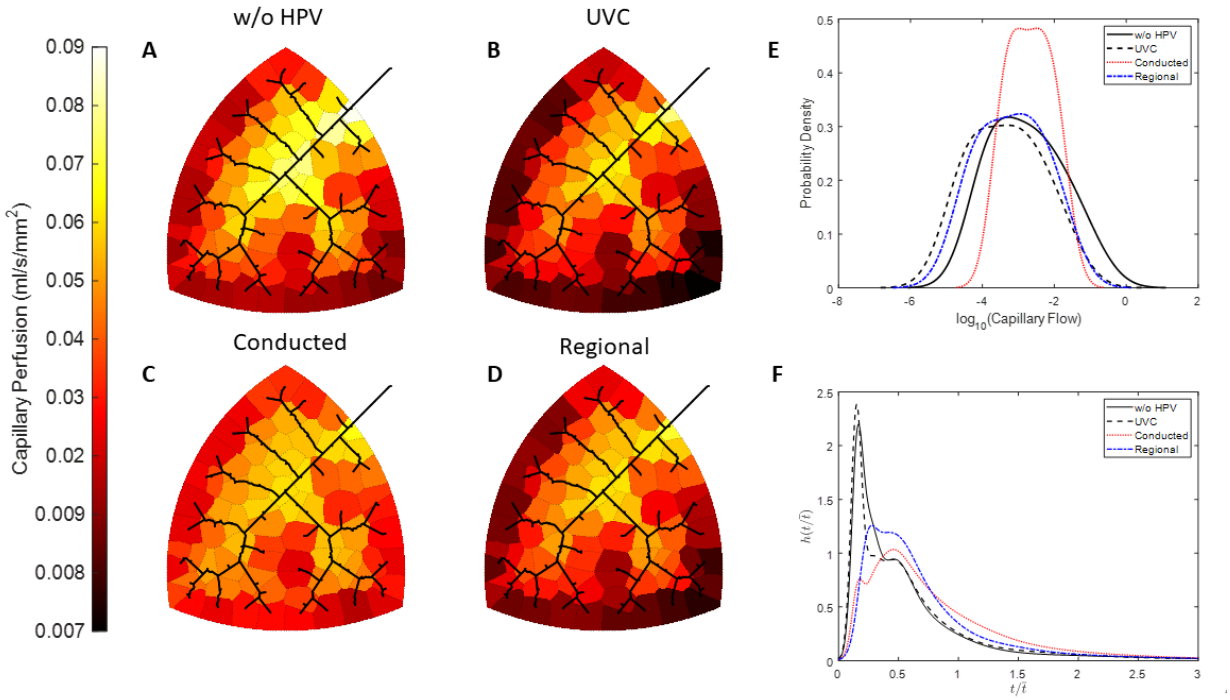


Figure 4.4 ***Effect of HPV and uniform vasoconstriction on V/Q matching.*** *(A) Simulation run without regulation from HPV. (B) Simulation run with uniform vasoconstriction (UVC). (C) Simulation run with the conducted vascular response model of HPV. (D) Simulation run with the regional oxygen sensing model of HPV. The panel of the right depicts the distribution of V/Q ratios.*

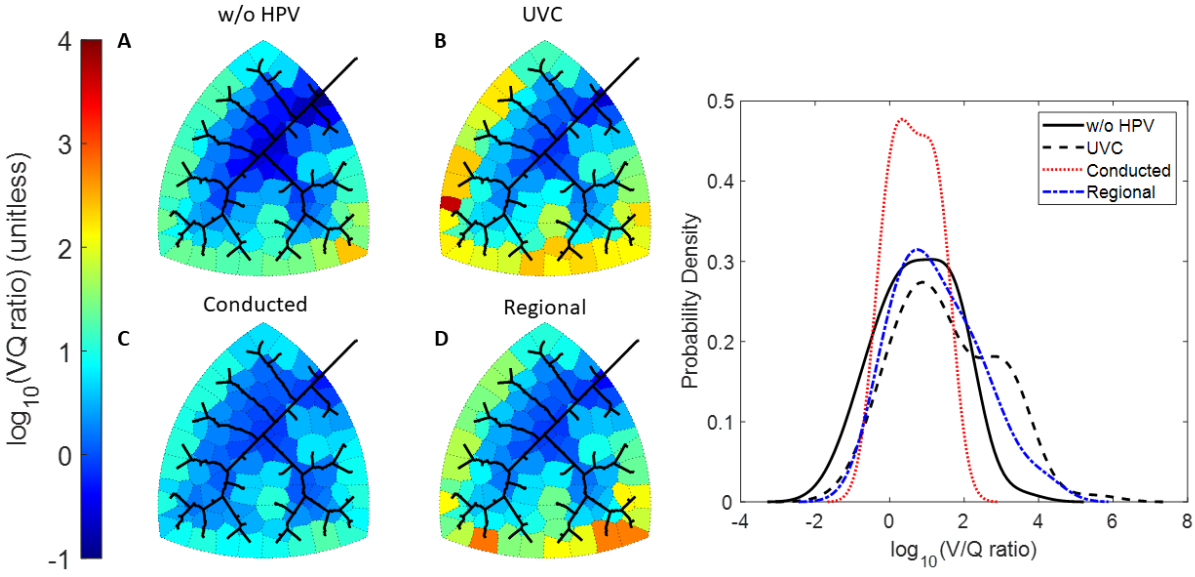


Figure 4.5 ***Effect of HPV and uniform vasoconstriction on oxygen flux.*** *(A) Simulation run without regulation from HPV. (B) Simulation run with uniform vasoconstriction (UVC). (C) Simulation run with the conducted vascular response model of HPV. (D) Simulation run with the regional oxygen sensing model of HPV. The panel of the right depicts the distribution of oxygen flux.*

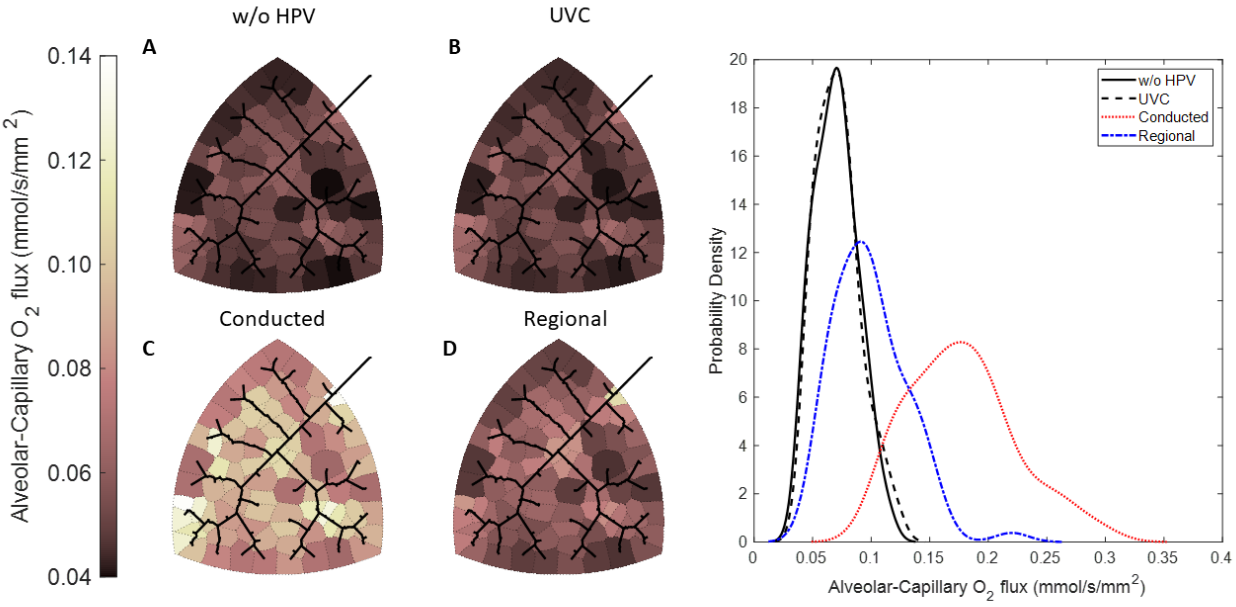


Figure 4.6 ***Strategy to progressively occlude the airway.*** *Each panel shows how airway starting at the southwest corner of the network is progressively occluded. The percentages above refer the fraction of the total airway occluded.*

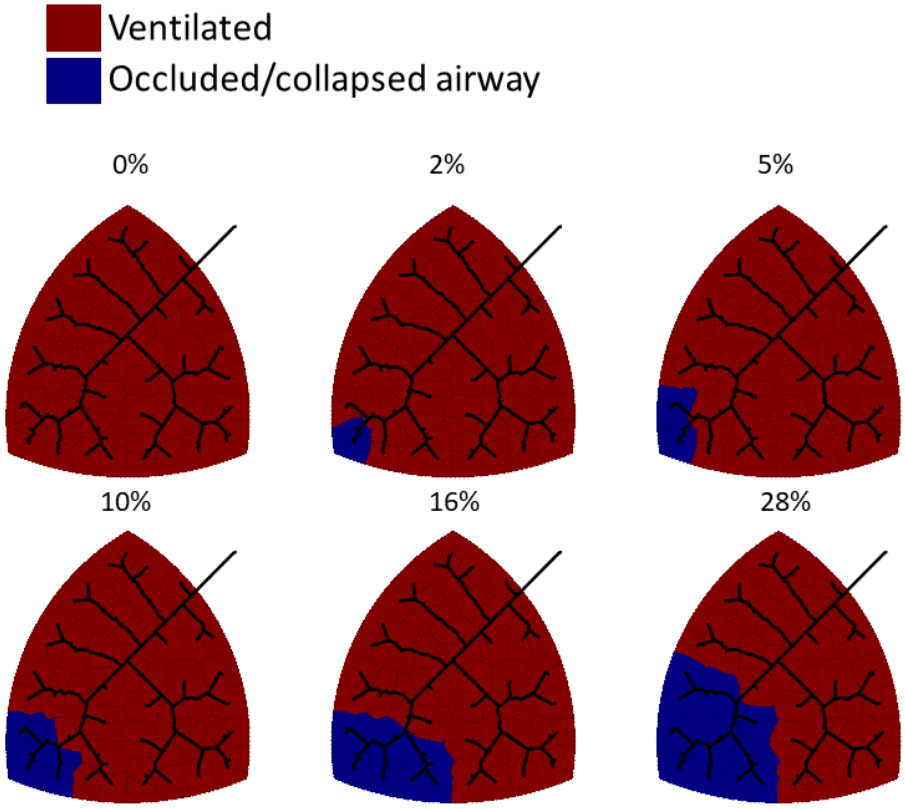


Figure 4.7 ***Effect of airway occlusions on tone from HPV.*** *(A-C) Simulations run with the conducted vascular response model of HPV. (D-F) Simulations run with the regional oxygen sensing model of HPV. (A,D) Simulations run with 0% of the airway occluded. (B,E) Simulations run with 16% of the airway occluded. (C,F) Simulations run with 28% of the airway occluded.*

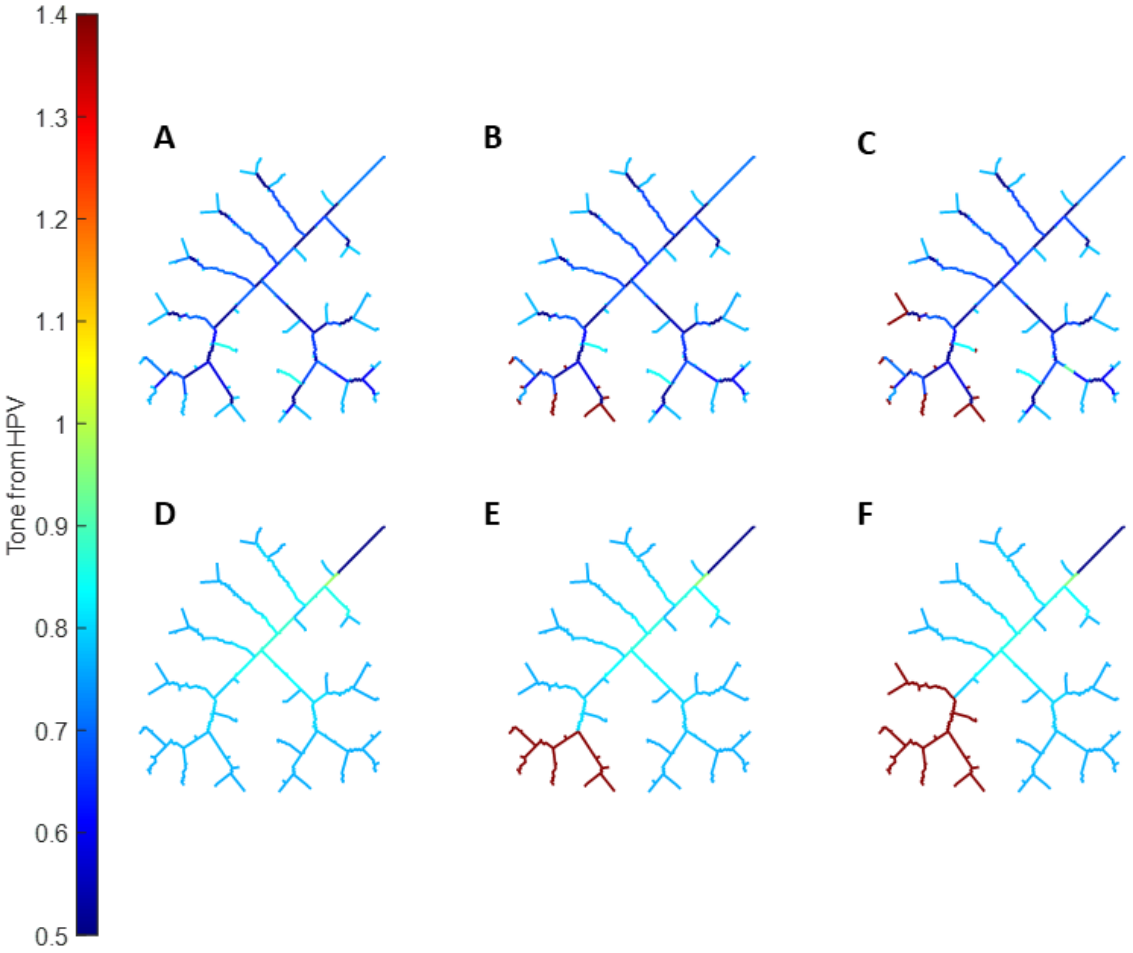


Figure 4.8 ***Effect of airway occlusions on HPV-mediated redistribution in hemodynamics.*** *(A-C) Simulations run with the conducted vascular response model of HPV. (D-F) Simulations run with the regional oxygen sensing model of HPV. (A,D) Simulations run with 0% of the airway occluded. (B,E) Simulations run with 16% of the airway occluded. (C,F) Simulations run with 28% of the airway occluded. (G) Distribution of blood flow.*

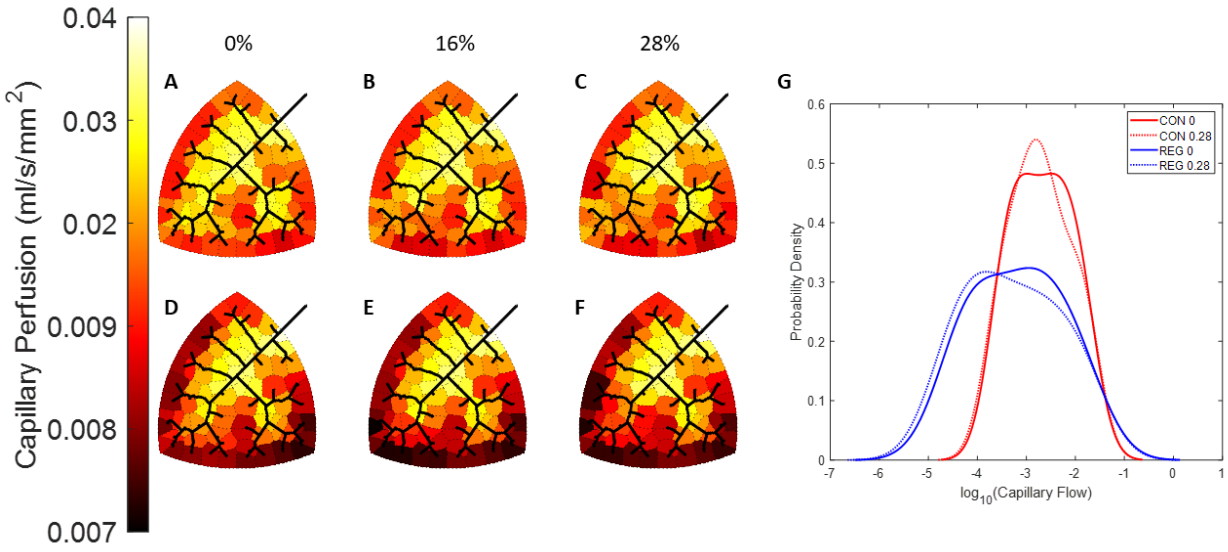


Figure 4.9 ***Effect of airway occlusions on HPV-mediated redistribution in V/Q matching.*** *(A-C) Simulations run with the conducted vascular response model of HPV. (D-F) Simulations run with the regional oxygen sensing model of HPV. (A,D) Simulations run with 0% of the airway occluded. (B,E) Simulations run with 16% of the airway occluded. (C,F) Simulations run with 28% of the airway occluded. (G) Distribution of V/Q ratios.*

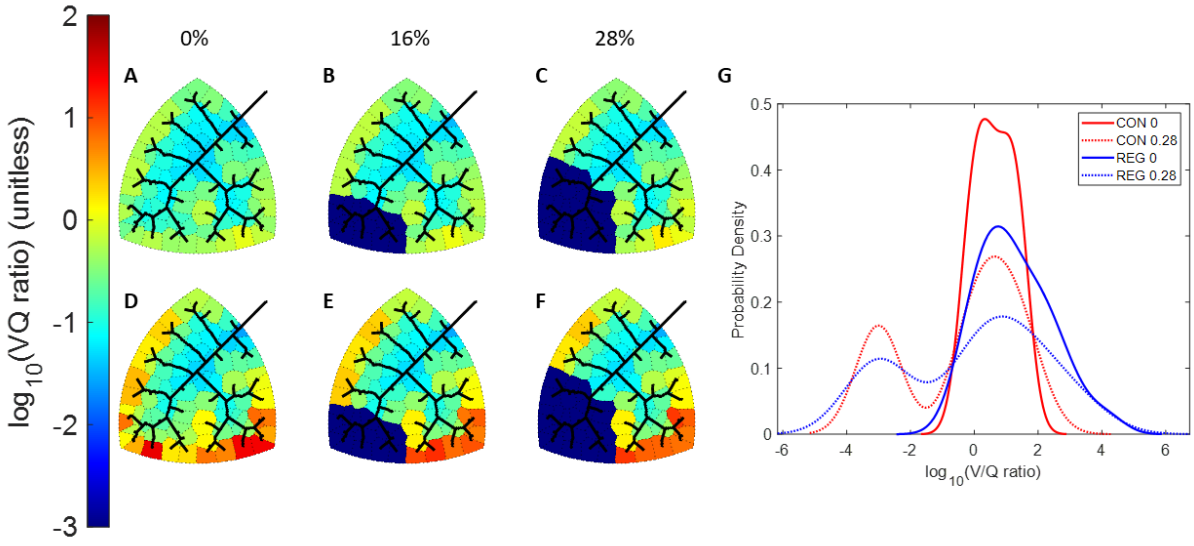


Figure 4.10 ***Effect of airway occlusions on HPV-mediated redistributions in oxygen flux.*** *(A-C) Simulations run with the conducted vascular response model of HPV. (D-F) Simulations run with the regional oxygen sensing model of HPV. (A,D) Simulations run with 0% of the airway occluded. (B,E) Simulations run with 16% of the airway occluded. (C,F) Simulations run with 28% of the airway occluded. (G) Distribution of oxygen flux.*

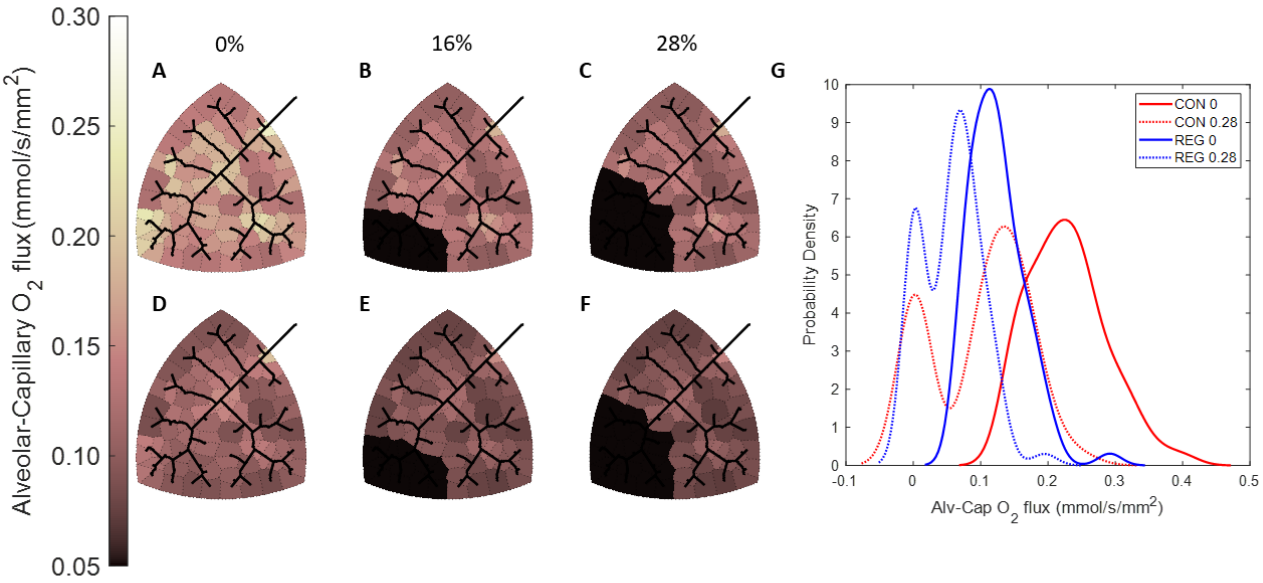


Figure 4.11 ***End-venous oxygen content as a function of the fraction of occluded alveoli.*** *(A) Oxygen tension. (B) Oxyhemoglobin saturation.*

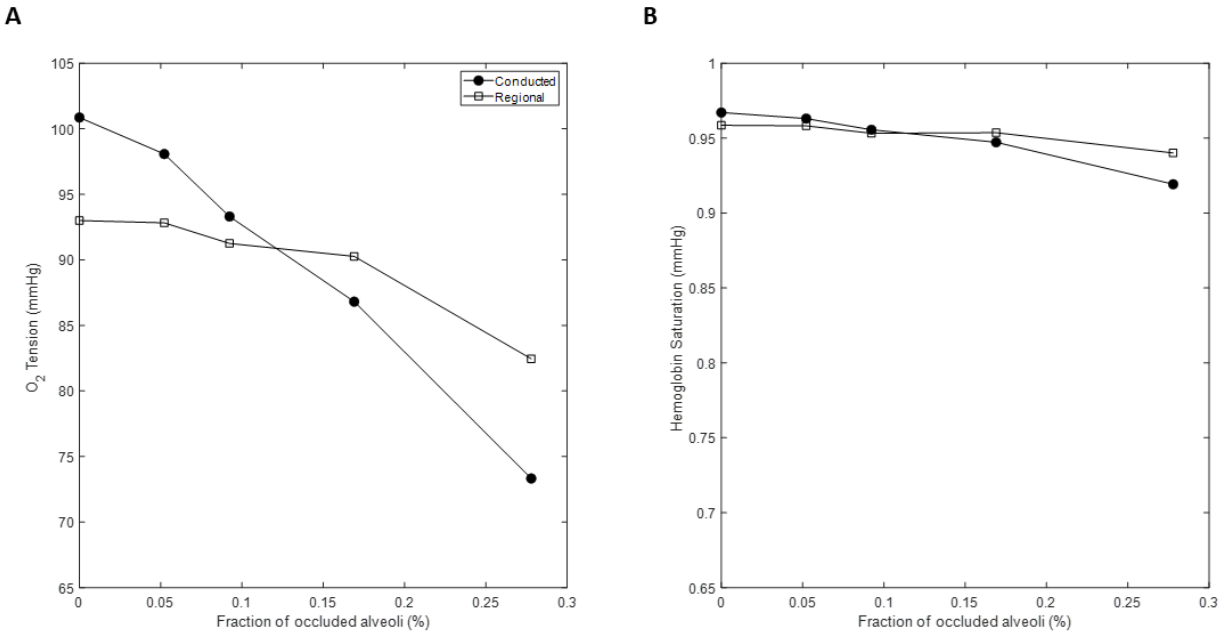
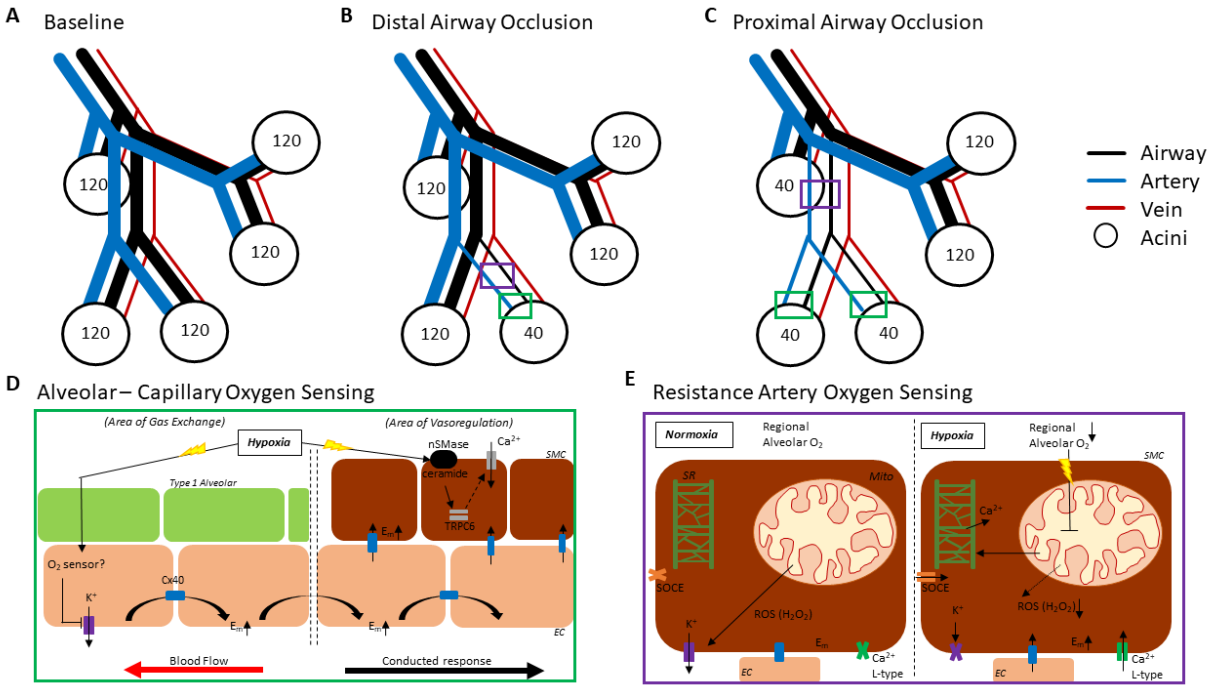


Figure 4.12 ***Proposed mechanism for HPV – multi-checkpoint system distributed throughout the tissue.*** *(A-C) Schematics of airways (black), arteries (blue), and veins (red) in the lungs. Diameter of airway and artery segments reflect flow - veins are left narrow for visual simplicity. Values within the acini are alveolar oxygen partial pressure in mmHg. (A) Baseline distribution of air and blood flow. (B) Distal segment of the airway is occluded, and HPV constricts the corresponding arterial segment. Green and purple boxes correspond to the molecular diagrams in panels D and E. (C) A more proximal segment of the airway is occluded, and HPV constricts the corresponding arterial segments. Green and purple boxes correspond to the molecular signaling diagrams in panels D and E. (D) Alveolar-capillary oxygen sensing. Hypoxia in the alveolar space stimulates a conducted vascular response that travels upstream in the oppositive direction of blood flow to depolarize PASMCs. Inhibition of Kv currents and activation of neutral sphingomyelinase (nSMase) and translocation of TRPC6 channels to PASMC membrane are potential mechanisms that operate at this spatial locus. Connexin-40 (Cx40) is the operative gap junction that transduces a wave of depolarization upstream. (E) Resistance artery oxygen sensing. Hypoxia-induced stimuli from a conducted vascular response, and/or direct oxygen sensing from the surrounding alveolar tissue drive HPV at this spatial locus. The mitochondrial ETC is inhibited by hypoxia. Decreased production of ROS, such as H_2O_2, inhibits Kv currents and further depolarizes the PASMC and activates L-type Ca^{2+} channels. A diversity of other augmented mitochondrial process are augmented which could activate the release of Ca2+ from the sarcoplasmic reticulum (SR) via IP3, ryanodine receptor, and/or store operated calcium entry (SOCE). (D-E) The signaling processes depicted are by not exhaustive, and there could be overlap of molecular events at distinct spatial locations. Ex: TRPC6 translocation could occur in PASMCs within a resistance artery*



Chapter 5 Conclusions and Roadmap for the Future

5.1 Summary

The work presented in this thesis was aimed at understanding how the distribution of ventilation-perfusion (V/Q) ratios affect pulmonary oxygen uptake and focused on how the physiological regulatory mechanism hypoxic pulmonary vasoconstriction (HPV) affects changes in blood flow distribution to maintain oxygenation of the bloodstream. *The central contribution here is a collection of computational model simulations that show the distribution of blood flow (and V/Q ratios) is an important determinant of pulmonary oxygen transport*. These model simulations are the foundation of a quantitative and mechanistic theory to understand how V/Q matching and HPV operate to ensure the bloodstream is adequately oxygenated.

In chapter 1, I reviewed what previous research efforts have revealed regarding the function and cellular/molecular basis of HPV. There has been more than 75 years of research efforts in this area which have yielded tremendous insights, however the governing molecular entities and signaling events remain elusive. In reviewing of this literature, I have identified a major gap: *many investigations do not use measurements of blood flow or V/Q ratio distributions as their functional assessment of HPV.* Isolated-ventilated-perfused organs have been used to measure whole-lung pressure-flow relationships (65), isolated vessels mounted on a myograph have been used to measure vessel diameter in response to application of exogenous stimuli (221), and patch-clamped pulmonary arterial smooth muscle cells (PASMCs) have been used to measure electrophysiological phenomena (114). These are valid, useful, and appropriate assays,

but each of them falls short in capturing and understanding the essential physiology of V/Q matching and HPV. Given the understanding that HPV operates to change the *distribution* of pulmonary blood flow to match the *distribution* of alveolar oxygen, I suggest that the field should use blood flow and/or V/Q ratio distribution measurements as the necessary evidence to uncover the molecular mechanism underlying HPV.

In chapter 2, I pose the ostensibly simple question "how does a V/Q ratio affect pulmonary oxygen uptake?" This is an important question, as to understand how the distribution of air and blood flow affect oxygen transport, as I first need to understand how V/Q matching within a single gas exchange unit operates. Intuitively, one could assume that when one refers to V/Q matching, ventilation and perfusion should be matched in a 1:1 manner and the ideal V/Q ratio is equal to one. And indeed, clinical V/Q measurements by single photon emission computed tomography (SPECT) support this intuition – however, this interpretation is confounded by the fact that V/Q ratios computed by SPECT are implicitly normalized by the maximum signal intensity of infused and inhaled tracers (147). To address this dissonance in interpretation of V/Q ratios, I analyze a series of a progressively more complicated models of pulmonary oxygen transport. This analysis reveals that V/Q ratios computing using flow rates is a non-linear relationship, and that V/Q ratios needed to adequately oxygenate the blood stream typically need to be larger than one. I posit that a physiological interpretation of idealized V/Q matching is in the algebraic form: $V = AQ/(B - CQ)$, where $A, B,$ and C are arbitrary positive real constants.

In chapter 3, I derive and make functional predictions with a multiscale multi-physics computational model of V/Q matching that includes an empirical representation of HPV. This model consists of spatially distributed vascular networks, vascular fluid and vessel wall

mechanics, and biophysical oxygen transport. This model enabled me to test the hypothesis that HPV operates to homogenize the distribution of blood flow and V/Q ratios, and that homogenizing the distribution of V/Q ratios increases net oxygen flux into the blood stream. In chapter 4, I use this model as a platform to test how two different proposed mechanisms of HPV could redistribute blood flow in response to regional occlusions of the airway. One mechanism posits that the oxygen sensor lies within PASMCs and pulmonary arteries directly sense the regional oxygen in the adjacent alveolar space (92). The other mechanism posits that the oxygen sensor is located at the alveolar-capillary interface and a wave of conducted depolarization is transduced through the endothelium to the upstream pulmonary arteries (120). Model simulations reveal that both mechanisms can affect changes in pulmonary blood flow, and the conducted vascular response mechanism appears to better oxygenate the blood stream under baseline conditions. However, when challenged with occlusions of the airway the regional oxygen sensing mechanism does a better job at redistributing blood flow away from the under ventilated regions. Based on these results, I hypothesize that both mechanisms could be operating in a synergistic manner to manifest the function of HPV.

5.2 Proposed Experimental Standard for Measuring HPV's Function

5.2.1 Defining HPV's function in terms of blood flow distribution

The central argument I make throughout this thesis is that the essential phenotype of HPV is to change pulmonary blood flow *distribution* to match the *distribution* of air flow (alveolar oxygen). The simulation results from my computational models demonstrate that different locations of oxygen sensors for HPV could differently affect *redistributions* in blood flow from perturbations like an occluded airway (chapter 4). However, my model simulations are certainly limited and demand experimental corroboration/refutation. However, the experimental systems

commonly employed in the field do not measure V/Q ratios or blood flow distribution and are therefore unable to test the hypotheses raised by my model simulations. Thus, *I propose an experimental standard for investigations of HPV's function*:

1. The operative **assay** or **metric** should be a direct measure of flow distribution (ex: SPECT) ***OR*** be defined as change in flow from one region of the lung to another (ex: diversion of blood flow from one anatomical lobe to the remainder of the organ)
2. A **baseline control** for these experiments must be a demonstration that perturbing the alveolar oxygen distribution (ex: differential ventilation of lobes by a double lumen endotracheal tube, regional occlusion of the airway by inflation of a balloon-tipped catheter) leads to a corresponding redistribution in blood flow ***AND*** that any redistribution in blood flow can be reversed by undoing the perturbation of the alveolar oxygen distribution
3. To test the contribution of a molecular entity to HPV, the **treatment group** (ex: pharmacological perturbation, recombinant genetic manipulation) should seek to reproduce the **baseline control**'s change in blood flow distribution due to the alveolar oxygen distribution perturbation; with the null hypothesis being that the treatment does not affect the control's change in blood flow distribution

These three general criteria are a framework that can be used to plan an experiment that captures the essential physiology of HPV. If the inhibition of a given molecular entity does not alter how blood flow is redistributed from a change alveolar oxygen distribution, then one can have some confidence in claiming that the molecular entity is not a direct mediator of HPV's molecular mechanism. Additionally, an experiment following these criteria should be able to thoroughly scrutinize the claims I've made based on my model simulations. To this end, I have begun to perform experiments to measure the distribution of blood flow in rat lungs by infusing

fluorescently labeled microspheres. Figure 5.1 shows a representative example of these data, and initial steps for analysis. Briefly, these data are generated by infusing 15 μm polystyrene microspheres into a rat's pulmonary arterial circulation, which then become lodged in the precapillary arterioles. The 3-dimensional location of each microsphere is recovered by an imaging cryomicrotome (212). Panels B and C of Figure 5.1 show how one can create an arbitrarily sized grid of voxels to analyze the regional properties of flow distribution.

A confounding factor experimentalist may encounter in performing these experiments is temporal dynamics and time scale of HPV's response. How long should one wait after the initial perturbation of the alveolar oxygen distribution to see a change in blood flow distribution? How long does it take for the blood flow distribution to be restored to baseline after the perturbation of the alveolar oxygen distribution has ended? How many times can one expect a single research subject (ex: mouse, rat) to experience a change in alveolar oxygen distribution without suffering physiological exhaustion that leads to an inability to redistribute blood flow? Some of these questions are partially answered by phenotypes reported in the literature – it is well appreciated HPV has both an acute (phase 1) and chronic (phase 2) response (17). Yet it will still be important to answer these practical questions in preliminary studies to perform experiments following the criteria I've listed above. Defining HPV's phenotype in terms of altered distribution of blood flow has the possibility to resolve some amount of the contentious disagreement within the field. Beyond the claims I've made based on model simulations, many of the proposed molecular integrators for HPV with conflicting evidence (ex: contribution of different mitochondrial electron transport chain complexes as oxygen sensors (86–92)) could possibly be resolved by using experiments following these criteria.

In contrast to my proposition on how to effectively measure HPV's function, I challenge the field to be skeptical about using global hypoxia and hyperoxia exposure as experimental perturbations when investigating HPV. A landmark study frequently cited in the field is from Arai et al, where they used CT scans of lungs from human subjects in response to ventilation with different fractions of inspired oxygen (171). They used hyperoxic gas mixtures as a perturbation to remove HPV from the lung and showed that hyperoxia does not significantly alter the distribution of blood flow in terms the coefficient of variation (standard deviation/mean) – a single number summary of heterogeneity. Based on this result, they claim that HPV does not contribute to the resting distribution of pulmonary blood flow, and HPV only becomes appreciable during hypoxic stress and is likely irrelevant during normoxia. Given that HPV operates to affect changes in the *regional* distribution of blood flow is response to changes in *regional* alveolar oxygen distribution, I am skeptical of *global* hyperoxia exposure being an effective perturbation to uniformly inhibit HPV. Under normoxic conditions there is heterogeneity in the distribution of airflow and oxygen in the airway. This means that it's possible vascular tone from HPV is heterogeneously dispersed throughout the pulmonary vasculature. Under global hyperoxic conditions the average oxygen content in the airway certainly increases, however the heterogeneity of the airway oxygen distribution is likely unchanged—as demonstrated by experiments where airflow distribution is measured when a pig is ventilated on different fractions of inspired oxygen (158). To state my criticisms of Arai et al's study clearly, their study used a *global* experimental perturbation (inspiration of hyperoxic/hypoxic gas) and a *global* metric of blood flow distribution (coefficient of variation) to make claims about a mechanism that is primarily operating at the *regional* level. Moreover, my model simulations shown in chapter 3 and 4 demonstrate how empirical implementations of

an HPV mechanism can affect the distribution of blood flow, V/Q ratios, and oxygen uptake under normoxic conditions. Taken together, I assert that the role of HPV during normoxic conditions remains an open question that needs further investigation.

5.2.2 Measuring the Distribution of Alveolar Oxygen Tension

An underlying theme in my proposed experimental standard to measure HPV's function is the manipulation of the alveolar oxygen distribution. While there are handful of ways one can perturb this distribution (ex: differential ventilation of lobes by a double lumen endotracheal tube, regional occlusion of the airway by inflation of a balloon-tipped catheter) with pros and cons to each, it is critical to acknowledge that alveolar oxygen tension is rarely, if not ever directly measured. The oxygen content of ambient air can and has been directly measured, and the oxygen content of oxygenated and deoxygenated blood is frequently measured in clinical settings (223). Given that the field has robust understanding of the oxygen tension in ambient air (~150 mmHg) and the bloodstream (~100 mmHg), one can reasonably conclude that alveolar oxygen must be between these two values. Yet in clinical practice, the actual oxygen tension in the alveolar space is inferred and not measured – it is determined by an empirical equation using blood carbon dioxide and pH measurements. There are potentially many limitations to this empirical manner of determining alveolar oxygen tension one could criticize, but I believe the largest one is that it is a measure of the *average* alveolar oxygen tension and gives no information about how the oxygen is *distributed* throughout the alveolar space. While radiolabeled oxygen molecules can be used as a tracer in imaging measurements like SPECT, these methods measure air flow distribution and do not provide a measure of oxygen tension (224). For many experiments investigating HPV, a direct measurement of alveolar oxygen tension distribution could be unnecessary. For example, if one completely clamped shut an

airway and observes no more inflation/deflation dynamics to that region of the lung then one can be reasonably confident that regional oxygen tension in that region has been reduced. But for some experiments investigating HPV, measurements of alveolar oxygen distribution could prove to be very valuable data. In the case of differentially ventilating regions of the lung one can control the upstream fraction of inspired oxygen, but the resultant alveolar oxygen tensions in these differentially ventilated regions are unknown. To my knowledge, there is not a standard method or technique to make measurements of alveolar oxygen distribution, and thus this technology might need to be developed to aid in conducting the types of experiments I am proposing.

5.3 Future Experiments to Corroborate/Refute Model Simulations

5.3.1 V/Q Ratios Using Flow Rates v/s Tracer Signal Intensities

In chapter 2, I analyze a series of models representing pulmonary oxygen transport and conclude that in contrast to the field's intuition, the optimal V/Q ratio to oxygenate the bloodstream is generally greater than 1. My analysis also shows that oxygenation is not only dependent upon the V/Q ratio, but also on the magnitude of air and blood flow – when oxygen demand increases in exercise, air flow must increase more than cardiac output to maintain a given level of oxygenation in the systemic arterial blood. These analyses represent a theoretical foundation to understand how V/Q matching determines pulmonary oxygen transport. However, this study is subject to limitations that demand further investigation. The models analyzed were all calibrated to the same cardiopulmonary exercise testing (CPET) data set, where ventilation and systemic arterial oxy-hemoglobin saturation as function of exercise work rate taken form O'Donnell et al (151). For the purposes of identifying model parameters and model validation,

this data set is extremely limited as these data do not cover the physiologically possible but extreme V/Q ratios. To further scrutinize the models in this study, more robust data are needed.

There are two types of experiments and corresponding data that could be generated to have more confidence in predications made from the models analyzed in chapter 2. The first experiment should make use of a an isolated-ventilated-perfused lung preparation, where the air flow and blood flow through the organ are explicitly controlled by the experimentalist and the oxygen content of the venous washout is measured. With such a preparation, one could determine the oxygenation of the blood stream for any combination of air and blood flow magnitude, and corresponding V/Q ratio. These data would be most appropriate for calibrating the open-loop model formulations. The second experiment should be a cardiopulmonary exercise testing (CPET) study, where human subjects are exercised at progressively higher work rates and total ventilation, cardiac output, both systemic and pulmonary arterial blood gases, and V/Q ratios are measured. This kind of data set would provide an understanding of how V/Q matching changes from rest to exercise, and the corresponding physiological changes in oxygen demand and consumption. These data would be most appropriate for calibrating the closed-loop model formulations. However, one caveat to this idealized experiment is that to my knowledge the technology to measure V/Q ratios in a person whilst actively exercising does not currently exist. V/Q ratio measurements using SPECT requires the subject to lay relatively still for a period, and the final measurement is averaged over the period of acquisition time (224). Assuming technology is developed in the future to measure V/Q ratios in an exercising subject, the data from such measurements would provide profound insight into the regime where these models predict that V/Q ratios significantly larger than 1 are important to maintain oxygenation.

5.3.2 Validating Multi-scale Multi-Physics Model of V/Q Matching and HPV

In chapters 3 and 4, I developed and made functional predictions with a multi-scale multi-physics model of V/Q matching governed by empirical implementations of putative HPV mechanisms proposed in the literature. Simulations with this model predict that HPV can affect the distribution of blood flow to increase regional alveolar-capillary oxygen flux and thus increase the total oxygen content in pulmonary venous outflow. This model is a conceptual platform to simulate and understand how the distribution air and blood flows, and V/Q ratios in spatially distributed networks affects oxygen transport. While the individual components of the model have been calibrated to different sources to data, this model is currently verified and not validated. Meaning that the underlying biophysics of sub-models have shown to be consistent and logically sound in isolation, however the complete model has not been appropriately compared to V/Q matching data, such as those acquired from SPECT. However, SPECT data (or V/Q matching measurements from other methods) in isolation are insufficient to validate my multi-scale multi-physics model. The ideal data set requires both V/Q ratios measurements, systemic and pulmonary arterial blood gases, AND imaging of the anatomy – namely the connectivity of the airway and vascular network – all within the same subject. I note that while methods to recover and segment the anatomical structure of the airway and vascular networks from imaging data do exist (225), these methods are non-trivial and demand substantial effort to process the raw data.

While a baseline measurement of V/Q ratios and anatomy would be sufficient to begin validating my model, additional experiments will be needed to effectively scrutinize my empirical implementations of HPV mechanisms. Specifically, an experiment following the three criteria I proposed previously on how the field should be define and measure the function of HPV. To reiterate, this experiment should perturb the distribution of alveolar oxygen (ex:

differential ventilation of lobes), and measure how the distribution of blood flow (and/or V/Q ratios) is altered by the physiological action of HPV. These data would be more than adequate to validate or refute the behavior of my multi-scale multi-physics model of V/Q matching and enable thorough scrutiny of any computational implementation of an HPV mechanism.

5.3.3 Methods to Measure Molecular Signaling Events Distributed Throughout the Lungs

In chapter 4, I use my multi-scale multi-physics model of V/Q matching to test and compare how two different proposed mechanisms for HPV could affect the distribution of flow and oxygen transport. One mechanism assumes that oxygen is regionally sensed by PASMCs from adjacent alveoli. The second mechanism assumes that oxygen sensor is located at the alveolar capillary interface and a conducted wave of depolarization through the endothelium is the critical transducer for vasoconstriction. Model simulations show that both mechanisms can increase the total oxygen content in the pulmonary venous outflow, and the conducted vascular response mechanism appears to be better than the regional oxygen sensing at oxygenating the blood stream under basal conditions. However, when the model is challenged with an occlusion of the airway, the regional oxygen sensing mechanism does a better job at diverting blood flow from the occluded region and maintaining oxygenation. Based on these results, I hypothesize that both putative mechanisms operate simultaneously in the form a multi-checkpoint system. This hypothesis is quite challenging to test, as implicit within it is the idea that that governing pathways for HPV are spatially distributed throughout the pulmonary vascular tissue, and thus spatially distributed measurements of signaling events (ex: endothelial and SMC membrane potential) would be the necessary to test my hypothesis. The ideal way to test this hypothesis would be to simultaneously measure lung anatomical structure (data input to my model), V/Q ratios (in the manner I have proposed previously) AND signaling events (ex: changes in

membrane potential) throughout the pulmonary vasculature. However, to my knowledge the technology to measure signaling events at the scale of the whole organ do not currently exist – as methods to measure membrane potential (electrophysiology), ROS signaling, protein interactions, etc. have generally been developed to make observations at the cellular level.

5.4 Future Model Refinements

To quote the statistician George Box, "all models are wrong, but some are useful." This wisdom certainly applies to models used throughout this thesis. The first improvement I can suggest to my multiscale multi-physics model of V/Q matching would be to represent 3-dimensional (3D) spatial networks. In addition to true lungs existing in 3D space rather than a flat plane, studies on angiogenesis and vascularization have shown how connectivity and branching patterns of vascular networks have different topological constraints when going from 2 dimensions to 3 dimensions (226,227). Along these lines, a 3D representation in these models might afford different model behavior for an HPV mechanism where a given pulmonary artery directly senses oxygen in the adjacent alveolar space. A second model improvement that one would naturally encounter in developing a 3D model of V/Q matching would be the mechanical coupling of the airway and vasculature. I have accounted for the effect of alveolar pressure on vascular fluid and wall mechanics in the model presented in chapter 3, but this is only a first effort. Since HPV is a process that operates on the background of other physiology, a more nuanced model of this anatomical coupling could prove very important. A particular example would be in disease states characterized by loss of alveolar surfactant, such as ARDS (51) – it has been hypothesized the mechanically stiffened airways in ARDS stents open the adjacent vasculature and thus limit HPVs ability to affect changes in the distribution of blood flow.

A third improvement to models of HPV and V/Q matching would be a robust representation of the electrophysiological coupling of vascular tissue. I have proposed a hypothesis wherein multiple oxygen sensors are located at different locations throughout the organ and converge on the PASMCs to affect vasoconstriction. To begin evaluating such a hypothesis, we will need to move beyond the empirical models of HPV presented in this thesis and work to derive and validate models of pulmonary endothelial and PASMC electrophysiology, and potentially other signaling transduction and amplification mechanisms that underly HPV. A fourth improvement would be to account for the transport and elimination of carbon dioxide (CO_2) and corresponding the plasma acid-base balance. Not only is the exhalation of CO_2 a parallel process to the uptake of oxygen in the lungs, but it has also been observed that alkalosis inhibits, and acidosis amplifies HPV (9). Moreover, HPV-mediated redistributions in blood flow and V/Q ratios could have advantageous or deleterious effects on the plasma acid-base balance.

A fifth and final improvement would be to couple this model of V/Q matching to an appropriate model of oxygen transport and utilization by systemic tissues. This improvement is likely the most conceptually challenging to implement. The parallel physiological process to V/Q matching is the matching of perfusion the metabolic activity of systemic tissues – which could be referred to as "Perfusion-Metabolism" (Q/M) matching. As complex as V/Q matching is, Q/M matching is arguably more complicated as different systemic tissues have different oxygen demands and blood flows. Moreover, some tissues like skeletal muscle and the gastrointestinal tract can undergo profound changes in oxygen demand and corresponding blood flows when going from rest to exercise (228,229). A complete model of V/Q and Q/M matching would fully encapsulate whole-body oxygen transport (from the atmosphere to a mitochondrion). In Figure

5.2 we depict how these parallel physiological processes interact and feedback to one another. The operative challenge in designing such a Q/M matching model to couple to my V/Q matching model is the scale and scope of model complexity. What aspects of metabolism need to be modeled? Should there be different metabolism models for different tissues? Should one account for the spatially distributed nature of the systemic oxygenation in the same we have for the pulmonary side of the circuit? These are extremely challenging questions both in concept and computational feasibility. I highlight that these kinds of questions are natural extensions of the landmark studies from August Krogh on oxygen transport and capillary recruitment (161–163). There have many efforts since Krogh to model the complete path of physiological oxygen transport (230–232). Some of these efforts use a very literal interpretation of diagrams like that in Figure 5.2B in the form of compartmental mass transfer, others have more granular representations of spatial transport with multiple intermediate compartments or use partial differential equations to account for the spatially distributed nature of this process. These models have undoubtedly been useful in advancing our understanding of the physiology of oxygen transport, however the current frontier of what remains unknown is how the *spatially distributed* nature of the vasculature networks affords, augments, and limits pathophysiology.

5.5 Clinical Considerations for Interpreting V/Q Ratios

This thesis raises an interesting possibility for how physicians and healthcare providers could interpret the results of V/Q scans. Generally, a V/Q scan is ordered for a patient when they have clinical symptoms that suggest V/Q mismatching (ex: blood gas derangement, alveolar hemorrhage, isolated dyspnea, etc.) (233). While V/Q scans are a mapping of air and blood flow distributions, they are in practice used to identify structural abnormalities, such a pulmonary embolism or collapsed/occluded airway. This use of V/Q scans is tremendously useful, as the

V/Q scans can function as a literal map to aid in surgical interventions to navigate surgical tools to the local region affected by pathology (234). However, to my knowledge, V/Q scans in clinical settings are not used to directly infer anything about gas exchange. *Perhaps there could be clinical value in using V/Q scans to infer how region of lungs contributes to a patient's gas exchange*? The model simulations performed in chapters 3 and 4 show how different distributions of regional blood flow can dramatically alter the regional flux of oxygen into the blood stream, and overall oxygenation of the pulmonary venous outflow. Using this understanding of how V/Q matching affects gas exchange could potentially be leveraged in making a diagnosis or developing a treatment plan to restore gas exchange to a homeostatic regime.

Let's consider chronic thromboembolic pulmonary hypertension (CTEPH). CTEPH is characterized by multiple distributed thromboemboli in the lungs, which can cause profound redistributions of blood flow, elevated pulmonary arterial and capillary wedge pressures, and remodeling of the pulmonary vasculature (235,236). At the extreme end of pathophysiology, these patients can have V/Q mismatching, and hemodynamic complications can lead to diastolic and systolic cardiac dysfunction. Of the various forms of pulmonary hypertension, CTEPH is unique in that some patients can be fully cured by surgical removal of thrombi (pulmonary endarterectomy). In the case of surgical intervention to remove these thrombi, a practical decision needs to be made – *which thrombi are the priority to remove*? In some situations, it is often infeasible to exhaustively excise every thrombus as there is a limited time frame a patient can tolerate a procedure, and some thrombi are so small they are inaccessible by modern intravascular surgical tools (microemboli) (237). Moreover, a patient might need to undergo multiple rounds of surgery to adequately restore gas exchange to a homeostatic regime. Patient-

specific model simulations or a generalized mechanistic theory of how V/Q ratio distributions affect gas exchange could potentially be used here to predict which thrombi are the most strategic to excise first. One can appreciate how this kind of understanding could further refine the standard of care when treating patients with kind of complex disease.

The inherent challenges of treating a patient with multiple distributed pulmonary emboli is particularly relevant in 2022 with the ongoing COVID-19 pandemic. While the clinical presentation and optimal treatment for critically ill-patients with COVID-19 is an actively evolving area of research, *many of these patients suffer and die from hypoxemia due to V/Q mismatching that is downstream of distributed microthrombi* (238). Epidemiology studies have predicted that COVID-19 will likely continue to be a part of our lives in a seasonal manner comparable to influenza viral infections (239,240), so while immunization from vaccines, social distancing, and wearing facemasks are important structural strategies to limit the spread of and prevent infections (241–243), the world needs more efficacious therapeutic interventions for the patients who are afflicted. The models developed in this thesis could potentially be used to simulate how microthrombi affect V/Q matching and gas exchange but could also be extended to predict how thrombolytic drugs are transported to and dissolve clots, and corresponding changes in gas exchange. Regardless of how the COVID-19 pandemic will resolve, this thesis represents a framework and inspiration for how measurements of V/Q ratios can be used to make mechanistic inferences on the spatially distributed nature of pulmonary gas exchange.

Figure 5.1 ***Fluorescent Microspheres to Measure Rat Lung Blood Flow Distribution.*** *15 μm polystyrene microspheres conjugated to fluorescent tags are infused into rat pulmonary arterial circulation and become lodged in the precapillary arterioles. (A) Distribution of microspheres in 3-dimensional space. (B) Voxel grid to analyze regional properties of blood flow distribution. (C) Density of flow per voxel. Voxels are colored to reflect the number of microspheres within them.*

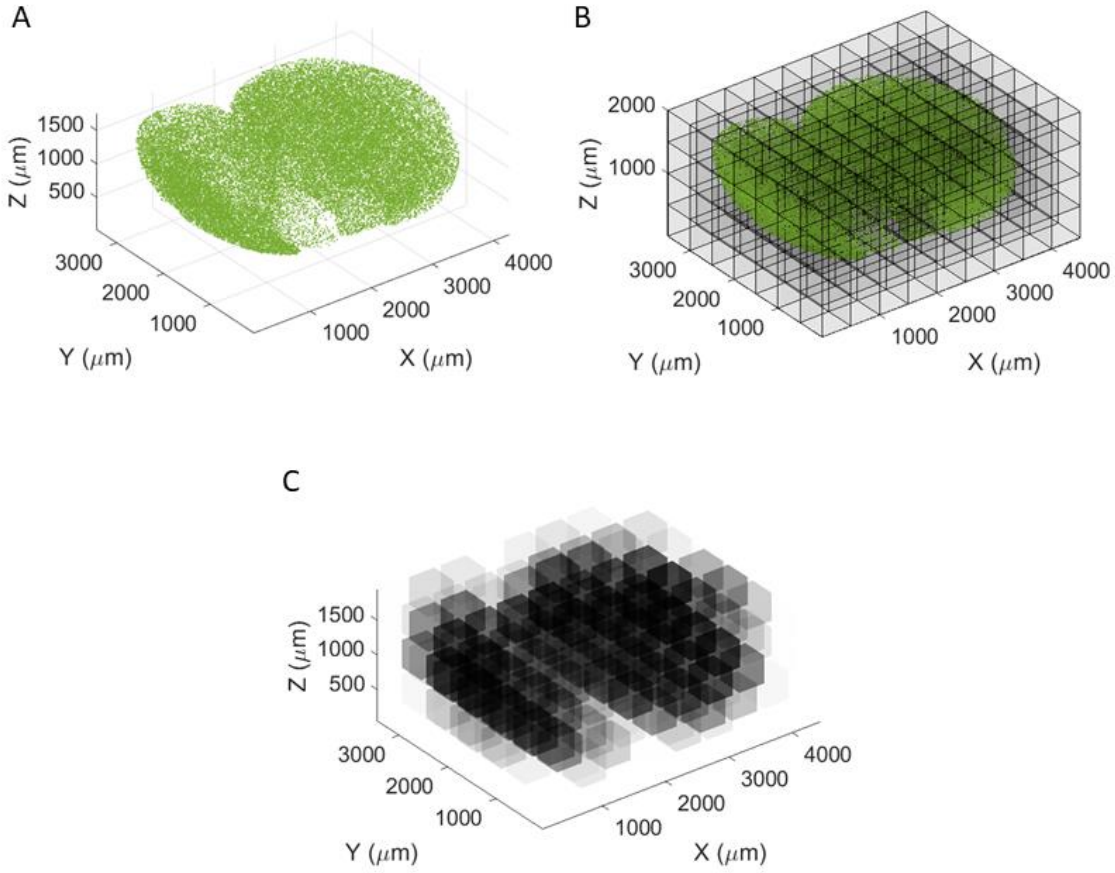
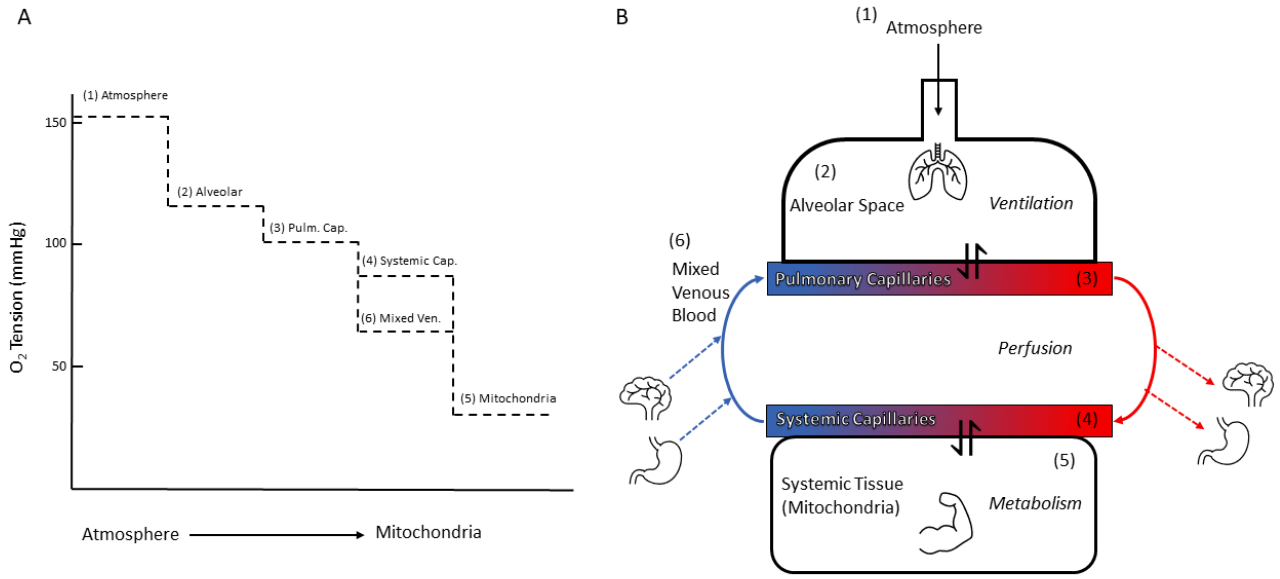


Figure 5.2 ***Whole Body Oxygen Transport****. (A) The Oxygen Cascade. The dashed line illustrates the oxygen tensions in various areas of the body as it is transported to and consumed by the systemic tissues. (B) Ventilation – Perfusion – Metabolism Matching. This diagram shows the directionality of how oxygen is transported into the blood stream by the lungs, distributed to systemic tissues, and then mixed venous blood returns to the lungs. The labels (1) – (6) correspond to the labels in panel A. This diagram depicts skeletal muscle as the operative systemic tissue, but there are many parallel paths within the circulatory system to provide oxygen to all other tissues (such as the brain and gastrointestinal tract). In the lungs, ventilation and perfusion need to be properly matched to ensure the bloodstream is adequately oxygenated. In the systemic tissues, perfusion needs to be matched the oxygen demand and metabolic activity of tissue to continue physiological function.*



Appendix A

A.1 Steady state alveolar and vascular oxygen tension

The steady-state behavior of each model is simulated by setting time derivatives to zero and determining the steady-state values of oxygen in the alveolar and vascular compartments.

A.1.1 Model A

Setting the time derivatives of the governing equations equal to zero yields

$$0 = V(P_{air} - P^*_{alv}) - D(P^*_{alv} - P^*_{vasc}), \text{and} \qquad \text{Eqn. (A1)}$$

$$0 = Q(P_{in} - P^*_{vasc}) + D(P^*_{alv} - P^*_{vasc}).$$

We use a superscripted asterisk (*) to denote the steady state values of alveolar and vascular oxygen tension. This system of algebraic equations can be solved to find

$$P^*_{alv} = \frac{P_{air}Dv + P_{in}DQ + P_{air}QV}{QV + DQ + DV}, \text{and} \qquad \text{Eqn. (A2)}$$

$$P^*_{vasc} = \frac{P_{in}QV + P_{in}DQ + P_{air}DV}{QV + DQ + DV}.$$

A.1.2 Model B

Setting the time derivatives equal to zero and substituting the vascular oxygen concentration-partial pressure relationship produces two non-linear algebraic equations:

$$0 = V(P_{air} - P^*_{alv}) - \alpha\beta D(P^*_{alv} - P^*_{vasc}), \text{and} \quad \text{Eqn. (A3)}$$

$$0 = Q\left(C_{in} - \alpha P^*_{vasc} - C_{Hb}\frac{P^{*n}_{vasc}}{P^{*n}_{vasc} + P^n_{50}}\right) + \alpha D(P^*_{alv} - P^*_{vasc}).$$

This system of algebraic equations does not have an analytic solution. We employ MATLAB's a numerical root-finding algorithm *fzero* to solve for P^*_{alv} and P^*_{vasc}.

A.1.3 Model C

Setting the time derivates of the governing equations equal to zero yields

$$0 = V(P_{air} - P^*_{alv}) - D(P^*_{alv} - \langle P^*_{vasc}\rangle), \text{and} \quad \text{Eqn. (A4)}$$

$$\frac{dP^*_{vasc}}{dx} = \frac{D}{Ql}(P^*_{alv} - P^*_{vasc}).$$

Our steady-state assumption reduces the partial differential equation to an ordinary differential equation (ODE) with the boundary condition $P^*_{vasc}(0) = P_{in}$. This ODE can be analytically solved and yields

$$P^*_{vasc}(x) = P^*_{alv} + (P_{in} - P^*_{alv})\exp\left(-\frac{D}{Ql}x\right). \quad \text{Eqn. (A5)}$$

It follows that the steady state oxygen tension leaving the vascular tube is

$$P^*_{vasc}(l) = P^*_{alv} + (P_{in} - P^*_{alv})\exp\left(-\frac{D}{Q}\right). \quad \text{Eqn. (A6)}$$

We use equation (18), which is represents the steady state vascular oxygen tension as a function of space, to determine the average oxygen tension across the vascular tube as

$$\langle P^*_{vasc}\rangle = \frac{1}{l}\int P^*_{vasc}(x)dx = P^*_{alv} + \frac{q}{D}(P_{in} - P^*_{alv})\left(1 - \exp\left(-\frac{D}{q}\right)\right). \quad \text{Eqn. (A7)}$$

We substitute $\langle P^*_{vasc}\rangle$ into the Eqn. (17) to solve for steady state alveolar oxygen tension as

$$P^*_{alv} = \frac{QP_{in}\left(\exp\left(-\frac{D}{Q}\right) - 1\right) - VP_{air}}{Q\left(\exp\left(-\frac{D}{Q}\right) - 1\right) - V}. \quad \text{Eqn. (A8)}$$

A.1.4 Model D

Setting the time derivatives equal to zero yields

$$\frac{dC^*_{vasc}}{dx} = \frac{\alpha D}{Ql}(P^*_{alv} - P^*_{vasc}), \quad \text{Eqn. (A9)}$$

$$0 = V(P_{air} - P^*_{alv}) - \alpha\beta D(P^*_{alv} - \langle P^*_{vasc}\rangle), \text{and}$$

$$C^*_{vasc} = \alpha P^*_{vasc} + C_{Hb}\frac{P^{*n}_{vasc}}{P^{*n}_{vasc} + P^n_{50}}.$$

This system of algebraic and differential equations does not have an analytic solution. To solve for the steady state alveolar and oxygen tension we employ a strategy of numerical relaxation detailed in the below.

A.1.5 Model E

Setting the time derivatives equal to zero yields

$$P^*_{alv} = P_{air} - \frac{\beta V_{O2}}{V}, \text{and} \quad \text{Eqn. (A10)}$$

$$P^*_{vasc} = P_{air} - V_{O2}\left(\frac{\beta}{V} + \frac{1}{\alpha D}\right).$$

A.1.6 Model F

Since Model F has the same governing equations as Model D, setting the time derivatives equal to zero yields equations (A9). We solve for the steady state alveolar and oxygen tension with a numerical relaxation strategy detailed below.

A.2 Numerical stability for relaxing Model D and F to steady state

To numerically solve Model D and F we discretize and recast Equation (A7) as

$$\frac{dC^*_{vasc,i}}{dx} = \frac{\alpha D}{Ql}\left(P^*_{alv} - P^*_{vasc,i}\right), \qquad \text{Eqn. (A11)}$$

$$P^*_{alv} = \frac{vP_{air} + \alpha\beta D\langle P^*_{vasc,i}\rangle}{V + \alpha\beta D}$$

$$C^*_{vasc,i} = \alpha P^*_{vasc,i} + C_{Hb}\frac{P^{*n}_{vasc,i}}{P^{*n}_{vasc} + P^n_{50}}.$$

where $C^*_{vasc,i}$ and $P^*_{vasc,i}$ are oxygen concentration and tension respectively equally spaced along the length of the capillary, and $\langle P^*_{vasc,i}\rangle$ is the arithmetic average of P^*_{vasc}. $C^*_{vasc,i}$ and $P^*_{vasc,i}$ are spaced $\Delta x = 1/n$ distance apart, where n the total number of nodes. We approximate the solution to this system by successive over-relaxation. We define the error of our approximation as

$$\epsilon = \left|\frac{C_{vasc,i+1} - C_{vasc,i}}{C_{vasc,i}}\right|$$

and relax the system until $\epsilon < 10^{-12}$

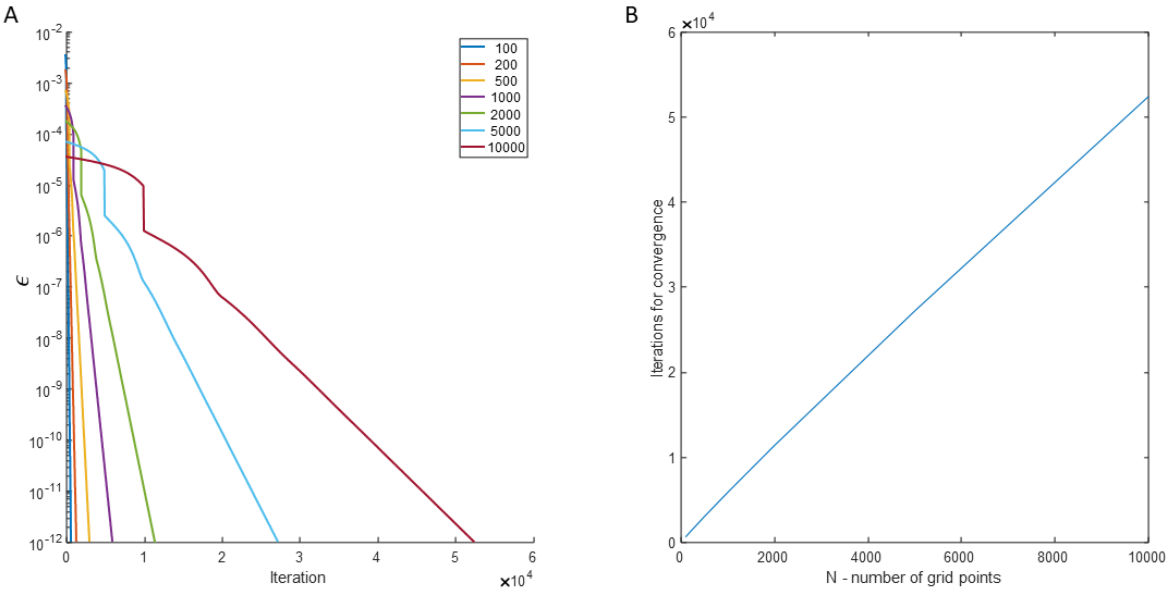
Figure A1 in illustrates the numerical stability of this relaxation strategy. We evaluate the stability of our relaxation strategy by using different amounts of grid points to discretize the vascular tube. Figure A1A shows error as a function of relaxation iterations and each curve represents simulations using different amounts of grid points. One can appreciate that for any amount of grid points used, the error monotonically decreases. Figure A1B shows the number of

iterations required to relax the system as a function of grid points used. We define our error threshold to be 10^{-12}, and observe a linear trend for the iterations required for the relaxation to converge.

A.3 Sensitivity of model behavior to apparent diffusivity parameter

To globally explore how the apparent diffusion (D) parameter affects our models' behavior, we re-made the panels shown in Figure 4 and 5 using a wide range of values for D. Using each discrete value of D as a frame, we created animated .gif files that illustrate how the value of D affects the oxygen tension isoclines. In total there are 3 .gif files for Models A-E (15 total) – one for the alveolar, vascular, alveolar-vascular oxygen difference. Animated. gif's for model F have been excluded, as they are extremely computationally intensive to generate and model F has a similar dependence on the parameter D as model E.

Figure A.1 ***Numerical stability for approximating the fixed points of Model D****. (A) Error in our approximation as a function of the number of iterations. The legend refers to the number of grid points used to discretize the spatial domain. (B) Iterations required to converge as a function of N – the number of grid points used to discretize the spatial domain.*



Appendix B

B.1 Network morphometry

Table B.1 summaries the morphometry of the generated vascular networks. The information in the bottom block of this table corresponds to the data plotted in Fig 3.3.

B.2 Airway model

In contrast to the detail of our vascular networks, we use a relatively simplified airway model. Fig B.1 illustrates how the airway and alveolar compartments are connected to each other.

B.3 Effect of tidal volume on oxygenation

To understand how tidal ventilation affects gas exchange in our model, we adjust the parameter Q_V^* which represents bulk airflow. Tidal volume (TV) is proportional to airflow (TV/Q_V^*=272), so increasing this parameter increases tidal volume, and decreasing this parameter decreases tidal volume. Fig B.2 shows how tidal volume impacts oxygen uptake. Increasing tidal volume increases oxygen uptake in a manner that asymptotically approaches oxygen partial pressure in the air (150 mmHg).

B.4 Effect of HPV and uniform vasoconstriction on regional oxygen tension distribution

While vasomotion does alter the distribution of blood flow, another functional consequence of this action is to alter the distribution of oxygen in the alveolar and vascular

space. Fig B.3 shows the distribution of oxygen tension in network A under conditions of no regulation, with regulation from HPV, and with uniform vasoconstriction.

B.5 Effect of airway occlusions on vascular tone from HPV

In Fig 10, we show airway occlusions affect the distribution of hemodynamics, V/Q matching, and oxygen flux. In Fig S4, we show the underlying changes in tone from HPV that mediate the changes in blood flow, V/Q matching, and oxygenation. southwestern perfusion zone, and progressive airway occlusions are made following the structure of the vascular network.

Table B.1 ***Pulmonary vascular network and perfusion zone morphometry*** *Descriptive statistics for each vascular network. Quantities are presented as mean ± standard deviation. The top block summaries the size of the perfusion zones, and the bottom block summarizes the diameters and lengths for each diameter-defined Strahler order.*

Network	A			B			C		
Area of perfusion zone (μm^2)	907.34 ± 227.68			594.19 ± 150.69			639.47 ± 165.07		
dd Strahler Order	Segments	Diameter (μm)	Length (μm)	Segments	Diameter (μm)	Length (μm)	Segments	Diameter (μm)	Length (μm)
12	1	540.53	2,250.00	2	600.90 ± 0.67	525.00 ± 300.00	3	589.10 ± 0.83	625.00 ± 304.14
11	4	533.91 ± 2.28	375.00 ± 75.00	26	485.95 ± 3.63	452.88 ± 51.88	8	568.70 ± 1.92	487.50 ± 40.09
10	5	510.21 ± 4.13	405.00 ± 137.48	29	360.15 ± 4.44	375.00 ± 39.74	4	517.90 ± 1.35	450.00 ± 61.24
9	14	385.69 ± 6.42	514.28 ± 72.85	32	255.61 ± 3.36	473.44 ± 40.75	21	407.19 ± 4.47	442.85 ± 52.25
8	34	266.08 ± 4.20	555.88 ± 47.62	136	185.18 ± 1.14	266.91 ± 20.35	29	322.25 ± 3.61	411.21 ± 40.37
7	89	185.16 ± 1.41	317.70 ± 30.53				22	253.83 ± 4.09	507.95 ± 52.21
6							122	184.13 ± 1.11	288.32 ± 18.47

Figure B.1 ***Schematic of our airway model****. Blue boxes denote compartment in our airway model. Airway 1 interacts with the atmospheric air and airway 2. Airway 2 functions as a mixing chamber and interacts with all of the alveolar compartments. Each alveolar compartment exchanges oxygen with a capillary compartment.*

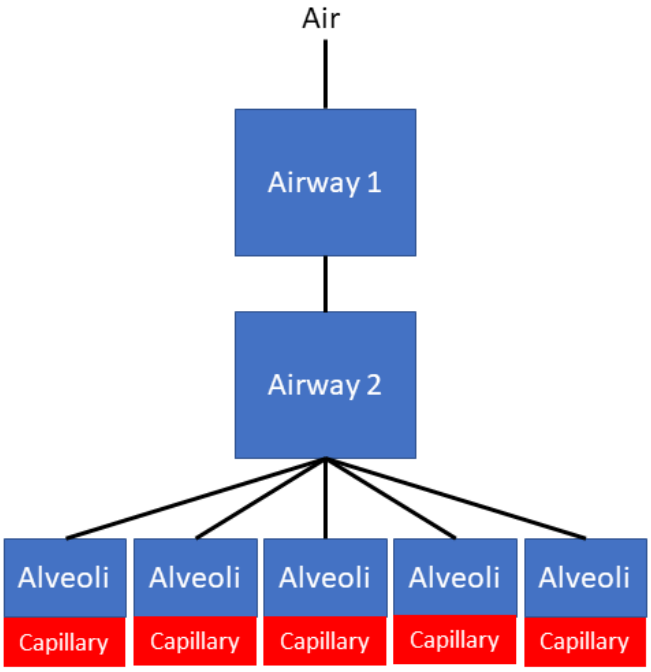


Figure B.2 ***Effect of tidal volume on oxygenation*** *(A) Oxygen tension in the primary vein and mean and standard deviation in the alveolar compartments as a function of tidal volume; (B) Total oxygen flux as a function of tidal volume.*

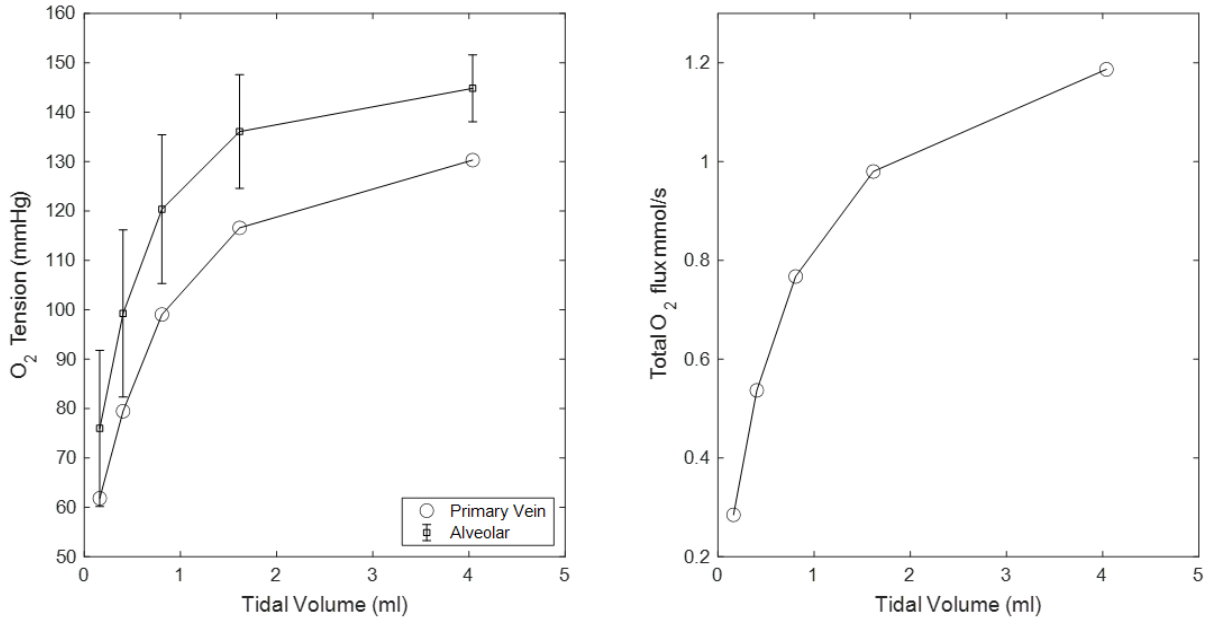


Figure B.3 ***Effect of HPV and uniform vasoconstriction on Network A regional oxygen tension distribution.*** *Leftmost column of networks are without regulation from HPV, middle column of networks are with regulation from HPV, and the rightmost column of networks are with uniform vasoconstriction, where $T^* = 0{:}8$ is used for the global vascular tone. The black scale bar is 1000 µm. (A) End-capillary oxygen tension; (B) Alveolar Oxygen tension; (C) Tone from HPV.*

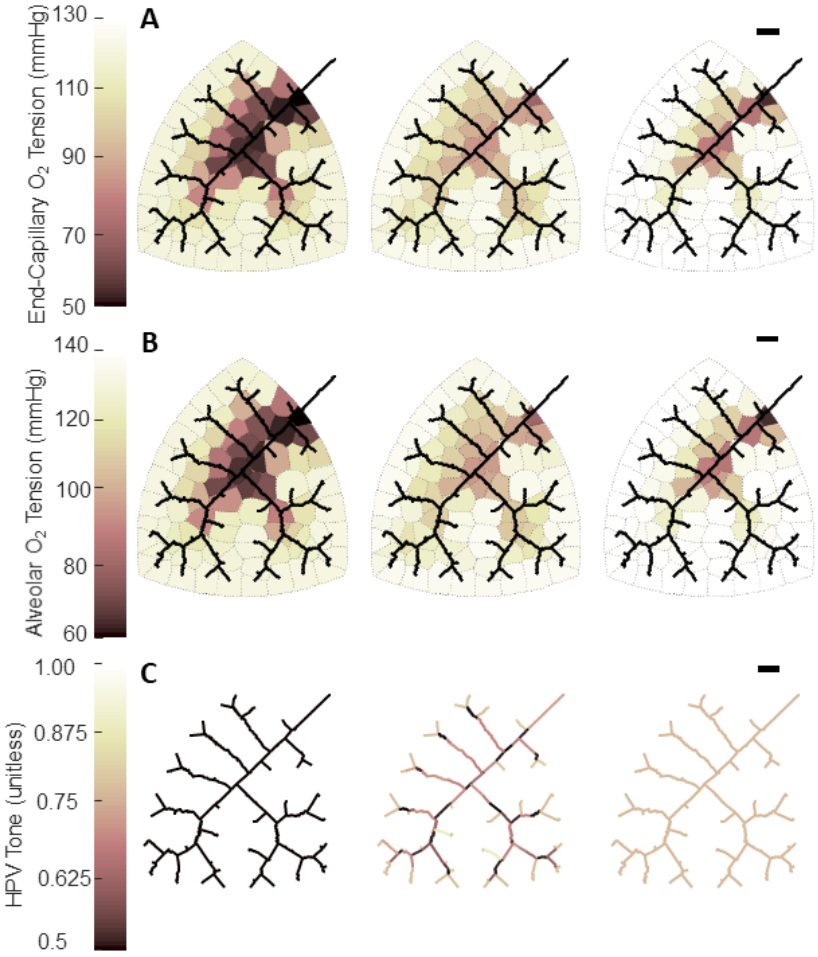
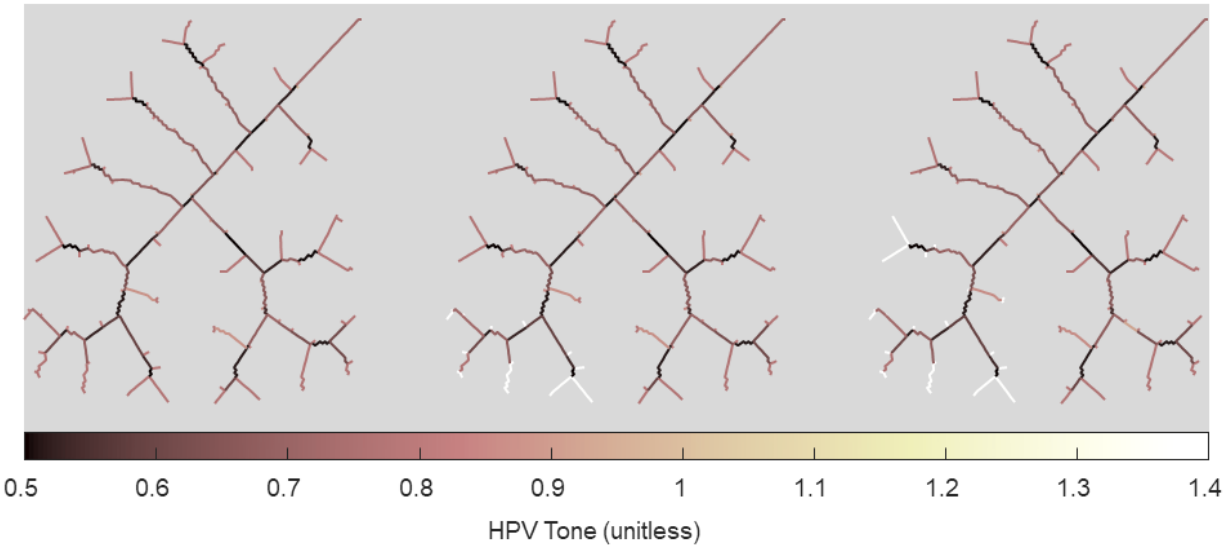


Figure B.4 ***Effect of airway occlusions on the distribution of vascular tone from HPV This figure corresponds to simulations shown in Fig 3.10****. Leftmost network is with 0% of the alveoli occluded, middle network is with 17% of the alveoli occluded, and the rightmost network is with 28% of the alveoli occluded. The first airway occlusion is at the most southwestern perfusion zone, and progressive airway occlusions are made following the structure of the vascular network.*



Bibliography

1. Hsia CCW, Hyde DM, Weibel ER. Lung Structure and the Intrinsic Challenges of Gas Exchange.
2. Derenoncourt PR, Felder GJ, Royal HD, Bhalla S, Lang JA, Matesan MC, et al. Ventilation-Perfusion Scan: A Primer for Practicing Radiologists. https://doi-org.proxy.lib.umich.edu/101148/rg2021210060 [Internet]. 2021 Oct 22 [cited 2021 Nov 15];41(7):2047–70. Available from: https://pubs-rsna-org.proxy.lib.umich.edu/doi/abs/10.1148/rg.2021210060
3. West JB, Dollery CT, Naimark A. Distribution of blood flow in isolated lung; relation to vascular and alveolar pressures. https://doi.org/101152/jappl1964194713 [Internet]. 1964 Jul 1 [cited 2021 Nov 15];19(4):713–24. Available from: https://journals.physiology.org/doi/abs/10.1152/jappl.1964.19.4.713
4. Burrowes KS, Tawhai MH. Computational predictions of pulmonary blood flow gradients: Gravity versus structure. Respiratory Physiology & Neurobiology. 2006 Dec 1;154(3):515–23.
5. Hubmayr RD, Walters BJ, Chevalier PA, Rodarte JR, Olson LE. Topographical distribution of regional lung volume in anesthetized dogs. https://doi.org/101152/jappl19835441048 [Internet]. 1983 [cited 2021 Nov 15];54(4):1048–56. Available from: https://journals.physiology.org/doi/abs/10.1152/jappl.1983.54.4.1048

6. Cortney Henderson A, Sá RC, Theilmann RJ, Buxton RB, Kim Prisk G, Hopkins SR. The gravitational distribution of ventilation-perfusion ratio is more uniform in prone than supine posture in the normal human lung. Journal of Applied Physiology [Internet]. 2013 Aug 1 [cited 2021 Nov 15];115(3):313–24. Available from: https://journals.physiology.org/doi/abs/10.1152/japplphysiol.01531.2012
7. Glenny RW, Robertson HT. Spatial Distribution of Ventilation and Perfusion: Mechanisms and Regulation. In: Comprehensive Physiology [Internet]. Hoboken, NJ, USA: John Wiley & Sons, Inc.; 2011 [cited 2021 Mar 14]. p. 373–95. Available from: http://doi.wiley.com/10.1002/cphy.c100002
8. Sylvester JT, Shimoda LA, Aaronson PI, Ward JPT. Hypoxic pulmonary vasoconstriction. Physiological Reviews [Internet]. 2012 [cited 2021 Nov 15];92(1):367–520. Available from: https://journals.physiology.org/doi/abs/10.1152/physrev.00041.2010
9. EULER US v., LILJESTRAND G. Observations on the Pulmonary Arterial Blood Pressure in the Cat. Acta Physiologica Scandinavica. 1946;12(4):301–20.
10. Elliott AR, Steffey EP, Jarvis KA, Marshall BE. Unilateral hypoxic pulmonary vasoconstriction in the dog, pony and miniature swine. Respiration Physiology. 1991 Sep 1;85(3):355–69.
11. Santolicandro A, Prediletto R, Fornai E, Formichi B, Begliomini E, Giannella-Neto A, et al. Mechanisms of hypoxemia and hypocapnia in pulmonary embolism. Am J Respir Crit Care Med. 1995;152(1):336–47.
12. Jain L, Eaton DC. Physiology of Fetal Lung Fluid Clearance and the Effect of Labor. Seminars in Perinatology. 2006 Feb 1;30(1):34–43.

13. Weichert J, Hartge DR, Axt-Fliedner R. The Fetal Ductus Arteriosus and Its Abnormalities—A Review. Congenital Heart Disease [Internet]. 2010 Sep 1 [cited 2021 Nov 15];5(5):398–408. Available from: https://onlinelibrary-wiley-com.proxy.lib.umich.edu/doi/full/10.1111/j.1747-0803.2010.00424.x

14. Laudy JAM, Wladimiroff JW. The fetal lung 1: Developmental aspects. Ultrasound in Obstetrics and Gynecology. 2000;16(3):284–90.

15. Gao Y, Raj JU. Regulation of the pulmonary circulation in the fetus and newborn. Physiological Reviews [Internet]. 2010 Oct [cited 2021 Nov 15];90(4):1291–335. Available from: https://journals-physiology-org.proxy.lib.umich.edu/doi/abs/10.1152/physrev.00032.2009

16. Sartori C, Rimoldi SF, Duplain H, Stuber T, Garcin S, Rexhaj E, et al. Developmental Origins of Hypoxic Pulmonary Hypertension and Systemic Vascular Dysfunction: Evidence from Humans. Advances in Experimental Medicine and Biology [Internet]. 2016 [cited 2021 Nov 15];903:17–28. Available from: https://link-springer-com.proxy.lib.umich.edu/chapter/10.1007/978-1-4899-7678-9_2

17. Bennie RE, Packer CS, Powell DR, Jin N, Rhoades RA. Biphasic contractile response of pulmonary artery to hypoxia. https://doi-org.proxy.lib.umich.edu/101152/ajplung19912612L156 [Internet]. 1991 [cited 2021 Nov 15];261(2 5-1). Available from: https://journals-physiology-org.proxy.lib.umich.edu/doi/abs/10.1152/ajplung.1991.261.2.L156

18. Weissmann N, Akkayagil E, Quanz K, Schermuly RT, Ghofrani HA, Fink L, et al. Basic features of hypoxic pulmonary vasoconstriction in mice. Respiratory Physiology and

Neurobiology [Internet]. 2004 Jan 15 [cited 2021 Jun 20];139(2):191–202. Available from: https://pubmed.ncbi.nlm.nih.gov/15123002/

19. I S, NC K, N S, RT S, HA G, F G, et al. Hypoxic pulmonary vasoconstriction in isolated mouse pulmonary arterial vessels. Exp Physiol [Internet]. 2018 Sep 1 [cited 2021 Jul 27];103(9):1185–91. Available from: https://pubmed.ncbi.nlm.nih.gov/29917290/

20. LM H, TC R, NL J. RhoA increases ASIC1a plasma membrane localization and calcium influx in pulmonary arterial smooth muscle cells following chronic hypoxia. Am J Physiol Cell Physiol [Internet]. 2018 Feb 1 [cited 2021 Jul 26];314(2):C166–76. Available from: https://pubmed.ncbi.nlm.nih.gov/29070491/

21. Grimmer B, Kuebler WM. The endothelium in hypoxic pulmonary vasoconstriction. J Appl Physiol [Internet]. 2017 [cited 2020 Sep 16];123:1635–46. Available from: http://www.jappl.org

22. Zhao Y, Packer CS, Rhoades RA. Pulmonary vein contracts in response to hypoxia. American Journal of Physiology - Lung Cellular and Molecular Physiology [Internet]. 1993 [cited 2020 Aug 31];265(1 9-1). Available from: https://pubmed.ncbi.nlm.nih.gov/8338186/

23. Houston CS. Acute pulmonary edema of high altitude. N Engl J Med [Internet]. 1960 Sep 8 [cited 2021 Nov 15];263(10):478–80. Available from: https://pubmed.ncbi.nlm.nih.gov/14403413/

24. West JB, Mathieu-Costello O. High altitude pulmonary edema is caused by stress failure of pulmonary capillaries. In: International Journal of Sports Medicine [Internet]. Int J Sports Med; 1992 [cited 2020 Aug 31]. Available from: https://pubmed.ncbi.nlm.nih.gov/1483792/

25. Stream JO, Grissom CK. Update on High-Altitude Pulmonary Edema: Pathogenesis, Prevention, and Treatment. Wilderness & Environmental Medicine. 2008 Dec 1;19(4):293–303.

26. Swenson ER. Carbonic anhydrase inhibitors and high altitude illnesses. Subcell Biochem [Internet]. 2014 [cited 2022 Mar 6];75:361–86. Available from: https://pubmed.ncbi.nlm.nih.gov/24146388/

27. Pei SX, Chen XJ, Si Ren BZ, Liu YH, Cheng XS, Harris EM, et al. Chronic Mountain Sickness in Tibet. QJM: An International Journal of Medicine [Internet]. 1989 Jun 1 [cited 2021 Nov 15];71(3):555–74. Available from: https://academic-oup-com.proxy.lib.umich.edu/qjmed/article/71/3/555/1530067

28. Y P, C C, Y H, None O, H Z, D Y, et al. Down-Regulation of EPAS1 Transcription and Genetic Adaptation of Tibetans to High-Altitude Hypoxia. Mol Biol Evol [Internet]. 2017 Apr 1 [cited 2021 Jul 26];34(4):818–30. Available from: https://pubmed.ncbi.nlm.nih.gov/28096303/

29. HY Y, SJ K. Disappearance of hypoxic pulmonary vasoconstriction and o2-sensitive nonselective cationic current in arterial myocytes of rats under ambient hypoxia. Korean J Physiol Pharmacol [Internet]. 2013 Oct [cited 2021 Jul 21];17(5):463–8. Available from: https://pubmed.ncbi.nlm.nih.gov/24227949/

30. Simonneau G, Galiè N, Rubin LJ, Langleben D, Seeger W, Domenighetti G, et al. Clinical Classification of Pulmonary Hypertension. J Am Coll Cardiol. 2004;43:S5–12.

31. Burger CD, DuBrock HM, Cartin-Ceba R, Moss JE, Shapiro BP, Frantz RP. Topic-Based, Recent Literature Review on Pulmonary Hypertension. Mayo Clinic Proceedings. 2021 Aug 31;

32. Vitali SH, Hansmann G, Rose C, Fernandez-Gonzalez A, Scheid A, Mitsialis SA, et al. The Sugen 5416/hypoxia mouse model of pulmonary hypertension revisited: long-term follow-up. Pulm Circ [Internet]. 2014 Dec 1 [cited 2021 Nov 15];4(4):619–29. Available from: http://www.ncbi.nlm.nih.gov/pubmed/25610598

33. Tuder RM. Pulmonary vascular remodeling in pulmonary hypertension. Cell and Tissue Research [Internet]. 2017 Mar 1 [cited 2021 Dec 1];367(3):643–9. Available from: https://link-springer-com.proxy.lib.umich.edu/article/10.1007/s00441-016-2539-y

34. Shimoda LA, Laurie SS. Vascular remodeling in pulmonary hypertension.

35. Sylvester JT, Gordon JB, Malamet RL, Wetzel RC. Prostaglandins and Estradiol-induced Attenuation of Hypoxic Pulmonary Vasoconstriction. Chest [Internet]. 1985 Oct [cited 2020 Aug 27];88(4):252S-254S. Available from: https://pubmed.ncbi.nlm.nih.gov/3840073/

36. Lahm T, Crisostomo PR, Markel TA, Wang M, Wang Y, Weil B, et al. Exogenous estrogen rapidly attenuates pulmonary artery vasoreactivity and acute hypoxic pulmonary vasoconstriction. Shock [Internet]. 2008 Dec [cited 2021 Jun 27];30(6):660–7. Available from: https://pubmed.ncbi.nlm.nih.gov/18461023/

37. D X, W N, Y L, B Z, M L, H D, et al. Endogenous estrogen attenuates hypoxia-induced pulmonary hypertension by inhibiting pulmonary arterial vasoconstriction and pulmonary arterial smooth muscle cells proliferation. Int J Med Sci [Internet]. 2013 [cited 2021 Jul 21];10(6):771–81. Available from: https://pubmed.ncbi.nlm.nih.gov/23630443/

38. Cheron C, McBride SA, Antigny F, Girerd B, Chouchana M, Chaumais MC, et al. Sex and gender in pulmonary arterial hypertension. Eur Respir Rev [Internet]. 2021 Dec 31

[cited 2021 Nov 15];30(162):200330. Available from: https://pubmed.ncbi.nlm.nih.gov/34750113/

39. Longo DL, Musher DM, Thorner AR. Community-Acquired Pneumonia. http://dx.doi.org.proxy.lib.umich.edu/101056/NEJMra1312885 [Internet]. 2014 Oct 22 [cited 2021 Nov 15];371(17):1619–28. Available from: https://www-nejm-org.proxy.lib.umich.edu/doi/full/10.1056/NEJMra1312885

40. Gharib AM, Stern EJ. RADIOLOGY OF PNEUMONIA. Medical Clinics of North America. 2001 Nov 1;85(6):1461–91.

41. Watkins RR, Lemonovich TL. Diagnosis and Management of Community-Acquired Pneumonia in Adults. American Family Physician [Internet]. 2011 Jun 1 [cited 2021 Nov 16];83(11):1299–306. Available from: www.aafp.org/afpAmericanFamilyPhysician1299

42. Kalil AC, Metersky ML, Klompas M, Muscedere J, Sweeney DA, Palmer LB, et al. Management of Adults With Hospital-acquired and Ventilator-associated Pneumonia: 2016 Clinical Practice Guidelines by the Infectious Diseases Society of America and the American Thoracic Society. Clinical Infectious Diseases. 2016 Sep 1;63(5):e61–111.

43. Gea J, Roca J, Torres A, Agusti AGN, Wagner PD, Rodriguez-Roisin R. Mechanisms of abnormal gas exchange in patients with pneumonia. Anesthesiology [Internet]. 1991 [cited 2020 Aug 31];75(5):782–9. Available from: https://pubmed.ncbi.nlm.nih.gov/1952203/

44. Fischer SR, Bone HG, Powell WC, McGuire R, Traber LD, Traber DL. Pyridoxalated hemoglobin polyoxyethylene conjugate does not restore hypoxic pulmonary vasoconstriction in ovine sepsis. Critical Care Medicine [Internet]. 1997 [cited 2020 Sep 2];25(9):1551–9. Available from: https://pubmed.ncbi.nlm.nih.gov/9295831/

45. Frank DU, Lowson SM, Roos CM, Rich GF. Endotoxin alters hypoxic pulmonary vasoconstriction in isolated rat lungs. Journal of Applied Physiology [Internet]. 1996 [cited 2020 Sep 2];81(3):1316–22. Available from: https://pubmed.ncbi.nlm.nih.gov/8889769/

46. Stevens T, Morris K, McMurtry IF, Zamora M, Tucker A. Pulmonary and systemic vascular responsiveness to TNF-α in conscious rats. Journal of Applied Physiology [Internet]. 1993 [cited 2020 Aug 31];74(4):1905–10. Available from: https://pubmed.ncbi.nlm.nih.gov/8514709/

47. Spöhr F, Cornelissen AJM, Busch C, Gebhard MM, Motsch J, Martin EO, et al. Role of endogenous nitric oxide in endotoxin-induced alteration of hypoxic pulmonary vasoconstriction in mice. American Journal of Physiology - Heart and Circulatory Physiology [Internet]. 2005 Aug [cited 2021 Jun 21];289(2 58-2). Available from: https://pubmed.ncbi.nlm.nih.gov/15778287/

48. N J, RR L, CJ B, MT V, T B, MJ KS, et al. Inhaled carbon monoxide protects time-dependently from loss of hypoxic pulmonary vasoconstriction in endotoxemic mice. Respir Res [Internet]. 2015 Sep 29 [cited 2021 Jul 25];16(1). Available from: https://pubmed.ncbi.nlm.nih.gov/26415503/

49. X C, J W, Y L, ZG C, TF R, M M, et al. Bacillus anthracis edema toxin inhibits hypoxic pulmonary vasoconstriction via edema factor and cAMP-mediated mechanisms in isolated perfused rat lungs. Am J Physiol Heart Circ Physiol [Internet]. 2021 Jan 1 [cited 2021 Aug 1];320(1):H36–51. Available from: https://pubmed.ncbi.nlm.nih.gov/33064559/

50. Morrell NW, Nijran KS, Biggs T, Seed WA. Regional matching of ventilation and perfusion during lobar bronchial occlusion in man. Clinical Science [Internet]. 1995 [cited 2020 Sep 1];88(2):179–84. Available from: https://pubmed.ncbi.nlm.nih.gov/7720342/

51. McCann UG, Schiller HJ, Gatto LA, Steinberg JM, Carney DE, Nieman GF. Alveolar mechanics alter hypoxic pulmonary vasoconstriction. Critical Care Medicine [Internet]. 2002 [cited 2021 Jun 20];30(6):1315–21. Available from: https://pubmed.ncbi.nlm.nih.gov/12072688/

52. BJ T, J K, EM S, TP O, BD J. Pulmonary capillary recruitment in response to hypoxia in healthy humans: a possible role for hypoxic pulmonary venoconstriction? Respir Physiol Neurobiol [Internet]. 2011 Jul 31 [cited 2021 Jul 19];177(2):98–107. Available from: https://pubmed.ncbi.nlm.nih.gov/21513822/

53. Tanner TN, Hall BR, Oran J. Pneumoperitoneum. [cited 2021 Nov 16]; Available from: https://doi.org/10.1016/j.suc.2018.06.004

54. Strang CM, Fredén F, Maripuu E, Hachenberg T, Hedenstierna G. Ventilation - Perfusion distributions and gas exchange during carbon dioxide-pneumoperitoneum in a porcine model. British Journal of Anaesthesia [Internet]. 2010 [cited 2021 Jun 29];105(5):691–7. Available from: https://pubmed.ncbi.nlm.nih.gov/20693177/

55. CM S, F F, E M, U E, T H, G H. Improved ventilation-perfusion matching with increasing abdominal pressure during CO(2) -pneumoperitoneum in pigs. Acta Anaesthesiol Scand [Internet]. 2011 Aug [cited 2021 Jul 19];55(7):887–96. Available from: https://pubmed.ncbi.nlm.nih.gov/21689075/

56. Wagner PD. Ventilation-Perfusion Matching during Exercise. Chest. 1992 May 1;101(5):192S-198S.

57. TK R, TW S. Effects of pulmonary flow heterogeneity on oxygen transport parameters in exercise. Respir Physiol Neurobiol [Internet]. 2019 Mar 1 [cited 2021 Jul 27];261:75–9. Available from: https://pubmed.ncbi.nlm.nih.gov/30321626/

58. Touyz RM, Alves-Lopes R, Rios FJ, Camargo LL, Anagnostopoulou A, Arner A, et al. Vascular smooth muscle contraction in hypertension. Cardiovascular Research [Internet]. 2018 Mar 15 [cited 2021 Nov 16];114(4):529–39. Available from: https://academic-oup-com.proxy.lib.umich.edu/cardiovascres/article/114/4/529/4831102

59. McMurtry IF, Davidson AB, Reeves JT, Grover RF. Inhibition of hypoxic pulmonary vasoconstriction by calcium antagonists in isolated rat lungs. Circulation Research [Internet]. 1976 [cited 2020 Aug 26];38(2):99–104. Available from: https://pubmed.ncbi.nlm.nih.gov/1245025/

60. Harder DR, Madden JA, Dawson C. Hypoxic induction of Ca2+-dependent action potentials in small pulmonary arteries of the cat. Journal of Applied Physiology [Internet]. 1985 [cited 2020 Aug 27];59(5):1389–93. Available from: https://pubmed.ncbi.nlm.nih.gov/4066569/

61. McMurtry IF. BAY K 8644 potentiates and A23187 inhibits hypoxic vasoconstriction in rat lungs. American Journal of Physiology - Heart and Circulatory Physiology [Internet]. 1985 [cited 2020 Aug 27];18(4). Available from: https://pubmed.ncbi.nlm.nih.gov/2413777/

62. Tolins M, Weir EK, Chesler E, Nelson DP, From AH. Pulmonary vascular tone is increased by a voltage-dependent calcium channel potentiator. Journal of Applied Physiology [Internet]. 1986 [cited 2020 Aug 27];60(3):942–8. Available from: https://pubmed.ncbi.nlm.nih.gov/2420778/

63. Ohe M, Ogata M, Shirato K, Takishima T. Effects of Verapamil and BAY K 8644 on the Hypoxic Contraction of the Isolated Human Pulmonary Artery. The Tohoku Journal of Experimental Medicine [Internet]. 1989 [cited 2020 Aug 30];157(1):81–2. Available from: https://pubmed.ncbi.nlm.nih.gov/2469135/

64. MJ C, J PL, S B, JP W, PI A. Hypoxic pulmonary vasoconstriction in the absence of pretone: essential role for intracellular Ca2+ release. J Physiol [Internet]. 2013 Sep [cited 2021 Jul 21];591(18):4473–98. Available from: https://pubmed.ncbi.nlm.nih.gov/23774281/

65. PP J, S H, M X, A B, T Z, M R, et al. Revisiting the mechanism of hypoxic pulmonary vasoconstriction using isolated perfused/ventilated mouse lung. Pulm Circ [Internet]. 2020 [cited 2021 Aug 1];10(4). Available from: https://pubmed.ncbi.nlm.nih.gov/33282184/

66. Dipp M, Nye PCG, Evans AM. Hypoxic release of calcium from the sarcoplasmic reticulum of pulmonary artery smooth muscle [Internet]. Vol. 281, American Journal of Physiology - Lung Cellular and Molecular Physiology. American Physiological Society; 2001 [cited 2021 Jun 16]. Available from: https://pubmed.ncbi.nlm.nih.gov/11435205/

67. Morio Y, McMurtry IF. Ca2+ release from ryanodine-sensitive store contributes to mechanism of hypoxic vasoconstriction in rat lungs. Journal of Applied Physiology [Internet]. 2002 [cited 2021 Jun 20];92(2):527–34. Available from: https://pubmed.ncbi.nlm.nih.gov/11796660/

68. Uzun Ö, Demiryürek AT, Kanzik I. Role of Gs proteins in hypoxic constriction of sheep pulmonary artery rings. Pharmacology [Internet]. 2002 [cited 2021 Jun 20];64(4):214–6. Available from: https://pubmed.ncbi.nlm.nih.gov/11893903/

69. Fuchs B, Dietrich A, Gudermann T, Kalwa H, Grimminger F, Weissmann N. The role of classical transient receptor potential channels in the regulation of hypoxic pulmonary vasoconstriction. In: Advances in Experimental Medicine and Biology [Internet]. Adv Exp Med Biol; 2010 [cited 2021 Jun 27]. p. 187–200. Available from: https://pubmed.ncbi.nlm.nih.gov/20204731/

70. Tang C, To WK, Meng F, Wang Y, Gu Y. A role for receptor-operated Ca2+ entry in human pulmonary artery smooth muscle cells in response to Hypoxia. Physiological Research [Internet]. 2010 Dec [cited 2021 Jun 28];59(6):909–18. Available from: https://pubmed.ncbi.nlm.nih.gov/20533864/

71. B F, M R, HA G, RT S, W S, F G, et al. Diacylglycerol regulates acute hypoxic pulmonary vasoconstriction via TRPC6. Respir Res [Internet]. 2011 Feb 4 [cited 2021 Jul 19];12(1). Available from: https://pubmed.ncbi.nlm.nih.gov/21294865/

72. XY W, D M, W T, XX L, YG Z, Y S, et al. Inhibition of RhoA/ROCK signaling pathway ameliorates hypoxic pulmonary hypertension via HIF-1α-dependent functional TRPC channels. Toxicol Appl Pharmacol [Internet]. 2019 Apr 15 [cited 2021 Jul 27];369:60–72. Available from: https://pubmed.ncbi.nlm.nih.gov/30831131/

73. Post JM, Hume JR, Archer SL, Weir EK. Direct role for potassium channel inhibition in hypoxic pulmonary vasoconstriction. American Journal of Physiology - Cell Physiology [Internet]. 1992 [cited 2020 Aug 31];262(4 31-4). Available from: https://pubmed.ncbi.nlm.nih.gov/1566816/

74. Dumas M, Dumas JP, Rochette L, Advenier C, Giudicelli JF. Comparison of the effects of nicorandil, pinacidil and nitroglycerin on hypoxic and hypercapnic pulmonary vasoconstriction in the isolated perfused lung of rat. British Journal of Pharmacology

[Internet]. 1996 [cited 2020 Sep 1];117(4):633–8. Available from: https://pubmed.ncbi.nlm.nih.gov/8646407/

75. Lee SH, Ho WK, Earm YE. Effects of intracellular Na+, Mg2+ and metabolites on Ca2+-activated K+ channels in pulmonary and ear arterial smooth muscle cells of the rabbit. Experimental Physiology [Internet]. 1998 [cited 2020 Oct 28];83(6):707–15. Available from: https://pubmed.ncbi.nlm.nih.gov/9782181/

76. Osipenko ON, Tate RJ, Gurney AM. Potential role for Kv3.1b Channels as oxygen sensors. Circulation Research [Internet]. 2000 Mar 17 [cited 2020 Oct 28];86(5):534–40. Available from: http://www.circresaha.org

77. Coppock EA, Tamkun MM. Differential expression of Kv channel α- and β-subunits in the bovine pulmonary arterial circulation. American Journal of Physiology - Lung Cellular and Molecular Physiology [Internet]. 2001 [cited 2021 Jun 16];281(6 25-6). Available from: https://pubmed.ncbi.nlm.nih.gov/11704530/

78. Bakhramov A, Evans A, Kozlowski R. Differential effects of hypoxia on the intracellular Ca2+ concentration of myocytes isolated from different regions of the rat pulmonary arterial tree. Experimental Physiology [Internet]. 1998 May 1 [cited 2020 Oct 27];83(3):337–47. Available from: http://doi.wiley.com/10.1113/expphysiol.1998.sp004117

79. Platoshyn O, Yu Y, Golovina VA, McDaniel SS, Krick S, Li L, et al. Chronic hypoxia decreases Kv channel expression and function in pulmonary artery myocytes. American Journal of Physiology - Lung Cellular and Molecular Physiology [Internet]. 2001 [cited 2021 Jun 14];280(4 24-4). Available from: https://pubmed.ncbi.nlm.nih.gov/11238022/

80. Platoshyn O, Brevnova EE, Burg ED, Yu Y, Remillard C v., Yuan JXJ. Acute hypoxia selectively inhibits KCNA5 channels in pulmonary artery smooth muscle cells. American Journal of Physiology - Cell Physiology [Internet]. 2006 Mar [cited 2021 Jun 21];290(3). Available from: https://pubmed.ncbi.nlm.nih.gov/16236819/

81. Diesen DL, Hess DT, Stamler JS. Hypoxic vasodilation by red blood cells: evidence for an S-nitrosothiol–based signal. Circ Res. 2008;103(5):545–53.

82. Silva C, Specht A, Wegiel B, Ferran C, Kaczmarek E. Mechanism of purinergic activation of endothelial nitric oxide synthase in endothelial cells. In: PURINERGIC SIGNALLING. 2008. p. S87–S87.

83. Platoshyn O, Yu Y, Ko EA, Remillard C v., Yuan JXJ. Heterogeneity of hypoxia-mediated decrease in IK(V) and increase in [Ca2+]cyt in pulmonary artery smooth muscle cells. American Journal of Physiology - Lung Cellular and Molecular Physiology [Internet]. 2007 Aug [cited 2021 Jun 22];293(2). Available from: https://pubmed.ncbi.nlm.nih.gov/17526598/

84. Archer SL, London B, Hampl V, Wu X, Nsair A, Puttagunta L, et al. Impairment of hypoxic pulmonary vasoconstriction in mice lacking the voltage-gated potassium channel Kv1.5. The FASEB Journal [Internet]. 2001 Aug 1 [cited 2022 Mar 24];15(10):1801–3. Available from: https://onlinelibrary.wiley.com/doi/full/10.1096/fj.00-0649fje

85. Papa S, Martino PL, Capitanio G, Gaballo A, de Rasmo D, Signorile A, et al. The Oxidative Phosphorylation System in Mammalian Mitochondria. Advances in Experimental Medicine and Biology [Internet]. 2012 [cited 2022 Mar 9];942:3–37. Available from: https://link-springer-com.proxy.lib.umich.edu/chapter/10.1007/978-94-007-2869-1_1

86. Leach RM, Hill HM, Snetkov VA, Robertson TP, Ward JPT. Divergent roles of glycolysis and the mitochondrial electron transport chain in hypoxic pulmonary vasoconstriction of the rat: Identity of the hypoxic sensor. Journal of Physiology [Internet]. 2001 Oct 1 [cited 2021 Jun 16];536(1):211–24. Available from: https://pubmed.ncbi.nlm.nih.gov/11579170/

87. Paddenberg R, Ishaq B, Goldenberg A, Faulhammer P, Rose F, Weissmann N, et al. Essential role of complex II of the respiratory chain in hypoxia-induced ROS generation in the pulmonary vasculature. American Journal of Physiology - Lung Cellular and Molecular Physiology [Internet]. 2003 May 1 [cited 2021 Jun 20];284(5 28-5). Available from: https://pubmed.ncbi.nlm.nih.gov/12676762/

88. R P, M T, P F, A G, B G, U P, et al. Mitochondrial complex II is essential for hypoxia-induced pulmonary vasoconstriction of intra- but not of pre-acinar arteries. Cardiovasc Res [Internet]. 2012 Mar 15 [cited 2021 Jul 20];93(4):702–10. Available from: https://pubmed.ncbi.nlm.nih.gov/22215723/

89. Sommer N, Pak O, Schörner S, Derfuss T, Krug A, Gnaiger E, et al. Mitochondrial cytochrome redox states and respiration in acute pulmonary oxygen sensing. European Respiratory Journal [Internet]. 2010 Nov 1 [cited 2021 Jun 29];36(5):1056–66. Available from: https://pubmed.ncbi.nlm.nih.gov/20516051/

90. N S, N A, O P, F K, I S, S S, et al. Bypassing mitochondrial complex III using alternative oxidase inhibits acute pulmonary oxygen sensing. Sci Adv [Internet]. 2020 Apr 1 [cited 2021 Aug 1];6(16). Available from: https://pubmed.ncbi.nlm.nih.gov/32426457/

91. GB W, JD M, RD G, PT M, JM S, D D, et al. Superoxide generated at mitochondrial complex III triggers acute responses to hypoxia in the pulmonary circulation. Am J Respir

Crit Care Med [Internet]. 2013 Feb 15 [cited 2021 Jul 21];187(4):424–32. Available from: https://pubmed.ncbi.nlm.nih.gov/23328522/

92. Dunham-Snary KJ, Wu D, Potus F, Sykes EA, Mewburn JD, Charles RL, et al. Ndufs2, a Core Subunit of Mitochondrial Complex I, Is Essential for Acute Oxygen-Sensing and Hypoxic Pulmonary Vasoconstriction. Circulation Research [Internet]. 2019 Jun 7 [cited 2020 Aug 26];124(12):1727–46. Available from: https://pubmed.ncbi.nlm.nih.gov/30922174/

93. Wu W, Platoshyn O, Firth AL, Yuan JXJ. Hypoxia divergently regulates production of reactive oxygen species in human pulmonary and coronary artery smooth muscle cells. American Journal of Physiology - Lung Cellular and Molecular Physiology [Internet]. 2007 Oct [cited 2021 Jun 22];293(4). Available from: https://pubmed.ncbi.nlm.nih.gov/17693484/

94. Weissmann N, Grimminger F, Voswinckel R, Conzen J, Seeger W. Nitro blue tetrazolium inhibits but does not mimic hypoxic vasoconstriction in isolated rabbit lungs. American Journal of Physiology - Lung Cellular and Molecular Physiology [Internet]. 1998 [cited 2020 Sep 2];274(5 18-5). Available from: https://pubmed.ncbi.nlm.nih.gov/9612287/

95. Pourmahram GE, Snetkov VA, Shaifta Y, Drndarski S, Knock GA, Aaronson PI, et al. Constriction of pulmonary artery by peroxide: role of Ca2+ release and PKC. Free Radical Biology and Medicine [Internet]. 2008 Nov 15 [cited 2021 Jun 27];45(10):1468–76. Available from: https://pubmed.ncbi.nlm.nih.gov/18805479/

96. Ahmad M, Kelly MR, Zhao X, Kandhi S, Wolin MS. Roles for Nox4 in the contractile response of bovine pulmonary arteries to hypoxia. American Journal of Physiology -

Heart and Circulatory Physiology [Internet]. 2010 Jun [cited 2021 Jun 29];298(6). Available from: https://pubmed.ncbi.nlm.nih.gov/20304813/

97. N S, M H, O P, S S, F K, C S, et al. Mitochondrial Complex IV Subunit 4 Isoform 2 Is Essential for Acute Pulmonary Oxygen Sensing. Circ Res [Internet]. 2017 Aug 4 [cited 2021 Jul 26];121(4):424–38. Available from: https://pubmed.ncbi.nlm.nih.gov/28620066/

98. Duprat F, Guillemare E, Romey G, Fink M, Lesage F, Lazdunski M, et al. Susceptibility of cloned K+ channels to reactive oxygen species. Proc Natl Acad Sci U S A [Internet]. 1995 Dec 5 [cited 2022 Mar 24];92(25):11796–800. Available from: https://www.pnas.org

99. Weissmann N, Zeller S, Schäfer RU, Turowski C, Ay M, Quanz K, et al. Impact of mitochondria and NADPH oxidases on acute and sustained hypoxic pulmonary vasoconstriction. American Journal of Respiratory Cell and Molecular Biology [Internet]. 2006 Apr [cited 2021 Jun 21];34(4):505–13. Available from: https://pubmed.ncbi.nlm.nih.gov/16357364/

100. Gupte SA, Okada T, McMurtry IF, Oka M. Role of pentose phosphate pathway-derived NADPH in hypoxic pulmonary vasoconstriction. Pulmonary Pharmacology and Therapeutics [Internet]. 2006 Aug [cited 2021 Jun 21];19(4):303–9. Available from: https://pubmed.ncbi.nlm.nih.gov/16203165/

101. Farah C, Michel LYM, Balligand JL. Nitric oxide signalling in cardiovascular health and disease. Nature Reviews Cardiology 2018 15:5 [Internet]. 2018 Feb 1 [cited 2021 Nov 16];15(5):292–316. Available from: https://www-nature-com.proxy.lib.umich.edu/articles/nrcardio.2017.224

102. Chi AY, Waypa GB, Mungai PT, Schumacker PT. Prolonged hypoxia increases ros signaling and RhoA activation in pulmonary artery smooth muscle and endothelial cells.

Antioxidants and Redox Signaling [Internet]. 2010 Mar 1 [cited 2021 Jun 28];12(5):603–10. Available from: https://pubmed.ncbi.nlm.nih.gov/19747063/

103. VR Y, T S, L M, L J, YM Z, YX W. PLCγ1-PKCε-IP 3 R1 signaling plays an important role in hypoxia-induced calcium response in pulmonary artery smooth muscle cells. Am J Physiol Lung Cell Mol Physiol [Internet]. 2018 May 1 [cited 2021 Jul 27];314(5):L724–35. Available from: https://pubmed.ncbi.nlm.nih.gov/29388468/

104. Smyth EM, Grosser T, Wang M, Yu Y, Fitzgerald GA, Smyth EM, et al. Prostanoids in health and disease. Journal of Lipid Research [Internet]. 2009 Apr 1 [cited 2021 Nov 16];50(SUPPL.):S423–8. Available from: http://www.jlr.org/article/S0022227520306507/fulltext

105. Benumof JL, Wahrenbrock EA. Local effects of anesthetics on regional hypoxic pulmonary vasoconstriction. Anesthesiology [Internet]. 1975 [cited 2020 Aug 26];43(5):525–32. Available from: https://pubmed.ncbi.nlm.nih.gov/1190522/

106. Lennon PF, Murray PA. Attenuated hypoxic pulmonary vasoconstriction during isoflurane anesthesia is abolished by cyclooxygenase inhibition in chronically instrumented dogs. Anesthesiology [Internet]. 1996 Feb [cited 2020 Sep 1];84(2):404–14. Available from: https://pubmed.ncbi.nlm.nih.gov/8602673/

107. Voelkel NF, Morganroth M, Feddersen OC. Potential Role of Arachidonic Acid Metabolites in Hypoxic Pulmonary Vasoconstriction. Chest [Internet]. 1985 Oct [cited 2020 Aug 27];88(4):245S-248S. Available from: https://pubmed.ncbi.nlm.nih.gov/3930165/

108. Gottlieb JE, McGeady M, Adkinson NF, Sylvester JT. Effects of cyclo- and lipoxygenase inhibitors on hypoxic vasoconstriction in isolated ferret lungs. Journal of Applied

Physiology [Internet]. 1988 [cited 2020 Aug 27];64(3):936–43. Available from: https://pubmed.ncbi.nlm.nih.gov/2835351/

109. Paterson NAM, Hamilton JT, Yaghi A, Miller DS. Effect of hypoxia on responses of respiratory smooth muscle to histamine and LTD4. Journal of Applied Physiology [Internet]. 1988 [cited 2020 Aug 27];64(1):435–40. Available from: https://pubmed.ncbi.nlm.nih.gov/3356661/

110. Miller DS, Yaghi A, Hamilton JT, Paterson NAM. Role of arachidonic acid metabolites in hypoxic contractions of isolated porcine pulmonary artery and vein. Experimental Lung Research [Internet]. 1989 [cited 2020 Aug 30];15(2):213–22. Available from: https://pubmed.ncbi.nlm.nih.gov/2707182/

111. Yamaguchi T, O'Brien RF, Hanson WL, Wagner WW, McMurtry IF. Prostacyclin contributes to inhibition of hypoxic pulmonary vasoconstriction by alkalosis. Prostaglandins [Internet]. 1989 [cited 2020 Aug 30];38(1):53–63. Available from: https://pubmed.ncbi.nlm.nih.gov/2546189/

112. McDonnell TJ, Westcott JY, Czartolomna J, Voelkel NF. Role of peptidoleukotrienes in hypoxic pulmonary vasoconstriction in rats. American Journal of Physiology - Heart and Circulatory Physiology [Internet]. 1990 [cited 2020 Aug 30];259(3 28-3). Available from: https://pubmed.ncbi.nlm.nih.gov/2118728/

113. Zhu D, Medhora M, Campbell WB, Spitzbarth N, Baker JE, Jacobs ER. Chronic hypoxia activates lung 15-lipoxygenase, which catalyzes production of 15-HETE and enhances constriction in neonatal rabbit pulmonary arteries. Circulation Research [Internet]. 2003 May 16 [cited 2021 Jun 20];92(9):992–1000. Available from: https://pubmed.ncbi.nlm.nih.gov/12690037/

114. Han WN, Li XH, Jiang ZY, Ji HY, Huang LJ, Wang ZM, et al. Effect of 15-HETE on potassium channels of rabbit pulmonary arterial smooth muscles during hypoxia - PubMed [Internet]. Acta Physiologica Sinica. 2004 [cited 2021 Jun 20]. Available from: https://pubmed.ncbi.nlm.nih.gov/15614421/

115. Chu X, Tang X, Guo L, Bao H, Zhang S, Zhang J, et al. Hypoxia suppresses KV1.5 channel expression through endogenous 15-HETE in rat pulmonary artery. Prostaglandins and Other Lipid Mediators [Internet]. 2009 Jan [cited 2021 Jun 27];88(1–2):42–50. Available from: https://pubmed.ncbi.nlm.nih.gov/18984061/

116. Wang Y, Liang D, Wang S, Qiu Z, Chu X, Chen S, et al. Role of the G-protein and tyrosine kinase - Rho/ROK pathways in 15-hydroxyeicosatetraenoic acid induced pulmonary vasoconstriction in hypoxic rats. Journal of Biochemistry [Internet]. 2010 [cited 2021 Jun 28];147(5):751–64. Available from: https://pubmed.ncbi.nlm.nih.gov/20139061/

117. Keserü B, Barbosa-Sicard E, Popp R, Fisslthaler B, Dietrich A, Gudermann T, et al. Epoxyeicosatrienoic acids and the soluble epoxide hydrolase are determinants of pulmonary artery pressure and the acute hypoxic pulmonary vasoconstrictor response. The FASEB Journal [Internet]. 2008 Dec [cited 2021 Jun 24];22(12):4306–15. Available from: https://pubmed.ncbi.nlm.nih.gov/18725458/

118. Cogolludo A, Moreno L, Frazziano G, Moral-Sanz J, Menendez C, Castañeda J, et al. Activation of neutral sphingomyelinase is involved in acute hypoxic pulmonary vasoconstriction. Cardiovascular Research [Internet]. 2009 May [cited 2021 Jun 27];82(2):296–302. Available from: https://pubmed.ncbi.nlm.nih.gov/19088082/

119. G F, L M, J MS, C M, L E, C G, et al. Neutral sphingomyelinase, NADPH oxidase and reactive oxygen species. Role in acute hypoxic pulmonary vasoconstriction. J Cell Physiol [Internet]. 2011 Oct [cited 2021 Jul 19];226(10):2633–40. Available from: https://pubmed.ncbi.nlm.nih.gov/21792922/

120. L W, J Y, HT N, H R, A T, J H, et al. Hypoxic pulmonary vasoconstriction requires connexin 40-mediated endothelial signal conduction. J Clin Invest [Internet]. 2012 Nov 1 [cited 2021 Jul 20];122(11):4218–30. Available from: https://pubmed.ncbi.nlm.nih.gov/23093775/

121. NM G, L W, H R, W L, A T, WM K. TRPV4 Is Required for Hypoxic Pulmonary Vasoconstriction. Anesthesiology [Internet]. 2015 Jun 20 [cited 2021 Jul 25];122(6):1338–48. Available from: https://pubmed.ncbi.nlm.nih.gov/25815455/

122. Tabeling C, Yu H, Wang L, Ranke H, Goldenberg NM, Zabini D, et al. CFTR and sphingolipids mediate hypoxic pulmonary vasoconstriction. Proc Natl Acad Sci U S A [Internet]. 2015 Mar 31 [cited 2021 Nov 16];112(13):E1614–23. Available from: https://www-pnas-org.proxy.lib.umich.edu/content/112/13/E1614

123. Kawanabe Y, Nauli SM. Endothelin. Cellular and Molecular Life Sciences 2010 68:2 [Internet]. 2010 Sep 17 [cited 2021 Nov 17];68(2):195–203. Available from: https://link.springer.com/article/10.1007/s00018-010-0518-0

124. Davenport AP, Hyndman KA, Dhaun N, Southan C, Kohan DE, Pollock JS, et al. Endothelin. Pharmacological Reviews [Internet]. 2016 Apr 1 [cited 2021 Nov 17];68(2):357–418. Available from: https://pharmrev-aspetjournals-org.proxy.lib.umich.edu/content/68/2/357

125. Weygandt GR, Kopman EA, Ludbrook PA. Mechanism of nitroglycerin-Induced hypoxemia. Catheterization and Cardiovascular Diagnosis [Internet]. 1980 [cited 2020 Aug 26];6(4):387–95. Available from: https://pubmed.ncbi.nlm.nih.gov/6781754/

126. Ogata M, Ohe M, Katayose D, Takishima T. Modulatory role of EDRF in hypoxic contraction of isolated porcine pulmonary arteries. In: American Journal of Physiology - Heart and Circulatory Physiology [Internet]. Am J Physiol; 1992 [cited 2020 Aug 31]. Available from: https://pubmed.ncbi.nlm.nih.gov/1558177/

127. Roberts JD, Chen TY, Kawai N, Wain J, Dupuy P, Shimouchi A, et al. Inhaled nitric oxide reverses pulmonary vasoconstriction in the hypoxic and acidotic newborn lamb. Circulation Research [Internet]. 1993 [cited 2020 Aug 31];72(2):246–54. Available from: https://pubmed.ncbi.nlm.nih.gov/8380356/

128. Weissmann N, Voswinckel R, Tadić A, Hardebusch T, Ghofrani HA, Schermuly RT, et al. Nitric oxide (NO)-dependent but not NO-independent guanylate cyclase activation attenuates hypoxic vasoconstriction in rabbit lungs. American Journal of Respiratory Cell and Molecular Biology [Internet]. 2000 [cited 2021 Jun 14];23(2):222–7. Available from: https://pubmed.ncbi.nlm.nih.gov/10919989/

129. Fagan KA, Fouty BW, Tyler RC, Morris KG, Hepler LK, Sato K, et al. The pulmonary circulation of homozygous or heterozygous eNOS-null mice is hyperresponsive to mild hypoxia. Journal of Clinical Investigation [Internet]. 1999 [cited 2021 Jun 14];103(2):291–9. Available from: https://pubmed.ncbi.nlm.nih.gov/9916141/

130. Deem S, Swenson ER, Alberts MK, Hedges RG, Bishop MJ. Red-blood-cell augmentation of hypoxic pulmonary vasoconstriction: Hematocrit dependence and the importance of

nitric oxide. American Journal of Respiratory and Critical Care Medicine. 1998 Dec 14;157(4 PART I):1181–6.

131. Deem S, Berg JT, Kerr ME, Swenson ER. Effects of the RBC membrane and increased perfusate viscosity on hypoxic pulmonary vasoconstriction. Journal of Applied Physiology [Internet]. 2000 May 1 [cited 2020 Oct 28];88(5):1520–8. Available from: https://www.physiology.org/doi/10.1152/jappl.2000.88.5.1520

132. Loer SA, Peters J. Effects of haemoconcentration and haemodilution on acute hypoxia-induced pulmonary hypertension and changes in vascular compliance of isolated rabbit lungs. Intensive Care Medicine [Internet]. 2000 [cited 2021 Jun 14];26(8):1124–30. Available from: https://pubmed.ncbi.nlm.nih.gov/11030170/

133. Moens AL, Goovaerts I, Claeys MJ, Vrints CJ. Flow-Mediated Vasodilation: A Diagnostic Instrument, or an Experimental Tool? Chest. 2005 Jun 1;127(6):2254–63.

134. Han TH, Qamirani E, Nelson AG, Hyduke DR, Chaudhuri G, Kuo L, et al. Regulation of nitric oxide consumption by hypoxic red blood cells. Proc Natl Acad Sci U S A [Internet]. 2003 Oct 14 [cited 2021 Jun 20];100(21):12504–9. Available from: https://pubmed.ncbi.nlm.nih.gov/14523233/

135. Deem S. Nitric oxide scavenging by hemoglobin regulates hypoxic pulmonary vasoconstriction [Internet]. Vol. 36, Free Radical Biology and Medicine. Elsevier Inc.; 2004 [cited 2021 Jun 20]. p. 698–706. Available from: https://pubmed.ncbi.nlm.nih.gov/14990350/

136. Takemoto M, Sun J, Hiroki J, Shimokawa H, Liao JK. Rho-kinase mediates hypoxia-induced downregulation of endothelial nitric oxide synthase. Circulation [Internet]. 2002

Jul 1 [cited 2021 Jun 20];106(1):57–62. Available from: https://pubmed.ncbi.nlm.nih.gov/12093770/

137. Nozik-Grayck E, Huang YCT, Carraway MS, Piantadosi CA. Bicarbonate-dependent superoxide release and pulmonary artery tone. American Journal of Physiology - Heart and Circulatory Physiology [Internet]. 2003 [cited 2021 Jun 20];285(6 54-6). Available from: https://pubmed.ncbi.nlm.nih.gov/12842815/

138. Helset E, Kjæve J, Bjertnæs L, Lundberg JM. Acute alveolar hypoxia increases endothelin-1 release but decreases release of calcitonin generelated peptide in isolated perfused rat lungs. Scandinavian Journal of Clinical and Laboratory Investigation [Internet]. 1995 [cited 2021 Jun 14];55(5):369–76. Available from: https://pubmed.ncbi.nlm.nih.gov/8545594/

139. Wang Y, Coe Y, Toyoda O, Coceani F. Involvement of endothelin-1 in hypoxic pulmonary vasoconstriction in the lamb. The Journal of Physiology [Internet]. 1995 Jan 15 [cited 2020 Sep 1];482(2):421–34. Available from: https://pubmed.ncbi.nlm.nih.gov/7714833/

140. Takeda S, Nakanishi K, Inoue T, Ogawa R. Delayed elevation of plasma endothelin-1 during unilateral alveolar hypoxia without systemic hypoxemia in humans. Acta Anaesthesiologica Scandinavica [Internet]. 1997 [cited 2020 Sep 2];41(2):274–80. Available from: https://pubmed.ncbi.nlm.nih.gov/9062613/

141. Sato K, Morio Y, Morris KG, Rodman DM, McMurtry IF. Mechanism of hypoxic pulmonary vasoconstriction involves ET(A) receptor- mediated inhibition of K(ATP) channel. American Journal of Physiology - Lung Cellular and Molecular Physiology

[Internet]. 2000 [cited 2020 Oct 28];278(3 22-3):434–42. Available from: http://www.ajplung.org

142. Liu Q, Sham JSK, Shimoda LA, Sylvester JT. Hypoxic constriction of porcine distal pulmonary arteries: Endothelium and endothelin dependence [Internet]. Vol. 280, American Journal of Physiology - Lung Cellular and Molecular Physiology. American Physiological Society; 2001 [cited 2021 Jun 14]. Available from: https://pubmed.ncbi.nlm.nih.gov/11290508/

143. Goirand F, Bardou M, Guerard P, Dumas JP, Rochette L, Dumas M. ETA, mixed ETA/ETB receptor antagonists, and protein kinase C inhibitor prevent acute hypoxic pulmonary vasoconstriction: Influence of potassium channels. Journal of Cardiovascular Pharmacology [Internet]. 2003 Jan 1 [cited 2021 Jun 20];41(1):117–25. Available from: https://pubmed.ncbi.nlm.nih.gov/12500029/

144. Zhang WM, Yip KP, Lin MJ, Shimoda LA, Li WH, Sham JSK. ET-1 activates Ca2+ sparks in PASMC: Local Ca2+ signaling between inositol trisphosphate and ryanodine receptors. American Journal of Physiology - Lung Cellular and Molecular Physiology [Internet]. 2003 Sep 1 [cited 2021 Jun 20];285(3 29-3). Available from: https://pubmed.ncbi.nlm.nih.gov/12740215/

145. Santolicandro A, Prediletto R, Fornai E, Formichi B, Begliomini E, Giannella-Neto A, et al. Mechanisms of hypoxemia and hypocapnia in pulmonary embolism. American Journal of Respiratory and Critical Care Medicine. 1995 Dec 20;152(1):336–47.

146. Wagner PD. The multiple inert gas elimination technique (MIGET). In: Applied Physiology in Intensive Care Medicine (Second Edition) [Internet]. Springer Berlin

Heidelberg; 2009 [cited 2021 Mar 16]. p. 29–36. Available from: https://link-springer-com.proxy.lib.umich.edu/chapter/10.1007/978-3-642-01769-8_8

147. Bajc M, Schümichen C, Grüning T, Lindqvist A, le Roux PY, Alatri A, et al. EANM guideline for ventilation/perfusion single-photon emission computed tomography (SPECT) for diagnosis of pulmonary embolism and beyond. European Journal of Nuclear Medicine and Molecular Imaging [Internet]. 2019 Nov 1 [cited 2021 Mar 16];46(12):2429–51. Available from: https://doi.org/10.1007/s00259-019-04450-0

148. Wagner PD. VENTILATION-PERFUSION RELATIONSHIPS. Ann Rev Physiol [Internet]. 1980 [cited 2021 Dec 15];42:235–82. Available from: www.annualreviews.org

149. Petersson J, Glenny RW, Chemla D, Vonk-Noordegraaf A, Dinh-Xuan Affiliations A, Respir E. Gas exchange and ventilation–perfusion relationships in the lung. European Respiratory Journal [Internet]. 2014 Oct 1 [cited 2022 May 5];44(4):1023–41. Available from: https://erj.ersjournals.com/content/44/4/1023

150. Palmer J, Bitzén U, Jonson B, Bajc M. Comprehensive Ventilation/Perfusion SPECT. Vol. 42, THE JOURNAL OF NUCLEAR MEDICINE •. 2001.

151. O'Donnell DE, Elbehairy AF, Berton DC, Domnik NJ, Alberto Neder J. Advances in the evaluation of respiratory pathophysiology during exercise in chronic lung diseases [Internet]. Vol. 8, Frontiers in Physiology. Frontiers Media S.A.; 2017 [cited 2021 Feb 28]. p. 82. Available from: www.frontiersin.org

152. Kara T, Narkiewicz K, Somers VK. Chemoreflexes–physiology and clinical implications. Acta Physiol Scand. 2003;177(3):377–84.

153. Powers KA, Dhamoon AS. Physiology, Pulmonary Ventilation and Perfusion. StatPearls [Internet]. 2022 Jan 28 [cited 2022 May 5]; Available from: https://www.ncbi.nlm.nih.gov/books/NBK539907/

154. Riley MS, Porszasz J, Engelen MPKJ, Brundage BH, Wasserman K. Gas exhange responses to continuous incremental cycle ergometry exercise in primary pulmonary hypertension in humans. European Journal of Applied Physiology [Internet]. 2000 [cited 2021 Feb 28];83(1):63–70. Available from: https://link-springer-com.proxy.lib.umich.edu/article/10.1007/s004210000240

155. Stringer WW, Hansen JE, Wasserman K. Cardiac output estimated noninvasively from oxygen uptake during exercise. Journal of Applied Physiology [Internet]. 1997 [cited 2021 Feb 28];82(3):908–12. Available from: https://journals-physiology-org.proxy.lib.umich.edu/doi/abs/10.1152/jappl.1997.82.3.908

156. Grainge CL, Lau LCK, Ward JA, Dulay V, Lahiff G, Wilson S, et al. Effect of bronchoconstriction on airway remodeling in asthma. New England Journal of Medicine. 2011;364(21):2006–15.

157. Bousquet J, Jeffery PK, Busse WW, Johnson M, Vignola AM. Asthma: from bronchoconstriction to airways inflammation and remodeling. Am J Respir Crit Care Med. 2000;161(5):1720–45.

158. Starr IR, Lamm WJE, Neradilek B, Polissar N, Glenny RW, Hlastala MP. Regional hypoxic pulmonary vasoconstriction in prone pigs. Journal of Applied Physiology [Internet]. 2005 Jul [cited 2021 Nov 28];99(1):363–70. Available from: https://journals-physiology-org.proxy.lib.umich.edu/doi/abs/10.1152/japplphysiol.00822.2004

159. Hlastala MP, Lamm WJE, Karp A, Polissar NL, Starr IR, Glenny RW. Spatial distribution of hypoxic pulmonary vasoconstriction in the supine pig. Journal of Applied Physiology. 2004;96(5):1589–99.

160. Hantzidiamantis PJ, Amaro E. Physiology, Alveolar to Arterial Oxygen Gradient. StatPearls [Internet]. 2021 Feb 22 [cited 2021 Oct 6]; Available from: https://www.ncbi.nlm.nih.gov/books/NBK545153/

161. Krogh A. The supply of oxygen to the tissues and the regulation of the capillary circulation. J Physiol. 1919;52(6):457–74.

162. Krogh A. The anatomy and physiology of capillaries. Vol. 18. Yale University Press; 1922.

163. Krogh A. The number and distribution of capillaries in muscles with calculations of the oxygen pressure head necessary for supplying the tissue. J Physiol. 1919;52(6):409–15.

164. Barstow TJ. Characterization of VO2 kinetics during heavy exercise. Medicine and Science in Sports and Exercise [Internet]. 1994 Nov 1 [cited 2021 Mar 21];26(11):1327–34. Available from: https://europepmc.org/article/med/7837952

165. Gharahi H, Figueroa CA, Tune JD, Beard DA. Multiscale model of the physiological control of myocardial perfusion to delineate putative metabolic feedback mechanisms. bioRxiv [Internet]. 2021 Aug 6 [cited 2022 Jan 11];2021.08.04.455088. Available from: https://www.biorxiv.org/content/10.1101/2021.08.04.455088v1

166. Bassingthwaighte JB, Beard DA, Li Z. The mechanical and metabolic basis of myocardial blood flow heterogeneity. Basic Res Cardiol [Internet]. 2001 [cited 2022 Jan 11];96(6):582–94. Available from: https://pubmed.ncbi.nlm.nih.gov/11770077/

167. Glenny RW, Robertson HT. Fractal modeling of pulmonary blood flow heterogeneity. Journal of Applied Physiology [Internet]. 1991 [cited 2021 Mar 14];70(3):1024–30. Available from: https://journals-physiology-org.proxy.lib.umich.edu/doi/abs/10.1152/jappl.1991.70.3.1024

168. Hughes JMB. Hypoxic pulmonary vasoconstriction: Clinical implications [Internet]. Vol. 47, European Respiratory Journal. European Respiratory Society; 2016 [cited 2021 Mar 14]. p. 31–4. Available from: http://ow.ly/Uh54o

169. Glenny RW, Lamm WJE, Bernard SL, An D, Chornuk M, Pool SL, et al. Selected Contribution: Redistribution of pulmonary perfusion during weightlessness and increased gravity. Journal of Applied Physiology [Internet]. 2000 Sep 1 [cited 2021 Mar 14];89(3):1239–48. Available from: https://www.physiology.org/doi/10.1152/jappl.2000.89.3.1239

170. Marquis AD, Jezek F, Pinsky DJ, Beard DA. Hypoxic pulmonary vasoconstriction as a regulator of alveolar-capillary oxygen flux: A computational model of ventilation-perfusion matching. PLOS Computational Biology [Internet]. 2021 May 1 [cited 2021 Jul 15];17(5):e1008861. Available from: https://journals.plos.org/ploscompbiol/article?id=10.1371/journal.pcbi.1008861

171. Arai TJ, Henderson AC, Dubowitz DJ, Levin DL, Friedman PJ, Buxton RB, et al. Hypoxic pulmonary vasoconstriction does not contribute to pulmonary blood flow heterogeneity in normoxia in normal supine humans. Journal of Applied Physiology [Internet]. 2009 Apr [cited 2021 Mar 14];106(4):1057–64. Available from: https://www.physiology.org/doi/10.1152/japplphysiol.90759.2008

172. Sander R. Compilation of Henry's law constants (version 4.0) for water as solvent. Atmospheric Chemistry & Physics. 2015;15(8).

173. Cartheuser CF. Standard and pH-affected hemoglobin-O2 binding curves of Sprague-Dawley rats under normal and shifted P50 conditions. Comp Biochem Physiol Comp Physiol. 1993;106(4):775–82.

174. Larson BL, Ormiston EE. Respiration and Circulation. Journal of Dairy Science. 1972;55(9):1332.

175. Moudgil R, Michelakis ED, Archer SL. Hypoxic pulmonary vasoconstriction. J Appl Physiol. 2005;98(1):390–403.

176. Sylvester JT, Shimoda LA, Aaronson PI, Ward JPT. Hypoxic pulmonary vasoconstriction. Physiol Rev. 2012;92(1):367–520.

177. West JB, Dollery CT, Naimark A. Distribution of blood flow in isolated lung; relation to vascular and alveolar pressures. J Appl Physiol. 1964;19(4):713–24.

178. Hubmayr RD, Walters BJ, Chevalier PA, Rodarte JR, Olson LE. Topographical distribution of regional lung volume in anesthetized dogs. Journal of Applied Physiology. 1983;54(4):1048–56.

179. Domino KB, Swenson ER, Hlastala MP. Hypocapnia-induced ventilation/perfusion mismatch: a direct CO2 or pH-mediated effect? Am J Respir Crit Care Med. 1995;152(5):1534–9.

180. Lele EE, Hantos Z, Bitay M, Sz\'\ivós B, Bogáts G, Peták F, et al. Bronchoconstriction during alveolar hypocapnia and systemic hypercapnia in dogs with a cardiopulmonary bypass. Respir Physiol Neurobiol. 2011;175(1):140–5.

181. Starr IR, Lamm WJE, Neradilek B, Polissar N, Glenny RW, Hlastala MP. Regional hypoxic pulmonary vasoconstriction in prone pigs. Journal of Applied Physiology. 2005;99(1):363–70.

182. Ball MK, Waypa GB, Mungai PT, Nielsen JM, Czech L, Dudley VJ, et al. Regulation of hypoxia-induced pulmonary hypertension by vascular smooth muscle hypoxia-inducible factor-1α. Am J Respir Crit Care Med. 2014;189(3):314–24.

183. Richalet JP, Gratadour P, Robach P, Pham I, Déchaux M, Joncquiert-Latarjet A, et al. Sildenafil inhibits altitude-induced hypoxemia and pulmonary hypertension. Am J Respir Crit Care Med. 2005;171(3):275–81.

184. Visovatti SH, Hyman MC, Goonewardena SN, Anyanwu AC, Kanthi Y, Robichaud P, et al. Purinergic dysregulation in pulmonary hypertension. American Journal of Physiology-Heart and Circulatory Physiology. 2016;311(1):H286–H298.

185. Chlopicki S, Bartus JB, Gryglewski RJ. Hypoxic pulmonary vasoconstriction in isolated blood-perfused rat lung; modulation by thromboxane A2, platelet-activating factor, cysteinyl leukotrienes and endothelin-1. Pol J Pharmacol. 2002;54(5):433–41.

186. Cruickshank S, Hirschauer N. The alveolar gas equation. Continuing Education in Anaesthesia, Critical Care & Pain. 2004;4(1):24–7.

187. Ellwein LM, Pope SR, Xie A, Batzel JJ, Kelley CT, Olufsen MS. Patient-specific modeling of cardiovascular and respiratory dynamics during hypercapnia. Math Biosci. 2013;241(1):56–74.

188. Carlson BE, Anderson JC, Raymond GM, Dash RK, Bassingthwaighte JB. Modeling oxygen and carbon dioxide transport and exchange using a closed loop circulatory system. In: Oxygen Transport to Tissue XXIX. Springer; 2008. p. 353–60.

189. Burrowes KS, Tawhai MH. Coupling of lung tissue tethering force to fluid dynamics in the pulmonary circulation. International Journal for Numerical Methods in Biomedical Engineering. 2010;26(7):862–75.

190. Clark AR, Burrowes KS, Tawhai MH. Contribution of serial and parallel microperfusion to spatial variability in pulmonary inter-and intra-acinar blood flow. J Appl Physiol. 2010;108(5):1116–26.

191. Hasler D, Anagnostopoulou P, Nyilas S, Latzin P, Schittny J, Obrist D. A multi-scale model of gas transport in the lung to study heterogeneous lung ventilation during the multiple-breath washout test. PLoS Comput Biol. 2019;15(6):e1007079.

192. Burrowes KS, Clark AR, Wilsher ML, Milne DG, Tawhai MH. Hypoxic pulmonary vasoconstriction as a contributor to response in acute pulmonary embolism. Ann Biomed Eng. 2014;42(8):1631–43.

193. Wang L, Yin J, Nickles HT, Ranke H, Tabuchi A, Hoffmann J, et al. Hypoxic pulmonary vasoconstriction requires connexin 40–mediated endothelial signal conduction. J Clin Invest. 2012;122(11):4218–30.

194. Wang L, Yin J, Nickles HT, Ranke H, Tabuchi A, Hoffmann J, et al. Hypoxic pulmonary vasoconstriction requires connexin 40–mediated endothelial signal conduction. The Journal of Clinical Investigation. 2012 Nov 1;122(11):4218–30.

195. Wang CY, Bassingthwaighte JB, Weissman LJ. Bifurcating distributive system using Monte Carlo method. Math Comput Model. 1992;16(3):91–8.

196. Talischi C, Paulino GH, Pereira A, Menezes IFM. PolyMesher: a general-purpose mesh generator for polygonal elements written in Matlab. Structural and Multidisciplinary Optimization. 2012;45(3):309–28.

197. Jiang ZL, Kassab GS, Fung YC. Diameter-defined Strahler system and connectivity matrix of the pulmonary arterial tree. Journal of Applied Physiology. 1994;76(2):882–92.

198. Erwig M. The graph Voronoi diagram with applications. Networks: An International Journal. 2000;36(3):156–63.

199. Safaei S, Blanco PJ, Müller LO, Hellevik LR, Hunter PJ. Bond graph model of cerebral circulation: toward clinically feasible systemic blood flow simulations. Front Physiol. 2018;9:148.

200. Fung YC, Sobin SS. Theory of sheet flow in lung alveoli. Journal of Applied Physiology. 1969;26(4):472–88.

201. Zhong Z, Dai Y, Mei CC, Tong P. A micromechanical theory of flow in pulmonary alveolar sheet. Cmes-computer MODELING in engineering & sciences. 2002;3(1):77–86.

202. Crane GJ, Neild TO, Segal SS. Contribution of active membrane processes to conducted hyperpolarization in arterioles of hamster cheek pouch. Microcirculation. 2004;11(5):425–33.

203. Blanco PJ, Watanabe SM, Passos MARF, Lemos PA, Feijóo RA. An anatomically detailed arterial network model for one-dimensional computational hemodynamics. IEEE Transactions on biomedical engineering. 2014;62(2):736–53.

204. Gelman S. Venous function and central venous pressure: A physiologic story. Anesthesiology: The Journal of the American Society of Anesthesiologists. 2008;108(4):735–48.

205. Molthen RC, Karau KL, Dawson CA. Quantitative models of the rat pulmonary arterial tree morphometry applied to hypoxia-induced arterial remodeling. J Appl Physiol. 2004;97(6):2372–84.

206. Cheng HY, Croft QPP, Frise MC, Talbot NP, Petousi N, Robbins PA, et al. Human hypoxic pulmonary vasoconstriction is unaltered by 8 h of preceding isocapnic hyperoxia. Physiol Rep. 2017;5(17):e13396.

207. Brimioulle S, Lejeune P, Naeije R. Effects of hypoxic pulmonary vasoconstriction on pulmonary gas exchange. Journal of Applied Physiology. 1996;81(4):1535–43.

208. Vinnakota KC, Bugenhagen SM. Optimization and parameter estimation, genetic algorithms. Encyclopedia of Systems Biology. 2013;1600–4.

209. Meier P, Zierler KL. On the theory of the indicator-dilution method for measurement of blood flow and volume. J Appl Physiol. 1954;6(12):731–44.

210. Murray CD. The physiological principle of minimum work applied to the angle of branching of arteries. J Gen Physiol. 1926;9(6):835.

211. Murray CD. The physiological principle of minimum work: I. The vascular system and the cost of blood volume. Proc Natl Acad Sci U S A. 1926;12(3):207.

212. Glenny RW, Bernard SL, Robertson HT. Pulmonary blood flow remains fractal down to the level of gas exchange. Journal of Applied Physiology. 2000;89(2):742–8.

213. Pries AR, Secomb TW, Gaehtgens P, Gross JF. Blood flow in microvascular networks. Experiments and simulation. Circ Res. 1990;67(4):826–34.

214. Pries AR, Secomb TW, Gessner T, Sperandio MB, Gross JF, Gaehtgens P. Resistance to blood flow in microvessels in vivo. Circ Res. 1994;75(5):904–15.

215. Tabeling C, Yu H, Wang L, Ranke H, Goldenberg NM, Zabini D, et al. CFTR and sphingolipids mediate hypoxic pulmonary vasoconstriction. Proceedings of the National Academy of Sciences. 2015;112(13):E1614–E1623.

216. Henderson AC, Sá RC, Theilmann RJ, Buxton RB, Prisk GK, Hopkins SR. The gravitational distribution of ventilation-perfusion ratio is more uniform in prone than supine posture in the normal human lung. J Appl Physiol. 2013;115(3):313–24.

217. Tapson VF, Humbert M. Incidence and prevalence of chronic thromboembolic pulmonary hypertension: from acute to chronic pulmonary embolism. Proc Am Thorac Soc. 2006;3(7):564–7.

218. Reeve HL, Michelakis E, Nelson DP, Weir EK, Archer SL. Alterations in a redox oxygen sensing mechanism in chronic hypoxia. Journal of Applied Physiology [Internet]. 2001 [cited 2021 Jun 14];90(6):2249–56. Available from: https://pubmed.ncbi.nlm.nih.gov/11356790/

219. DR P, LM H, TR Y, TC R, LV GB, BR W, et al. Chronic hypoxia limits H2O2-induced inhibition of ASIC1-dependent store-operated calcium entry in pulmonary arterial smooth muscle. Am J Physiol Lung Cell Mol Physiol [Internet]. 2014 Sep 1 [cited 2021 Jul 21];307(5). Available from: https://pubmed.ncbi.nlm.nih.gov/24993130/

220. Eyal FG, Hachey WE, Curtet-Eyal NL, Kellum FE, Alpan G. Effect of modulators of hypoxic pulmonary vasoconstriction on the response to inhaled nitric oxide in a neonatal model of severe pulmonary atelectasis. Seminars in Perinatology [Internet]. 1996 [cited 2020 Sep 2];20(3):186–93. Available from: https://pubmed.ncbi.nlm.nih.gov/8870121/

221. Broughton BRS, Jernigan NL, Norton CE, Walker BR, Resta TC. Chronic hypoxia augments depolarization-induced Ca2+ sensitization in pulmonary vascular smooth muscle through superoxide-dependent stimulation of RhoA. American Journal of Physiology - Lung Cellular and Molecular Physiology [Internet]. 2010 [cited 2021 Jun 27];298(2). Available from: https://pubmed.ncbi.nlm.nih.gov/19897743/

222. Langlands TAM, Henry BI, Wearne SL. Fractional cable equation models for anomalous electrodiffusion in nerve cells: infinite domain solutions. Journal of Mathematical Biology 2009 59:6 [Internet]. 2009 Feb 17 [cited 2022 Jan 13];59(6):761–808. Available from: https://link-springer-com.proxy.lib.umich.edu/article/10.1007/s00285-009-0251-1

223. Ortiz-Prado E, Dunn JF, Vasconez J, Castillo D, Viscor G. Partial pressure of oxygen in the human body: a general review. American Journal of Blood Research [Internet]. 2019 [cited 2022 Apr 11];9(1):1. Available from: /pmc/articles/PMC6420699/

224. Bajc M, Neilly B, Miniati M, Mortensen J, Jonson B. Methodology for ventilation/perfusion SPECT. Vol. 40, Seminars in Nuclear Medicine. W.B. Saunders; 2010. p. 415–25.

225. Colebank MJ, Mihaela Paun L, Umar Qureshi M, Chesler N, Husmeier D, Olufsen MS, et al. Influence of image segmentation on one-dimensional fluid dynamics predictions in the mouse pulmonary arteries. Journal of the Royal Society Interface [Internet]. 2019 Oct 31 [cited 2022 Apr 11];16(159). Available from: https://royalsocietypublishing-org.proxy.lib.umich.edu/doi/full/10.1098/rsif.2019.0284

226. Kopylova VS, Boronovskiy SE, Nartsissov YR. Fundamental principles of vascular network topology. 2017 [cited 2022 Jan 19]; Available from: http://portlandpress.com/biochemsoctrans/article-pdf/45/3/839/723786/bst-2016-0409c.pdf

227. Kassab GS. Scaling laws of vascular trees: Of form and function. American Journal of Physiology - Heart and Circulatory Physiology [Internet]. 2006 Feb [cited 2022 Jan 19];290(2):894–903. Available from: https://journals-physiology-org.proxy.lib.umich.edu/doi/abs/10.1152/ajpheart.00579.2005

228. Mortensen SP, Saltin B. Regulation of the skeletal muscle blood flow in humans. Experimental Physiology [Internet]. 2014 Dec 1 [cited 2022 Apr 11];99(12):1552–8. Available from: https://onlinelibrary-wiley-com.proxy.lib.umich.edu/doi/full/10.1113/expphysiol.2014.081620

229. ter Steege RWF, Kolkman JJ. Review article: the pathophysiology and management of gastrointestinal symptoms during physical exercise, and the role of splanchnic blood flow. Alimentary Pharmacology & Therapeutics [Internet]. 2012 Mar 1 [cited 2022 Apr 11];35(5):516–28. Available from: https://onlinelibrary-wiley-com.proxy.lib.umich.edu/doi/full/10.1111/j.1365-2036.2011.04980.x

230. Batzel JJ, Ellwein L, Olufsen MS. Modeling cardio-respiratory system response to inhaled CO 2 in patients with congestive heart failure. Proceedings of the Annual International Conference of the IEEE Engineering in Medicine and Biology Society, EMBS. 2011;2418–21.

231. McGuire BJ, Secomb TW. A theoretical model for oxygen transport in skeletal muscle under conditions of high oxygen demand. Journal of Applied Physiology [Internet]. 2001 [cited 2022 Apr 11];91(5):2255–65. Available from: https://journals-physiology-org.proxy.lib.umich.edu/doi/full/10.1152/jappl.2001.91.5.2255

232. Goldman D. Theoretical models of microvascular oxygen transport to tissue. Microcirculation. 2008;15(8):795–811.

233. Righini M, Robert-Ebadi H, le Gal G. Diagnosis of acute pulmonary embolism. Journal of Thrombosis and Haemostasis [Internet]. 2017 Jul 1 [cited 2022 Apr 11];15(7):1251–61. Available from: https://onlinelibrary-wiley-com.proxy.lib.umich.edu/doi/full/10.1111/jth.13694

234. Licha CRM, McCurdy CM, Maldonado SM, Lee LS. Current Management of Acute Pulmonary Embolism. Annals of Thoracic and Cardiovascular Surgery [Internet]. 2020 [cited 2022 Apr 11];26(2):65. Available from: /pmc/articles/PMC7184035/

235. Yandrapalli S, Tariq S, Kumar J, Aronow WS, Malekan R, Frishman WH, et al. Chronic Thromboembolic Pulmonary Hypertension. Cardiology in Review [Internet]. 2018 Mar [cited 2022 Apr 24];26(2):62–72. Available from: https://journals-lww-com.proxy.lib.umich.edu/cardiologyinreview/Fulltext/2018/03000/Chronic_Thromboembolic_Pulmonary_Hypertension_.2.aspx

236. Kim NH, Delcroix M, Jenkins DP, Channick R, Dartevelle P, Jansa P, et al. Chronic thromboembolic pulmonary hypertension. J Am Coll Cardiol [Internet]. 2013 Dec 24 [cited 2022 Apr 24];62(25 SUPPL.):D92–9. Available from: http://dx.doi.org/10.1016/j.jacc.2013.10.024

237. Madani MM. Surgical Treatment of Chronic Thromboembolic Pulmonary Hypertension: Pulmonary Thromboendarterectomy. Methodist DeBakey Cardiovascular Journal [Internet]. 2016 Oct 1 [cited 2022 Apr 25];12(4):213. Available from: /pmc/articles/PMC5344471/

238. Nitsure M, Sarangi B, Shankar GH, Reddy VS, Walimbe A, Sharma V, et al. Mechanisms of Hypoxia in COVID-19 Patients: A Pathophysiologic Reflection. Indian Journal of Critical Care Medicine : Peer-reviewed, Official Publication of Indian Society of Critical Care Medicine [Internet]. 2020 [cited 2022 Apr 11];24(10):967. Available from: /pmc/articles/PMC7689135/

239. Telenti A, Arvin A, Corey L, Corti D, Diamond MS, García-Sastre A, et al. After the pandemic: perspectives on the future trajectory of COVID-19. Nature 2021 596:7873

[Internet]. 2021 Jul 8 [cited 2022 Apr 11];596(7873):495–504. Available from: https://www-nature-com.proxy.lib.umich.edu/articles/s41586-021-03792-w

240. Liu X, Huang J, Li C, Zhao Y, Wang D, Huang Z, et al. The role of seasonality in the spread of COVID-19 pandemic. Environmental Research. 2021 Apr 1;195:110874.

241. Sallam M. COVID-19 Vaccine Hesitancy Worldwide: A Concise Systematic Review of Vaccine Acceptance Rates. Vaccines 2021, Vol 9, Page 160 [Internet]. 2021 Feb 16 [cited 2022 Apr 11];9(2):160. Available from: https://www-mdpi-com.proxy.lib.umich.edu/2076-393X/9/2/160/htm

242. Fazio RH, Ruisch BC, Moore CA, Granados Samayoa JA, Boggs ST, Ladanyi JT. Social distancing decreases an individual's likelihood of contracting COVID-19. Proc Natl Acad Sci U S A [Internet]. 2021 Feb 23 [cited 2022 Apr 11];118(8). Available from: https://doi.org/10.1073/pnas.2023131118

243. Wang Y, Deng Z, Shi D. How effective is a mask in preventing COVID-19 infection? Medical Devices & Sensors [Internet]. 2021 Feb 1 [cited 2022 Apr 11];4(1):e10163. Available from: https://onlinelibrary-wiley-com.proxy.lib.umich.edu/doi/full/10.1002/mds3.10163